An aptamer based biosensing platform for point-of-care diagnosis of cardiac biomarkers

THESIS

SUBMITTED FOR THE DEGREE OF

DOCTOR OF PHILOSOPHY

To

JAWAHARLAL NEHRU UNIVERSITY

NEW DELHI, INDIA

MAY 2022

IMTECH

SALONI KAKKAR

CSIR-INSTITUTE OF MICROBIAL TECHNOLOGY

CHANDIGARH-160036, INDIA

सीएसआईआर – इमटैक
CSIR-IMTECH

सीएसआईआर – सूक्ष्मजीव प्रौद्योगिकी संस्थान
सैक्टर 39 – ए, चण्डीगढ – 160 036 (भारत)
CSIR-INSTITUTE OF MICROBIAL TECHNOLOGY
(A CONSTITUENT ESTABLISHMENT OF CSIR)
Sector 39-A, Chandigarh-160 036 (INDIA)

CERTIFICATE

The research work embodied in this thesis entitled **"An aptamer based biosensing platform for point-of-care diagnosis of cardiac biomarkers"** has been carried by Ms. Saloni Kakkar at Immunodiagnostics and Biosensors Department under the guidance of Dr. Vijayender Bhalla (Principal Scientist) at CSIR-Institute of Microbial Technology, Sector 39-A, Chandigarh, India. This thesis is an original work performed by the candidate herself and has not been submitted in whole, or any part, for a degree or diploma in any other institute/university in India or abroad. To the best of my knowledge and belief, the work does not comprise any material published or written by some other person, except as acknowledged in the context.

Dr. Vijayender Bhalla

Principal Scientist

(Supervisor)

Saloni Kakkar

दूरभाष 0172-6665201 } Reception
0172-6665202 }
0172-6665..... (Direct)

फैक्स : 0091-172-2690632 (COA)
Fax : 0091-172-2690585 (Director)
0091-172-2690056 (Purchase)
एस. टी. डी. कोड : STD CODE : 172

Web : http://imtech.res.in


Dedicated to my family
&
the eternal supreme...

A glimpse of the years that rolled,

Well I must say a long journey toiled.

Endless it firstly seemed to stride,

My footsteps reminisce the time flied.

The breath of life in each moment,

Some ecstatic and some to torment.

All crafted me to own my present existence,

Strengthening me to persist and outdistance.

Affirmation in judgment that endeavors for perfection,

Each day I got to encounter a different perception.

Admirations to dejections, today I apprehend,

Carving me with the evolutions that mend.

Today, accustomed I feel with the accomplishment,

To pen my emotions with gratifying achievement.

The heart pounds with mixed sentiments,

Overwhelmingly today it leaves my temperament.

The journey commenced now paves a new way,

The blissfulness to embrace, Oh Lord, forever stay.

Saloni…

ACKNOWLEDGEMENT

Walking my last steps on a seemingly endless journey, first and foremost I extend glory and gratitude to ***the God, the almighty, the divinity*** *for his benevolent showers of bountiful blessings throughout this roller coaster ride of my research to attain its completion all through. I get a leaf to express my heartfelt gratitude to all those people whose comments, questions, criticism, support and most importantly considerate encouragement have gracefully contributed towards achieving the final landmark leaving an influential impact in my work.*

Firstly, I would like to express sincere indebtedness to my research guide ***Dr. Vijayender Bhalla****, Principal Scientist, CSIR-IMTECH, Chandigarh, for providing me all the freedom to explore on my own with his valuable guidance and scholarly inputs that I received throughout the research work. I will always be thankful to him for giving me the opportunity to be a part of his lab for conducting my research work under his supervision. His dynamic scientific vision and sincerity was an optimistic stimulation that has always been a great source of inspiration to strive hard for excellence. His friendly attitude and consistent conviction on my capabilities gathers privilege and honor for me to learn and grow under his guidance.*

I would also like to extend my obligation especially to our former Director ***Dr. Anil Koul*** *and current Director* ***Dr. Sandeep Khosla*** *for his undaunted academic support and facilities that reinforced my will to carry out research work at the institute. I am extremely grateful to* ***Dr. S. Karthikeyan****,* ***Dr. Charu Sharma, Dr. Balwinder, Mrs. Batra, Mrs. Indu, Janki Sir, Mrs. Neha*** *for smooth working of JNU-IMTech PhD programme. I am thankful to* ***Rajender sir*** *for always being there to solve our fellowship issues and suggesting ideas to get through odd situations. I am obliged towards the members of my research advisory committee (RAC)-* ***Dr. Manoj Raje, Dr. Raman Parkesh and Dr. Amit Tuli*** *for their scientific and helpful suggestions regarding assessment in presentations during the tenure of my PhD that inspired me to improvise upon the research work.*

I am exceptionally courteous to all other scientists of the institute for their considerate and cordial help at various phases of my research, whenever I approached them; I do hereby acknowledge all of them. I am grateful to ***Dr. Ashish*** *for his scientific recommendations, and invaluable suggestions that laid down the foundation of scientific vision in me. I sincerely appreciate the enduring support from* ***Dr. Rahul Prajesh*** *from CSIR-CEERI, Pilani for his gratefulness in collaborative worthwhile scientific learning regarding device fabrication. I owe my distinct appreciation to him for creating an amiable environment at CEERI steering towards*

an altogether different learning regarding FET (Field effect transistor) devices for his revering considerations that outstood in the form of a publication.

A special recognition to my mentor in masters ***Dr. Navin Bajpai****, Professor, Graphic Era University, Dehradun whose persistent confidence in my endeavors had a deep influence for inspiring me to make research as my cup of tea. The consistent guidance and support from my senior* ***Dr. Payal Gupta****, DBT-RA, IIT, Roorkee accustomed me with the research culture to fulfill my aims.*

Well, it feels really venerated to be a part of Immunodiagnostics and Biosensors group at IMTECH, Chandigarh where I shared all the trials and tribulations along with my success and satisfactions. It has been a great journey that acquainted me with a huge gang of diligent seniors, cooperative colleagues and enthusiastic juniors. I am thankful to my seniors ***Dr. Rajni, Dr. Beant, Dr. Pravin, Dr. Pargat, Dr. Virendra, Dr. Deepjyoti, Dr. Naresh*** *for their consistent support and troubleshooting sessions whenever I required them for smoothly overcoming my limitations. A special token of gratitude to my colleague* ***Bharti*** *for sharing aptamers synthesized by her along with the basic training to carry out research work in my initial days of joining the lab. I thank* ***Bhawna*** *for imparting optimistic attitude along with the pleasant and relaxing time we shared while having chit-chats over tea that crafted me well to escape the different shades during my PhD journey. She has been the best critic as a senior, best discussion partner as a colleague and the best buddy as a junior in the lab;* ***Jai*** *for creating lively environment in lab and saying his all-time set dialogue- "tension mat lo mam, sab hojya". His eagerness for food revealed by always saying "Canteen chalein" was a stress buster;* ***Manisha*** *and* ***Sanpreet*** *for our good times during discussions regarding protein preparation;* ***Aftab*** *for helping in electrochemical work and making my stay at CEERI memorable. A significant acknowledgement for* ***Sakshi*** *who came to lab as trainee but I really appreciate her sincere commitment that enabled to expand my work as an equivalent helping hand. Her hard work and perseverance in working with me during the last two years of research period along with her support to always gear up was unconditionally applaudable. I appreciate all other juniors* ***Tanvi, Kalyan, Amandeep, Nisha, Nitin, Manmeet, Sheetal, Rishika, Purva, Anshi,*** *especially* ***Jasmeet*** *and* ***Surbhi*** *(biggest thank you and sincere gratitude for being there while my final version of this journey-thesis printing and compilation) for maintaining an energetic and hilarious ambience during working hours in lab. I admire my junior* ***Shyamli*** *whose dramatic conversations worked as jovial fillers in between my thesis writing tenure.* ***Priya*** *whose enthusiastic and adorable nature melted all my tiredness and worries along with her hopeful attitude always imbibed more tolerance in me striving towards making of "The Mahal". Her optimism always fueled me up with the spark to again get up and make endeavors and most importantly polished the patience within me for everything to work at its own destined time.*

Let me take a moment to appreciate my friends-my team of best three that I share with ***Megha*** *and* ***Dr. Tina. Megha****-my roommate, my batchmate, my labmate is an amazing person who made me learn to roar for myself, who has been there throughout my journey of five years watching my highs and lows. Although at times, it seemed difficult but our Tom & Jerry fights anyhow made both of us reach through our destinations. Thanks megha for being there whenever I needed you.* ***Tina****-my partner in crime, has been a true darling with whom I share uncontrollable hilarious moments even on small and silly matters. She has been a bundle of "energy therapy" who mentored me in times of need with all her love and care as an elder sister. She has been a person whom I loved unconditionally and would go to any extent to see her face smiling and eyes shining.*

*Cheers to us-****"Imtech 3-idiots"*** *who laughed together, who cried together, who complained together; keeping the most important factor of "being together". Our instant mood tea, Tina ki coffee, short films, never-ending walks, unnecessary outings, street-food, cooking were always great stress busters as crazy bunches that made my PhD time smooth and eventful.*

Apart from lab members, I share great moments with many other seniors and juniors of the institute. I extend my heartfelt gratitude to ***Dr. Shiv Pratap Yadav*** *for his constructive criticism and righteous scoldings that organized and aligned me gearing towards the completion of this memorable research voyage. His perpetual scientific inputs along with the mantra of being self-motivated and developing a habit of self-encouragement in every phase have been selflessly boundless. I would also pay my warm appreciation to* ***Dr. Sachin*** *who have always been like an elder brother to me for his support whenever I needed. I also cherish memorable time with some other seniors* ***Dr. Vaidhvi****-my home trip partner,* ***Dr. Drishti*** *for helping me getting rid of my kidney stones,* ***Dr. Manjula*** *and* ***Dr. Pragya*** *for our conversations over meals,* ***Dr. Sarabjeet*** *and* ***Dr. Vandana*** *for guiding me regarding protein expression discussions,* ***Dr. Rakesh*** *for his gyan ki batein,* ***Dr. Amardeep*** *for his help in trouble-shooting when I used to work at night. I also embrace my other juniors and friends-****Kulvinder*** *for his endless tea sessions,* ***Lakhwinder*** *and* ***Shashi sir*** *for the homely food, care, love and affection****, Sahil*** *for always irritating me and making me smile by responding to his silly jokes****, Amber*** *for always asking "Mam party kab dere ho",* ***Nisha*** *for our mini happiness tea parties****, Kunika****-the cricket girl****, Khushboo****-mam kurkure dena muje****, Anita****-kahin ghumne chale****, Nishtha, Manpreet*** *and* ***Irfan*** *for their joyful and light-hearted conversations.*

I would always cling to my not so big but entertaining recollections of Throwball, Cricket, Marathon, Tug-of-war, Table-tennis and Saraswati Visarjan from our busy research schedule. All the motherly love and support from ***Paramjeet mam,***

Sharanjeet mam, Veerkanta mam *and* ***Sudesh mam*** *will be sweet reminisces that I will always adore. I also want to mention my recognition to our hostel warden* ***Dr. Deepak Sharma*** *for always being there to resolve our issues and* ***mess workers*** *for providing homely meals,* ***gardeners*** *for making Imtech bloom & blossom and guards, especially* ***Parvinder Uncle*** *as "my Chai wale uncle". I do hereby thank all my SB16 group-* ***Dr. Nancy, Dr. Amandeep, Arunima*** *for our coordination to solve DST related issues,* ***Harsh, Gaurav Kumar, Gunjan, Sangeeta*** *for momentous bhangra practice sessions,* ***Nishant, Manish*** *for melodious memories during singing sessions,* ***Rajesh-*** *"the kaala chashma" performance buddy ,* ***Rahul*** *and* ***Gaurav Chaubey*** *for joyful times during BLI experiments,* ***Manisha*** *and* ***Pooja*** *for late-night chit-chats,* ***Lucky*** *and* ***Neha mam*** *for giggles over tea,* ***Pradeep sir*** *and* ***Kailash sir*** *for solving my PTM issues. And all other batchmates-* ***Dr. Anuradhika, Shukla, Hilal, Jagrity, Khadim, Dr. Naushad, Happy, Padma, Sapna, Sumeeta, Sumit, Ramiz*** *and* ***Raghvendra*** *for all the amusing conversations of sharing PhD ki batein.*

At the end, I extend my imperatively paramount gratitude to my ***parents*** *for their persistent motivation and unconditional love whenever I needed emotional care. It was solely their blessings and faith in me that made me through my accomplishments. My brother* ***Anmol*** *has always been a friend with whose encouragement and support I reached this milestone and my sister-in-law* ***Sakshi*** *whose motherly tenderness always relieved me of my afflictions. I want to thank you all for always understanding the things I said and the ones I didn't. Their consistent statement-'Believe in yourself' you've almost made through' always sustained my confidence to rise again and endeavor. I would also mention* ***Zoe****-my furball at home whose wait and energetic welcome at home relieved all my stress. At long last, I would like to self-appreciate* ***myself*** *for my perseverance echoing within my soul that no matter what you can and you will do it.*

I owe it all to the supreme eternal, for empowering wisdom and health…

To fight the storm that stayed internal, with all the bestowed strength…

Saloni…

ABSTRACT

Cardiac biomarker Troponin I (TnI) is the inhibitory subunit of Troponin complex which binds to actin in thin myofilaments. It holds the actin-tropomyosin complex in place for calcium mediated regulation of cardiac muscle contraction. TnI have acquired significant diagnostic value since last two decades for its recognition as gold standard biomarker for Acute Myocardial Infarction (AMI). An elevated concentration of TnI in serum is associated with the occurrence of myocardial injury eventually leading to heart attack. Although, remarkable progress has been made in the diagnostics of cardiovascular diseases, nevertheless, the current medical techniques are unable to predict the rapid and cost-effective strategies. Since few years, the high sensitive TnI detection Abott iSTAT is used in hospitals and advanced healthcare systems but the cost being the major deterrent limits its accessibility to common mass. Other TnI biosensing platforms based on antibodies also pose limitations of non-specificity and high cost due to its production. Therefore, DNA aptamers have been introduced in various therapeutic and diagnostic interventions to develop highly sensitive and cost-effective biosensing platforms. As compared to conventional antibodies based detection methods, aptamers offers stability acting as high affinity bioprobes for specific target recognition. Drawing conclusions from the previous reported studies of aptamer generation; our group has adopted a novel strategy for screening aptamers against TnI. The aptamers have been chemically synthesized by Systematic Evolution of Ligands by Exponential Enrichment (SELEX) methodology against apical regions of the biomarker instead of whole TnI protein. The aforementioned unique technique of selecting apical peptides was followed to render specificity and achieve sensitivity in designing aptamer based TnI biosensing platforms.

The study initiates with heterologous expression of human cardiac TnI protein following ion metal affinity chromatography (IMAC) based purification along with its validation for stability and purity. Additionally, several biochemical and biophysical techniques were employed for studying the interaction and binding ability of synthesized DNA aptamers against C-terminal apical region (Tc18 and Tc35p) and N-terminal apical region (Tn13.2a and Tn24.1) with full length biomarker TnI. Only C-

terminal aptamer-Tc18 was propagated for further studies due to its unique secondary structure folding that enabled better binding with TnI.

After studying the interaction, both the aptamers were incorporated to design biosensing platforms for rapid diagnosis of AMI by detecting TnI levels. Preliminary, aptamer based immunodiagnostic microtiter sandwich assays were performed introducing a novel match-pair of aptamer with synthetic peptide for sensitive detection of TnI. The peptide used as bioreceptor was selected from studies previously reported in literature for effectively targeting TnI, thus eliminating the utility of antibodies. Furthermore, dot-blot based dipstick immunoassay has been demonstrated utilizing surface plasmon resonance of gold nanoparticles conjugated with Tc18 aptamer enabling visual signal readout. Moreover, the dot-blot assay was also expanded as Lateral-flow Immunoassay using Tc18 gold nanoconjugates for on-site rapid detection of TnI.

Additionally, in order to design rapid and cost-effective diagnostics for heart-failure, the novel match-pair of aptamer and peptide was used in developing an aggregator-free gold nanoparticle assay for colorimetric detection of TnI. The assay comprised dual site-directed nanobioprobes of aptamer and peptide conjugated gold nanoparticles that interact with TnI at discrete binding sites causing their aggregation. The detection methodology was validated in human clinical samples for which AMI blood specimens were procured from our clinical partner Dr. Manojkumar Rohit, Cardiology Centre, PGIMER, Chandigarh under collaborative Mission project (PGI/IEC-11/2019-1398).

Furthermore, to achieve ultra-sensitive TnI detection systems, electrochemical sensing platforms were implemented for rapid targeting of TnI. This study was accomplished in collaboration with CSIR-CEERI who developed gold metal coated electrodes and polysilicon Field Effect Transistor device comprising metallic gold coated gate terminal. Both the devices were manufactured using photolithographic microfabrication technology for on-site detection of TnI to diagnose myocardial injury. The functionality of the devices was potentially verified to detect TnI using biofunctionalization of thiolated Tc18 onto gold-surface. Moreover, another study comprising an advanced nanohybrid of graphene-oxide with aptamer conjugated gold

nanoparticles has been developed for increasing the sensitivity of TnI detection. The study discovered novel charge conducting properties attributed by conformational switching of aptamer upon binding TnI.

Comprehensively, the entire study encapsulates synthesis of cardiac biomarker TnI with detailed biochemical and biophysical characterization of Tc18 and Tc35p aptamers generated against C-terminal peptide fragment to interact with full length recombinant protein. These high affinity aptamers have been further demonstrated to target native human heart TnI spiked in complex serum matrix as well. In addition to this, the nanomolar binding strength of these aptamers have been investigated to design various biosensing platforms for early, rapid and cost-effective detection of TnI. Each biosensing platform surpasses the limit of detection from the preceding one. Majorly, the favorable binding competence of Tc18 aptamer for TnI was implemented to fabricate microtiter immunoassays, lateral-flow assays, colorimetric and electrochemical aptasensing platforms for point-of-care diagnostics of Myocardial Infarction.

TABLE OF CONTENTS

LIST OF FIGURES

LIST OF TABLES

LIST OF ABBREVIATIONS

Weights and Measurements

%	:	percent
°C	:	degree Celsius
µA	:	micro Ampere
Å	:	Angstrom
bp,kb	:	base pair, kilo base pair
kDa	:	kilo Dalton
M. wt.	:	molecular weight
mL, L	:	mili-, litre
mV, V	:	milli volts, Volts
nm	:	nanometre
nM, µM, mM, M	:	nano-, micro-, mili-, molar
nmoles, µmoles	:	nano-, micromoles
O.D.	:	optical density
pg, µg, mg, g	:	pico-, micro-, mili-, gram
pH	:	*potentia hydrogenii*
pI	:	isoelectric point
psi	:	pounds per square inch
rpm	:	rounds per minute
RT	:	room temperature
s/sec, min, h	:	seconds, minutes, hours

Symbols

@	:	at
<	:	less than
=	:	equals to
>	:	greater than
±	:	plus or minus
≤	:	less than equal to
≥	:	greater than equal to
°	:	degree
KD	:	Dissociation Constant
ln	:	Natural logarithm
log	:	Logarithm
α	:	Alpha
β	:	Beta

γ	:	Gamma
Δ	:	Delta
ζ	:	Zeta
π	:	Pi
ε	:	Epsilon
λ	:	Lambda
θ	:	Theta
σ	:	Sigma
~	:	approximately

Amino acids

Gln (Q)	:	Glutamine
Glu (E)	:	Glutamate
Gly (G)	:	Glycine
His (H)	:	Histidine
Leu (L)	:	Leucine
Phe (F)	:	Phenylalanine
Pro (P)	:	Proline
Tyr (Y)	:	Tyrosine
Val (V)	:	Valine
Thr (T)	:	Threonine
Ser (S)	:	Serine
Met (M)	:	Methionine
Arg (A)	:	Arginine
Lys (K)	:	Lysine
Asp (D)	:	Aspartate
Asn (N)	:	Aspargine
Ala (A)	:	Alanine
Cys (C)	:	Cysteine
Ile (I)	:	Isoleucine
Trp (W)	:	Tryptophan

Chemicals

Kan	:	Kanamycin
APS	:	Ammonium per sulphate
ATP	:	Adenosine triphosphate
β- ME	:	Beta mercaptoethanol
DTT	:	Dithiothretol
EDTA	:	Ethylene diamine-tetra acetate
$CaCl_2$	:	Calcium chloride

HCl	:	Hydrochloric acid
H2SO4	:	Sulphuric acid
HEPES	:	(4-(-2-hydroxyethyl)-1-piperazineethanesulphonic acid
IPTG	:	Isopropyl-beta-D-1-thiogalactopyranoside
KCl	:	Potassium chloride
KH2PO4	:	Potassium dihydrogen phosphate
LB Broth	:	Luria-Bertani Broth
MgCl2	:	Magnesium chloride
Na2CO3	:	Sodium carbonate
NaCl	:	Sodium chloride
$NaHCO_3$	:	Sodium bicarbonate
Na2HPO4	:	Sodium dihydrogen phosphate
$Ni2^{+}$-NTA	:	Nickel-nitrilotriacetic acid
PBS	:	Phosphate buffered saline
PB	:	Phosphate buffer
PMSF	:	Phenylmethylsuphonyl fluoride
SDS	:	Sodium dodecyl sulphate
TEMED	:	N,N',N'N'-tetramethylethylenediamine
Tris	:	Tris(hydroxymethyl)aminomethane
SiO_2	:	Silicon dioxide
H_2O_2	:	Hydrogen peroxide
$[Fe(CN)_6]^{3-/4-}$	:	Ferrocyanide/Ferricyanide

Techniques

FPLC	:	Fast Protein Liquid Chromatography
UV-Vis Spectroscopy	:	Ultra Violet And Visible Light Spectroscopy
PAGE	:	Poly Acrylamide Gel Electrophoresis
CD	:	Circular Dichroism
BLI	:	Bio-layer Interferometry
ELISA	:	Enzyme Linked Immuno Sorbent Assay
HPLC	:	High Performance Liquid Chromatography
PDB	:	Protein Data Bank
AFM	:	Atomic force microscopy
DLS	:	Dynamic light scattering
CV	:	Cyclic voltammetry
SWV	:	Square wave voltammetry
EIS	:	Electrochemical impedance spectroscopy
LPCVD	:	Low pressure chemical vapor deposition
PECVD	:	Plasma enhanced chemical vapor deposition
IMAC	:	Ion metal affinity chromatography

Introduction

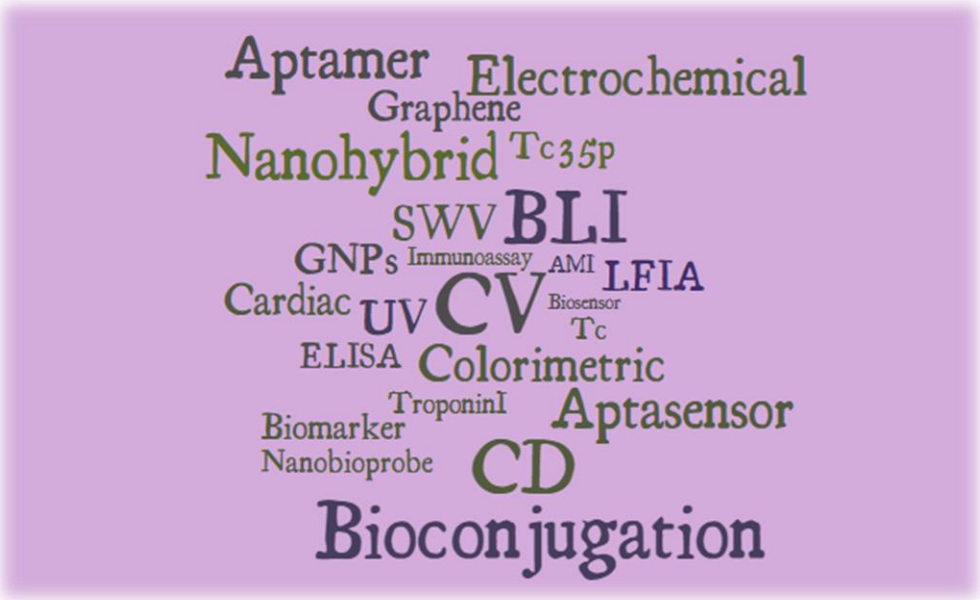

Introduction

Cardiovascular diseases (CVDs) involve heart and blood vessels comprising coronary heart disease, congenital heart disease, heart failure, thrombosis, etc. Amongst various CVDs, Acute Myocardial Infarction (AMI)/heart attack is the sudden cardiac muscle injury causing irreversible myocardial necrosis due to low or no blood supply (ischemia) to heart. AMI being considered as the leading cause of death accounted for 17.9 million (32%) deaths globally reported by World Health Organization (WHO) in 2019 [1][2][3]. The typical diagnosis of CVDs starts with ECG that in severe cases is followed by expensive techniques of computerized tomography (CT) and magnetic resonance imaging (MRI). ECG produces a static picture of cardiac condition with only 50% sensitivity and does not show the underlying severity of condition [4].

In order to develop effective diagnostic strategies, we need to fill the gaps pertaining to high cost, lack of diagnostic precision following unreliable prognosis and delayed identification/diagnosis of patients. Early stratification of risk factors associated with AMI holds utmost importance for reducing costs by screening the hospitalization and streamlining the standard diagnosis for patients. The rapid and early diagnosis of AMI in good time owing to the symptoms is predominantly crucial for patient's survival. Acknowledging the consistent progress in the diagnostics and therapeutics of cardiac diseases, still the current medical techniques are unable to predict the rapid treatment strategies [5]. European Society of Cardiology (ESC) and American College of Cardiology (ACC) guidelines of 2018 have defined CVD diagnosis as per fourth universal definition of AMI for patients meeting any of the three conditions: chest pain, alteration in ECG measurements and elevation of cardiac biomarkers in blood. Therefore, analytical measurements of cardiac biomarkers is a key important factor and is required for assisting and managing AMI diagnosis [6] [7].

The earliest known cardiac biomarkers employed for AMI detection limited their applicability in diagnostics due to lack of specificity to cardiac tissues producing false positive results [8]. Relatively, cardiac biomarker troponin (cTn) became the biomarker of supreme choice for diagnosis of AMI as it has been considered the most sensitive and specific marker of myocardial necrosis [9]. Troponin protein as a

complex of three subunits: Troponin T (cTnT), Troponin C (cTnC) and Troponin I (cTnI) regulate calcium mediated integral component of contractile apparatus leading to contraction and relaxation of heart muscles [8]. Furthermore, among all the three variants, the inhibitory subunit Troponin I (TnI) is considered as the gold standard biomarker for AMI due to its myocardial specificity [10]. After the onset of myocardial injury, TnI level hikes to 50ng/ml in 3-6 hours and saturates to a concentration of about 500ng/ml, finally depleting to its normal concentration within 6-8 days [11–13]. This long diagnostic window with parameters of kinetic release in blood circulation distinguishes TnI from other biomarkers as an ultrasensitive and specific detection biomarker for AMI.

Conventional TnI biosensing techniques of microtiter immunoassays and polymerase chain reaction (PCR) suffer various drawbacks associated with low sensitivity and high cost yet constraining their practical applications. Moreover, huge and complex instruments such as Roche E 2010/602 TnI and Abott TnI testing have been implemented in clinical settings but cost-effective strategy still needs to be addressed concerning the unavailability of AMI diagnosis to poor masses [14]. The limitations pertaining to sophisticated laboratory set ups, high cost and long hours of detection restricts successful commercialization of present diagnostic strategies compromising with patient health. To this context, affordable, portable and low-cost TnI sensing platforms are required for AMI diagnostics. Studies have reported various biosensing platforms for the detection of TnI that use biological antibodies as biorecognition elements. However, disadvantages of batch to batch variation, *in vivo* production and short shelf life restrict their utility to some extent on commercial grounds. In this regard, artificial antibodies known as aptamers have discovered great potential for developing cost-effective, specific and reproducible detection strategies. Aptamers are generated using SELEX method (Systematic Evolution of Ligands by Exponential enrichment) an *in vitro* selection and amplification method for generation of target-specific aptamers [15]. Considering the emerging requirement to address point-of-care-testing (POCT) for AMI, aptamers can result in designing specific detection platforms that can hold a potential for affordable, rapid and early diagnosis of AMI. The parameters of sensitivity and physicochemical stability addressed by aptamer

based biosensing assays have gained extreme interest in detecting biomarker proteins with high affinity. Since long, aptamers have been incorporated for TnI detection in a wide range of biosensing platforms viz. optical [16], electrochemical [17], fluorescence [18], SERS [19], FET sensors (Field Effect Transistors) [20] and microfluidics based lab-on-a-chip assays [21].

A viewpoint needs to be implemented to define and shape the heterogeneous nature of biosensing assays for cardiac biomarkers and narrow down our research to sensitize the present detection limits. This will elucidate the optimum treatment required within a particular time frame to the patient. Despite improvements in both sensitivity and cost effectivity, problems in assay standardization, interferences, imprecision, and pre-analytical variability may affect their clinical use persistence. In order to address all these issues, the current study has been focused towards designing platforms for early, rapid, low cost, accessible and sensitive methods for diagnosing AMI. The overall approach would be to increase the sensitivity of existing methods or to device novel methods using latest developments in the field of nanotechnology and surface immobilization techniques. The work emphasizes upon fabrication of portable and highly sensitive biosensors without compromising the point-of care testing for AMI diagnosis.

To explore more work done and unfold the knowledge gaps pertaining to point-of-care detection of cardiac biomarkers for management of myocardial infarction, the objectives of the study were framed as follows:

Aims and Objectives

1. **Expression and purification of cardiac Troponin I and selection of DNA aptamers binding with biomarker protein.**
2. **Biophysical and biochemical characterization of aptamers interacting with Troponin I.**
3. **Designing of biosensing platforms for sensitive detection of Troponin I along with the validation studies addressing early and rapid point of care diagnostics for Acute Myocardial Infarction.**

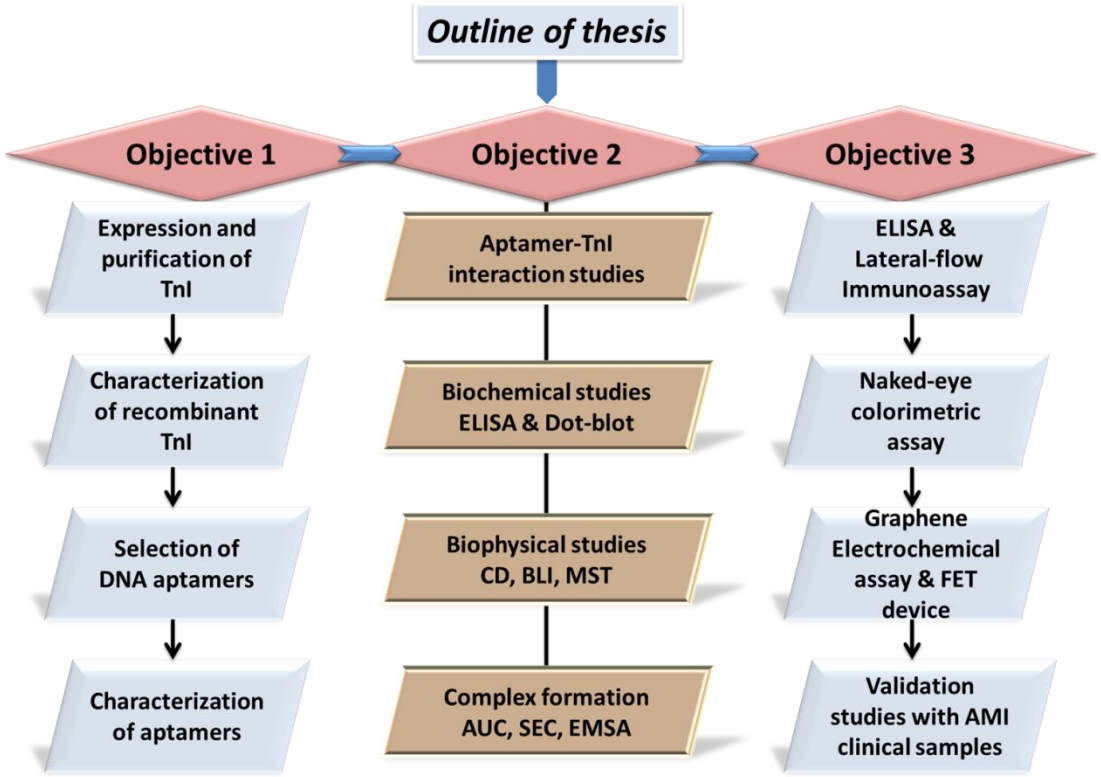

Based on outline of the proposed study and defined objectives, the thesis has been categorized into seven chapters which are summarized as follows. Each division addresses consecutive and oriented series of studies determined towards ***"development of aptamer based biosensing platforms for point-of-care diagnosis of cardiac biomarkers of Acute Myocardial Infarction (AMI)".***

Chapter 1: ***Review of literature***

The chapter consists of present state-of-art for prevalence of global mortality due to cardiovascular diseases owing to the importance of cardiac biomarkers for risk stratification. It highlights the progress achieved for detecting human cardiac Troponin I-the biomarker of choice for Myocardial Injury. Moreover, thorough information about release of Troponin I and its clearance is explained in terms of occurrence of cardiac injury. Along with the current status of advancements established in the area of biosensors, the chapter provides detailed information about various biosensing techniques applied for detection of Troponin I. The major emphasis has been laid towards the advantages of DNA aptamers as efficient high-affinity biorecognition elements over conventional antibodies in AMI diagnostics. A

background study pertaining to the developments proposed in aptamers mediated detection of Troponin I have been discussed.

Chapter 2: ***Heterologous expression & purification of human cardiac Troponin I and selection of DNA aptamers binding biomarker protein***

This chapter describes about overexpression of human cardiac Troponin I in prokaryotic system along with purification of biomarker protein. The integrity and purity of recombinant Troponin I was characterized by various methods such as gel electrophoresis and mass spectrometry. Secondary structure analysis was performed using CD spectroscopy and binding efficiency was confirmed by ELISA. Moreover, homology models of Troponin I protein was made using I-TASSER server due to absence of high resolution crystal structure.

The chapter also comprises of selection of DNA aptamers generated against apical peptide fragments of cardiac Troponin I through SELEX. The aptamers were characterized *in silico* by predicting their secondary structure using Mfold and tertiary structure via RNA composer. Moreover, biophysical techniques such as BLI explained binding strength of aptamers in terms of dissociation constant and CD studies explained the structural folding of aptamers. Other bioreceptors such as polyclonal antibodies and synthetic peptide specific to Troponin I are also introduced in this chapter.

Chapter 3: ***Interaction studies of aptamers binding to cardiac Troponin I***

The studies in this section elucidate the ability of aptamers generated against the peptide fragment of Troponin I for binding full length biomarker protein. A combined approach of biochemical and biophysical characterization was adopted to study the effect of varying concentration of target Troponin I binding with aptamer. BLI studies incorporating binding kinetics provided information pertaining to binding affinity of aptamers. While CD studies were performed to examine structural changes in aptamers post interacting with target Troponin I. Both the techniques have unfolded various aspects of aptamer-target interaction. Moreover, the stability of complex formation of aptamers with Troponin I was studied via gel electrophoresis, EMSA and AUC. Moreover, *in silico* docking of aptamers and

Troponin I by HDOCK accompanied with PBDsum generate analysis predicted the binding residues at interface further elaborating the understanding of interaction. And microtiter assays revealed the efficiency of aptamers to target Troponin I in sandwich ELISA platform.

Chapter 4: ***Immunoassays for detection of cardiac Troponin I***

This chapter discusses about aptamer based immunodiagnostic assays for detecting Troponin I. The proficiency of aptamers to bind Troponin I in a sandwich configuration has been demonstrated with synthetic peptide as novel match-pair bioreceptors. Aptamers are displayed to bind Troponin I as both capture and target bioprobes with high affinity in complex serum matrix as well. Additionally, the capability of aptamers to detect Troponin I have been validated in AMI clinical samples procured from PGIMER, Chandigarh. Another fast and reliable immunoassay known as dot-blot assays comprising aptamer conjugated gold nanoparticles as nanobioprobes to detect Troponin I have been discussed. Moreover, the competency of aptamers to detect Troponin I have been extended in paper based lateral-flow immunoassay as well.

Chapter 5: ***Aggregator-free gold nano-sandwich based colorimetric detection of cardiac Troponin I***

This section of the study focuses upon a colorimetric biosensing platform for Troponin I detection using a unique match-pair combination of bioreceptors. Aptamer and peptide conjugated gold nanoparticles are implemented as site directed nanobioprobes that interacts with Troponin I at distant interface. This binding of both nanoconjugates to Troponin I reduce the inter-particle distance causing aggregation which changes color of the solution. Both the nanoconjugates of aptamer and peptide have been well characterized for their stability. The colorimetric assay produces instant naked-eye visual signal upon detecting Troponin I in serum samples abolishing interference of non-specific targets. Additionally, the colorimetric biosensor has been validated in AMI clinical samples identifying the applicability of high-affinity aptamer for point-of-care detection of Troponin I.

Chapter 6: ***Aptamer based electrochemical biosensing for sensitive detection of cardiac Troponin I***

The current study describes an aptamer mediated electrochemical biosensing platform for rapid sensing of Troponin I. The work was conceived under collaboration with partners at CSIR-CEERI who synthesized gold electrodes/chips and polysilicon FET device for aptasensing of Troponin I. The synthesized devices were characterized for their conductivity, stability and reproducibility proposing point-of-care electrochemical devices for monitoring myocardial infarction. The gold-thiol bonding enabled biofunctionalization of aptamer onto gold surface forming homogenized self-assembled monolayer. The aptamer biofunctionalization was verified by various surface immobilization techniques such as Atomic Force Microscopy, Raman spectroscopy and contact angle measurements. Consequently, aptamer based sensing have been depicted to provide sensitive targeting of Troponin I.

Chapter 7: ***A graphene-gold nanohybrid for electrochemical aptasensing of cardiac Troponin I***

The last chapter comprises nanohybrid of graphene oxide and gold nanoparticles that have been designed for enhanced synergistic electrochemical conductivity contributed by both nanomaterials. Aptamer conjugated gold nanoparticles biointerfacing graphene oxide have been implemented to fabricate nanohybrid based electrochemical aptasensor to improvise the Troponin I detection sensitivity. The designed nanohybrid has been well characterized for its stable chemical conjugation determining morphological and optical features. The developed aptasensor have been proposed in this section to exhibit instant Troponin I detection at ultralow concentrations further validated in human serum samples as well. An enhancement in the electrochemical signal has been explained emphasizing on Troponin I induced conformational rearrangement of aptamer.

Summary and future perspectives

In this chapter, I have summarized all the conclusions and findings obtained from each section of the proposed work. It also compiles and sums up the entire objectives of carrying studies further imparting a deep sense of knowledge connecting the results

achieved. In addition, this final division of the work recollects the conclusions discussing loopholes in current scenario of cardiovascular diseases point-of-care management. Finally, future implications of generated aptamers along with the designed aptasensing platforms have been discussed for their applicability in diagnostics of Acute Myocardial infarction.

Chapter 1

Review of Literature

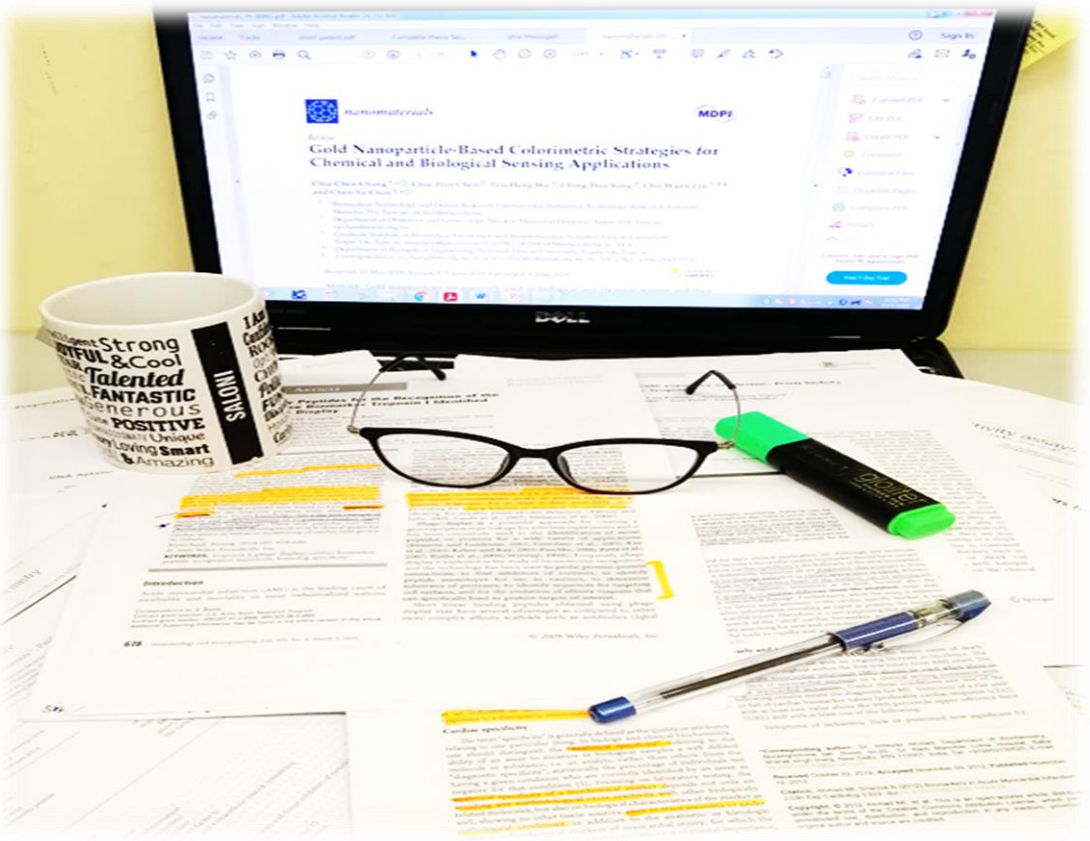

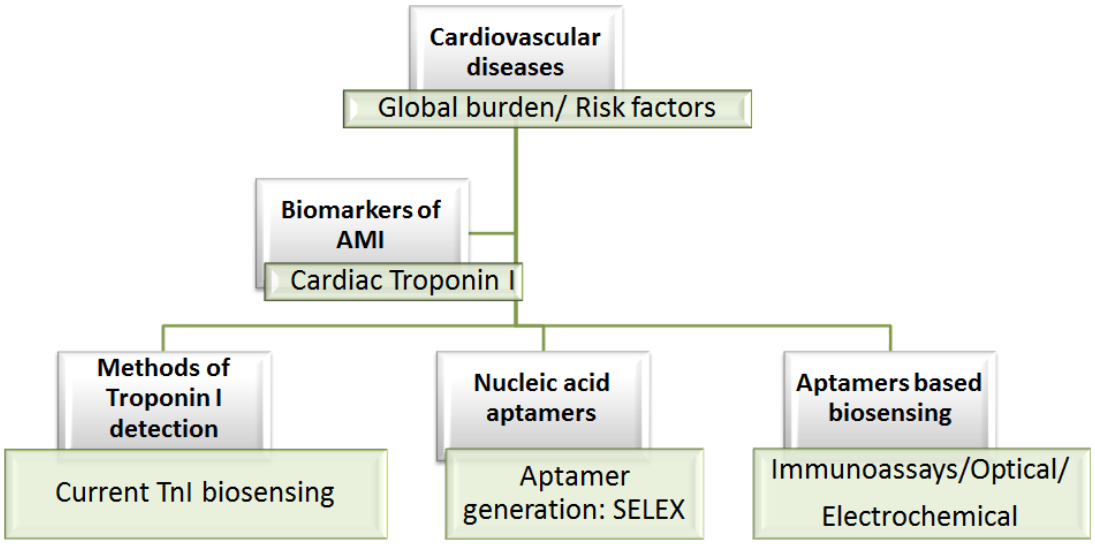

1.1 Global burden of cardiovascular diseases

Cardiovascular diseases (CVDs) have emerged as the leading cause of mortality and morbidity worldwide [22]. World Health Organization (WHO) in 2019 have estimated a death rate of 31% taking lives of 17.9 million people every year. With these rising death rates, according to WHO it is estimated that by 2030, it is supposed to take a toll of 25 million people annually (Fig.1.1)[23].

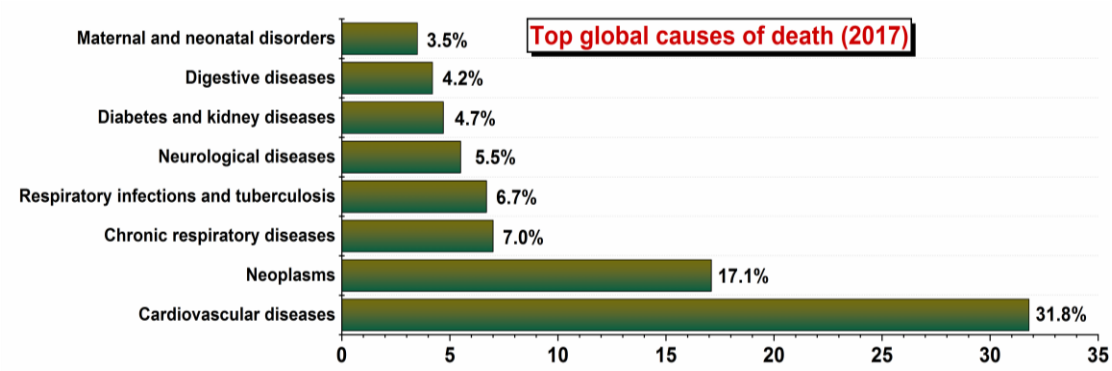

Fig.1.1 Statistical data for global cause of death due to cardiovascular disease [27]

Various heart heath care guidelines by American College of Cardiologists (ACC), European Society of Cardiology (ESC) and American Heart Association (AHA) and have been working for primary prevention of CVDs in terms of associated risk factors [24]. They claim that the potential risk factors of CVDs can be split into two categories: modifiable and non-modifiable. A person's age, ethnicity, family history, socio-economic background contributes to non-modifiable risk factors. While modifiable risk factors that leads to CVD includes diabetes, hypertension, obesity,

elevated cholesterol levels, consistent consumption of tobacco, physical inactivity and most common improper nutritional practices [24][25]. Amongst mentioned risks, hypertension is one of the strongest factors that affect people of all the age groups, especially young adults (generally females) [26].

After being recognized as dominant and chief cause of death worldwide in 2001, 80% of CVD death toll globally is devoted to under-developed and developing countries such as India where burden of risk factors are high due to ongoing epidemiological transition [28]. Clinical reports have suggested a convincing association of CVDs with the ongoing pandemic as COVID-19 patient is prone to cardiovascular manifestations intervened by the route of entry of SARS-Cov-2 into host cells. Increased risk of mortality due to Covid-19 has reported repercussions from pre-existing cardiovascular diseases. Latest studies have also reported a reverse scenario where Covid-19 itself can lead to various cardiovascular ailments such as myocardial injury, acute coronary syndrome and venous thromboembolism [29].

1.2 Acute Myocardial Infarction (AMI)

1.2.1 Pathophysiology of AMI

Being the most severe instances of CVDs, Acute myocardial infarction (AMI) is considered as one of the paramount causes of cardiac deaths globally despite substantial advancements in prognosis over the last decade [30]. The pathogenic mechanism underlying the cascade of thrombotic events starts with the blockage in blood flow of coronary arteries due to the potential risk factors that causes damage of myocardial tissue forming a plaque in arteries (Fig.1.2) [31]. The initiation of AMI marks the rupture or erosion of coronary plaque which results in exposure of circulating blood to a series of thrombotic core proteins causing platelet activation [32]. This atherosclerotic plaque interrupts the blood supply and oxygen to the myocardium that results in formation of an infarct as displayed by coronary arteries in [33]. Myocardial necrosis due to infarction ultimately leads to heart failure and inflammatory processes. Common symptoms underlying AMI is angina that originates from center of the heart or left side and travels through shoulder and back [34]. AMI is associated with chest pain/discomfort, vomiting, sweating, weakness,

arrhythmias and nausea and sometimes loss of consciousness. The immediate disturbance of coronary blood flow along with aforementioned symptoms defines it a life-threatening medical emergency that demands sudden risk management and treatment [35].

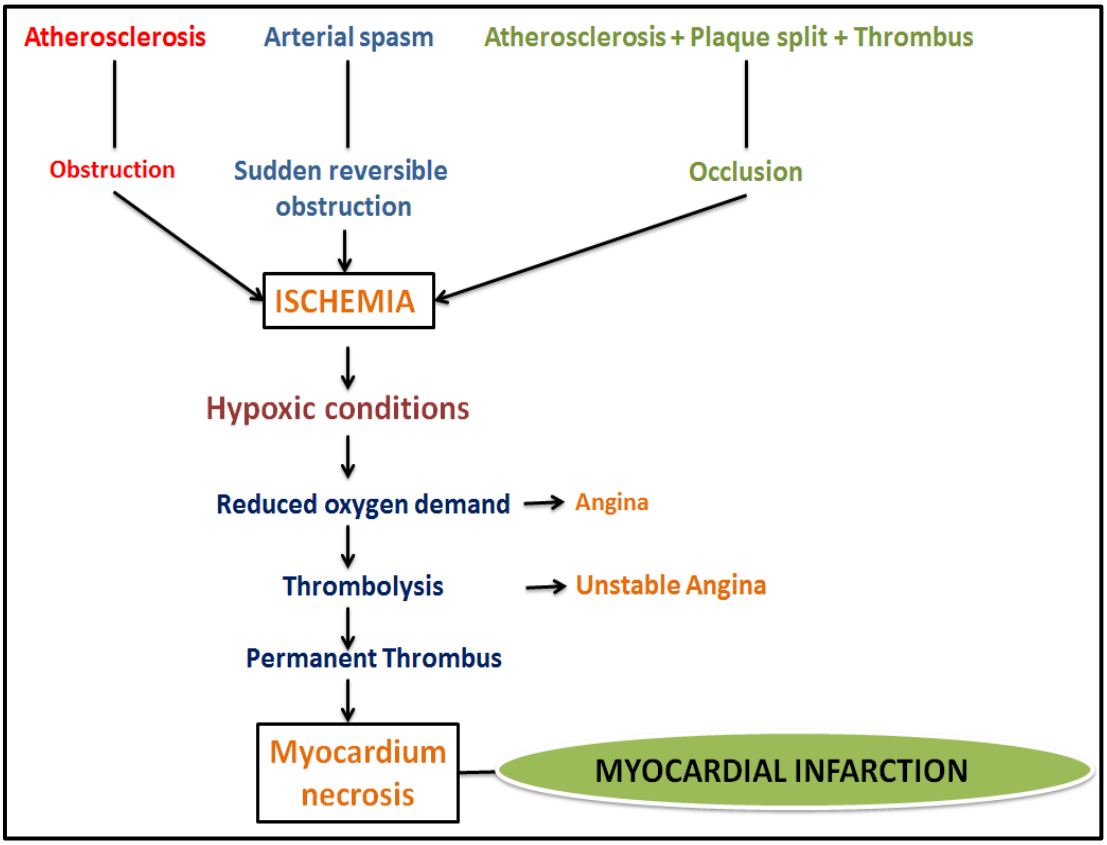

Fig.1.2 Pathophysiology of events underlining the occurrence of Acute Myocardial Infarction

1.2.2 Cardiac biomarkers of AMI

As defined by ACC and ESC-"A biomarker is a component/parameter that is measured and quantified as a characteristic indicator of a biological process of therapeutic intervention" [36]. Cardiac biomarkers are reliable diagnostic solutions for management of CVDs as they can differentiate any changes in the pathogenic processes corresponding to heart disease or any other disease relatively correctly and rapidly [31]. They hold great importance enabling timely and accurate diagnosis and prognosis of acute coronary syndrome such as MI.

In 1954, aspartate transaminase (AST) was reported by Karmen et al as first cardiac biomarker used in clinical practice [37]. Then lactate dehydrogenase (LDH) (1955) and creatine kinase (CK) (1960) were introduced as biomarkers for MI. But neither of

respective biomarkers were specific to cardiac tissues thereby compromising the applicability in AMI therapy [38]. Thereafter, Myoglobin-globular oxygen carrying protein was prioritized for differential diagnosis of myocardial necrosis [39]. Although being a sensitive indicator of cardiac damage, Myoglobin lacks myocardial specificity and gets excreted from circulation within 24 hours [40].

The ideal cardiac biomarker for AMI should (a) possess cardiac specificity as pivotal significance, (b) rapidly release in sufficient detectable amount providing severity of condition, (c) detectable in blood circulation for long duration, (d) not be found in non-cardiac tissues [33][40]. Generally, apart from AST, LDH, CK/CK-MB and Myoglobin, myocardial necrosis appearance is marked by several other cardiac biomarkers such as Troponin. Ischemic cardiac biomarkers comprises Heart-type Fatty Acid-Binding Protein (H-FABP). While biomarkers of hemodynamic stress are natriuretic peptides- N-terminal brain natriuretic peptide (NT-Pro-BNP), Brain natriuretic peptide (BNP) and inflammatory and prognostic markers such as Interleukin-6 (IL-6), C-reactive protein (CRP) and Tumor necrosis factor-α (TNF-α) are reported. Another novel biomarkers include Choline, growth differentiation factor-15 (GDF-15) and Copeptin have been explored [36,40]. In this regard, Ahmad et al in 2012 discussed about the biomarkers implicated in each consecutive pathogenesis of AMI. Additionally, Table 1.1 enlists the comparative analysis of all the characteristic features of cardiac biomarkers.

Biomarker	First assay (year)	First detection (hours)	Maximum value (hours)	Return to normal value (days)	Sensitivity to myocytes	Specificity to myocytes
AST	1954	3-4	15-28	5	++	+
LDH	1955	5-10	60-144	12	++	+
CK	1960	3-9	10-20	3	++	+
CK-MB	1972	3-8	10-20	3	++	++
Myoglobin	1978	1-3	4-7	1-1.5	+++	+
TnI	1987	3-7	10-20	10	++++	++++
TnT	1989	3-8	15-120	14	++++	++++

Table 1.1 Comparative analyses of cardiac biomarkers with their characteristic features [41]

1.3 Human cardiac biomarker Troponin I

1.3.1 Gold standard biomarker of choice

With the discovery of Troponin in 1965 followed by development of a radioimmunoassay in 1990s, cardiac troponin became the biomarker of choice for diagnosis of myocardial infarction[42][43][44]. Originally, Troponin was identified, purified and characterized by Professor Setsuro Ebashi in 1960 to establish molecular basis of muscle contraction regulated by Ca^{2+}[45]. Cardiac Troponin forms the integral component of muscle contractile apparatus on thin filaments of cardiac and skeletal muscle fibers. Troponin proteins forms a complex of three subunits: Troponin T (cTnT) which interacts with tropomyosin, Troponin C (cTnC) which binds Ca^{2+} and Troponin I (cTnI) which inhibits the ATPase activity of actomyosin complex. In presence of Ca^{2+}, a complex alteration in Troponin facilitates ATP-dependent interaction of myosin with actin leading to muscle contraction dislocating Troponin I. While in relaxed state, Troponin I binds with myosin and prevents its interaction with actin, holding the actin-tropomyosin complex in place [38]. TnC is not specific to MI as it is identically present in skeletal and cardiac muscle, whereas TnI and TnT differentiate their sequence identity in skeletal and cardiac muscle making them specific biomarkers for myocardial necrosis [46]. Furthermore, among all the three subunits, Troponin I (TnI) is considered as the gold standard biomarker for AMI due to its specific production site at the myocardium, prolonged diagnostic window and high specificity to cardiac diseases [47].

1.3.2 Structure-Function relationship of Troponin I

The three isoforms of TnI are expressed in humans: fast and slow skeletal isoforms along with a special cardiac predominant isoform which is exclusively confined to myocardial tissues [48][49]. Human TnI isoform consists of 209 amino acid residues, with a molecular weight estimating 24 kDa as first amino acid methionine is removed during synthesis. TnI comprises four α-helices with intercalating flexible disordered regions with its five domains: cardiac specific N-terminal domain (residues 1-33) with two phosphorylation sites, IT-arm (residues 40-136) having two α–helices binding to α–helices of C-terminal domain of TnT and the C-lobe of TnC, inhibitory domain (residues 137-146) interacting with actin-Tm and C-lobe of TnC, regulatory

domain/switch-peptide region (residues 147-163) that recognize hydrophobic patch of NcTnC and C-terminal mobile domain (residues 164-210) having a second actin-Tm binding site [50,51][49,52]. The important study proposed by Takeda et al in 2003 was partial crystal structure for core domain of Troponin complex in Ca^{2+} saturated form (RCSB-PDB ID:4Y99). It revealed 46 kDa L-shaped conformation comprising all five domains connected via flexible linkers[53].

TnI contains extra 32 to 33 extra amino acids at its N-terminus distinguished from the skeletal TnI comprising two adjacent serine residues at 22 and 23/23 and 24 positions. This N-terminal domain is exclusively found in cardiac isoform of TnI having an important role in interaction of TnI with TnC regulating contraction and relaxation of heart muscles. Posttranslational modification of phosphorylation via Protein Kinase-A at Ser-23/Ser-24 disrupts the respective interaction of TnC-TnI dislocating TnI to cause relaxation of heart muscles. This respective PTM decreases the affinity of Ca^{2+} for TnC altering interaction between two isoforms to cause contraction of cardiac muscles [48][54]. This Ca^{2+} switch of TnI can be explained as actomyosin complex formation which is sterically inhibited by TnI at low cytosolic Ca^{2+} due to phosphorylation at N-terminal serine residues. C-terminal of TnI binds to actin and lock tropomyosin inducing muscle relaxation. On the contrary, at high Ca^{2+} levels, single ion binds to regulatory N-terminal TnC provoking an intra-molecular conformational shift for interaction of TnC and TnI. This binding in turn pulls TnI away from actin permitting cross-bridge cycling by exposing all myosin binding sites free on actin inducing muscle contraction [52].

1.3.3 Troponin I release in blood

The contractile protein of TnI gets released in the blood stream post 3-9 hours of infarction having a half-life of 2 hours in blood [38]. After the onset of myocardial injury, TnI levels hike upto 50ng/ml in a time frame of 3-6 hours and finally saturates to a level of about 500ng/ml that remains detectable for few days, finally depleting to its normal concentration [46].

TnI increases in 4 to 6 hours, peaks at 12 hours returning to its basal levels in 3-10 days (Fig.1.3) [36][33]. This long diagnostic window distinguishes TnI from other biomarkers as an ultrasensitive and rapid diagnostic biomarker for AMI [43][55]. TnI is expressed only in cardiac muscle and after infarction, remains detectable for 4-7

days and gets cleared from the circulation primarily by the reticuloendothelial system fragmenting into molecules that are cleared via kidney route [56].

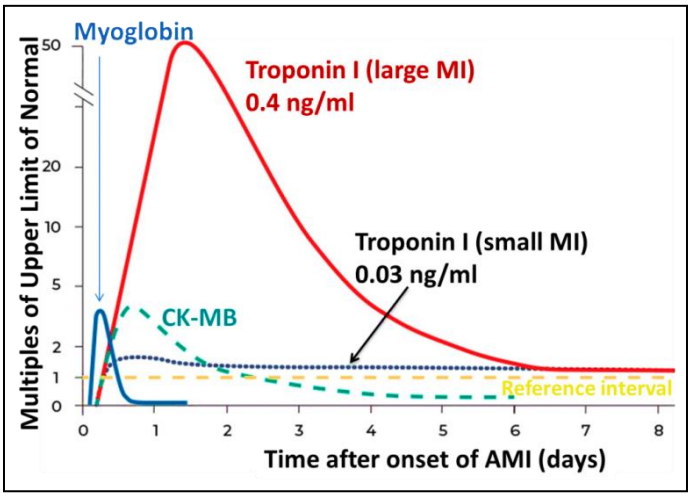

Fig.1.3 Release timing and persistence of various biomarkers after AMI [57]

After myocardial infarction, TnI is supposed to release in blood from the cytoplasm accompanied with an irreversible sustained release for days due to myofibrils degradation. The studies have even reported that myocardial strain during pressure overload, mechanical stress, membrane permealization (through stretch-responsive integrins) and shedding of "blebs" from membrane along with proteolysis of TnI from Troponin complex induced by ischemia has been hypothesized to excrete biomarker from cardiomyocytes [58]. Researchers also report that pathways such as death receptor apoptosis, mitochondrial apoptosis, death receptor necrosis and mitochondrial necrosis have roles in myocardial death causing release of TnI into circulation [59]. Moreover, studies have revealed TnI release from apoptotic myocytes as an alternative reasoning for TnI elevations without clinical signs of ischemic conditions. Additionally, absence of myocardial ischemia is also governed by rise in Left Ventricular Dysfunction After Transient Pressure Overload (LVEDP) leading to TnI apoptosis, release and reversible stretch-induced stunning [60,61]. Unrelated to ischemia, TnI subunit release through bleb formation, oxygen supply imbalance, apoptosis, acute cardiac stress releasing catecholamines and integrins, inflammation and myocardial stretching. Moreover release of Troponin peptides have also been studies in detail by Wu and his co-workers in 2017 [62]. Cardiomyocyte necrosis being the most obvious reason of TnI release into circulation is also evident via Ca^{2+} leakage into cardiomyocyte cytoplasm leading to contraction of sarcomere

thus causing necrosis. Recent reports have studied TnI washouts through renal clearance after membrane damage due to necrosis or cell wounds that causes sustained release of TnI for days. Prolonged release of TnI after ischemic events due to slow exit from local myocardial injury or delayed necroptosis nullifies the clearance of TnI after every 24 hours [63].

1.3.4 Clearance of Troponin I from circulation

After the formation of clot in coronary blood vessel following AMI occurrence, muscle tissues undergoes severe ischemia accompanied by necrotization of ischemic muscle. This necrotization is associated with release of proteases from lysosomes and proteolytic cleavage of various intracellular proteins. This discloses that TnI is highly susceptible to proteolysis and its degradation rapidly cleaves N- and C-terminal regions whereas the central region (30-110 amino acids) is substantially stable. The comparative higher stability of central region is related to the complex formation of TnI with TnC. As a result, after 20-40 hours of AMI onset, the biomarker protein TnI is not found intact in bloodstream rather occurs as heterogeneous mixture of proteolytic fractions and as complex with TnC. Adding more to what has been mentioned, this proteolytic degradation not only occur in necrotic cardiomyocytes but also in blood circulation or collected serum samples. Besides, the complex biophysical and pathophysiological background related to posttranslational modifications of TnI (Phosphorylation, Glycation, Acetylation, etc.), it also undergoes intra-myocardial proteolysis of N-terminal by caspase and calpain [64–66].

1.4 Current biosensing techniques and challenges

1.4.1 Limitations of state-of-art TnI biosensing

Over the years, various biosensing strategies have been employed to detect cardiac biomarkers relevant to avert the risk of AMI reducing cost of healthcare management. AMI diagnosis is generally based upon specification of atleast two of three criteria: chest pain, ECG (Electrocardiogram) elevation of ST segment and elevation in cardiac biomarker TnI. Since the ECG monitoring reflects less accuracy in demonstrating the severity of condition due to poor diagnostic analysis as it presents normal signals even for CVD patients in emergency department. In fact 50-60% patients experiencing chest pain display normal ECG readouts making early diagnosis difficult [5]. Additionally, hospital settings these days comprises of complex

instrumentation such as TnI Roche E 2010/602 and Abott TnI for testing. But these techniques are associated with huge cost that needs to be addressed concerning the unavailability of AMI diagnosis to poor masses [14]. Taking all the aspects into consideration, designing of ultra-sensitive assays and development of biosensors for evaluating TnI levels in serum was adopted along with feasibility for POCT integration.

1.4.2 Introduction to biosensors

Ever since the discovery of first biosensor by Leland Clark (Father of Biosensor) in 1962, biological sensors have unfolded various applications in therapeutics and diagnostics of biomedical sciences. Generally, a biosensor is a small device that is designed to detect and quantify biochemical target molecules applicative as impressive analytical objects in medical diagnostics and other research areas. It consists of three parts: biorecognition elements that recognize the biomarkers, a signal transducer depending upon biosensing strategy and a reader for recording response outcome (Fig1.4).

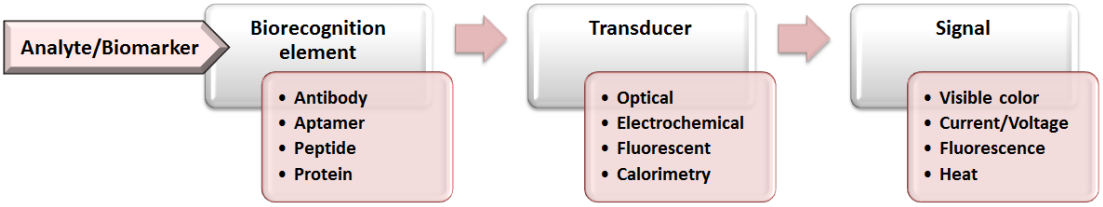

Fig.1.4 Schematic showing general working process of biosensors

It monitors the levels of different biomolecules such as proteins, nucleic acids or other biomolecular interaction. In principle, it is typically fabricated by immobilizing a bioreceptor moiety such as nucleic acids/proteins or antibodies on the transducer surface that modifies biochemical signal into quantifiable electronic readout. Here, cardiac biomarkers detection biosensing devices play a pivotal role to help improve diagnostic accuracy of AMI without any risk factors involved in the treatment [5]. Furthermore, biomarkers also aid in prognostic information about AMI that helps the clinicians towards desirable treatment protocols.

1.4.3 Biosensors for TnI detection

There is a huge range of biosensors developed for detecting biomarkers of CVD, most prominently TnI (Fig.1.5). Therefore, use of novel biosensors for targeting cardiac

TnI for rapid monitoring for AMI patients has been proved as a crucial diagnostic solution. Prior to fabrication of TnI detection devices, it becomes important to have an idea about the clinical cut-off levels of TnI in serum that are indicative of AMI occurrence [67]. TnI concentration of 0.03 ng/ml or 30 pg/ml has been implemented in clinical diagnostics to be dependent on its 99th percentile reference with coefficient of variation at limit of detection (LOD). The respective 99th percentile upper reference limit was employed to avoid mislead thresholds from higher for high-risk patients further reducing the false positive analysis rate to less than 1%. This threshold concentration of TnI is taken as the critical benchmark to differentiate between AMI and healthy individual as 99th percentile decision level for MI diagnosis [68] [69,70].

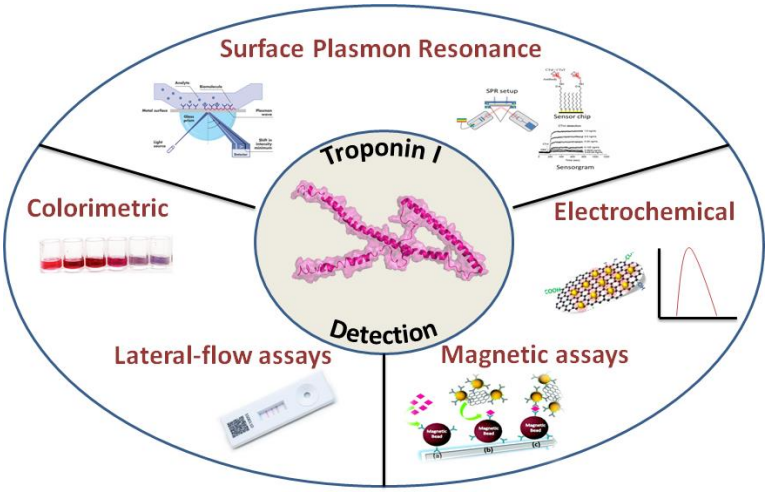

Fig.1.5 Biosensing methods for TnI detection [31]

For designing TnI detection biosensors, WHO guidelines of ASSURED (Affordable, Sensitive, Specific, User-friendly, Rapid and robust, Equipment-free and Deliverable to end-users) criteria should be used as reference for devising biomedical diagnostic assays for resource-limiting areas [71]. Currently, ACC and ESC guidelines for TnI biosensing relies upon the new 5th generation hs-TnI assays that can detect concentrations 10-100 fold lower than the conventional assays.

Moreover, hs-TnI assays has been very beneficial in non–ST-elevation myocardial infarction (NSTEMI) patients allowing single blood-test diagnosis permitting rapid treatment [36]. Various certified and clinically approved biosensor devices commercially used in hospitals are enlisted in Table 1.2 that has been designed in past years enabling hs-TnI detection. These assays empower in detecting TnI levels in

healthy individuals as an important decision making potential in emergency hospital departments.

Commercially available Troponin assays	99th percentile cut-off (ng/mL)	Time	Cost (USD)
i-STAT (Abott point-of-care, USA)	0.08	10 min	420
ACS:180 (Bayer, Germany)	0.07	24 h	1200
Dimension Vista (Siemens, Germany)	0.05	10 min	28,000
Architect (Abott, USA)	0.04	10 min	19,000

Table 1.2 Commercially available hs-TnI detection technologies [68]

Over the years, different biosensing techniques have emerged for detecting trace levels of TnI to develop varied types of biological sensors for rapid and point-of care diagnosis of AMI. Although, the conventional strategies being labor intensive require prolonged measurements time. Therefore, sensitive biosensing approaches such as electrochemical sensors (EC) [72], field-effect transistor based biosensors (FET) [20], ELISA (Enzyme linked immune sorbent assay) [73], surface plasmon resonance (SPR) based optical biosensors [74], fluorescence based biosensors [75] have taken up TnI detection for AMI surveillance. To which EC, SPR and FET based sensors have received phenomenal attention for POCT management [67]. Moreover, these techniques can be integrated with nanostructures or nanocomposites for sensitively enhanced operative devices. All these biosensor platforms enable highly sensitive detection of TnI aiding in rule in/rule out of AMI further combating the challenges encountered for serum measurements. Apart from what has been said, immobilization strategies onto biosensor devices, fluorescent/chemiluminiscent labeling, nanomaterials coatings or self-assembly monolayers (SAM) for biorecognition elements as-bioreceptors favor enhancement in signal readouts with improved sensor efficiency [76,77].

1.5 Nucleic acid DNA aptamers

1.5.1 Aptamers as potential biorecognition elements

The performance of any diagnostic assay/biosensing platform based upon sensitivity and specificity relies upon significance of biorecognition elements known as bioreceptors. These biological recognition elements bind or recognize specific

bioanalytes further transforming the signal measurement into a user-friendly readout. Majorly, bioreceptors such as enzymes, proteins, antibodies, nucleic acids and in some cases whole cells play a pivotal role in affecting the efficiency of target detection [78]. Since last 40 years from the production of first Mab in 1975 by Georges Kohler and Cesar Milstein, monoclonal antibodies (Mab) have been an integral part in diagnostics and therapeutics of biomedical research along with advancements in the improvisation of their binding potential. Although, in order to optimize the pharmacokinetics and binding affinity of antibodies towards their target, consistent intriguing research have been implemented, nevertheless their inherent limitations have impeded their progress in diagnostics [79]. After the magnitude of authentic research by scientific communities, the concluding rational acknowledged the antibodies not to be potent molecular probes. Various drawbacks pertaining to reproducibility issues, lengthy protocols of production employing animal models, high cost of antibody production, variation in binding efficacy due to batch-to-batch, undergoes salt or temperature induced denaturation, limited storage duration restricting their applicability in biomedical diagnostics. Moreover, their structural complexity, cross-reactivity, difficulty in synthesis against non-immunogenic targets, compromised sensitivity induced by steric hindrance due to large size and low target specificity ultimately has affected their reliability for development of biosensing platforms [79] [80].

Whereas, nucleic-acid based artificial antibodies as potent biorecognition elements have gained intense scientific interest in the form of next-generation attractive bioprobes for biosensing. Ideally, emerging requirements of real-time detection with on-field applicability for biosensors have gradually been emphasized beyond the traditional needs of sensitivity and selectivity for detection of bioanalytes. To this context, since last three decades the conventional antibodies based biosensing platforms have been replaced successfully by chemical antibodies as therapeutic "missile". Due to the shortcomings of antibodies, nucleic-acid aptamers have been integrated in a variety of biosensing applications as "*Aptasensors*" that possess the capability to recognize a broad range of targets [79][81].

Aptamers are termed as "chemical antibodies" due to their three-dimensional folding ability to bind a specific target with utmost sensitivity, distinguishing from conventional protein based antibodies. By their attractive nature, aptamers are chemically designed

sequence defined biomoieties that represent a cost-effective, consistent and modifiable substitutes for antibodies [82]. Their unique properties consider them as chemical rivals of antibodies because of their adaptable advantages. Aptamers offer their inherent attributes of their cell-free ease of chemical synthesis, cost-effective bulk-production without any batch-to-batch variation with controlled modifications and less immunogenicity fulfills the aspect of "perfect molecular probe".

Specific target detection property of aptamers, their molecular stability even at various temperature/salt based physiological conditions compliments their higher shelf life as compared to antibodies. There is no harm to animals for synthesizing aptamers with very less costs involved in their production along with their supreme flexibility that enables multiple sites for interacting with their target molecules. The small size of aptamers allows their access to even pre-blocked or intracellular remote targets along with ease of modifications using fluorophore/linkers/other chemical groups [83][79][82]. All these features of aptamers define their tremendous potential to be used as specific and sensitive biorecognition elements in therapeutic and diagnostic technologies. Alongside, diverse modifications in synthesis process of aptamers enables their applicability for targeted delivery systems, stable conjugations with cells, aptamer-drug bioconjugate. The supreme flexibility and infiltrate analyte positioning as compact biomolecules differentiates the aptamers in clinical diagnostics for targeting biomarkers [84].

1.5.2 SELEX

Aptamers are referred as single-stranded DNA/RNA that have capability to bind to their targets with high affinity and specificity diversifying from small organic compounds to large proteins and even live cells. The discovery of aptamers dates back to 1990s by an *in vitro* evolution procedure–SELEX (Systematic Evolution of Ligands by Exponential Enrischment) synthesized by two groups of researchers, Tuerk and Gold [15] and Ellington and Szostak [85]. The aptamer synthesis undergoes an iterative process- incubation of random oligonucleotide library sequence with target to screen high-affinity sequences. Next it consists of separation of bound aptamer sequences from unbound ones that are amplified by Polymerase Chain Reaction (PCR) (Fig.1.6). This process is repeated 10-15 times until an enriched pool of DNA aptamers is obtained which is further cloned and sequenced. A diversified

variation of SELEX methodologies has been studied including genomic SELEX, photo-SELEX, monoLEX, *in vivo*-SELEX, *in silico*-SELEX, whole cell-SELEX, etc. Moreover, Spiegelmers- L-ribonucleic acid aptamer is a RNA-like molecule having L-ribose units forming mirror-images of natural oligonucleotides [86]. SOMAmers (Slow off-rate modified aptamers) were introduced enhancing nuclease stability, specificity and affinity containing modified nucleic acid bases. Apart from this, other modifications incorporated phosphodiester linkage modification, truncations and end-capping for generation of high-affinity DNA aptamers [87]. Other non-SELEX methods consists of non-equilibrium capillary electrophoresis of equilibrium mixture (NECEEM) that comprise incubation of random oligonucleotide library with target followed by separation of bound fragments without the need of amplification [88]. Another non-SELEX technique includes HAPIscreen-high-throughput method [83].

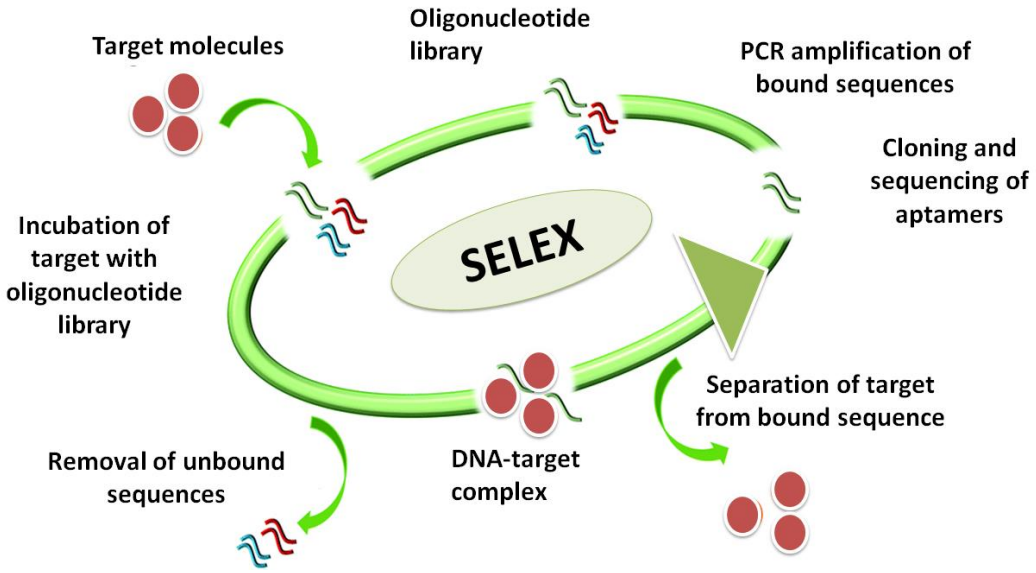

Fig.1.6 Schematic of steps followed in SELEX procedure

The aptamers generated by SELEX procedure have been a crucial part of designing various point-of-care biosensing platforms for instance immunoassays such as ELISA, Dot-blot assays, Lateral-flow immunoassays, Electrochemiluminescence (ECL), Fluorescent based assays, Electrochemical assays, Colorimetric/optical assays of nanoparticles to detect biomarkers relevant to biomedical diagnostics. The flexible conformational properties of aptamers conferring to target-binding induced structural rearrangement, competitive replacement due to small size, target induced displacement encourages their diverse applications in sensing of diagnostic biomarkers [89][90].

1.6 Aptamer based immunodiagnostic assays

1.6.1 ELISA

Immunoassays/Immunodiagnostic assays are biochemical methods for quantitative estimation of presence or concentration of bioanalytes using biological receptor moieties. Introduction of immunoassay dates back to 1975 for the development of monoclonal antibody by Kohler and Milstein. Since then immunoassays were implemented in a wide variety of scientific disciplines, specifically clinical diagnostics [91]. And the limitations offered by antibodies based ELISAs were compensated by introduction of aptamer based immunoassays. They have attracted extensive attention offering improvised sensitivity and specificity. Taking aptamers as molecular recognition reagent (MRE), they were adapted as potential candidates for replacement of antibodies in ELISA. Aptamer based immunoassays were referred to as ELASA (enzyme linked apta-sorbent assay), ELAA (enzyme-linked aptamer assay), ELONA (enzyme-linked oligonucleotide assay), ALISA (aptamer-linked immobilized sorbent assay). Different variants of aptamer being used in ELISA format is shown in Fig.1.7.

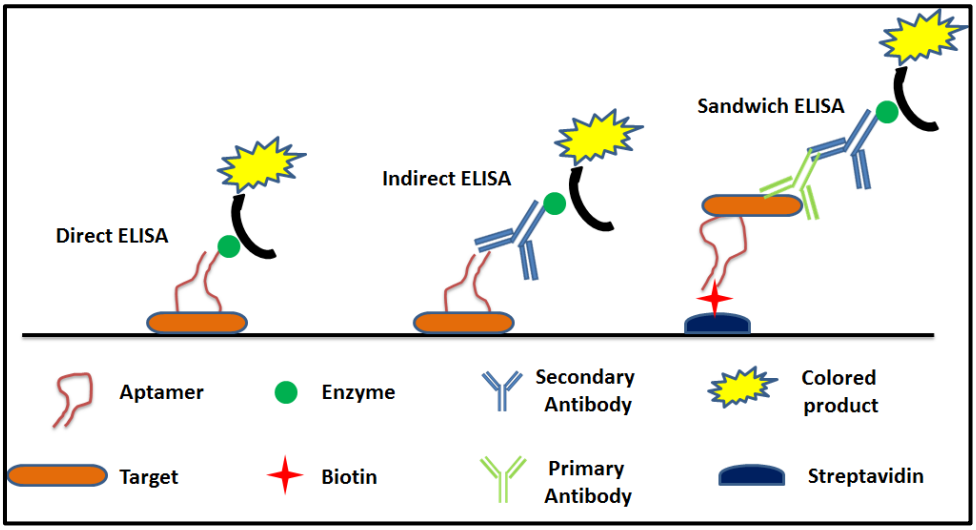

Fig.1.7 Schematic representation of aptamer-ELASA protocol [68]

Various reports have shown aptamers to be widely used as capturing agents because of their ability to specifically bind with their target. To this context, immobilization of aptamers on the solid support is achieved by covalent linkage with two methods- (a) direct attachment using linkers/proteins as bio-coated sensing surface, (b) conjugation

onto functionally active surface. To achieve this, aptamer should be modified with chemical moieties such as amine, thiol or biotin and in some cases modification with oligonucleotide linkers enables flexibility between aptamer and solid surface. All these specifications regarding aptamer immobilization offers great target capturing due to oriented adherence of aptamer onto the surface [92][93,94]. Most aptamers based TnI detection ELISA comprises a common linkage of avidin-biotin interaction wherein streptavidin coated surface is used to capture biotinylated aptamers for immobilization. Recently, Gopinathan et al displayed an integrated microfluidics platform for TnI detection upto 12 ng/L [21].

1.6.2 Dot-blot immunoassay

Another important classification of immunoassays is fast and simple dot-blots due to their advantage of requiring very less samples. Dot-blot immunoassays refers to deposition of analyte as small volume dots onto membrane for quantification of interaction between biomolecules (Fig.1.8) [95]. Aptamer based dot-blot assays have scrutinized in diagnostics as simple, fast, visual detection immunoassays as potent antibodies surrogates [96].

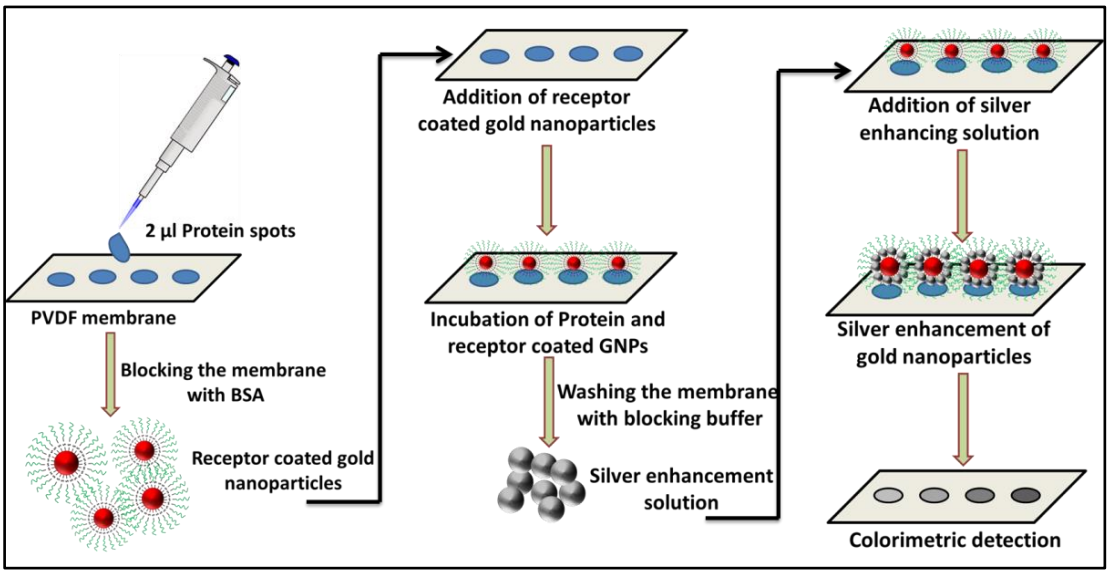

Fig.1.8 Schematic representation of dot-blot assay

With the use of gold nanoparticles as signal indicators, these dot-blot assays circumvent the incorporations of expensive enzymes/chemical substrates distinguishing from the basic ELISAs. They utilize the resonance light scattering of metal nanoparticles enhancing the sensitivity for detecting biomolecular interactions.

Dorraj and his co-workers in 2015 demonstrated an aptamer based dot-blot immunoassay to detect 5 ng/ml of TnI [16]. They used aptamer conjugated gold nanoparticles for detecting TnI and used silver enhancing solution for amplification of spot signals. In principle, gold particles reduce silver ions to metallic silver by acting as catalyst in presence of hydroquinone as reducing agent. This reduced silver deposits onto gold surface further enlarging the particles that enhances the visible signal [97]. Moreover thrombin biomarker and β-amyloid peptide for Alzheimer's disease was also detected via dot-blot assay integrated with aptamer as biorecognition elements [98,99].

1.7 Aptamer based colorimetric assays

Although, florescent dyes and enzymes such as HRP have been incorporated to amplify the visual signal, but the discovery of nanotechnology to use metallic nanoparticles have made through novel biosensing strategies [100]. In recent years, gold (Au) and silver (Ag) nanoparticles due to their diverse applications of being well-dispersed and having SPR (surface plasmon resonance) possess the ability to cause transition in color of solution/test-strip/paper/membrane due to change in inter-particle distance. Their spectroscopic change is a quantitative measure for aggregation or dispersion that corresponds to amount of target present. Specifically, gold nanoclusters have profound applicability in biological sensors owing to their exceptional optical and chemical properties. The feature of strong linkage with a wide range of biomolecular probes using thiol-gold covalent interaction allows diverse functional nanoconjugation. All these attributes have significantly focused on development of new-generation of nanoparticles based sensing strategies empowering specificity, enhanced sensitivity and stability [101][102]. Moreover, advantages of single-stranded DNA adsorption onto gold particles for specific biosensing have been dated back to conventional salt induced aggregation proposed by Chad A. Mirkin in 1996 (Fig.1.9). The combination comprising optical properties of gold nanoparticles and aptamers as molecular recognition elements since then were implemented in numerous bioanalytes detection of biomedical importance [103].

Various reports have been investigated for colorimetric detection of TnI incorporating aptamers and even peptides as replacement of antibodies. A previous study by Scott Banta in 2009 have shown peptide as biorecognition elements selected via phage display technique binding specifically to TnI [104]. Wang et al in 2011 demonstrated

PDMS gold nanoparticle sensing platform based on aptamer for TnI detection [105]. Moreover, an ultra-sensitive plasmon-exciton hybrid of gold particles-quantum dot based aptamer nanobiosensor have been designed for 0.4 fM detection of TnI [106]. Recently, a study reports change in color signal from purple to red based on self-assembled heparin stabilized gold-nanorods using enzyme-free colorimetric sensor for detecting cardiac TnI upto 0.5 ng/ml [107].

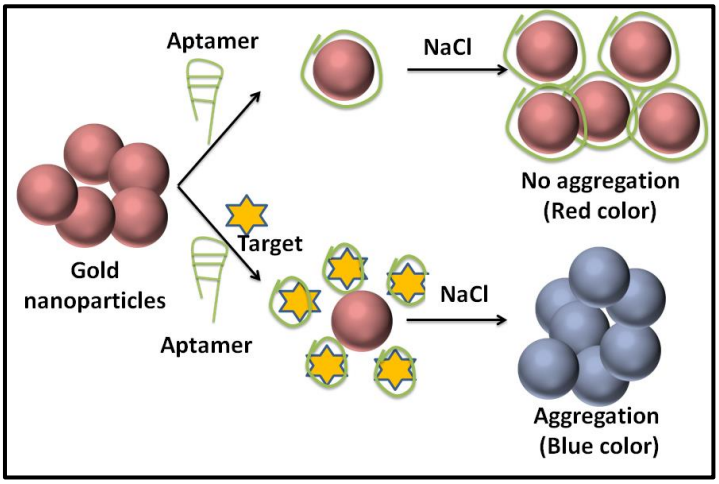

Fig.1.9 Schematic of salt based gold nanoparticle aggregation based assay [108]

1.8 Aptamer based electrochemical assays

Electrochemical biosensors rely on affinity based reactions undergoing due to interaction of immobilized biorecognition element and target molecules. The signal generation depends upon monitoring the change at transducer surface in terms of transition in current/voltage electrochemical signals. This change is subjected to charge based electron transfer as a resultant of target binding to bioreceptors such as antibodies, aptamers, peptide/proteins, thus converting chemical information to user-friendly measurable signal. There are a wide range of electrochemical sensors designed for sensitive detection of TnI detection based upon aptamers as specific bioprobes. The categorical classification of electrochemical biosensors is divided into amperometric, impedimetric, potentiometric, voltammetric and conductance based sensors based upon their operational mode (Fig.1.10) [5][31]. An electrochemical sensor is robust, requires low-power, provides ease of miniaturization and is cost-effective providing real time detection of analyte. The technique holds great promise for applications in detection of biological molecules relevant to biomedical diagnostics as point-of-care due to their sensitivity and reliability for target detection.

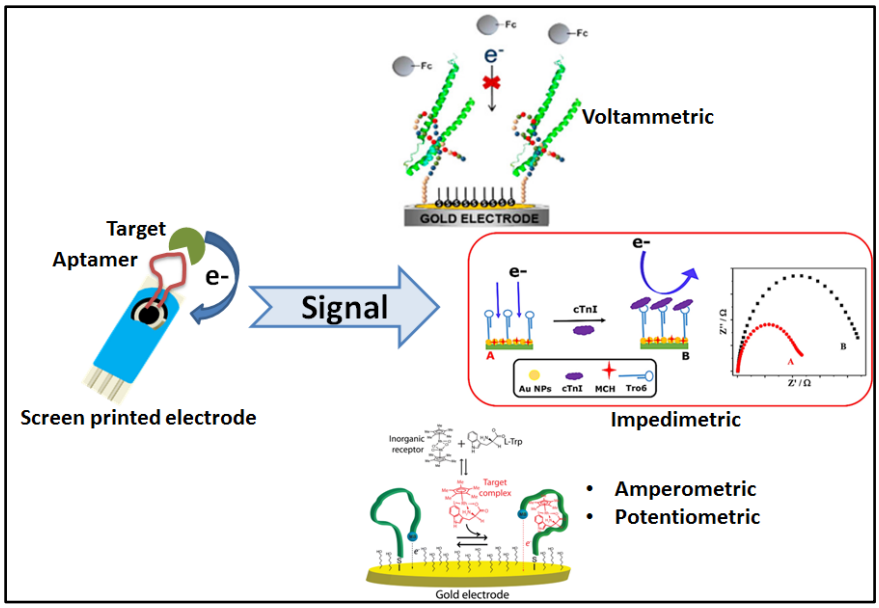

Fig.1.10 Schematic representation of different types of electrochemical biosensor [109][110][111]

Recently, profound attention has been centered on integration of nanomaterials such as gold nanoparticles and other advanced nanocomposites such as graphene, MoS_2, carbon nanotubes (CNT), etc. to increase sensitivity in electrochemical biosensing. Besides that, nanomaterials improve the electrochemical intensity due to their catalytic and electrical conductivity imparted by large surface area. Alongside nanomaterials impart reactivity, bioprobes conjugation, roughness enhancing electron transfer capacity [112]. Graphene oxide-an advanced nanomaterial possessing high mechanical strength and electrical conductivity has been implemented for sensitive detection of TnI lowering down the detection limit [113][114]. The nanohybrid of graphene-oxide and gold nanoparticles have also been applied for TnI detection using antibodies in sandwich configuration [115]. Lopa et al in 2019 developed AuNP integrated titanium metal substrate conjugated with DNA aptamer for TnI detection to address AMI in patients [116]. Changill Ban in 2015 designed an electrochemical aptasensor based on voltammetric measurements of TnI using silica nanoparticles modified with ferrocene with 24 pg/ml of detection limit [117]. Another novel aptasensor based on aptamer-MoS_2 nanoconjugates was designed for TnI sensing upto 1pM using impedance spectroscopic method [118].

Moreover, after the invention of FET systems by Bergveld in 1970, the evolutions of respective transducer in a wide range of biosensor applications have been witnessed. FET comprises of semiconductor sensing path, connecting source (S) and drain (D)

electrodes, to capture targets. Modulation of bias potential to third electrode (gate) is done where channel conductance is varied by detection of targets. This is further measured and processed by electrical system [119]. Silicon nanowire Field effect transistor (Si-FET) based real-time detection of TnI has also been demonstrated displaying aptamer-TnI interaction by various groups for biomedical diagnostics of AMI [20,120].

Chapter 2

Heterologous expression & purification of human Cardiac Troponin I and selection of DNA aptamers binding biomarker protein

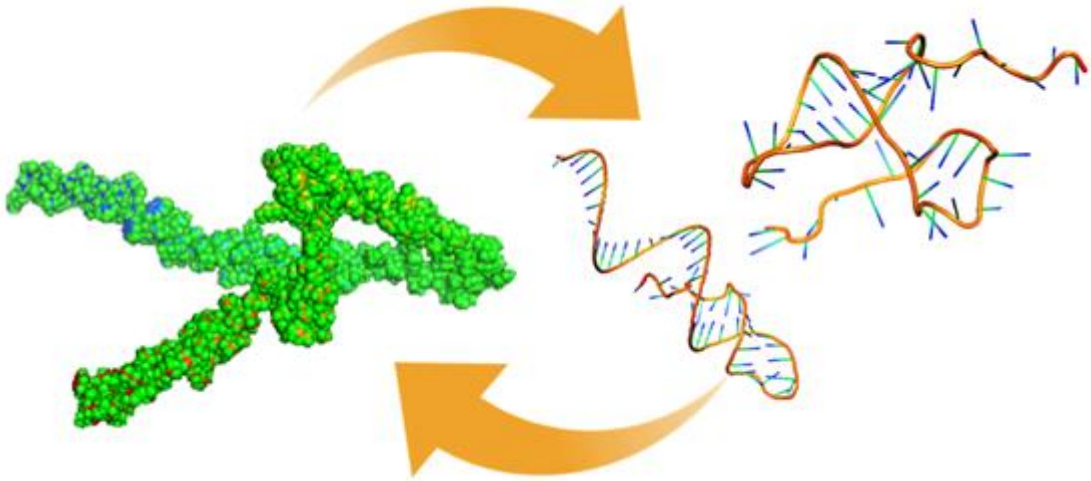

2.1 Overview

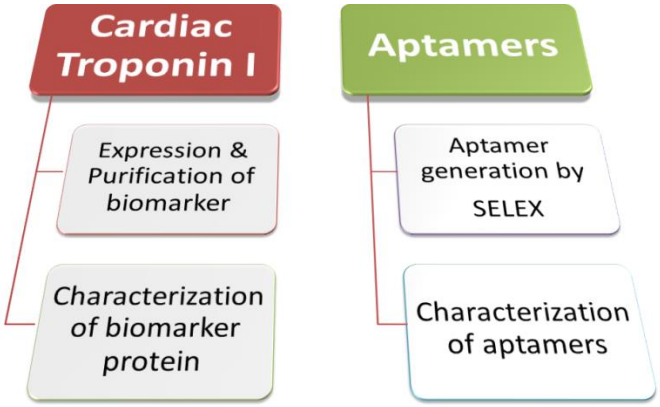

Human cardiac Troponin I is an important subunit of cardiac Troponin complex that coordinates calcium mediated interaction of actin-myosin regulating the contraction and relaxation of myocardial muscles [7]. TnI is presented as single isoform consisting of 209 amino acid residues, with molecular weight estimating ~ 24 kDa [121]. The requirement of TnI expression and purification became essential due to high costs associated with the naturally isolated TnI. However, the techniques utilized for TnI isolation from cardiac tissues were labor intensive yielding very less amount of pure protein. Therefore, recombinant DNA technology was incorporated for production of this crucial biomarker protein. Many studies have reported expression and purification of human TnI following mammalian expression system using complex expression plasmids**.** Heterologous systems such as *Escherichia coli* and yeast system of *Pichia pastoris* has been used by various groups for high yield stable expression of the protein along with different expression vectors. The other expression system was adding huge costs and produced unstable TnI offering posttranslational modifications of TnI [122]**.** Due to its unstable behavior owing to degradation by certain proteases, the protein was co-expressed with its other members of Troponin complex i.e. TnC and TnT [123]. Additionally, Ban and co-workers have reported comparatively facile and stable expression of TnI that has been followed in this work along with modifications at various stages of purification [110].

Cardiac TnI holds paramount therapeutic value in cardiac failure diagnostics which demands rapid detection strategies employing point-of-care management. High affinity biorecognition elements such as single-stranded DNA aptamers are highly selective for target binding without offering any batch-to-batch variation in their production unlike antibodies. Low-cost production, structural stability and ease of

chemical modification aligns with significant advances in aptamers based sensing platforms offering potential applications in the field of biomedical diagnostics [124]. Many groups have reported aptamers against full length TnI protein but their limitations pertaining to low binding affinity and lower detection limit or sensitivity in assay have restricted their utility. Dorraj and his group reported aptamer TnIApt 23 exhibiting its applicability in dot-blot assay [16]. Moreover, aptamers *Tro4* and *Tro6* were reported by Ban *et al* for electrochemical detection of TnI [110]. In both the cases, the aptamers lacked sensitivity in TnI detection assays. To this context, the major issue was to generated DNA aptamers exhibiting high affinity for TnI along with effective performance in TnI biosensing assays.

Consequently, this chapter describes about overexpression and purification of recombinant cardiac biomarker TnI along with some modifications for optimizing a high yield protein. Alongside, the characterization studies of aptamers against specific apical peptides of TnI have been discussed. The aptamers have been further investigated to bind full length TnI protein. Altogether, this approach of target selection for generating aptamers against TnI has been adopted for the first time.

2.2 Experimental approaches

2.2.1 Materials and instrumentation

The gene construct containing the full length protein sequence for human cardiac TnI was obtained from Genscript, HongKong. Primers sequences for T7 promoter and terminator sequence was from IDT technologies. Plasmid isolation kit was of Thermo Scientific. Fast digest restriction enzymes from New England Biolabs (NEB). Kanamycin monosulfate antibiotic, IPTG (Isopropyl β-D-1-thiogalactopyranoside), PMSF (Phenylmethylsulfonyl fluoride), Luria Bertani broth, Coomassie Brilliant blue dye G-250 for media preparation was from Sigma Aldrich /Merck. All the chemicals used were of analytical or molecular biology grade. Cardiac TnI protein from human heart tissues was procured from sigma for control experiments. HOOK™ Peptide Coupling Kit (Sulfhydryl Reactive) from G-Biosciences was purchased for coupling proteins. Trypsin in-gel digestion kit was used from Sigma. Lateral-flow TnI test cards were obtained from Recombinogen and Oscar. Anti-TnI monoclonal antibody was taken from Cloud-clone Corporation. PVDF membrane from Millipore, California, USA.

Gel electrophoresis assembly was of BioRad. GE healthcare nanodrop was used for measuring concentrations of DNA and protein. MALDI (Matrix assisted laser desorption ionization) Mass Spectrometry TOF/TOF 5800 was used for mass analysis from AB Sciex. GE healthcare Amersham semi-dry transfer was used for western blotting. Jasco J-815 CD instrument was used for CD spectroscopy. UV-spectroscopy measurements were taken using BioTek Synergy H1 spectrophotometer (UK). Octet K2 system (Pall Life sciences, Fremont, CA 94538) was used for performing binding kinetics studies. PCR thermal cycler was of BioRad. Western blotting transfer electroblotter was from Amersham. Syngene Gbox GG6 (Maddison, USA).gel doc instrument was used for acquiring images.

2.2.2 Bacterial strains, Media and Competent cells preparation

- **Cloning host:** *E. coli* strain DH5α
- **Expression host:** *E. coli* strain BL21 (DE3)
- **Media:** Luria Bertani (LB) broth was used to prepare media for bacterial cell culture in deionized water. The media was sterilized at 121˚C by autoclaving for 15 minutes at 15 lb/inch2 (psi) pressures.
- **Competent cells preparation:** Primarily, 5 ml of LB media was inoculated with 100 µl of frozen glycerol stock of BL 21 and DH5α. The cells were grown overnight at 37˚C for 12-16 hours under constant shaking at 220 rpm. A secondary culture of 50 ml LB was inoculated in a conical flask and cells were allowed to grow until OD_{600} reaches 0.4-0.6 at 37 ˚C. The bacterial cells were kept in ice-cold conditions and 40 ml of cells were centrifuged at 4000 rpm for 10 min. The cell pellet was resuspended gently in 1-2 ml following 20 ml of 0.1 M $MgCl_2$ (Ice cold). After then centrifuging bacterial cells at 4000 rpm for 10 min, supernatant was discarded. Finally, the bacterial cells were resuspended in ice-cold 0.1 M $CaCl_2$ and aliquots of 200 µl each were prepared. The cells were left undisturbed at 0˚C for 2 hours followed by long-term storage at -80˚C.

2.2.3 Transformation of bacterial cells

For transforming bacterial cells, 2 µl of recombinant plasmid was added to 200 µl of *E. coli* competent cells which were incubated in ice for 30 minutes and subjected to heat shock at 42˚C for 1 min in hot water bath. This was followed by an immediate

ice shock for 5 min to which 800 µl of pre-warmed sterile LB media was added. Incubation of the transformed cells at 37˚C for 1 hour was done under shaking at 220 rpm. The cells were gently spread onto the plate which was incubated at 37˚C for 12-16 hours till the bacterial colonies were grown.

2.2.4 Plasmid isolation and clone confirmation

The confirmation and validation of procured gene construct for harbouring the correct sequence of cardiac biomarker TnI was accomplished by performing restriction double digestion and sequencing PCR experimentation. To this context, DNA plasmid was isolated from transformed colonies of *E. coli* DH5α strain producing high copy number of recombinant plasmid pET28a(+).

Briefly, a single colony from transformed DH5α *E. coli* cells was inoculated in 10 ml LB broth and the culture was incubated at 37˚C for 12-16 hours under 220 rpm shaking. 5 ml of cultured cells were harvested by centrifugation at 5000 rpm for 8 min in a microcentrifuge tube. After discarding supernatant, the cell pellet was subjected to plasmid isolation performed using Thermo Scientific GeneJET Plasmid Miniprep Kit.

a. Restriction double digestion: Recombinant plasmid pET-28a (+) harbouring TnI gene was used as template for performing double digestion with two restriction enzymes BamHI and XhoI accommodating TnI gene sequence. Briefly, 50 µl of reaction mixture comprising the following composition was used:

- Plasmid DNA (90 µg/ml): 12 µl
- BamHI (NEB, 20 U/ µl): 2 µl
- XhoI (NEB, 20 U/ µl): 2 µl
- 10x Digestion buffer: 5 µl
- Nuclease free water: 29 µl

The reaction mixture was incubated at 37˚C for 1.5 hour. The digested DNA along with pET-28a (+) vector control and undigested plasmid was run on 0.8% agarose gel electrophoresis containing 0.5 µg/ml of EtBr. 1 kb DNA ladder was run for size demarcation. The bands were resolved under 80 Volts for 1.5 hour using 1x TAE buffer and DNA was visualized under Gel Doc for capturing image.

b. Sequencing PCR: A PCR reaction was set for amplifying TnI gene fragment using forward primer that hybridize with T7 promoter region lying upstream of template and reverse primer hybridizing with T7 terminator region lying downstream of template DNA. A reaction milieu of 10 µl each with composition as follows was set for forward and reverse primer mix:

Forward primer PCR mix	Reverse primer PCR mix
Template: 1 µl	Template: 1 µl
Sequencing buffer: 1.5 µl	Sequencing buffer: 1.5 µl
T7 promoter primer: 1 µl	T7 terminator primer: 1 µl
TRR mix: 1 µl	TRR mix: 1 µl
Nuclease free water: 5.5 µl	Nuclease free water: 5.5 µl

PCR amplification was performed by using BioRad thermal cycler which involved initial denaturation of plasmid at 96˚C for 1 min followed by 24-25 cycles of each of denaturation at 96˚C for 10 sec, annealing at 50˚C for 15 sec, extension at 60˚C for 4 min respectively. An eventual infinite hold was set at 4˚C.

2.2.5 Overexpression and Purification of human cardiac TnI

Full length TnI gene construct cloned in expression vector pET-28a(+) at multiple cloning site between restriction enzymes BamHI and XhoI along with 6x His tag at C-terminal region was designed. The designed gene construct in Fig.2.1 was procured from Genscript, HongKong with proper codon optimization for heterologous bacterial expression. The recombinant plasmid was overexpressed by primarily transforming the bacterial expression host strain BL21 (DE3). An isolated single bacterial colony from transformed plate was inoculated in 10 ml LB broth supplemented with 50 µg/ml kanamycin at 37°C under shaking at 220 rpm for 10-12 hours as primary culture. The secondary culture (1000 ml LB) was inoculated using 1% of primary culture along with 50 µg/ml kanamycin and incubated at 37°C under shaking till OD_{600} reaches 0.6. The culture was kept at 4°C for 2 hours followed by an induction in expression with 0.2 mM IPTG. Post induction, bacterial culture was incubated at 18°C for 16 hours under 200 rpm shaking. After incubation at low temperature,

harvesting of cells by centrifugation at 5500 rpm was done for 20 minutes in cold conditions and washed with 10 mM PBS pH 7.5. The cell pellets were stored at -20°C for short term and -80°C for long term preservation followed by running 12% SDS PAGE for confirmation of expression.

Fig.2.1 Gene construct of cardiac TnI protein

The harvested cells were subjected to lysis by suspending them in resuspension buffer containing 8 M urea along with protease inhibitor tablets and 1 mM PMSF under rotation at 4°C. The cells were further fragmented by sonication for 15 minutes at 25% amplitude under ice cold conditions. The ruptured cell debris was separated from clear supernatant by hard centrifugation at 12000 rpm for 50 min at 4°C. The supernatant containing the protein was purified by immobilized metal affinity chromatography (IMAC) mechanism of Ni-NTA to bind imidazole ring in 6-His tag amino acid residues of protein. The column was washed and equilibrated with resuspension buffer comprising 8M urea followed by loading of supernatant for binding of protein under rotation for 1 hour at 4°C. Urea refolding protocol was used to extract a high purity yield avoiding degradation of protein. After binding of protein to Ni-beads flow through was collected and column was washed with subsequent decreasing concentration of urea containing buffers (6 mM to 0 mM Urea). TnI bound to column was separated using elution buffer containing an immensely high concentration of imidazole. The eluted protein fractions were run on 12% SDS PAGE. The fractions with pure bands were dialyzed to remove imidazole with decreasing salt concentration of buffers and stored at -20°C for at most 10 days during which all the experiments from the respective batch of protein were performed.

The concentration of purified TnI was estimated by measuring UV absorbance value at 280 nm using nanodrop. The theoretical molar absorption coefficient ε was taken from ExPASY tool. All the physiochemical properties of human cardiac TnI such as molecular weight, isoelectric point (pI), number of amino-acid and molar extinction coefficient were calculated by submitting the respective full-length amino acid sequence to ProtParam tool of ExPASY server (http://web.expasy.org/protparam/).

2.2.6 SDS PAGE and MALDI-TOF

The expression pattern of recombinant TnI was analytically investigated by running 12% discontinuous SDS PAGE (Sodium Dodecyl Sulphate Polyacrylamide Gel Electrophoresis**)**. SDS-PAGE technique separates proteins based on their mass under the electric field. The proteins for separation migrate towards cathode as SDS being an anionic detergent denatures the proteins imparting negative charge. Briefly, 20 µl of cell lysates of cultures were mixed with 5 µl of laemmli buffer containing SDS and β-mercaptoethanol as reducing agent. The prepared samples were heated in a boiling water bath for 5-10 minutes and loaded into wells of stacking gel of 1mm thickness for separation along with a pre-stained protein marker. The electrophoretic separation was performed at 80 volts until protein bands reached resolving gel soaked in 1x TGS buffer after which gel was run at a constant voltage of 100 volts. Similarly, the eluted fractions of purified protein were also investigated under SDS-PAGE analysis. After completion of electrophoretic run, the gel was immersed in Coomassie blue staining solution for visualizing protein bands followed by destaining solution. MALDI-TOF (Matrix assisted laser desorption/ionization-Time of flight) or mass spectrometry was performed to characterize mass of purified TnI protein. The eluted protein fraction was concentrated in an Amicon concentrator tube (Millipore) to remove excess of salt and was subjected to intact mass analysis. Furthermore, MALDI-TOF MS/MS analysis was performed comprising of cleavage of protein to peptide fragments and measurement of m/z ratio of peptide ions determined with respect of time required for flight. The protein band was excised from gel followed by washing and destaining and subjected to trypsin digestion using Sigma trypsin in-gel digestion kit. Peptide mass-fingerprinting generated the absolute mass of individual peptide constituting to theoretical mass of the protein. This is conceived by database searching in Mascot that interprets mass spectral data into protein identities. Mascot provides comparison of the observed spectra to a database of known proteins and matches the most likely hits.

2.2.7 Lateral flow test card and Western blot analysis

Recombinant TnI was verified for its binding ability/functionality by testing it on commercial lateral-flow test card from Oscar and Recombinogen that consisted lining of anti-TnI monoclonal antibodies (Mab). Briefly, 50 µl purified TnI of varying

concentrations was added to sample pad and analyzed for formation of line in test area indicating presence of protein.

The homogeneity of purified recombinant TnI was confirmed through western blotting. The protein sample was resolved using 12% SDS-PAGE in a vertical electrophoretic system at 100 volts. The gel was fixed by incubating in transfer buffer (25 mM Tris, 192 mM Glycine, 20% methanol) for 10 minutes and transferred onto PVDF membrane using a semi-dry electroblotter at 30 volt for 3-4 hours. After washing with transfer buffer for 10 minutes, the membrane was blocked using 5% skim milk in 1x PBS (pH 7.5) at 4˚C for overnight to prevent non-specific absorption. After repeated washing with 1x PBST (0.1% Tween 20) three times, membrane was probed with anti-TnI Mab in 1:5000 µl dilution in block buffer. The membrane was incubated for 2 hours at room temperature following repeated washing as described before. Further, HRP conjugated anti-mouse antibody (1:3000 µl dilution in block buffer) was added and incubated for 1 hour in dark conditions under medium shaking. The membrane was washed again and blot was developed using Luminata Forte Western HRP substrate and image was taken using gel-doc.

2.2.8 Circular Dichroism spectroscopy

In principle, the difference in absorption pattern of left-handed circularly polarised light (L-CPL) and right-handed circularly polarized light (R-CPL) occurring with a molecule containing one/more chiral chromophores is referred as CD. CD was performed for secondary structure analysis of recombinant TnI. The spectrum was recorded in near-UV CD range of 190-260 nm λ under N_2 atmosphere equipped with quartz cuvette of 1.0 mm path length at scanning speed of 50 nm/min. 5 µM TnI diluted in 10 mM phosphate buffer (pH 7.5) to which the measurement scan was baseline corrected. To further substantiate the precision of measurement, commercial heart tissue isolated TnI was also scanned. A number of 3 CD scans were recorded for each sample measurement which was averaged for final signal.

2.2.9 Microtiter binding assay

The binding efficiency of TnI was evaluated by indirect ELISA using commercial anti-TnI Mab. Briefly, 2.5 µg/ml TnI was coated onto polystyrene plate using 100

mM bicarbonate buffer (pH 11) and incubated overnight at 4˚C. The plate was washed with 1x PBST (0.1% Tween 20) three times following blocking with 1% casein solution. Primary Ab anti-TnI Mab generated in mouse was added in a concentration gradient starting from 1:6k-1:192k dilution and incubated for another 2 hours at 37˚C. The wells were washed again and HRP labeled secondary Ab raised in mouse was added in dilution 1:5000 µl in 1x PBS. After incubating plate for 50 minutes at 37˚C, repeated washing was performed and addition of 80 µl of TMB substrate to each well was done. 60 µl of stop solution (2N H_2SO_4) was added to cease reaction until color developed in no protein control. The intensity of yellow color was measured by ELISA plate reader at 450 nm. The assay was performed along with negative control BSA and positive control commercial TnI.

2.2.10 *In silico* structure prediction of TnI

The crystal structure of TnI in RCSB PDB is present as a part of three Troponin subunits- Troponin T (cTnT), Troponin I (cTnI) and Troponin C (cTnC). Therefore, sequence based three-dimensional structure modeling of TnI subunit was performed by retrieving FASTA format amino-acids from Uniprot-a protein sequence database with ID: UniProtKB-P19429 (TNNI3_HUMAN). The sequence was submitted to I-TASSER (Iterative Threading ASSEmbly Refinement)-a protein structure prediction tool. First, it identifies from PDB the structural templates using multiple threading approach LOMETS, constructed by iterative template-based fragment assembly simulations with full-length atomic models.

2.3 Results and discussion

The plasmid isolation from DH5α bacterial cells yielded 90 ng/µl of DNA plasmid as measured by nanodrop which was subjected to restriction double digestion and sequencing PCR. Double digestion of plasmid which was performed using restriction enzymes BamHI and XhoI demonstrated a fall out corresponding to approximately 630 bp for TnI gene containing 210 amino acids in lane 3. While lane 1 represents vector pET-28a(+) and band in lane 2 shows recombinant vector pET-28a(+) containing TnI gene (Fig.2.2).

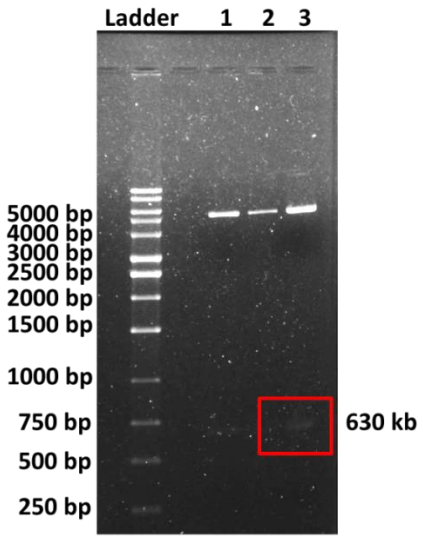

Fig.2.2 Double digestion of pET28a(+) plasmid carrying TnI gene

Subsequently, results of Sanger DNA sequencing PCR were analyzed by Finch TV server that confirmed sequence of human cardiac TnI when aligned with Genscript optimized nucleotide sequence with 100% sequence similarity. Moreover, the coding gene sequence of TnI optimized by Genscript was translated to protein sequence by ExpPASy Translate tool resulting in amino-acid sequence of human cardiac TnI in first open reading frame (https://web.expasy.org › translate). The derived amino-acid sequence gave 100% identity when aligned with Uniprot deposited TnI protein sequence using protein BLAST tool (https://blast.ncbi.nlm.nih.gov).

2.3.1 Expression and Purification of TnI

Post transformation of pET28a(+) plasmid bearing TnI gene in BL21 cells, bacterial colonies were screened by kanamycin antibiotic selection method. The overexpression of TnI was optimized at 0.2 mM IPTG induction at low temperature of 18˚C for 16 hours. Subsequently, after harvesting cells, the expression was confirmed by running 12% SDS-PAGE that demonstrated an intense band post IPTG induction in lane 2. Additionally, lane 3 and 4 shows soluble expression of protein after treatment with resuspension buffer containing 8M urea in Fig.2.3(a). TnI containing 6x His tag was purified via Ni-NTA affinity chromatography following on-column urea refolding purification. The elution fractions displays a band near 28.5 kDa along with the flow through and wash fraction in Fig.2.3(b). Further characterization via western blot using anti-TnI Mab also confirmed the purity of TnI. When estimated by nanodrop, 1-2 mg/ml yield of purified TnI was obtained as calculated using theoretical molar extinction coefficient derived from ExPASy tool.

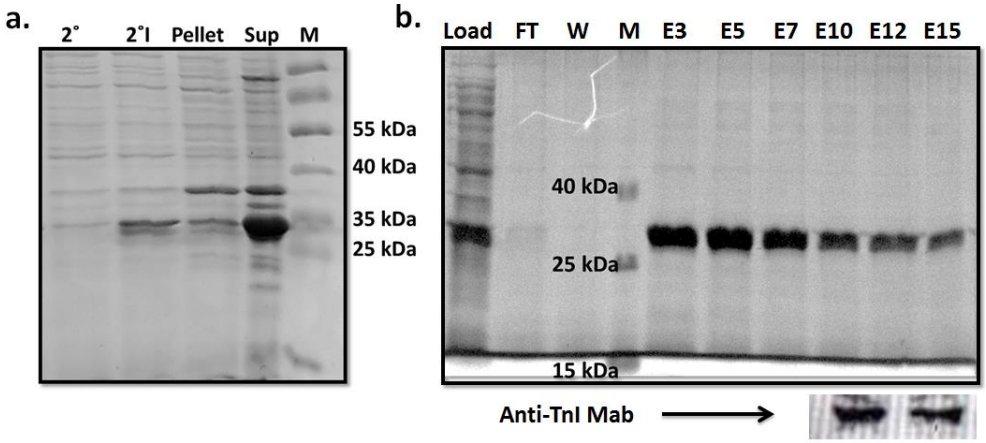

Fig.2.3 SDS-PAGE for (a) Expression of TnI (b) Purification of TnI with western blot (below)

2.3.2 Characterization of recombinant TnI

a. MALDI was used for validating purity and homogeneity of purified recombinant TnI that displayed a peak for intact mass of protein at 28.5 kDa in Fig.2.4(a). This 3 kDa extra mass was attributed to 6x His tag along with sequence from pET-28a (+) vector region. Further, peptide mass finger-printing via MALDI-TOF MS implementing tryptic digestion of TnI into peptide fragments was analyzed by MASCOT server. The observed peptide fingerprint spectra complied with cardiac TnI of *Homo sapiens* origin aligned with protein database search displaying probable matching hits with sufficient promising scoring in Fig.2.4(b).

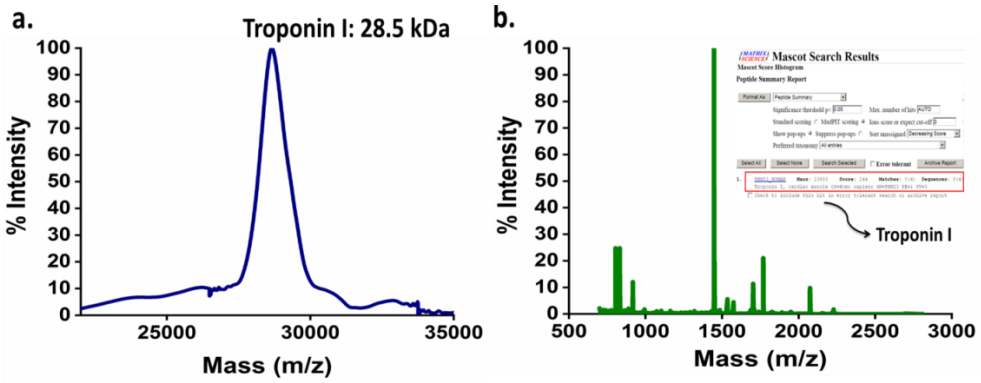

Fig.2.4 MS analysis of TnI (a) MALDI (b) MALDI-TOF MS with MASCOT search

b. Lateral flow test card analysis demonstrated a positive signal in test line area when purified TnI in varying concentrations was made to flow via sample pad elucidating the recombinant TnI holds functional properties for binding to its corresponding receptor moieties Fig.2.5(a).

c. CD spectroscopy in near-UV region for λ 190-260 nm depicted a negative peak at 208 nm corresponding to secondary structure fold of α-helix for recombinant which

coincided with commercial human heart TnI signature. Moreover, the CD profile of recombinant TnI also complied with the already reported 3-D structures of TnI subunit of Troponin complex (RCSB-PDB: 4Y99, 1J1E and 1J1D) [125]. The α-helical content was found to be 56.26% Fig.2.5(b).

d. An indirect binding microtiter ELISA was performed for exploring the capability of recombinant TnI to interact with commercial antibodies wherein TnI along with a negative and positive control was reacted with monoclonal anti-TnI antibody. The assay demonstrated efficient recognizing activity of recombinant TnI when compared to positive control of commercial TnI as seen in Fig.2.5(c). This investigated the diagnostically active properties of TnI for detecting antibodies and other bioreceptors.

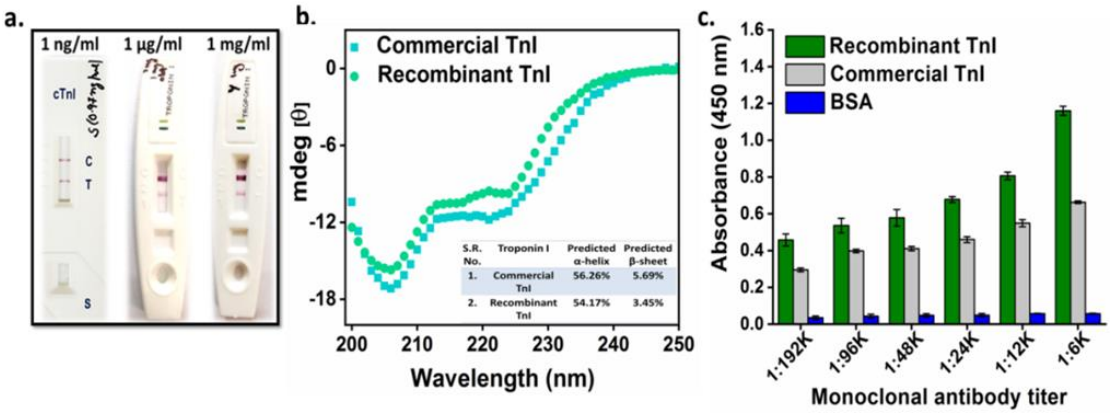

Fig.2.5 Characterization of recombinant TnI binding ability (a) Lateral-flow test card analysis showing band in test line area (b) CD spectra of recombinant and commercial TnI with inset table depicting α-helical content (c) Indirect binding ELISA for TnI sensing with Mab

In silico structure prediction analysis for TnI subunit was performed due to absence of availability for its 3-D structure in RCSB-PDB repository. To this context, sequence based structure threading by I-TASSER server revealed filamentous structure of TnI comprising presence of α-helices linked by flexible loops (Fig.2.6).

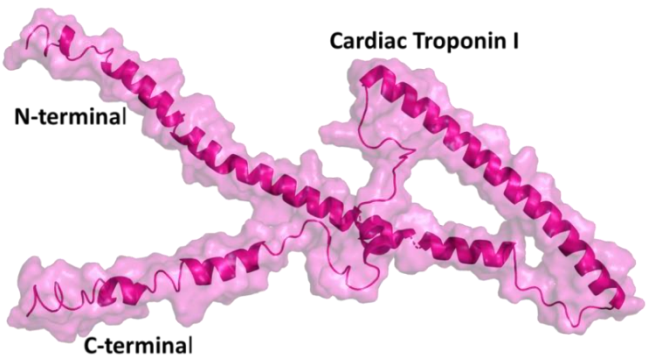

Fig.2.6 Three-dimensional structure of TnI predicted by I-TASSER server

2.4 DNA aptamers specific to cardiac TnI

Generally, delineating from the already reported approaches to synthesize aptamers against TnI in literature [16,126–129], our technique was inclined towards generating extremely specific DNA binders by taking peptide fragments of TnI as template to design aptamers. Linear peptides were predicted by using bioinformatics tool SVMTriP (Support Vector Machine utilized by combining the Tri-peptide similarity and Propensity scores). It uses machine learning algorithms such as Support Vector Machine (SVM), Artificial Neural Network (ANN) and Hidden Markov Model (HMM) to locate linear epitopes in protein sequence.

2.4.1 Aptamer generation using SELEX

SELEX, an *in vitro* selection method was used as a combinatorial chemical approach for generating DNA aptamers against TnI. A library of 86 nucleotides comprising a random DNA sequence of 40 bases flanked by 23 bases forward and reverse primer sequences was used. The affinity based SELEX method was utilized in which TnI peptide as target molecules were covalently conjugated to column matrix followed by selection and enrichment of efficient DNA binders. The procedure occurs in column with all the spatial conformation of the target peptides in the column matrix. In this SELEX procedure, alternating cycles of positive and negative binding were facilitated to create a natural selective pressure on the oligos selecting specific aptamers against target peptides of TnI.

Affi-Gel 10 affinity matrix (BioRad) was used for coupling that utilizes esters of N-hydroxysuccinimide derivatized cross-linked agarose gel bead support. The Affi-Gel 10 support contains a neutral 10-atom carboxyl spacer arm that covalently binds to amide group of TnI peptide molecules by anhydrous coupling mechanism.

2.4.2 Biochemical assays and electrophoretic separation of aptamers

a. **Indirect binding ELISA:** A microtiter binding ELISA was performed to examine the binding ability of aptamers specific to TnI peptide towards full length TnI protein. Briefly, 2.5 µg/ml recombinant TnI was coated onto polystyrene wells of microtiter ELISA plate using 100 mM bicarbonate buffer (pH 11) and was incubated for overnight at 4˚C. Next day, plate was washed thrice using 1x PBST (0.1% Tween 20) and blocked with 2% BSA for an hour at room temperature. After repeated washing, biotin labeled aptamers were added in a concentration

gradient of 7-500 nM along with a positive control binder and negative non-binder. After incubating the plate for two hours at 37˚C, anti-biotin HRP labelled secondary antibody raised in mouse was added using a dilution factor of 1:5000 in 1x PBS (pH 7.5). After 45 min of incubation following repeated washing, 80 µl of TMB was added and 60 µl stop solution 2N H_2SO_4 was added to cease color development after which absorbance was recorded at 450 nm for yellow color.

b. Gel electrophoresis: The synthesized aptamers were characterized for their purity and size by running 1% agarose gel and 10% native PAGE to analyze their migration pattern. DNA samples of 50 ng/µl were prepared and mixed with loading dye and was run on agarose gel for 1 hour under 70 volts with 1x TBE (Tris Borate EDTA) as running buffer. While, continuous native PAGE was run to analyze the native conformational folding state of aptamers using 1x TBE as running buffer under a constant voltage of 80 volts. Samples were mixed with tracking dye and heated at 95°C for 5min prior to loading in the wells along with 50 bp DNA ladder. SyBr green dye staining was used for illuminating the gel and visualization.

2.4.3 Biophysical characterization of aptamers specific to TnI

a. Bio-Layer Interferometry (BLI): It is an optical dip and read label-free technique to study and evaluate the strength of biomolecular interactions in real-time. It comprises ligand such as protein or nucleic acid immobilized on a matrix of fibre optic sensor chip to analyze its interaction with target sample. The interaction of biomolecules in turn alters interference pattern of white light reflected from sensor tip producing a change in optical thickness at bio-sensor tip. This induces wavelength shift proportional to binding intensity measured in terms of equilibrium dissociation constant K_D. ForteBio software analysis 9.0 directly provides binding affinities, rate of association and rate of dissociation in less than 20 minutes of time using very small concentration of sample (nM) once the conditions are optimized.

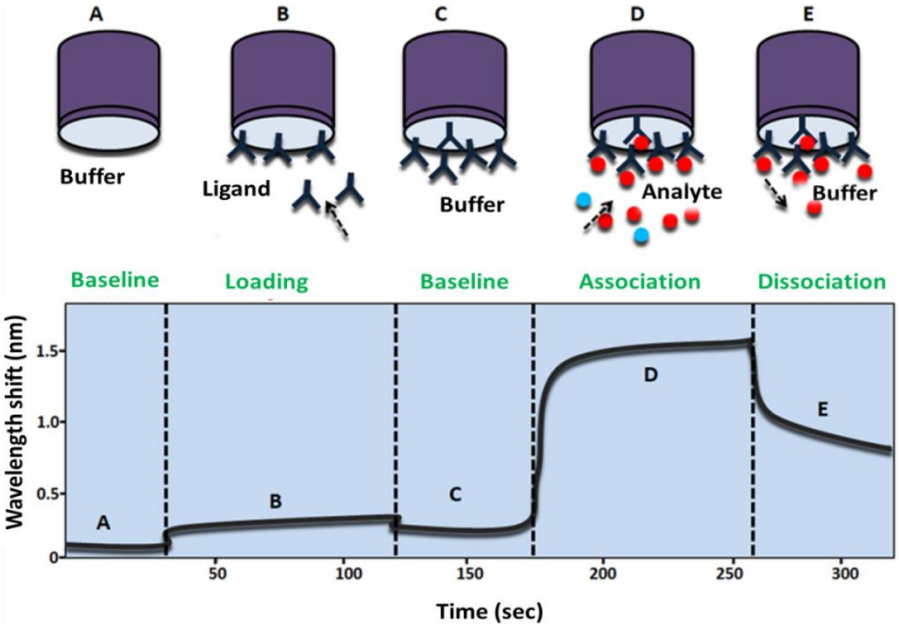

Fig.2.7 Schematic illustration of basic experimental assay steps in BLI

BLI was performed to examine affinity of aptamers generated against TnI peptide regions towards full length TnI protein. Sample preparations require a range of concentrations for the immobilized protein/aptamer and analyte, appropriate buffer controls are taken to check non-specific binding. Briefly, an optimized concentration of 50 nM biotin conjugated aptamers were immobilized on streptavidin conjugated sensor tip and further dipped in well of greinier black microtiter plate containing 50 nM TnI along with blocking and washing in 1x PBS solution. The sample volume required for each well is 200µl and experimental steps consisted of baseline for 60 sec, followed by aptamer loading for 300 sec on sensor tip and 300 sec of association and dissociation steps individually. Additionally, reference sensors were used for removal of any non-specific interactions with aptamers (Fig.2.7).

Alternative binding experiment was performed by immobilizing 50 nM of His tagged recombinant TnI onto Ni-NTA sensor tip and binding was observed with both aptamers separately. 200 µl of 50 nM Tc18 and Tc35p were prepared with buffer controls that were subtracted by reference sensors. The sensors were saturated with TnI for 300 sec loading followed by washing to remove unbound TnI and dipped in aptamer containing wells for 300 sec as association and dissociation each to evaluate dissociation constant.

b. Circular Dichroism: The secondary structural analysis to decipher conformational folding of DNA aptamers was inspected using CD spectroscopic

measurements. When circularly polarized light interacts with asymmetric chiral molecules in solution; extent of difference in absorption is recorded as change of ellipticity (Δε) measured in degrees which further provide information about secondary structure of biomolecules attained in solution. CD spectra were recorded in quartz cuvette of path length 0.2 cm with a bandwidth of 1.0 nm and a resolution under the far-UV wavelength range 200 to 320 nm for DNA aptamers. Experimentally, 2.5 μM aptamers in 10 mM PB (pH 7.5) were heated at 95˚C with every measurement recorded as 3 scans in continuous mode at 50 nm/min scan speed and then averaged to achieve better signal to noise ratio.

2.4.4 Secondary structure prediction of synthesized aptamers

a. The nature of folding pattern of single stranded DNA aptamers was determined by predicting their secondary structures. Their two-dimensional structures were deduced by using Mfold server (http://www.bioinfo.rpi.edu/applications/mfold) with folding parameters similar to experimental conditions *in vitro* as: NaCl=137 mM; Mg^{2+}=0 mM; temp=25˚C [130].

b. While, 3-dimensional tertiary structures of DNA aptamers were predicted by using webserver RNA Composer- an automated RNA structure 3D modeling tool (due to unavailability of 3D structure prediction software for single-stranded DNA). [131].

2.5 Results and Discussion

Instead of synthesizing aptamers against full length biomarker, purpose behind generating aptamers against apical peptide fragments TnI was to screen extremely specific nucleic acid binders that can target full length biomarker by targeting its peripheral regions. This method was practiced to achieve DNA aptamers that can detect TnI with high specificity avoiding non-specific interactions. The strategy moreover enabled the fabrication of match-pair based immunoassays and biosensing platforms for ultrasensitive biosensing of TnI.

SVMTriP server predicted two linear peptide regions of TnI from both apical regions for generation of aptamers based upon highest score (Fig.2.8). It takes latest input sequence from IEDB database (Immune Epitope Database) and Support Vector Machine (SVM) that combines Tri-peptide similarity and Propensity scores (SVMTriP) to achieve better prediction performance. A 13 residues sequence from N-

terminal region 27-39 amino acid and 12 residues linear peptide C-terminal apical region 187-198 amino acid were selected (Table 2.1). The peptide fragments thus selected for aptamer generation was predicted to be helix and loop regions of TnI protein. The selected peptide was chemically synthesized by solid phase peptide synthesis mechanism and further purified by HPLC (High Performance Liquid Chromatography). The purified products were obtained as lyophilized powdered peptides of approximately 12 mg each with proper mass analysis by MALDI.

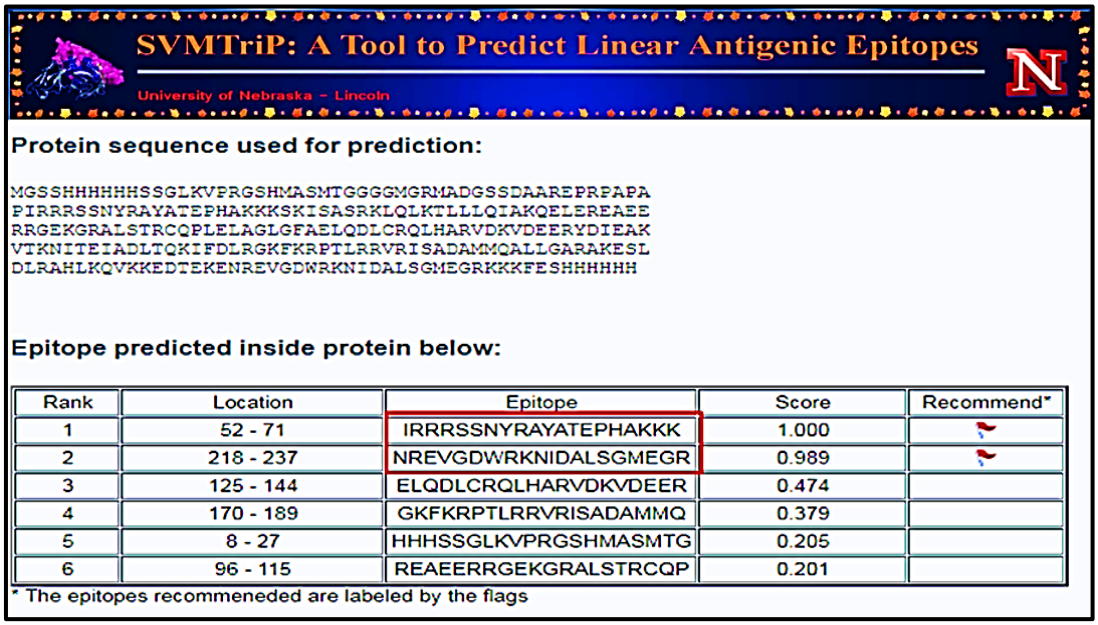

Fig.2.8 SVMTriP analysis for peptide prediction of TnI

S.R. No.	Peptide fragment	Region	No. of amino acids	Terminal
1.	RAYATEPHAKKKS	27-39	13	N-terminal
2.	VGDWRKNIDALS	187-198	12	C-terminal

Table 2.1 Selected peptide fragments from both apical regions of TnI

2.5.1 Selection of aptamers

Single stranded DNA library of 40 nucleotides random region flanked by forward and reverse primer of 23 nucleotides each is mentioned: **DNA Library (86 nucleotides)**

5'-TAGGGAAGAGAAGGACATATGAT-(N40)-TTGACTAGTACATGACCACTTGA-3'

A total of 10 cycles were run for multiple and repeated incubation rounds of positive DNA binders with target TnI peptides followed by their isolation and PCR amplification to generate specific DNA aptamers. The screened set of DNA aptamers

were cloned in bacterial vectors along with their sequencing. Eventually, the selected set of nucleic-acid sequences were synthesized commercially and procured sequences were investigated for their affinity based characterization towards full length biomarker cardiac TnI. The sequential layout of basic protocol followed for generating DNA aptamers by using SELEX is mentioned in Fig.2.9.

Four aptamers were screened and enriched by SELEX procedure- Tn13.2a and Tn24.1 against N-terminal peptide region of TnI protein while Tc18 and Tc35p against C-terminal region of TnI (Table 2.2). Fig.2.10 displays 3-D structural representation of apical regions of TnI protein selected for aptamer generation.

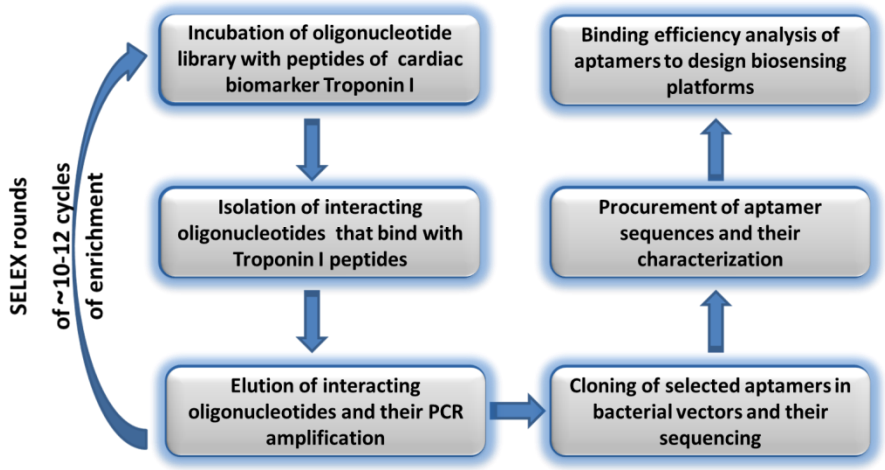

Fig.2.9 Schematic representation of SELEX cycles for aptamer screening against TnI peptides

SR. No.	Aptamers	Sequence	Length (base)	Target fragment	Target sequence
1.	Tn13.2a	TAGGGAAGAGAAGGACATA TGATCGACAGATCATATGG CCGAGAATATTAGCGTGCA AAGCTATTGACTAGTACAA GATCACTTGA	86	N-terminal	RAYATEPH AKKKS
2.	Tn24.1	TAGGGAAGAGAAGGACATA TGATCGACAGATCATATGG CCGAGAATATTAGCGTGCA AAGCTATTGGCTAGTACAT GATCATTTGA	86	N-terminal	RAYATEPH AKKKS
3.	Tc18	TAGGGAAGAGAAGGACATA TGATCACGGCATGTTGACT AGTACATGACCACTTGA	55	C-terminal	VGDWRKNI DALS
4.	Tc35p	TATTGGAGCGATCGGTCCG CGAAGGACATCATATGTCC TTCTCTTCCCTA	50	C-terminal	VGDWRKNI DALS

Table 2.2 List of aptamer sequence screened for both apical regions of TnI protein

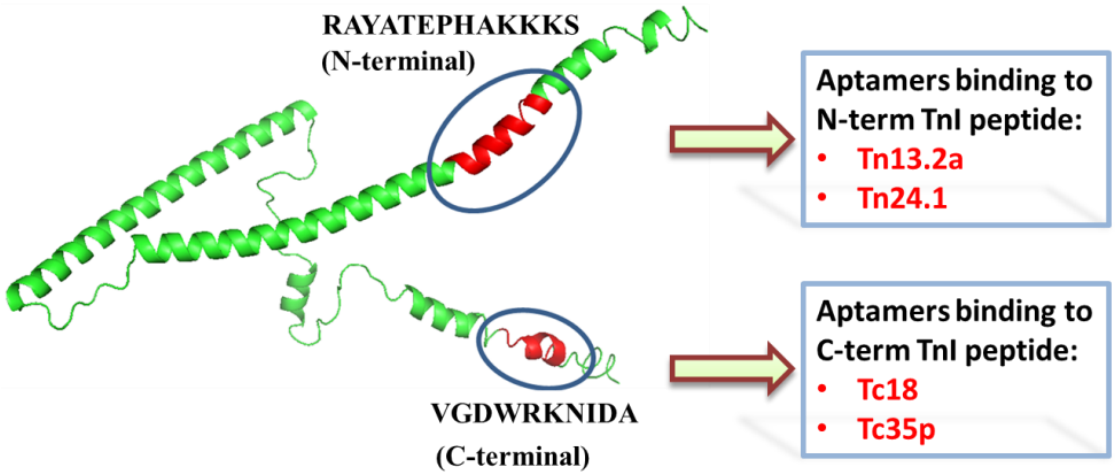

Fig.2.10 Structural representation highlighting both apical regions of TnI chosen for synthesis of DNA aptamers

2.5.2 Biochemical assays and electrophoretic separation

a. **Indirect microtiter ELISA:** All four aptamers generated against TnI peripheral peptides were investigated by indirect binding ELISA to detect full recombinant biomarker TnI. According to absorbance curves at 450 nm, only aptamers targeting C-terminal apical region of TnI (Tc18 and Tc35p) displayed efficient interaction while aptamers synthesized for N-terminal apical region of TnI (Tn13.2a and Tn24.1) did not bind actively (Fig.2.11).

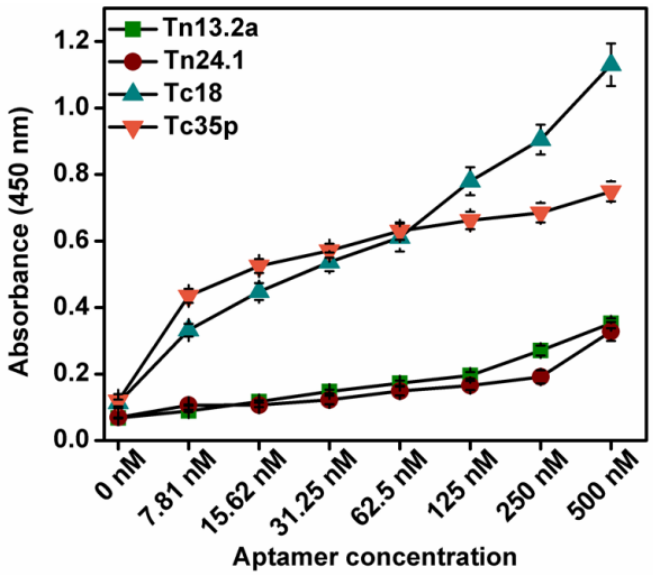

Fig.2.11 Microtiter binding ELISA for aptamers binding to both apical regions of TnI

The reason for non-efficacious interaction of N-terminal aptamers could be speculated as unavailability/masking of binding interface on TnI protein due to its

folding pattern. **Consequently, C-terminal specific aptamers-Tc18 and Tc35p were propagated in further studies.** The curves elucidate more concentration dependent occupancy of Tc18 binding interface on TnI protein than Tc35p. Therefore, ELISA results suggests better binding of Tc18>Tc35p when compared to positive control Tro4 aptamer from literature and a negative control aptamer avoiding non-specific binding with TnI [110].

b. Gel electrophoresis: In order to confirm presence of oligomerization or association states of screened aptamers, electrophoretic mobility assays were performed. 1% agarose gel was run for mass characterization of aptamers showing restricted mobility of Tc18 as compared to Tc35p corresponding to their size and purity in Fig.2.12(a). Additionally, series of acrylamide cross-linking were tried to optimize gel running conditions to which 10% acrylamide gave reproducible results. After SyBr green staining native PAGE gel displays an intense band of Tc18 near 55 bp and an accelerated migration of Tc35p near 50 bp ladder Fig.2.12(b). This indicates that aptamers comprises monomeric units which not only depends upon charge to mass ratio, but on physical shape/structure attained by aptamers/molecules in solution.

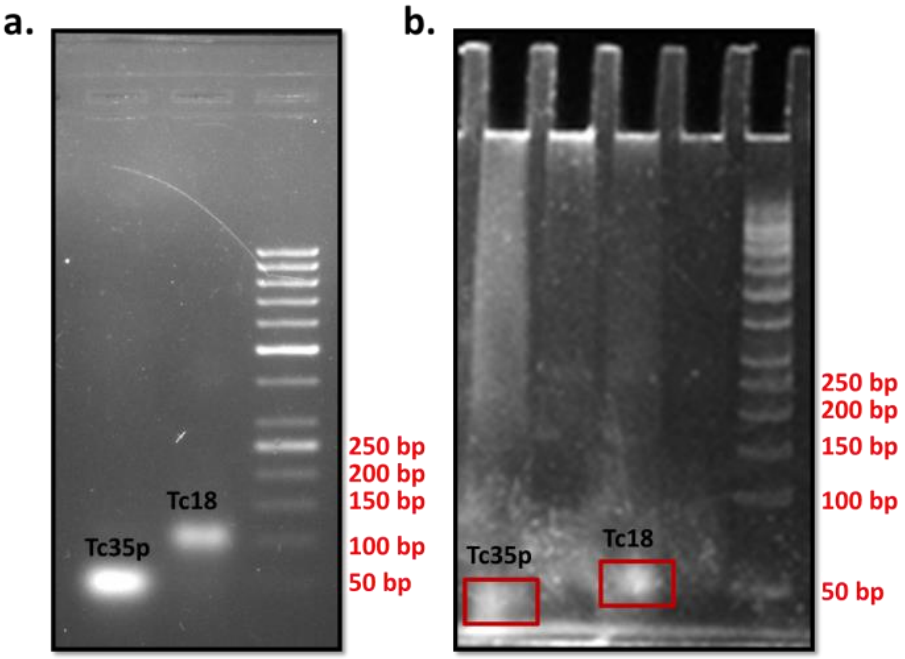

Fig.2.12 Migration profile of aptamers (a) Agarose gel electrophoresis (b) Native PAGE

2.5.3 Biophysical characterization of aptamers

a. BLI: The binding strength in terms of dissociation constant (K_D) of aptamers Tc18 and Tc35p for full length cardiac biomarker protein TnI was deciphered using BLI. Biotin labeled aptamers-Tc18 and Tc35p were immobilized onto streptavidin sensors and their binding was investigated with equimolar TnI. As evidenced from global fitting analysis of k_{on} and k_{off} curves in Fig.2.13, Tc18 exhibits higher binding affinity of $1.06\pm0.7x10^{-9}$ M as compared to Tc35p with $1.84\pm1.05x10^{-7}$ M suggesting the results to be in support with microtiter binding ELISA. The higher binding affinity of Tc18 can be attributed to its hair-pin loop conformation for interaction with TnI. Subsequently, binding affinity analysis performed using Ni-NTA sensor immobilized His tag recombinant TnI with DNA aptamers also generated similar K_D values. This reverse binding analysis was performed to further validate ability of aptamers to bind TnI protein suggesting role of aptamers both as capture and target bioreceptor moieties.

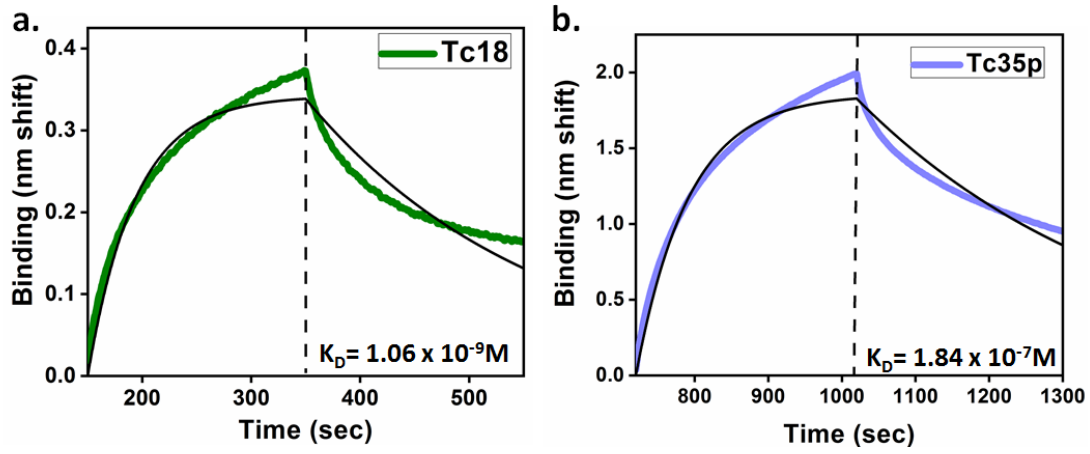

Fig.2.13 BLI curves showing dissociation constant K_D for aptamers binding TnI (a) Tc18 (b) Tc35p

b. CD Spectroscopy: The conformational folding pattern of DNA aptamers attained during *in vitro* experiments in physiological buffer was examined by CD spectroscopy. Both the aptamers- Tc18 and Tc35p depicts similar CD signature corresponding to B-form of DNA helix [132]. The spectroscopic scans were recorded under far-UV wavelength range of 200 to 320 nm in 10 mM PB (pH 7.5). A negative signal at 245 nm and positive peak signal at 270 nm along with a negative peak between 220-230 nm relates to poly[d(AT)] configuration of B-DNA [133] (Fig.2.14).

GC content and other parameters were calculated by GC content calculator which was found to be 43.63% for Tc18 and 50% for Tc35p (http://mcb.berkeley.edu) (Table 2.3). The moderate GC% content establishes the DNA aptamer stability for high temperature enabling easy unfolding and folding while performing *in vitro* interaction experiments.

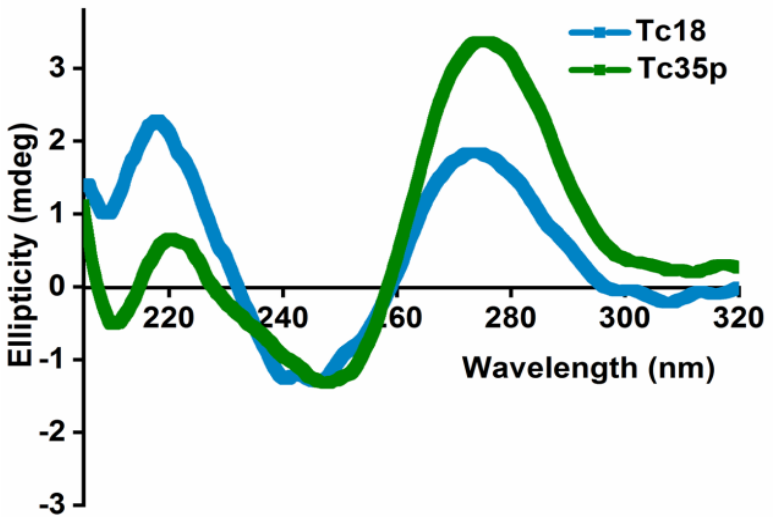

Fig.2.14 Secondary structure conformation of aptamers binding TnI by CD spectroscopy

S.R. No.	Aptamer	GC content	Length	Mol Wt	Tm
1.	Tc18	43.63%	55	17 kDa	71˚C
2.	Tc35p	50%	50	15 kDa	72˚C

Table 2.3 Calculation of GC% content of aptamers binding TnI

2.5.4 Structure prediction of aptamers

a. Mfold server was used for predicting **secondary structure** of aptamers to reveal their nature of folding pattern. The sequence of aptamers along with *in vitro* experimental conditions parameters was submitted. The server predicted structure of Tc18 aptamer with hair pin loop like conformation and Tc35p having stem-like extension with protruding arms (Fig.2.15). These secondary structures might play role in interacting with TnI elucidating their mechanism of binding or might be assisting in further folding of aptamers into more stable tertiary structures.

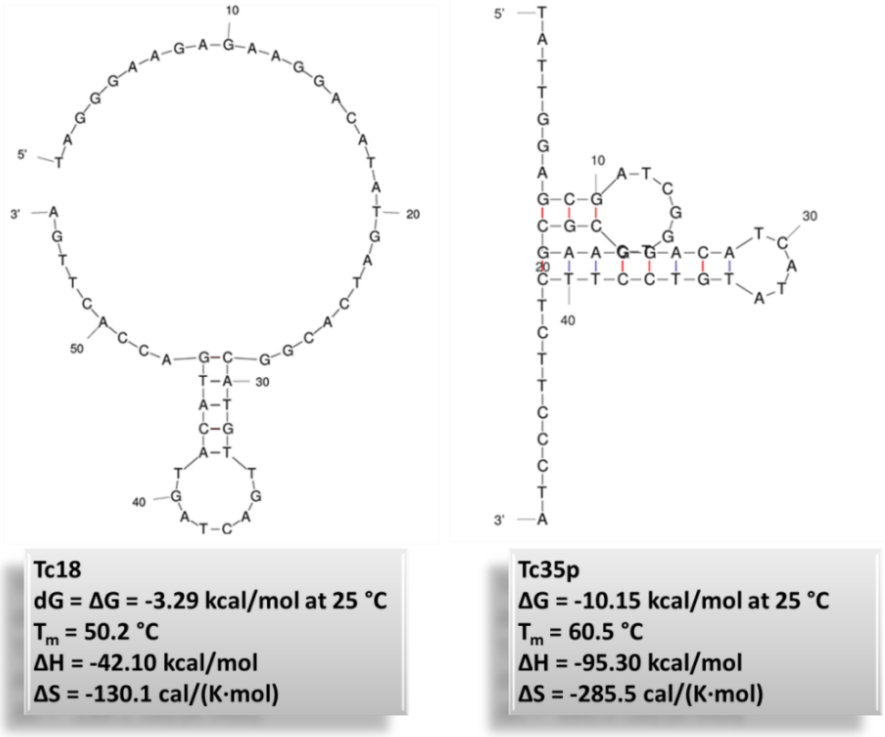

Fig.2.15 Secondary structures of aptamers predicted by Mfold server

b. Furthermore, **tertiary structures** of aptamers were deduced using RNA Composer by submitting vienna file format as input obtained from Mfold. As seen in Fig.2.16, 3-D structure of Tc18 depicted a uniform helical conformation and Tc35p attained a two-way opposite folding pattern. As a result, tertiary structure can provide critical information regarding the TnI-aptamer interaction giving insights for binding interface of their interaction.

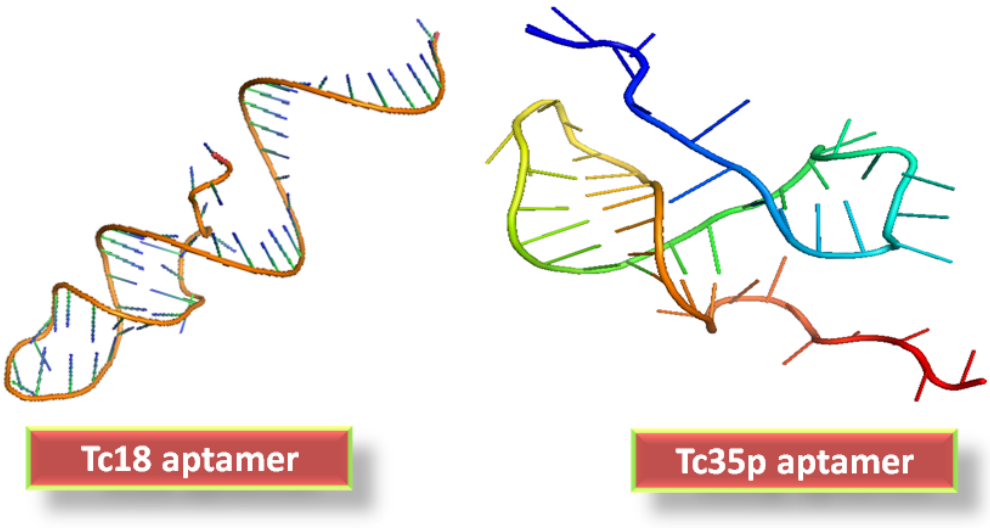

Fig.2.16 Tertiary structures of aptamers predicted by RNA composer

2.6 Development and characterization of polyclonal antibodies against recombinant TnI

Polyclonal antibodies (PolyAb) were synthesized in 4-6 weeks old New Zealand white (NZW) rabbit by subcutaneously injecting 250-300 µg/ml of recombinant TnI emulsified with Freund's complete adjuvant (FCA). After first immunization, five successive secondary boosters doses of TnI emulsified with Freund's incomplete adjuvant (FICA) were injected at intervals of every 21 days. The blood from the immunized rabbit was collected on every 5^{th} day of injection by making it bleed via ear vein. The serum was separated by centrifugation and complement system was inactivated by heating at 56°C for 20 min. The antibodies were purified by passing through Protein-A packed agarose bead column to isolate IgG fraction of antibody followed by ammonium-sulphate salt based purification technique [134][135].

Characterization of polyclonal antibodies

a. The ability of synthesized PolyAb to bind TnI was investigated by performing **indirect binding ELISA**. Briefly, 2.5 µg/ml of TnI was coated onto ELISA polystyrene wells using 100 mM bicarbonate buffer (pH 11) at 4˚C allowing overnight incubation. After washing plate with 1x PBST (pH 7.5), vacant sites were blocked with 1% casein solution for 2 hours at room temperature. Following repeated washing, all five booster antibodies along with pre-immune sera were added in a titer gradient from 1:1k to 1:62k for two hours at 37˚C. After washing the plate again, anti-rabbit HRP labeled secondary antibody was added (dilution 1:10k) and plate was kept for 50 min incubation at 37˚C. TMB substrate was added and reaction was stopped using H_2SO_4. As a result, Fig.2.17(a) shows III booster antibody displaying maximum binding response with TnI in each titer as compared to other boosters. Another indirect ELISA was performed to elucidate specific TnI binding of III booster PolyAb along with positive and negative control proteins that revealed specificity of generated PolyAb towards TnI in Fig.2.17(b).

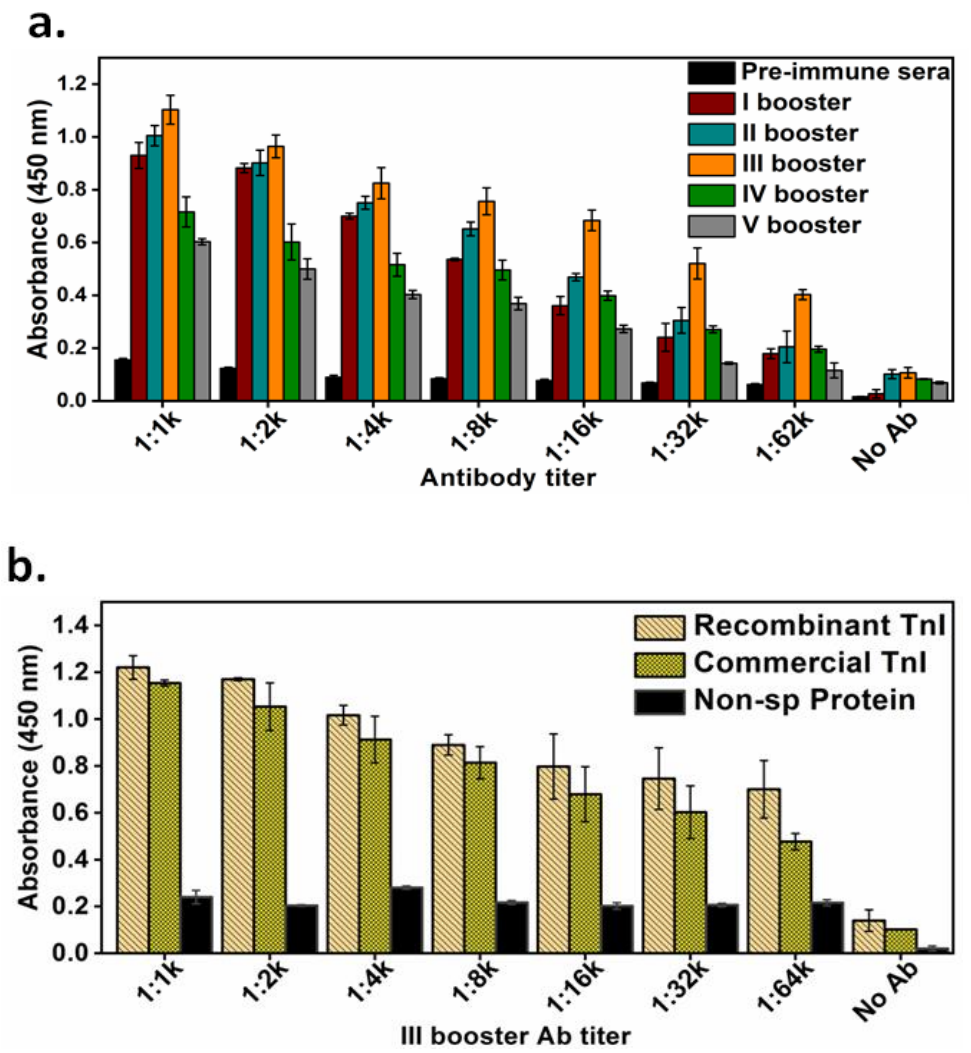

Fig.2.17 (a) Microtiter ELISA for all 5 boosters PolyAb synthesized against TnI (b) Microtiter binding ELISA of III booster antibody with TnI and other controls

b. The binding strength of PolyAb for TnI was quantified using **BLI** in terms of dissociation constant K_D. 50 nM III booster PolyAb was immobilized onto AR2G sensor by using amine-coupling chemistry. After blocking the sensor with ethanolamine following washing with 1x PBST (pH 7.5), sensor tip was dipped in equimolar TnI solution for association and dissociation along with reference sensors in working buffer. A comparison with anti-TnI commercial monoclonal antibody was performed for reference. As a result, comparable K_D values for PolyAb were calculated as Mab demonstrating proportionate binding affinity towards TnI (Fig.2.18).

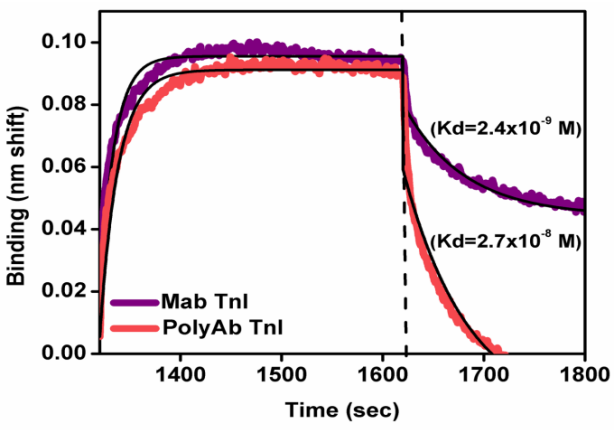

Fig.2.18 BLI curves of Mab and PolyAb with their dissociation constant

2.7 Selection and characterization of peptide specific for cardiac TnI

Scott Banta and his co-workers generated **peptide fragment as a bioreceptor** moiety specific against cardiac TnI by using polyvalent phage display technique [104]. They have isolated linear peptide motifs that can recognize human cardiac TnI which were synthesized by peptide-synthesis facility and purified by HPLC. The 12 amino-acid peptide was modified with lysine and alternatively cysteine at C-terminal for ease of conjugation. The peptide parameters were analyzed using ExPASy Protparam enlisted in Table 2.4

Peptide	Sequence	Size (kDa)	Length	Iso-electric point	Nature of peptide
Pep-C	FYSHSFHENWPSC	1.6	13 amino-acids	6.92	Acidic
Pep-K	FYSHSFHENWPSK	1.7	13 amino-acids	7.69	Basic

Table 2.4 Peptides selected from literature specific to TnI

Characterization of peptide

a. The synthesized peptide was characterized for its purity by using **mass spectrometry** analysis in Fig.2.19(a) showing a peak at 1.6 kDa with 100% intensity.

b. **CD spectroscopy** was performed to gather information about secondary structure folding of 10 µM of peptide dilution in 10 mM PB (pH7.5). A negative CD ellipticity at λ 195 nm corresponding to random coil was observed under far-UV CD range in Fig.2.19(b).

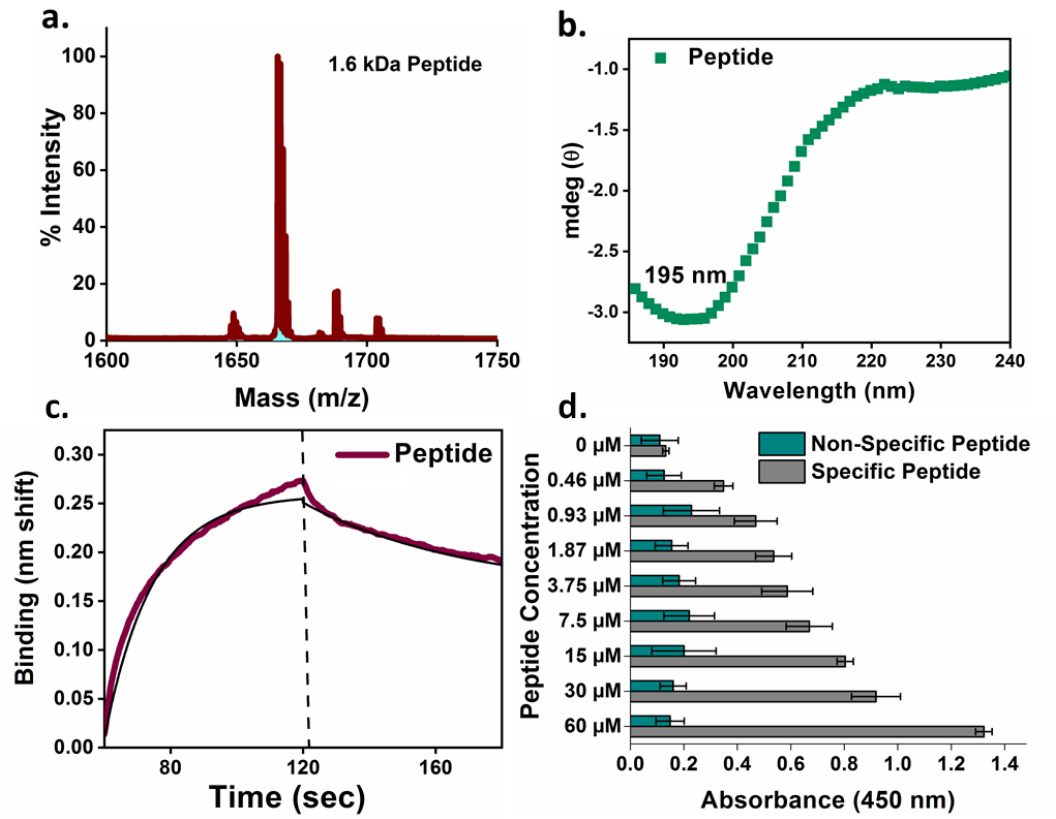

Fig.2.19 Characterization of peptide specific to TnI (a) MALDI showing peak of 1.6 kDa (b) CD spectroscopy showing random coil folding of peptide (c) BLI sensogram showing binding analysis of peptide with TnI (d) Indirect binding ELISA of peptide with TnI

c. The binding strength of peptide towards recombinant TnI was evaluated using **BLI** technique by immobilizing lysine modified 50 µM of peptide onto AR2G sensor via amine-coupling chemistry. Binding towards equimolar TnI was analyzed with association and dissociation curves deducing K_D=1.33±0.7x10^{-8} M with R^2=0.93 Fig.2.19(c).

d. To further investigate interaction of peptide with TnI, indirect binding ELISA was performed for which peptide was labeled with biotin. Briefly, 2.5 µg/ml TnI was coated for overnight onto plate which was blocked with 2% BSA solution for 2 hours. Biotinylated peptide was added from 0-60 µM followed by incubation for 2 hours at 37˚C. The detection was done by using HRP labeled streptavidin. Peptide was able to target TnI at low concentration as well without any non-specific interaction in Fig.2.19(d).

e. ***In silico*** analysis for 3-dimensional structure prediction of peptide was done by using PEP-FOLD3-*de novo* peptide structure prediction server that employs

coarse-grained force field providing a high resolution best model using default parameters of 100 set of simulations [136]. As a result, peptide attained a helical conformation along with loop region which might hold binding properties to interact with TnI in Fig.2.20.

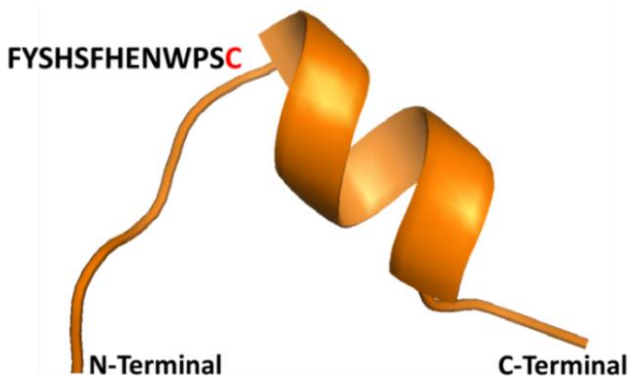

Fig.2.20 Tertiary structure of peptide predicted by PEP-FOLD3 server

f. Additionally, the peptide was conjugated to BSA carrier with peptide coupling kit utilizing sulfhydryl group (cysteine) of peptide. Using heterobifunctional cross-linker, NHS ester in sulfo-SMCC reacts first with primary amines on carrier protein BSA forming covalent amide bonds followed by reaction of maleimide group with peptide's sulfhydryl groups with stable thio-ether bonds. The conjugation was characterized by MALDI analysis deciphering 71 kDa intact mass of peptide-BSA bioconjugate compared to BSA in Fig.2.21(a). Additionally, 10% SDS-PAGE demonstrated restricted mobility of BSA-peptide conjugate as compared to peptide in Fig.2.21(b).

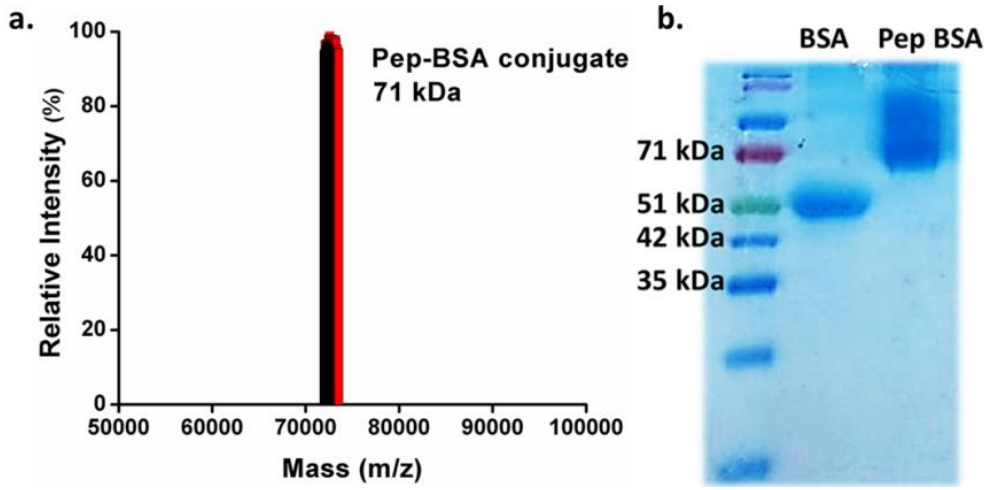

Fig.2.21 Characterization of Peptide-BSA conjugates by (a) MALDI (b) SDS-PAGE

2.8 Conclusion

In this chapter, we have discussed about **expression of human cardiac TnI** and its stable purification using modified urea refolding protocol. Recombinant TnI has been characterized for its purity through MALDI showing a peak at 28.5 kDa, SDS-PAGE showing gel bands without any impurities and indirect ELISA exhibiting the binding ability. The structural stability of TnI was confirmed by comparing its CD signature with commercial human heart TnI that depicts α-helical content.

This division of work also entails **DNA aptamers** synthesized by SELEX against both apical peptides of TnI. As a conclusion, C-terminal peptide specific aptamers-Tc18 and Tc35p at a low concentration of 7 nM were able to recognize and bind recombinant TnI as envisaged by microtiter binding ELISA. The binding affinity of aptamers as revealed by BLI was K_D=1.06x10^{-9} for Tc18 and 1.84x10^{-7} for Tc35p respectively. The migration pattern of both the aptamers was investigated by gel electrophoresis that demonstrated their monomeric subunit existence and respective size based mobility under the effect of voltage. Mfold deciphered aptamers with unique secondary structures comprising hair-pin loop (Tc18) and stem-loop (Tc35p) folding which was corroborated with B-DNA polymorphic form CD signature with negative dip at 245 nm along with positive signal at 270 nm and another negative dip at 220-230 nm relating to poly[d(AT)] configuration. This structural integrity at physiological buffer (pH 7.5) enabled specific recognition of TnI through C-terminal peptide in biochemical ELISA. *In silico* 3-D structure prediction analysis of aptamers using RNA composer and TnI via I-TASSER server was performed to provide deep insights for studying their interaction interface which will aid in developing AMI diagnostic platforms. Moreover, **PolyAb** and **specific peptide** have been incorporated as additional bioreceptors specific against TnI.

Taking into account the protein preparation and selection of aptamers performed for N-terminal and C-terminal peptide fragments of TnI, only C-terminal DNA binders were found to bind full TnI protein. For now, we have characterized these aptamers but still there are many aspects regarding their behavior of interaction

with peptide tail of TnI that are to be studied in detail. To this context, next chapter will focus upon certain investigations-firstly, the effect of TnI binding on aptamers; secondly, nature of interaction of aptamers with TnI; thirdly, does aptamer-TnI form a stable complex or is it just a surface immobilization based binding?

Chapter 3

Interaction studies of aptamers binding to cardiac Troponin I

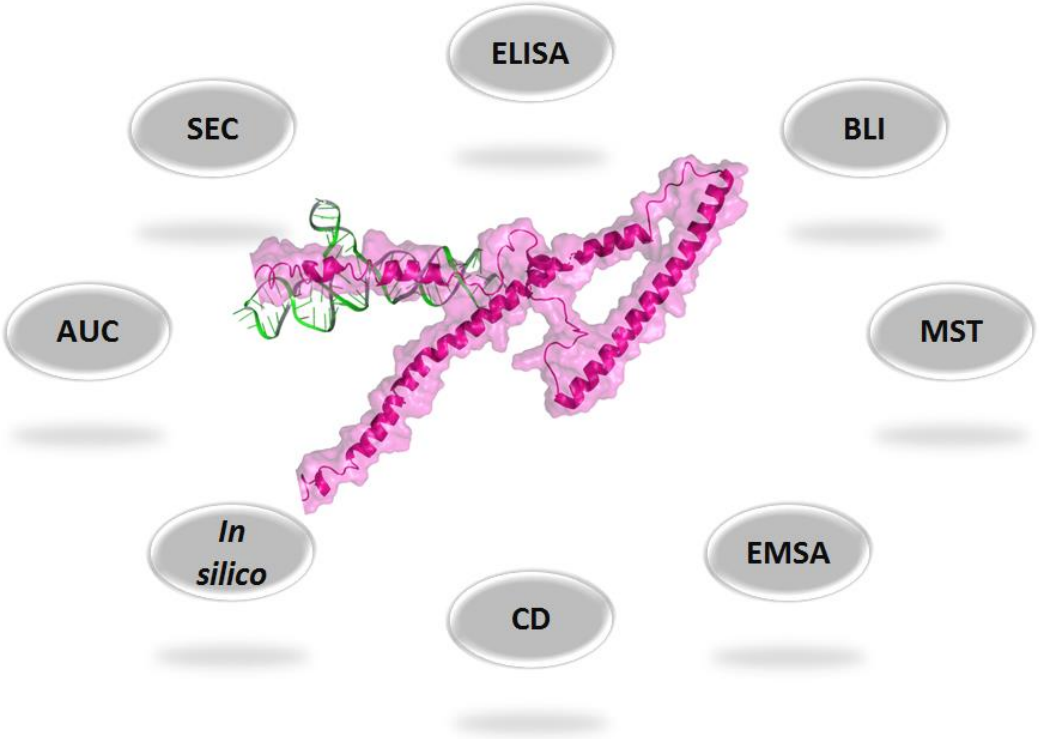

3.1 Overview

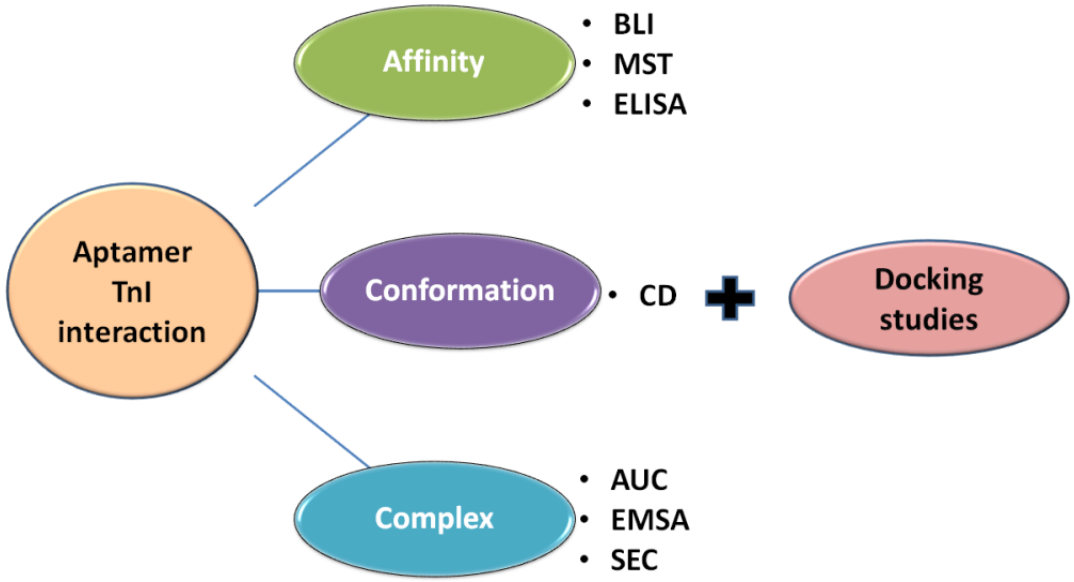

The subsequent approach highlighted in this chapter was to investigate the binding pattern of aptamers generated against C-terminal peptide region with full length recombinant TnI biomarker protein. The binding properties are driven by the secondary and tertiary structures/nature of folding pattern of aptamers that includes base pairing forming loops, hairpins, stem, bulges, etc. Moreover, the shape complementarity between the aptamer and TnI along with hydrogen bonding, ionic bonding, dipole-dipole bond, aromatic π-π stacking and London dispersion forces forms their intermolecular interactions. **The biomolecular recognition between aptamers and TnI defines the utility of aptamers to be used as high-affinity bioreceptor molecules for fabricating biosensing platforms** [137].

Therefore, this chapter comprises biochemical method of microtiter binding assays and other biophysical methods of Circular Dichroism (CD) spectroscopy, Microscale Thermophoresis (MST) and Biolayer Interferometry (BLI) to study interaction of aptamers with TnI. The respective studies were executed to provide information regarding structural changes and binding strength of aptamers defining their affinity for TnI. Moreover, aptamer-TnI complex formation has been intensively studied using other high-end characterization methods of analytical ultracentrifugation (AUC), gel filtration chromatography and electrophoretic mobility shift assay (EMSA).

Additionally, a broad learning regarding structural binding for aptamer with TnI C-terminal region has been addressed by *in silico* docking studies. Adding more to what has been mentioned is the major missing link for unavailability of three-dimensional structure prediction tools for single-stranded (ss) DNA. To date, researchers use RNA 3D structure determination servers considering the folding pattern of RNA similar to ss DNA [131]. The chapter also describes about the residues of TnI engaged in binding to nucleic acid residues of DNA aptamers. All the characterization techniques in conjunction with docking studies have provided a better conceptualization pertaining to interaction patterns of aptamer with target TnI. Moreover, studies regarding the binding of synthetic peptide as parallel bioreceptor have also been discussed.

3.2 Experimental approaches

3.2.1 Materials and Instrumentation

Recombinant cardiac TnI, Human heart isolated natural TnI (Sigma) for reference, Aptamers Tc18 and Tc35p (IDT Technologies). All the interaction study experiments were performed using physiological buffer 10 mM phosphate buffer (pH 7.5) referred to as 1x PBS along with Tween 20 (0.1%). Each experiment was repeated three times to which data is averaged and mean values were plotted against the protein concentration with standard deviation.

Spectroscopic measurements for ELISA were taken using BioTek Synergy H1 spectrophotometer (UK). Binding studies were performed using MST-Nanotemper Technologies (Monolith NT.115) and BLI Octet K2 system (Pall Life sciences, Fremont, CA 94538 USA). Conformational studies were performed using Jasco J-815 CD instrument for spectroscopic analysis. Sedimentation experiments were done on Beckman Coulter Life Sciences, Proteome Lab XL-A/XL-I (US). BioRad gel electrophoresis assembly was run for non-radioactive gel shift assay (EMSA).

3.2.2 Microtiter binding assays

a. The binding ability of both aptamers were primarily inspected using indirect ELISA by coating 1-20 ng/ml of TnI along with non-specific protein using 10 mM bicarbonate buffer (pH 11) for 12-16 hours at 4˚C. The wells were washed three times with 300µl 1x PBST (pH 7.5) followed by blocking vacant sites using 2% BSA in 1x PBS for 2 hours. After again washing the plate, 500 nM of both

biotinylated aptamers Tc18 and Tc35p were added and incubated for 2 hours at 37˚C. Post repeated washing, 1:5000 µl HRP labeled streptavidin was allowed to bind biotinylated aptamers. TMB substrate solution was added for signal development and 2N H_2SO_4 stop solution was used to cease reaction until color developed in control. Absorbance was recorded at 450 nm.

b. The binding efficiency of aptamers for detecting TnI in combination with commercial anti-TnI monoclonal antibodies (Mab) was investigated using sandwich ELISA. Briefly, 2 µg/ml anti-TnI Mab was coated onto polystyrene plate for overnight. The wells were blocked using 3% BSA for 2 hours followed by washing with 1x PBST (pH 7.5). Afterwards, 1-10 ng/ml TnI was added and incubated for 2 hours at 37˚C. Post repeated washing, 500 nM of biotinylated Tc18 and Tc35p were added alternatively and incubated for another 2 hours. HRP conjugated streptavidin in 1:5000 µl dilution was used for detection. Post incubation for 1 hour, TMB substrate along with stop solution was added for signal development and plate was read at 450 nm.

3.2.3 Biolayer Interferometry (BLI)

The affinity of aptamers specific to TnI as a function of TnI concentration was explored with binding kinetics experiment of BLI. Briefly, biotin labeled 50 nM Tc18 and Tc35p was immobilized onto streptavidin sensors for 600 sec until saturation was achieved. After washing step of 60 sec in 1x PBS, series of association and dissociation for 300 sec each with TnI dilutions (40-160 nM) were examined for binding. Regeneration of sensor tips as removal of bound TnI was performed with intermittent washing with glycine-HCl (pH 2.5). The results were analyzed in *Fortebio* software analysis 9.0.

The binding affinity of aptamers generated against TnI peptide fragment was also interrogated in serum matrix with 1:10 µl dilution in 1x PBST. 100 nM of biotinylated aptamers were immobilized onto streptavidin sensor until saturation. The aptamers were dipped sequentially in wells containing human serum spiked with natural heart tissue isolated TnI (4-35 nM) with recurrent washing and regeneration.

3.2.4 Microscale Thermophoresis (MST)

It is biophysical analysis for studying interactions between biomolecules based on detection of change in target fluorescence induced by temperature as a function of dilutions of a non-fluorescent ligand. This observed fluorescence change is based on a) temperature related intensity change (TRIC) of fluorescently labelled probe affected by binding, b) thermophoresis and particles movement in microscopic temperature gradient. The change in chemical microenvironment of fluorescent probe and alterations in biomolecular hydration shell result in relative fluorescence change. This is in turn induced by temperature gradient used to determine binding affinities. Without any surface immobilizations, MST offers measurement of biomolecular interactions directly in solution.

For experimentation, 100 µg/ml TnI was tagged with 80 µl solution of 1mg/ml fluorescent dye FITC which employs isothiocyanate group to react with amino terminal and primary amines in protein suspended in bicarbonate buffer pH 9. Varying dilutions of unlabeled aptamers (0.006-200 nM) in 1x PBST were titrated upto sixteen dilutions and mixed with 100 nM FITC labeled TnI. The mixture was allowed to interact and loaded on Monolith NT.115TM capillaries. The results were analyzed in Monolith NT.115 instrument (Nanotemper) software.

3.2.5 Circular Dichroism (CD) Spectroscopy

In order to study changes in secondary structures of aptamers Tc18 and Tc35p as a function of increasing concentration of target biomarker TnI, CD spectroscopy was performed. 2.5 µM of Tc18 and Tc35p was heated at 95˚C and cooled to normal temperature prior taking the scans. Far-UV CD measurements were taken as DNA bases absorb light differentially in λ range 200-320 nm [7]. Different dilutions of TnI from 10-80 µg/ml in 10 mM phosphate buffer (pH 7.5) were incubated with both aptamers alternatively for 15 min under shaking conditions. CD scans for each aptamer-TnI complex was recorded in a quartz cuvette of 0.2 cm path length with bandwidth 1.0 nm and 50 nm/sec scan rate. Each scan was baseline corrected to minimize signal to noise ratio and was averaged for 3 accumulations.

Furthermore, differential CD spectroscopy was performed wherein only Tc18 aptamer was titrated with 0-1 molar concentration TnI with an interval of 0.25 M. Each concentration of complex was incubated for 15 min and CD scan was accumulated for average three measurements.

3.2.6 Analytical Ultracentrifugation (AUC)

AUC is a quantitative method to analyze biomolecules in complex mixture by monitoring their optical behavior and their sedimentation in real time under influence of a strong gravitational force. The basic principle of ultracentrifugation is similar to normal centrifugation: separation of components of a solution on the basis of their size and density (viscosity) of the medium (solvent) for their dynamic behavior (sedimentation velocity) or systems in equilibrium (sedimentation equilibrium) [138]. Sedimentation velocity experiment (SV-AUC) was performed where solute movement in high centrifugal field is related to hydrodynamic shape, size and interaction of molecules. The experiment was performed on Beckman Coulter that provided sedimentation coefficient value (s) based on movement of molecules under centrifugal force achieved by solving the Lamn equation as Svedberg unit [139].

SV-AUC of aptamers Tc18 and Tc35p and their complex with TnI was performed to study their complex-formation tendency. Briefly, 400 µl of 100 nM aptamers and equimolar ratio of aptamer-TnI complex was centrifuged at 10,000 rpm. AUC continuous distribution measurement was done with An50 Ti Rotor at 260 nm for aptamers and at two different wavelengths 260 nm and 280 nm for aptamer-TnI complex. AUC data was analyzed using SEDFIT that displays a plot of sedimentation coefficient as svedbergs (S) vs continuous distribution model for sedimentation coefficient distribution.

3.2.7 Electrophoretic Mobility shift assay (EMSA)

A label-free EMSA/gel shift assay was performed to study interaction of DNA aptamers with TnI without use of radioactive probes to qualitatively detect the formation of aptamer-TnI complex formation [140]. Briefly, 1.5% agarose gel of around 1 cm thickness was prepared in 0.5x TBE buffer containing EtBr. Different concentrations of 10 µl TnI (0-150 µM) were incubated with 10 µl 50 nM aptamer in EMSA binding buffer at 37˚C for 30 minutes. The samples were loaded onto gel and run for 1 hour at 70 volts and migration pattern in the gel was observed under BioRad Gel Doc system for imaging.

3.2.8 Size exclusion chromatography (SEC)

SEC or molecular sieve chromatography is a method in which biomolecules are separated according to their size and molecular weight. Larger molecules are excluded from stationary gel matrix and flow through the column more quickly than smaller

molecules suggesting the phenomenon- smaller the molecule, longer the retention time. Analytical grade column Superdex® 200 10/300 GL from GE healthcare with 25 ml of bed volume was used along with AKTA pure chromatography/fast protein liquid chromatography system (FPLC) system in a cool cabinet at 4°C. Aptamer Tc18 and Tc35p separately and their complexes with TnI was loaded onto the column in equimolar dilution after incubation for 30 min at 0.5 ml/min flow-rate. The column matrix was pre-equilibrated with 100 ml of 1x PBS (pH 7.5) experimental buffer prior to separation of aptamer-TnI complex.

3.2.9 *In silico* analysis of aptamer-TnI interaction

Primarily, electrostatic potential of TnI was deduced using PDB2PQR-an automated pipeline for Adaptive Poisson-Boltzmann solver (ABPS) online web server (https://www.cgl.ucsf.edu). This was performed to determine overall charge on TnI at physiological pH 7.4 that could decipher probable binding sites for negatively charged aptamers.

Further, in order to recognize the interaction of aptamers generated against C-terminal apical peptide fragment with full TnI protein, docking studies were performed. HDOCK: protein–protein and protein–DNA/RNA interaction server was used based on hybrid strategy (http://hdock.phys.hust.edu.cn). It utilizes FFT-based global docking program, referred as HDOCKlite that globally samples putative modes of binding in HDOCK server, incorporating evaluation of an improved shape-based pairwise scoring function. PDB structure of TnI (I-TASSER) as receptor and aptamers (RNA Composer) as ligand were submitted to input query of HDOCK, along with adding of C-terminal apical fragment residues for which aptamers were generated. Furthermore, residues involved in interaction were determined by PDBsum cleft analysis (PDBsum Generate) - an EMBL-EBI server that provides an overview of contents for each 3D macromolecular structure deposited in the PDB (https://http://www.biochem.ucl.ac.uk/bsm/pdbsum/).

3.3 Results and Discussion

3.3.1 Biochemical assay of aptamers binding to TnI

An indirect binding ELISA was performed where varying TnI concentration was immobilized on surface and both aptamers were investigated for binding. As a result, Tc18 and Tc35p aptamers could detect even 1 ng/ml TnI displaying high affinity of aptamers towards TnI in Fig.3.1.

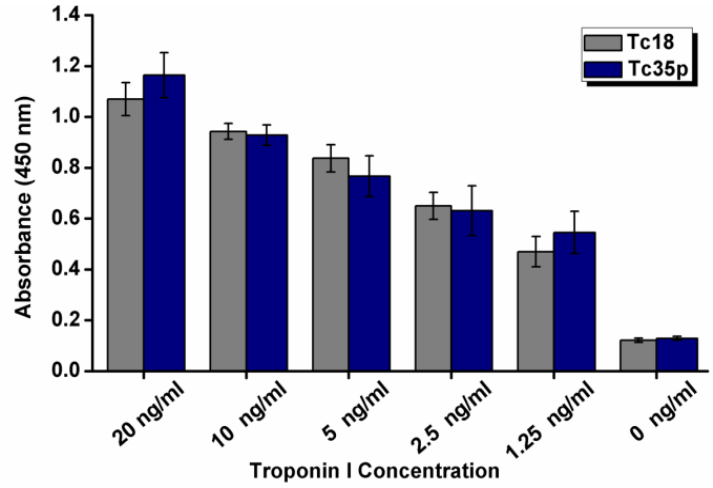

Fig.3.1 Indirect ELISA of aptamers binding varying dilutions of TnI

Moreover, when efficiency of aptamers was analyzed as match-pair in sandwich ELISA with commercial Mab, Tc18 surpassed Tc35p in binding TnI at low concentrations of 0.1 ng/ml avoiding any non-specific interactions [Fig.3.2(a) and (b)]. Therefore, it can be concluded that aptamers can function as efficient match-pair bioreceptors to design immunoassays for detecting TnI in trace levels.

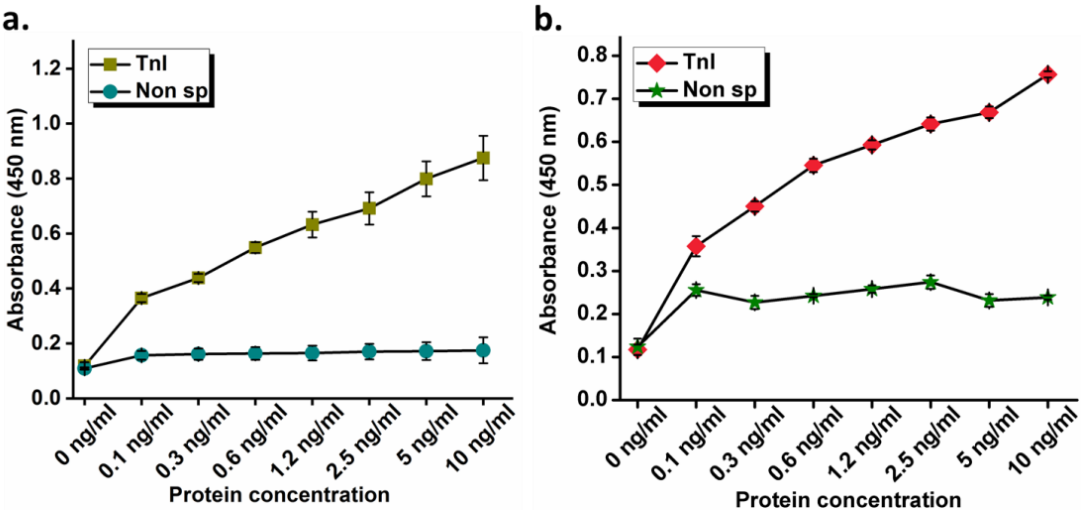

Fig.3.2 Sandwich microtiter assay of aptamers with Mab to detect TnI (a) Tc18 (b) Tc35p

3.3.2 Binding kinetics of aptamers with TnI

a. **Biolayer Interferometry:** The affinity of binding for aptamers with respect to varying dilutions of rTnI was estimated by performing BLI kinetics experiment. The dissociation constant (K_D) was calculated with *ForteBio* software analysis 9.0 using global fitting for association (k_{on}) and dissociation (k_{off}) curves in equimolar stoichiometric ratio that provided R^2 values of regression for data fitting (Table 3.1).

SR. No.	Aptamer	K_D	R^2
1.	Tc18	$2 \pm 0.16 \times 10^{-9}$	0.97
2.	Tc35p	$3.5 \pm 0.54 \times 10^{-8}$	0.95

Table 3.1 Dissociation constant values (K_D) of aptamers binding recombinant TnI protein

The K_D value represented an average of three independent runs for each TnI concentration [Fig.3.3(a) and (b)]. As evident from table, Tc18 shows higher binding affinity in terms of K_D that can be substantiated with its hair-pin loop like structural conformation studied in chapter 2. The structural integrity of both the aptamers enables their better interaction with TnI further supporting the ELISA results. Moreover, somewhat similar K_D values were obtained for BLI kinetics performed in serum with association and dissociation curves fitted globally providing a strong affinity of aptamers to recognize TnI in complex serum matrix [Fig.3.3(c) and (d)].

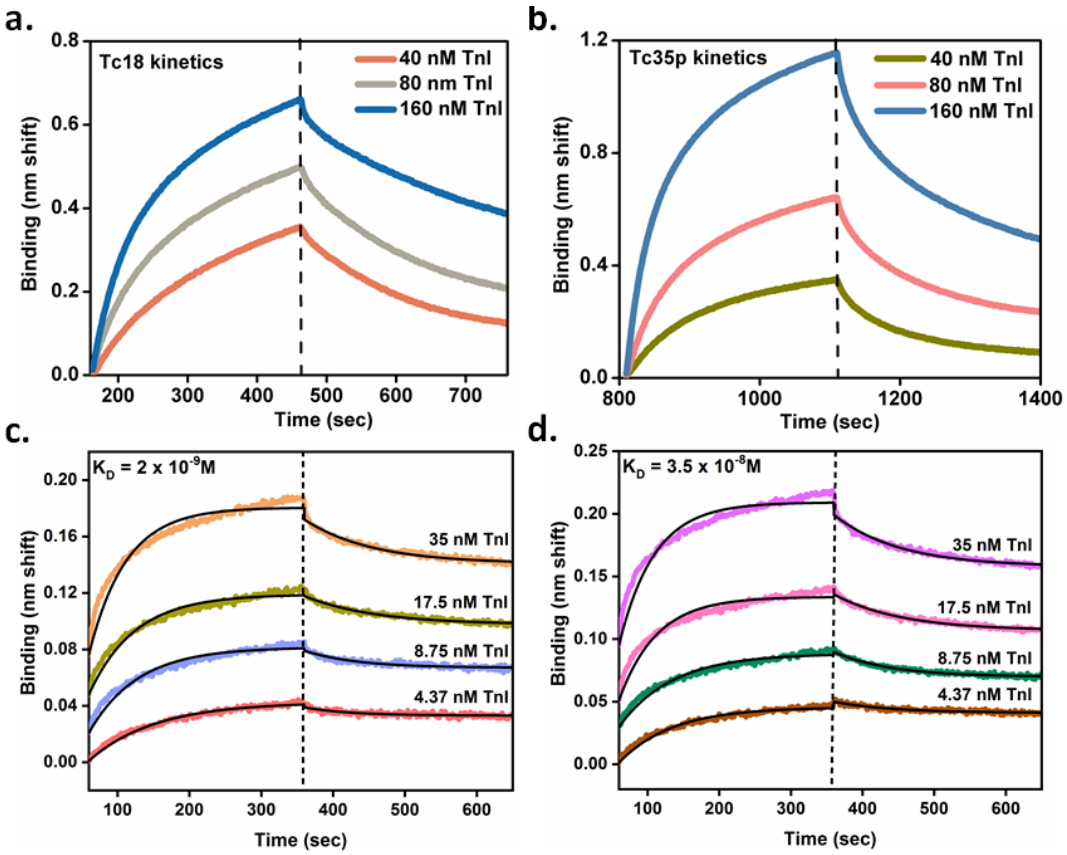

Fig.3.3 BLI sensograms showing binding kinetics for aptamers Tc18 and Tc35p respectively with varying dilutions of TnI (a and b) Assay in buffer and (c and d) Assay in spiked serum

b. Microscale Thermophoresis: MST technique was employed to validate the binding affinities of aptamers towards TnI protein obtained irrespective of dissociation coefficient calculated using BLI. An average dissociation constant of three MST experiments for each aptamer was calculated which was found in agreement with BLI data. Tc18 affinity of interaction with TnI was evaluated as K_D=27±0.47 nM and Tc35p was K_D=0.28±0.17x10^{-7}M.

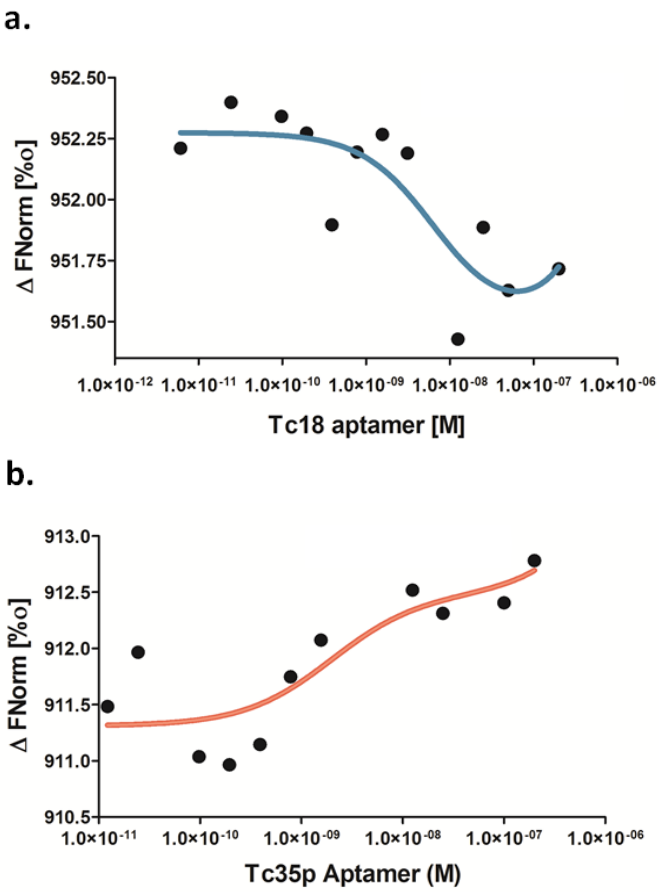

Fig.3.4 MST curves for affinity studies of aptamer towards TnI (a) Tc18-TnI (b) Tc35p-TnI

3.3.3 Conformational studies of aptamer-TnI interaction

CD spectroscopy with varying concentration of TnI was performed to decipher the alteration in secondary structures of aptamers upon binding with TnI. Each concentration was allowed to incubate prior to scan in 320-200 nm wavelength range. As evident from Fig.3.5(a) and (b) a consistent drop in peak at 220 nm with each increasing concentration of TnI was observed. This change from positive to negative ellipticity displaying a transition from B-DNA form to A-DNA (B-A transition) was indicative of strong conformational polymorphism in Tc18 and Tc35p secondary structure upon TnI binding [132]. Comparatively, Tc35p aptamer demonstrated subtle

changes in ellipticity measure than Tc18 which can be attributed to their respective secondary structure folding and nature of interaction with TnI. Both aptamers presented TnI induced structural switching corresponding to increase in TnI concentration.

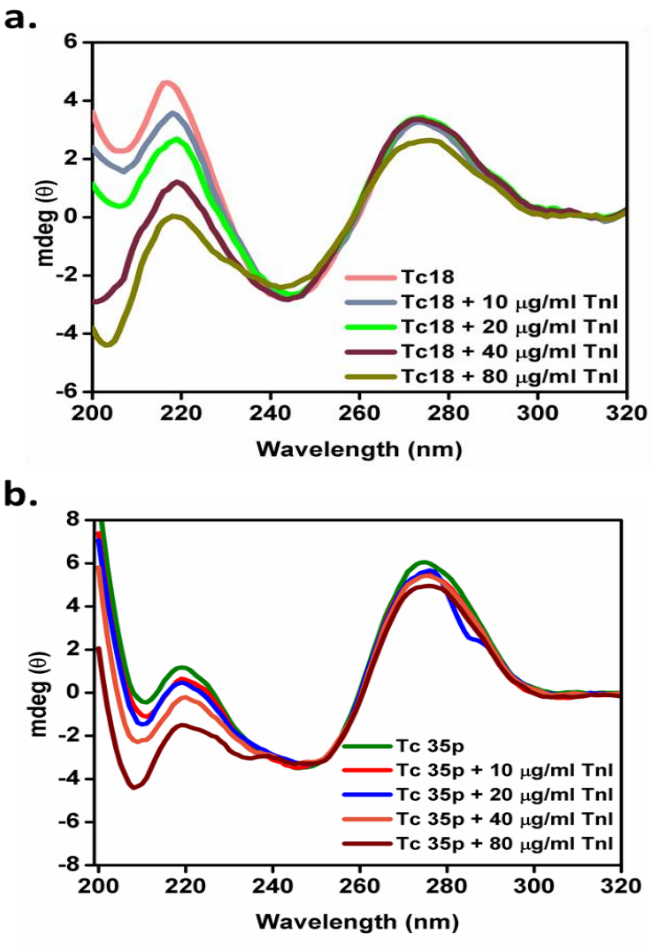

Fig.3.5 CD scans of aptamers showing structural-switching with increasing TnI (a) Tc18 (b) Tc35p

Moreover, differential CD experimentation was performed to analyze the efficiency of aptamer to sustain its structural integrity after interacting with TnI. CD scans of Tc18-TnI complex in Fig.3.6 deciphered B-DNA form of Tc18 which upon titration with consecutively increasing protein was dominated by α-helical CD signature of TnI. Gradual loss of Tc18 aptamer secondary structural content with appearance of TnI at equimolar ratio explained interaction of many aptamer molecules to single TnI molecule. This target induced conformational isomerization has been further corroborated with progressive signal loss of aptamer near 240 nm and 270 nm. As a consequence, we can infer that very small amounts of aptamers are required for designing TnI detection platforms.

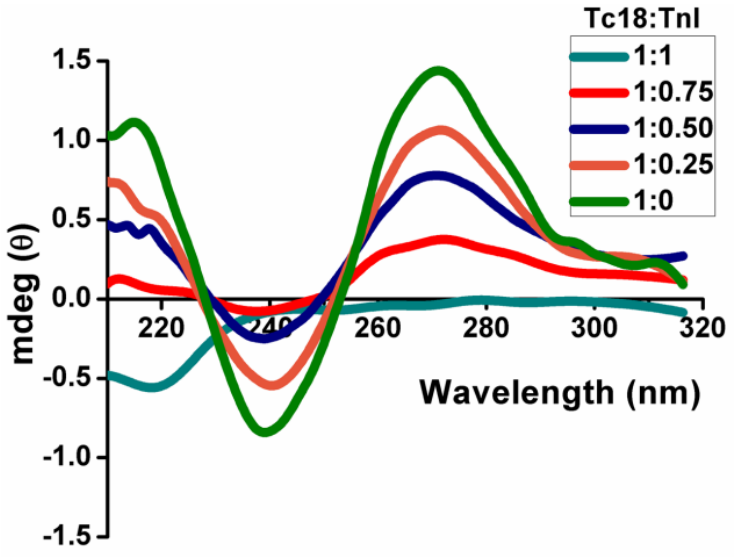

Fig.3.6 Differential CD of aptamer-TnI interaction showing loss in aptamer signal at equimolar ratio

3.3.4 Biophysical analysis for aptamer-TnI complex formation

a. Non-radioactive EMSA: Both aptamers were investigated for their ability to form complex with full TnI biomarker protein. Different concentrations of TnI were incubated at room temperature with both aptamers separately. As evident from Fig.3.7, a decrease in band intensity of Tc18 and Tc35p was observed with increasing TnI concentration suggesting the involvement of aptamers in forming complex with TnI [140]. Alternatively, it can be concluded that aptamer involved in complex formation experiences restricted mobility in agarose gel due to bulkiness of band that can be seen in the form of smearing. A non-specific aptamer was observed for binding with TnI as negative control.

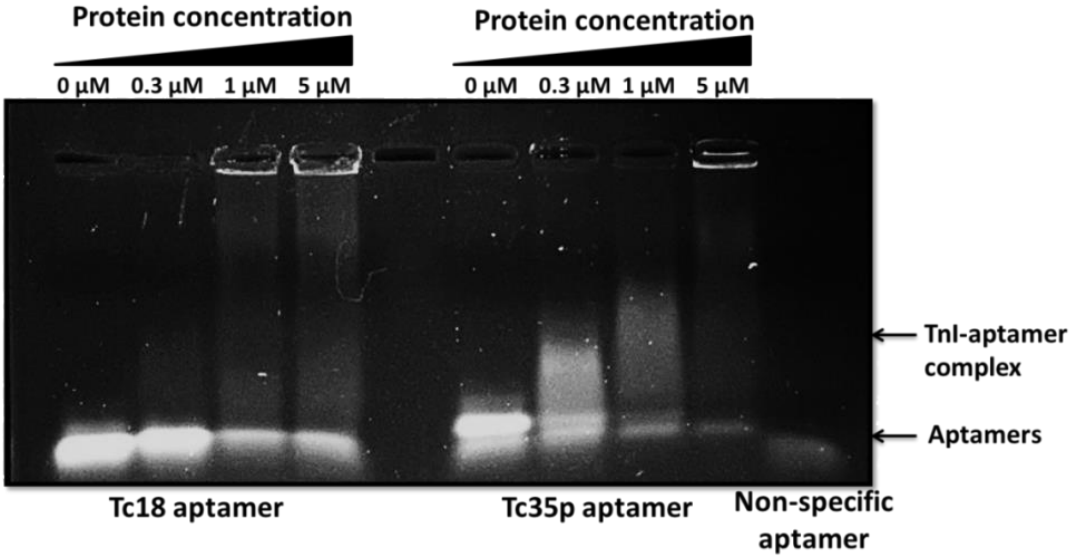

Fig.3.7 Non-radioactive EMSA gel of aptamer-TnI complex formation

The label-free gel shift assay for studying aptamer-TnI complex formation was further observed for a wide range of TnI from 0-150 µM. The relative difference in migration pattern of aptamer-TnI complex was compared to aptamer alone. Moreover, quantification of gel-shift assay was estimated in terms of measuring decrease in intensity of free aptamer with diminishing band using image processing software Image J. This decrease corresponded to engagement of aptamer Tc18 [Fig.3.8(a) and (b)] and Tc35p [Fig.3.8(c) and (d)] in complex formation with TnI [141].

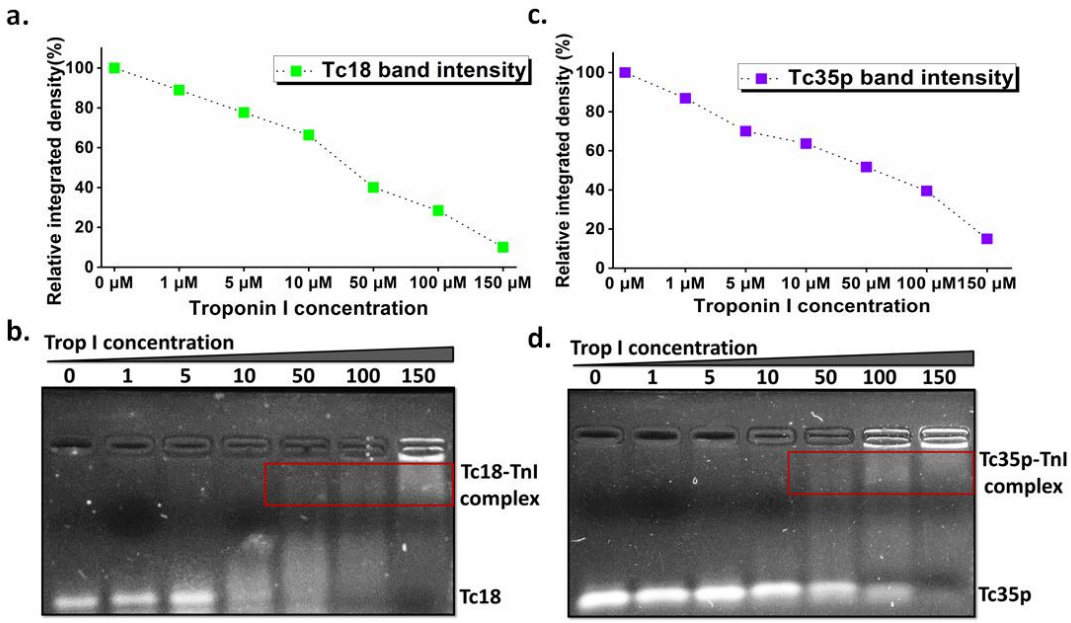

Fig.3.8 ImageJ analysis of decreasing unbound aptamer band intensity with gel-shift image showing bands for (a and b) Tc18 (c and d) Tc35p

b. AUC: Sedimentation velocity experiment (SV-AUC) was performed to analyze complex formation of aptamer-TnI that provided continuous distribution model for sedimentation coefficient distribution. The experiment provided sedimentation coefficient value (s) by solving the Lamn equation as Svedberg unit based on settling of complex and aptamers alone. The data was solved using SEDFIT-a software for analysis of AUC and other hydrodynamic data (NIH) [142]. As evident from Fig.3.9(a) and (b) an increase in sedimentation coefficient measured in Svedberg unit (S) was observed for aptamer-TnI complex as compared to aptamers. This was explained as heavier particles sediment faster and has higher Svedberg (s) due to change in shape after forming complex. The shape difference is resultant of mass to size ratios of complex compared to their individual shapes in unbound form. The bulky behavior as represented by enhanced sedimentation

coefficient is evident of stable complex formation in the form of single peak. It performs data analysis by setting meniscus from each end for raw data and processing parameters such as density, frictional ratio and output with least rmsd and accepted residuals.

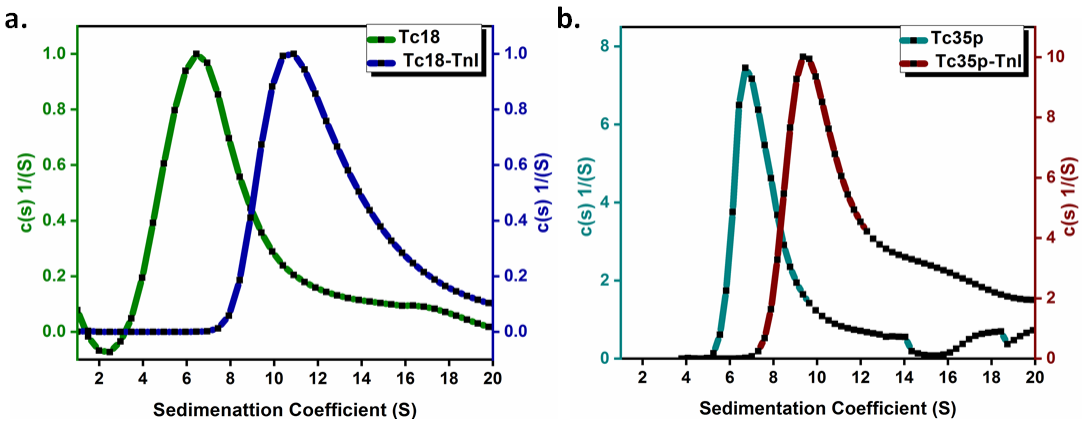

Fig.3.9 SV-AUC curves showing increase in sedimentation coefficient for (a) Tc18-TnI complex and (b) Tc35p-TnI complex; as compared to aptamers only

c. **Size exclusion chromatography:** SEC or gel filtration chromatography was employed for analyzing aptamer-TnI complex formation. An equimolar ratio of TnI-aptamer complex and TnI separately was injected into the column and examined for elution at different volumes. A single peak of Tc18-TnI and Tc35p-TnI complexes [Fig.3.10(a and b)] was observed deciphering their stable interaction in solution forming a complex. This can be verified by bulkiness of complex which elutes out prior than TnI.

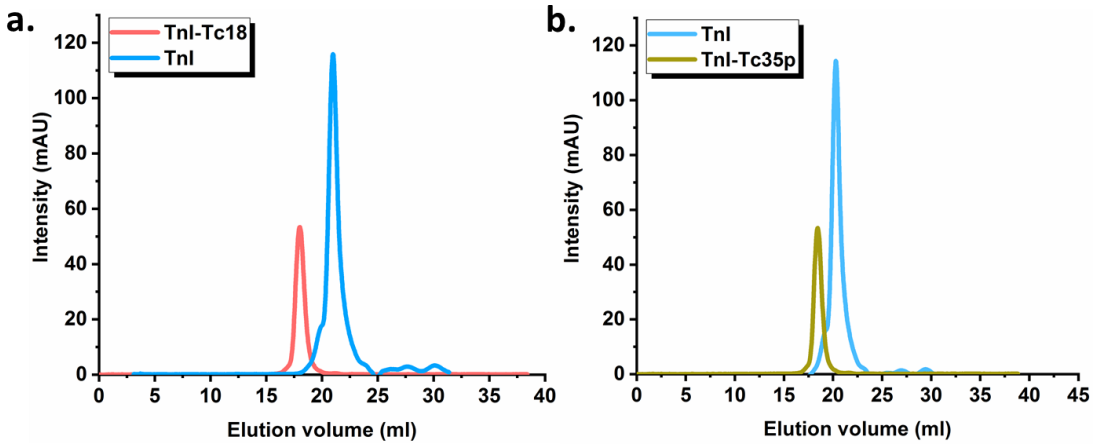

Fig.3.10 SEC purification curves of (a) Tc18-TnI complex (b) Tc35p-TnI complex; and TnI

3.3.5 Electrostatic surface potential and *in silico* docking studies

Electrostatic surface potential map of TnI was generated using PDB2PQR with color codes showing an overall charge of ±54.33 V which quantifies atom potentials and atom-by-atom contributions to solvation energy. The red (electronegative) and blue (electropositive) color depicted relatively more positive charge residues on clefts corresponding to C-terminal TnI fragment. This renders that region as an ideal docking site for negatively charged DNA aptamers (Fig.3.11).

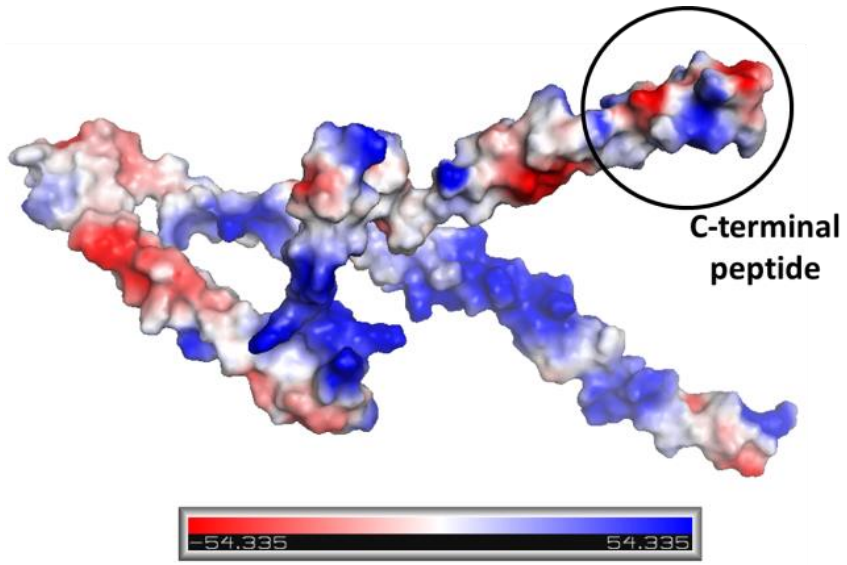

Fig.3.11 Electrostatic potential analysis of charge distribution on TnI structure

An elaborated flow-chart demonstrating the protocol followed for docking is depicted in Fig.3.12. HDOCK server was used for aptamer-protein docking by providing PDB files of receptor (TnI) and ligand (aptamers). HDOCK renders a user-friendly web server access to hybrid algorithm of template-mediated modeling and docking of protein–DNA complexes. It performed sequence similarity search and structure prediction providing top ten docked models as deduced by template based modeling. It efficiently integrates various sequence search components, model building, template selection and global docking exhibiting the binding site of both aptamers at C-terminal apical region of TnI. The first model with highest scoring was analyzed for identifying the binding residues involved in interaction of aptamer and TnI by using PDBsum generate.

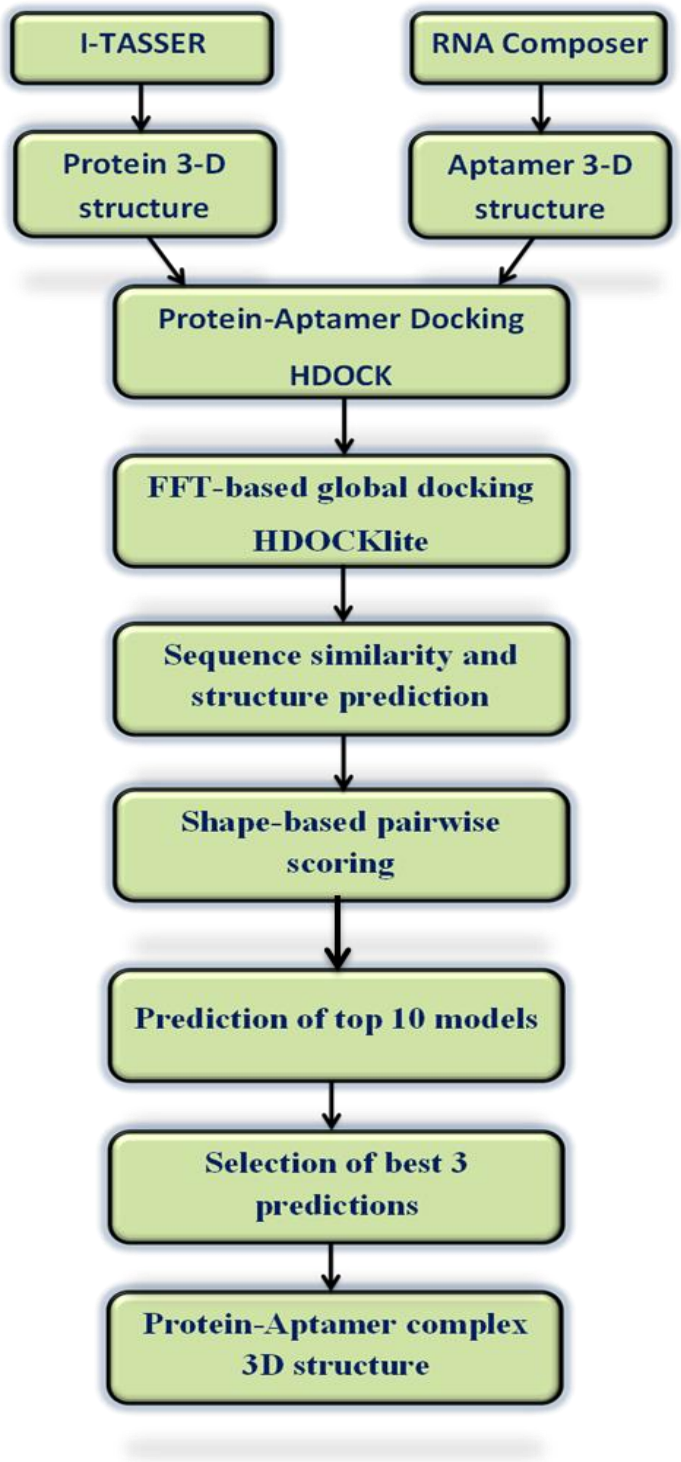

Fig.3.12 Flow-chart of aptamer-TnI docking studies

PDBsum Cleft analysis provided cavity/pockets present over the protein and their volumes that are involved in binding with ligand via hydrogen bonding. Table 3.2 enlists binding residues highlighted in structural map of TnI-Tc18 (Fig.3.13) and TnI-Tc35p (Fig.3.14) interactions with C-terminal fragment. PyMOL was used as visualization software to display binding residues within 4Å distance range [143].

S.R. No.	Troponin I-Aptamer	Residues of TnI and aptamer at binding interface	
1.	TnI-Tc18	Asp190-C43	2.2 Å
		Trp191-A42	3.3 Å
		Trp191-T33	2.6 Å
2.	TnI-Tc35p	Asp196-G8	2.9 Å
		Leu198-C37-P-C38	3.8 Å
		Asn194-A22	2.7 Å

Table 3.2 List of predicted binding residues involved in aptamer-TnI interaction

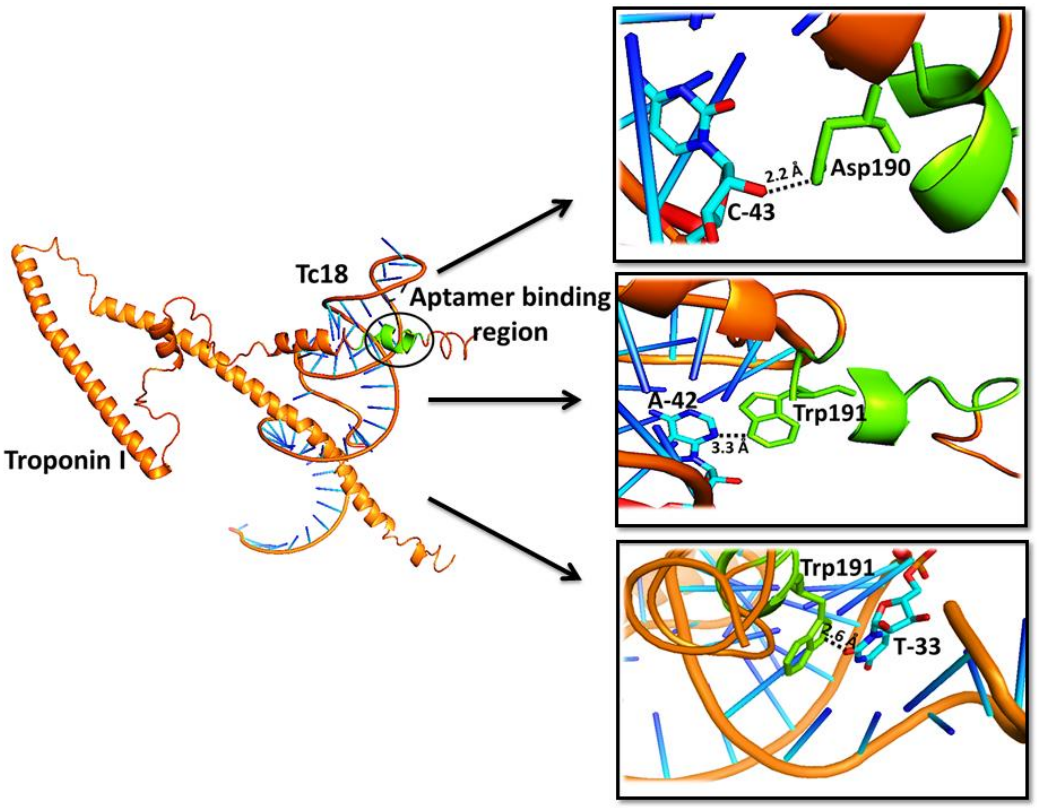

Fig.3.13 PDBsum generate analysis predicting binding-interface residues for Tc18-TnI interaction

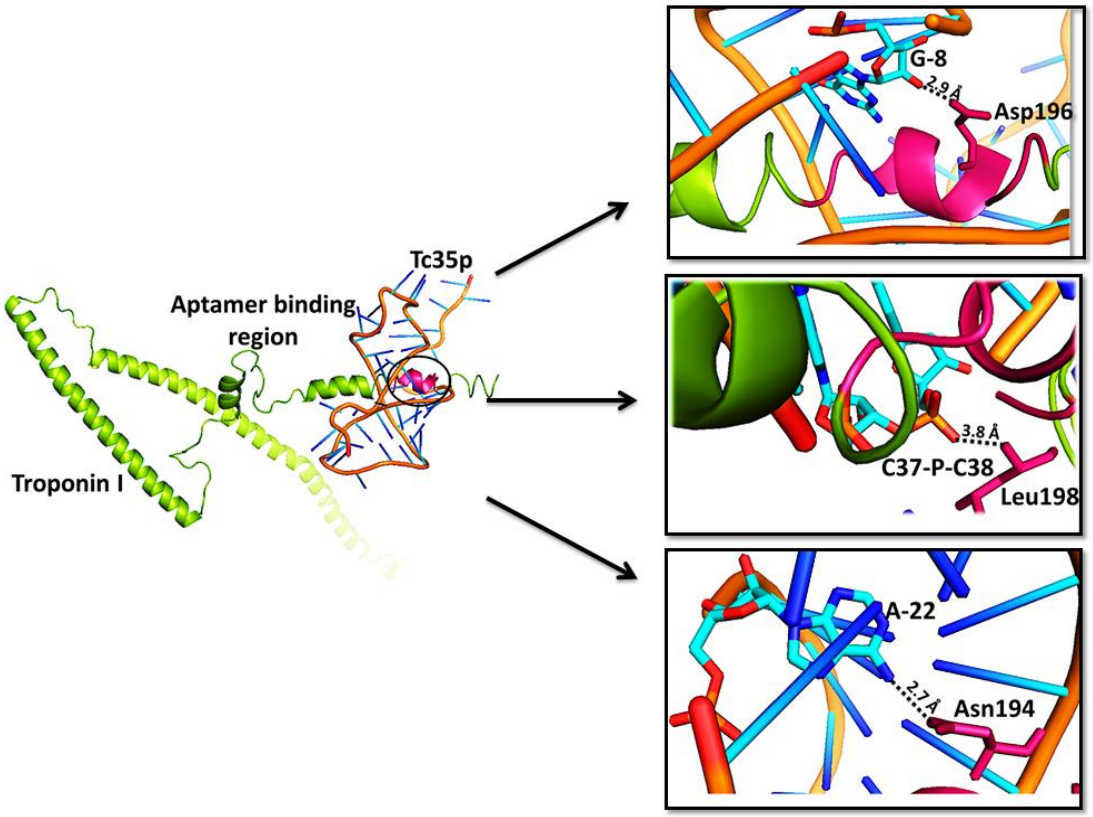

Fig.3.14 PDBsum generate analysis predicting binding-interface residues for Tc35p-TnI interaction

3.3.6 Peptide interaction studies with TnI

The development of aptamer-aptamer assays may pose similar charge based repulsion; therefore, synthetic peptide synthesized by Banta et al as discussed in the last chapter (Section 2.7) was studied for its interaction with TnI. Moreover, dual aptamer poses the limitation of steric hindrance in designing platforms.

a. BLI binding kinetics was performed with peptide as a function of TnI concentration with intermittent washing and regeneration. AR2G sensor was immobilized with 50 µM peptide and was dipped in wells containing varying TnI dilutions for 300 sec of association and dissociation each. K_D=4.46±1.5x10^{-8} M was achieved by using global fitting analysis with R^2=0.96 Fig.3.15(a).

b. *In silico* docking studies were performed to predict interaction of peptide specific for TnI using GRAMM X-a protein-protein docking tool. PDB files of TnI receptor generated by I-TASSER and peptide ligand by PEP-FOLD was submitted as input. It employed smoothed potentials, knowledge-based scoring to produce an average of 100 predictions as output. Our findings in conjunction to a recent

report also predicted that Lys58 and Glu66 of TnI are non-covalently linked with Trp10 of peptide in Fig.3.15(b) [144]. PyMOL was used for molecular visualization of PDB files [143].

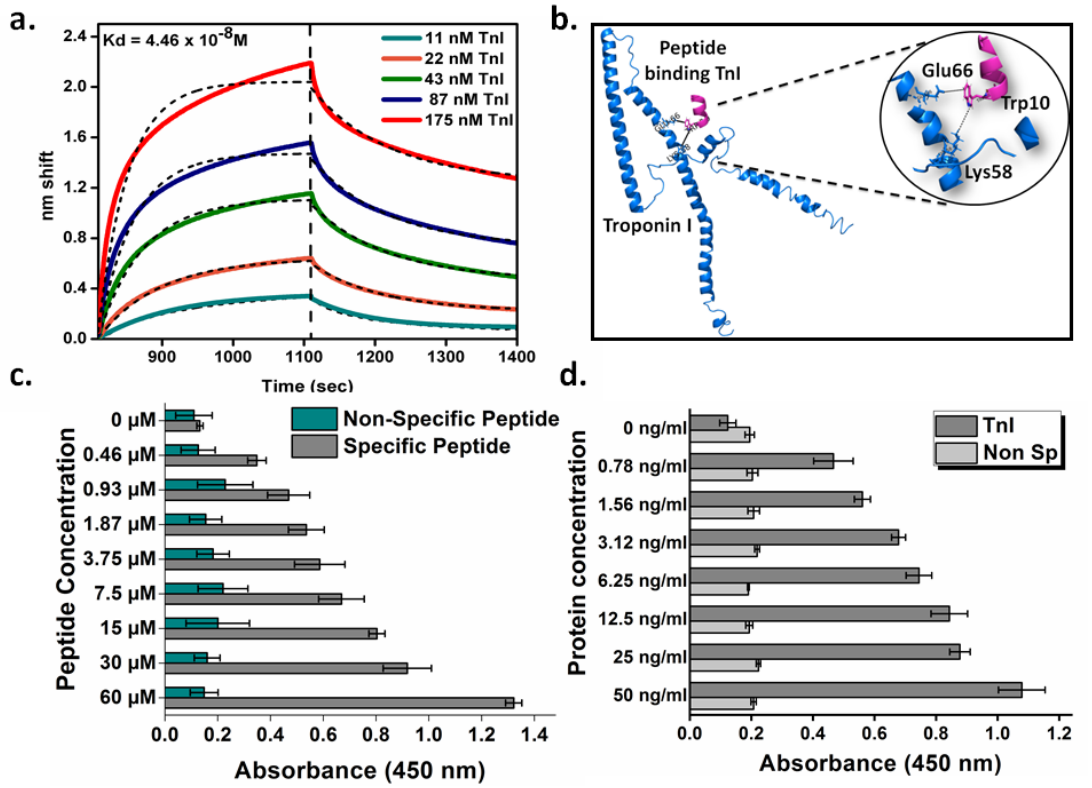

Fig.3.15 Peptide-TnI binding characterization (a) BLI sensogram of peptide binding with varying TnI dilutions (b) Docking studies of peptide-TnI highlighting binding residues (c) Indirect binding ELISA of varying peptide dilutions with TnI (d) Sandwich ELISA of peptide to detect TnI with commercial Mab

c. To further investigate interaction of peptide with TnI, indirect binding ELISA was performed for which peptide was labeled with biotin. Briefly, 2.5 µg/ml TnI was coated for overnight onto plate which was blocked with 2% BSA solution for 2 hours. Biotinylated peptide was added from 0-60 µM followed by incubation for 2 hours at 37˚C. The detection was done by using HRP labeled streptavidin. Peptide was able to target 0.1 ng/ml TnI without any non-specific interaction displayed in Fig.3.15(c). Additionally, sandwich ELISA of peptide was performed wherein, 10 µg/ml of BSA peptide conjugate was immobilized and TnI dilutions was detected using anti-TnI commercial Mab in Fig.3.15(d). Peptide is able to detect TnI in sandwich ELISA configuration as well upto 0.7 ng/ml.

3.4 Conclusion

This segment of work encompasses interaction patterns of aptamers-Tc18 and Tc35p towards full cardiac TnI protein. The **binding affinity** of aptamer was quantified with respect to TnI concentration by various biophysical techniques comprising **BLI and MST** in terms of dissociation constant (K_D). As a result, Tc18 displayed $K_D=2x10^{-9}M$ that certainly surpasses $K_D=3.5x10^{-8}M$ of Tc35p in binding kinetics studies. BLI kinetics experimentation performed in human serum spiked with varying TnI deduced similar K_D values as with physiological buffer experiments. This was further substantiated by MST calculated K_D values that further validated the dissociation constant values as $K_D=0.60x10^{-9}M$ for Tc18 and $K_D=0.28x10^{-7}M$ for Tc35p.

To this context, both aptamers were subjected to **microtiter binding assays** where aptamers was examined to bind varying TnI dilutions which demonstrated the ability of aptamers to efficaciously bind 1 ng/ml TnI. Further, sandwich microtiter ELISA demonstrated 0.1 ng/ml TnI detection by both aptamers suggesting their applicability as match-pair bioreceptors. Both the approaches of binding affinity studies by BLI/MST and quantification studies via microtiter assays displayed Tc18 as compared to Tc35p a better binder interacting with TnI.

Furthermore, **conformational changes in aptamer** upon TnI binding were investigated through **CD spectroscopy**. The apparent structural modification upon TnI binding in Tc18 was comparatively significant due to hair pin loop-like conformation that opens up to bind the target as compared to Tc35p. Additionally, differential CD experiment deciphered the requirement of only trace amounts of aptamer to detect TnI.

Next, we studied the **complex formation property of aptamer**-TnI by using biophysical characterization techniques of **AUC, SEC and non-radioactive EMSA**. The increase in sedimentation coefficient Svedberg's unit confers to formation of aptamer-TnI bulky complex as single entity compared to aptamer as control. Moreover, the restriction in mobility of bulky aptamer-TnI complex was analyzed by non-radioactive gel shift assay. As concentration of TnI increased in aptamer-TnI mixture, the band intensity of aptamer diminished due to indulgence of aptamer in

complex formation with TnI. Simultaneously, GFC purification as per its principle eluted aptamer-TnI complex prior to TnI protein as a single peak. Thus, consequently we can conclude that aptamer can interact with TnI via its C-terminal tail and forms a stable complex in solution as single biomolecular entity. The attribute of stable complex formation can enable these aptamers to pursue relevance in immunodiagnostic assays for TnI detection. The *in vitro* results of aptamer-TnI interaction studies have been supported by *in silico* docking studies that has provided nucleoside bases of aptamer involved in binding with amino-acid residues of C-terminal region of TnI. The residues of Tc18 have been predicted from the bottom loop region whereas residues of Tc35p have been predicted from stem region to bind TnI. This further supports our study inferences of all the assays stating **Tc18 to be a better binder than Tc35p**.

After digging deeply into interaction and binding pattern of aptamers with TnI, it was concluded that aptamers undergo structural changes that can be targeted for designing detection platforms. As deciphered from biophysical and biochemical characterization of aptamer-TnI binding, Tc18 has demonstrated better competency towards interacting with TnI protein via its C-terminal region. Moreover, their stable complex formation can render development of rapid detection strategies with utmost sensitive targeting of TnI. In this regard, preliminary biosensing platforms were designed using simple immunodiagnostic assays discussed in the next chapter to detect TnI.

Chapter 4

Immunoassays for detection of cardiac Troponin I

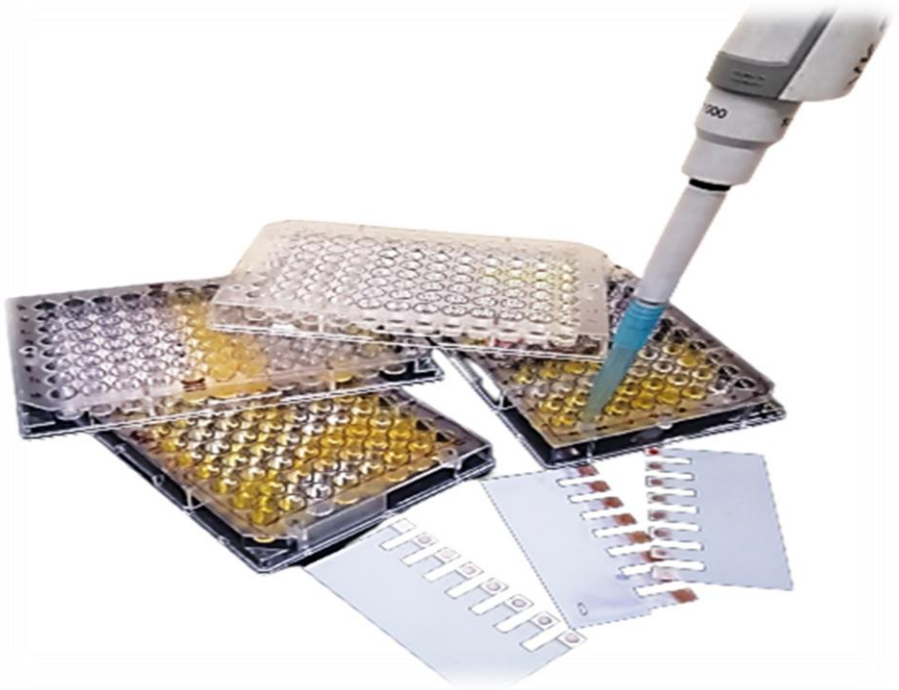

4.1 Overview

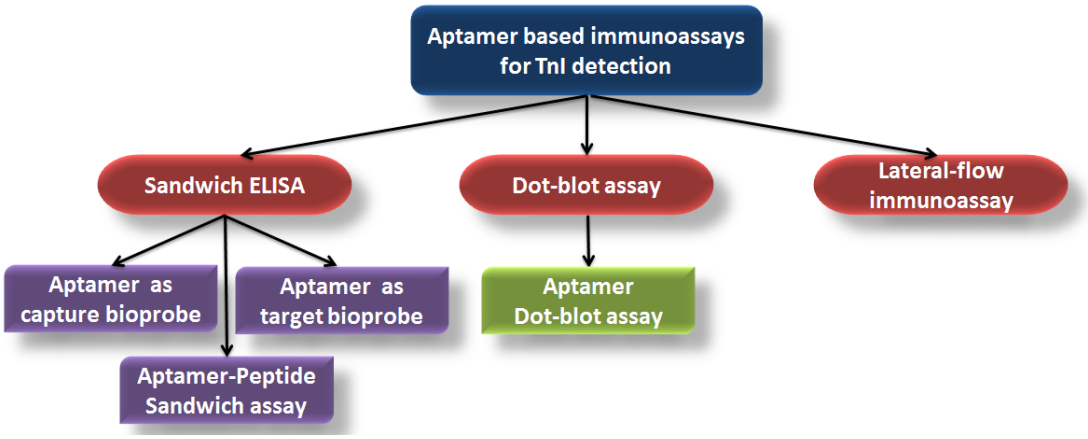

Microtiter immunoassays employ antigen-antibody interactions to study presence of any protein biomarker [145]. Antibodies based ELISA adds more cost to the entire test due to its production requiring animal that causes batch-to-batch variation. Moreover, the steric hindrance associated with huge molecular weight of antibodies compromise with sensitivity of the assays promoting non-specific interactions. In marked contrast to this, aptamers or synthetic peptides based assays deliver stable molecular probe replacements for antibodies in assays known as ELASA/ELONA [146–148]. This chapter describes the utility of aptamers generated against the apical C-terminal region of TnI in developing sandwich immunoassay TnI detection platform. Alongside, a novel match-pair of aptamer-peptide bioreceptors have been used to design the immunoassay completely eliminating the utility of polyclonal antibodies.

Simultaneously, aptamer based dot blot/aptablotting have been discussed in this chapter that is an easy, rapid and cost effective technique commonly used in detection of biomarker proteins in a biological sample [149]. As compared to ELISA, they are distinct type of diagnostic assays that circumvent the need of enzyme conjugates and can be performed within shorter duration of time requiring very less sample spotted directly onto membrane. Tc18 aptamer has been conjugated onto gold nanoparticles (GNPs) to investigate their binding efficacy as nanobioprobe for detection of TnI. The corresponding LSPR effect generated by aptamer gold nanoconjugates further allows visible naked-eye sensitive detection of TnI [150]. This has been further extended to develop lateral-flow immunoassay.

4.2 Experimental approaches

4.2.1 Materials and Instrumentation

Trisodium citrate dehydrate, Hydrogen tetrachloroaurate (III) trihydrate, (3-Glycidyloxypropyl) trimethoxysilane (GOPS), Monobasic dihydrogen phosphate and Dibasic monohydrogen phosphate, Bovine serum albumin (BSA), TMB substrate and Silver enhancement kit were from Sigma Aldrich (India). 5′ biotin labeled aptamers Tc18 and Tc35p and thiol modified Tc18 aptamer with a -S-S-$(CH_2)_6$ linker at 5′ end was procured from IDT technologies. The selected TnI binding peptide with a cysteine moiety at 5′ end was chemically synthesized and HPLC purified by our own peptide synthesis facility [104]. Recombinant TnI and commercial human heart TnI (Sigma) was used as targets. Dipstick nitrocellulose (NC) membrane used for dot-blot assay was taken from MDI. Anti-TnI monoclonal antibody was taken from Cloud-clone Corporation. HRP-labeled secondary antibodies were purchased from Sigma. All experiments were performed in 1xPBS (pH 7.4) and glasswares were rinsed with aqua regia further retreated with GOPS prior to use.

UV-Visible spectroscopy measurements were taken using BioTek Synergy H1 spectrophotometer (UK). Transmission electron microscopy (TEM) was performed using JEOL 2100 (USA). Gel based characterizations were done with BioRad gel assembly. Malvern Zetasizer was used for DLS measurements.

4.2.2 Immunodiagnostic assays

The assay is composed of aptamers based sandwich ELISA platform in two formats to detect TnI. Firstly, aptamers serve as capture bioprobes wherein the aptamers are immobilized onto the surface of microtiter plate. Secondly, aptamers serve as target bioprobes that comprises of reverse configuration targeting TnI from above. In both variants, anti-TnI PolyAb is used in combination serving as second bioreceptor to form sandwich. Lastly, an aptamer-peptide based sandwich ELISA is performed as novel match-pair to detect TnI. The efficacy of aptamers in sandwich assays is validated by spiking commercial human heart TnI in serum.

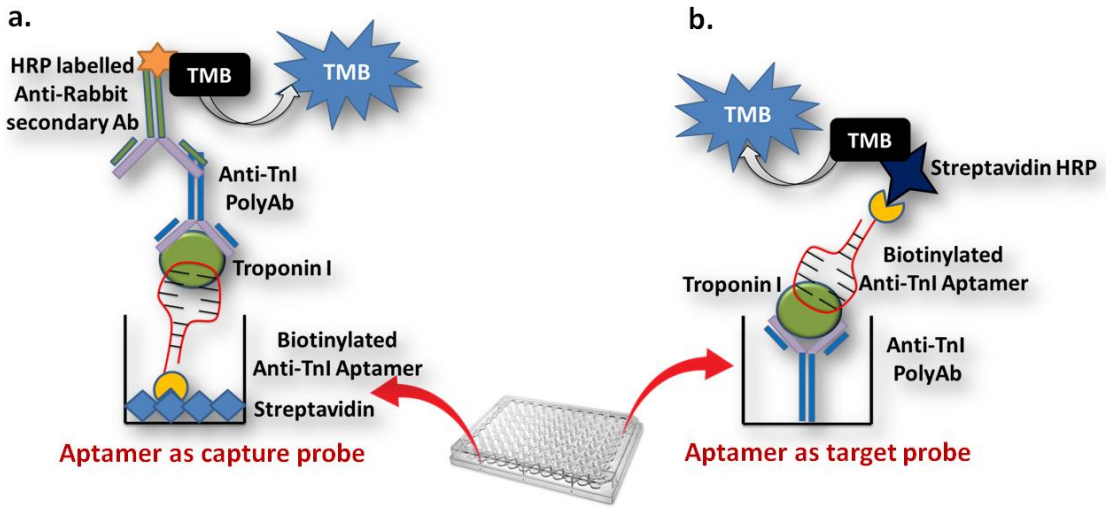

Fig.4.1 Schematic representation of aptamers in sandwich ELISA platform for TnI detection as (a) Capture probes (b) Target probes

a. Aptamer as capture probes

A sandwich microtiter assay was performed wherein biotin labeled aptamers Tc18 and Tc35p were captured onto the surface as illustrated in Fig.4.1(a). Briefly, 3 µg/ml streptavidin in 10 mM bicarbonate buffer (pH 9.5) was incubated overnight at 4˚C. After 3x washing using 1x PBST (0.1% Tween 20), wells of microtiter plate was blocked with 3% BSA made in 1x PBS (pH 7.5) for 2 hours. Then, 500 nM biotin labeled Tc18 and Tc35p aptamers preheated at 95˚C was added and allowed to bind with streptavidin at 37˚C for 2 hours. Post washing unbound aptamer, TnI along with non-specific protein control was added in 0.4-25 ng/ml dilutions following incubation at 37˚C for another 2 hours. Afterwards, rabbit anti-TnI PolyAb was added in 1:1500 µl dilution (approx. 30 µg/ml) into each well and was allowed to bind TnI for another 2 hours. Anti-rabbit HRP labeled secondary antibody was added following 1 hour incubation. TMB solution was added for color development which was ceased by adding 2N H_2SO_4 stop solution when signal started to develop in no protein control.

b. Aptamer as target probes

Aptamers were used in reverse configuration wherein 3 µg/ml PolyAb was coated onto microtiter wells using 10 mM bicarbonate buffer (pH 9.5) with overnight incubation at low temperature. The wells were washed using 1x PBST for removal of excess unbound Ab and blocked with 3% BSA solution for 2 hours. TnI was added in a concentration varying from 0.1-20 ng/ml and plate was kept for 2 hours

at 37˚C. After repeated washing, 500 nM biotinylated Tc18 and Tc35p aptamers were added as target bioprobes [(as illustrated in Fig.4.1(b)] alternatively after heating for 5 min at 95˚C and cooling back to normal in ice. HRP labeled streptavidin in 1:5000 µl dilution was added for 1 hour for obtaining signal.

The capability of aptamers to detect TnI in real samples was investigated by performing the above designed sandwich assay platforms in serum spiked with commercial human heart isolated TnI. Both versions of aforementioned assays were adopted in 1:10 µl diluted serum sample of healthy subject. The assays were optimized by performing in triplicates. A standard calibration curve for sandwich assays of aptamers was plotted as TnI concentration (ng/ml) against mean absorbance at 450 nm to identify TnI concentration in any unknown sample.

c. Peptide-Aptamer match-pair immunodiagnostic assay

Aptamer was also interrogated in combination with commercial peptide to detect TnI studied from literature by Banta's group, previously mentioned in second chapter. A sandwich based microtiter assay was performed wherein 10 µg/ml peptide conjugated with BSA carrier protein was coated onto polystyrene wells using 10 mM bicarbonate buffer (pH 9.5). Next day, plate was washed with 1x PBST and blocked with 5% skim milk for 1.5 hours and 0.4-50 ng/ml dilutions of TnI was added. The plate was incubated for another 2 hours at 37˚C and 500 nM biotinylated Tc18 and Tc35p aptamers were added in alternate assays. Both aptamers were heated at 95˚C for 5 min and cooled to normal to attain its conformational folding for binding TnI. After repeated washing, streptavidin-HRP in 1:5000 µl dilution was added for detection. Similarly, the unique combination of aptamer-peptide match-pair was used to detect commercial TnI spiked in human serum along with a standard curve.

4.2.3 Aptamer based immunodiagnostic assay verification in clinical samples

A total of 40 AMI clinical samples and 20 healthy samples were obtained from PGIMER, Chandigarh. Serum was separated from blood and stored for long term at -20˚C.

a. For performing aptamer based sandwich immunoassay with clinical samples, 3 µg/ml streptavidin was coated for overnight onto polystyrene wells of ELISA nunc plate at 4˚C. The plate was washed three times with 1x PBST and blocked

with 3% BSA solution for 2 hours. Afterwards, biotinylated Tc18 and Tc35p aptamers were added post denaturing them for 5 min at 95˚C. After 2 hours of incubation, all positive and negative samples (1:1 dilution in 1x PBST) were added in duplicates and allowed to bind for another 2 hours at 37˚C. Rabbit anti-TnI PolyAb was added for 2 hours and detection was done via HRP labeled anti-rabbit secondary antibody.

b. The selectivity of both aptamers to specifically detect TnI in clinical specimens was examined by spiking probable biomarkers in 1:10 µl diluted serum that can be found in circulation. Thyroglobulin, Lactalbumin, Lysozyme, BSA, NT-Pro-BNP, BNP, Myoglobulin were spiked in sufficiently higher concentrations in healthy serum along with a clinical sample of AMI patient containing TnI. Sandwich ELISA was performed wherein Tc18 and Tc35p aptamers were used as capture probes along with anti-TnI PolyAb.

c. The control experiments were performed with two randomly selected AMI positive samples. Briefly, streptavidin coated plates were used to capture biotinylated Tc18 and Tc35p aptamers and both AMI serum samples were added followed by incubating plate for 2 hours. Anti-TnI PolyAb was added in 1:1500 µl dilution which was recognized by HRP labeled anti-rabbit secondary antibody.

4.2.4 Aptamer as nanobioprobe: Dot-blot assay

Drawing conclusions from the results discussed in last chapter, Tc18 was found to be a better binder as compared to Tc35p. Therefore, applicability of Tc18 aptamer was expanded to design nanobioprobe for performing naked-eye visible analytical dot-blot assay. To this context, thiolated Tc18 aptamer was conjugated onto gold nanoparticles for directly detecting TnI spotted on nitrocellulose (NC) membrane dipsticks. The assay was further extended to detection of commercial TnI spiked in human serum as well. Moreover, the sandwich novel match-pair of aptamer-peptide was also examined separately.

a. Synthesis of aptamer gold nanoconjugates and its characterization

GNPs were synthesized by citrate reduction method as reported in literature [151]. Briefly, 50 ml solution of 0.01% (w/v) $HAuCl_4$ in milli-Q water was boiled following subsequent addition of 1 ml tri-sodium citrate 0.1% (w/v) with vigorous

stirring. Gradually, red color colloid solution started forming within fraction of minutes when tri-sodium citrate reduced Au (III) ions. The gold colloid solution was put to boiling again under stirring for another 10 minutes.

Freshly prepared GNPs were primarily washed and concentrated to OD 1 @ 520 nm corresponding to approximately 7.00×10^{11} particles/ml which were used to perform all the experimentation [152]. For bioconjugation, 1 μM Tc18 aptamer thiol-linkage was reduced with 0.1 M DTT solution with 37˚C incubation for 30 minutes making final volume to be 200 μl [153]. DTT prevents formation of any disulphide bond between aptamers allowing direct contact of free SH groups with GNPs [154]. After reduction, thiolated aptamer was dialyzed for 2 hours against 10 mM PB (pH 8) and added dropwise to concentrated GNPs under constant rotation in a round bottom flask [155] [156]. Afterwards, GNP-A solution was purified by washing 3x by milli-Q water at 9500 g for 20 minutes and pellet was suspended in PB (pH 7.5). The prepared GNPs and GNP-A were characterized by UV-spectroscopy, DLS, TEM and agarose gel shift.

Characterization: Diluted samples of GNPs and nanoconjugates of GNP-A were prepared by resuspending in 10 mM PB (pH 7.5). Respective drops of both samples were placed onto carbon coated TEM grids until drying. Extra solution was removed and negative staining via 2% phosphotungstic acid (PTA) was done for 30 minutes for GNP-A. Diluted samples of GNP and nanoconjugates GNP-A were subjected to size measurement in Malvern zetasizer. UV measurement for both GNP and GNP-A was measured by taking spectrum at λ 400-700 nm to measure shift in gold plasmon post conjugation of aptamer.

b. Aptamer nanobioprobe based dot-blot assay

3 μl TnI dilutions from 0.001-1000 ng/ml was spotted onto NC membrane dipsticks containing 50 μg/ml BSA in 1x PBS (pH 7.5) and incubated at room temperature for 2 hours. The vacant sites on membrane were blocked with 2% BSA solution for 30 minutes. After blocking, membrane was dipped in concentrated GNP-A solution for 2 hours. Post binding of GNP-A with TnI, membrane was washed thrice for 1 minute each with block buffer. The blots

were developed by adding equimolar volume of both solutions in silver enhancing kit until desired intensity coloration was seen with respect to control. The membrane was rinsed in DI water to remove extra silver stain solution. The photographic images were captured and quantification of spots was done using ImageJ analyzer that determined raw integrated density of spots corresponding to TnI concentration. Various other cardiac biomarkers such as N-terminal-pro BNP (NTP), Brain Natriuretic peptide (BNP), Myoglobin and other proteins BSA were also investigated for the unambiguous selectivity and specificity of assay. Similarly, dot-blot assay was performed for commercial human heart TnI spiked in 1:10 µl diluted healthy sera samples in 1x PBST. A calibration curve was plotted for spot density corresponding to TnI concentrations using ImageJ.

4.2.5 Aptamer based Lateral-flow immunoassay (LFIA)

The Tc18 aptamer was further studied to detect TnI on paper based LFIA for developing a rapid TnI detection test. Briefly, Tc18 were conjugated onto GNPs as discussed above to develop gold nanobioprobes which was adsorbed onto conjugate pads along with 10 µl of 5% sucrose followed by speed drying under vacuum at 30˚C for 30 min hours. Alternatively, 2mg/ml of anti-TnI PolyAb was lined onto NC membrane and dried at 37˚C for 1 hour. The membrane was then blocked with 2% PVA containing 1% skim milk for 15-20 min under shaking conditions. Post blocking, the strips were washed twice with blocking buffer for 5-10 min under shaking and dried at 37˚C for 20 min. The various components of LFIA were assembled as sample pad and conjugate pad containing GNP-A nanobioprobe at one extreme end and absorbent pad on the other side of NC membrane. Various Tn dilutions from 0.1-1000 ng/ml along with two non-specific control cardiac biomarker-BNP and NT-Pro-BNP were added onto sample pad and capillary action was observed for development of color onto test line.

4.3 Results and discussion

4.3.1 Aptamer based sandwich ELISA

Tc18 and Tc35p aptamers were investigated as efficient probes to detect TnI via sandwich microtiter assay. In first version, both aptamers were used as **capturing**

bioreceptors using avidin-biotin linkage to bind TnI from its apical peptide region. While PolyAb targeted TnI from above by multiple epitopic sites; thereby enhancing the signal intensity. Both the aptamers displayed sensitivity upto 0.4 ng/ml of TnI as seen from absorbance at 450 nm without any non-specific interactions in Fig.4.2(a).

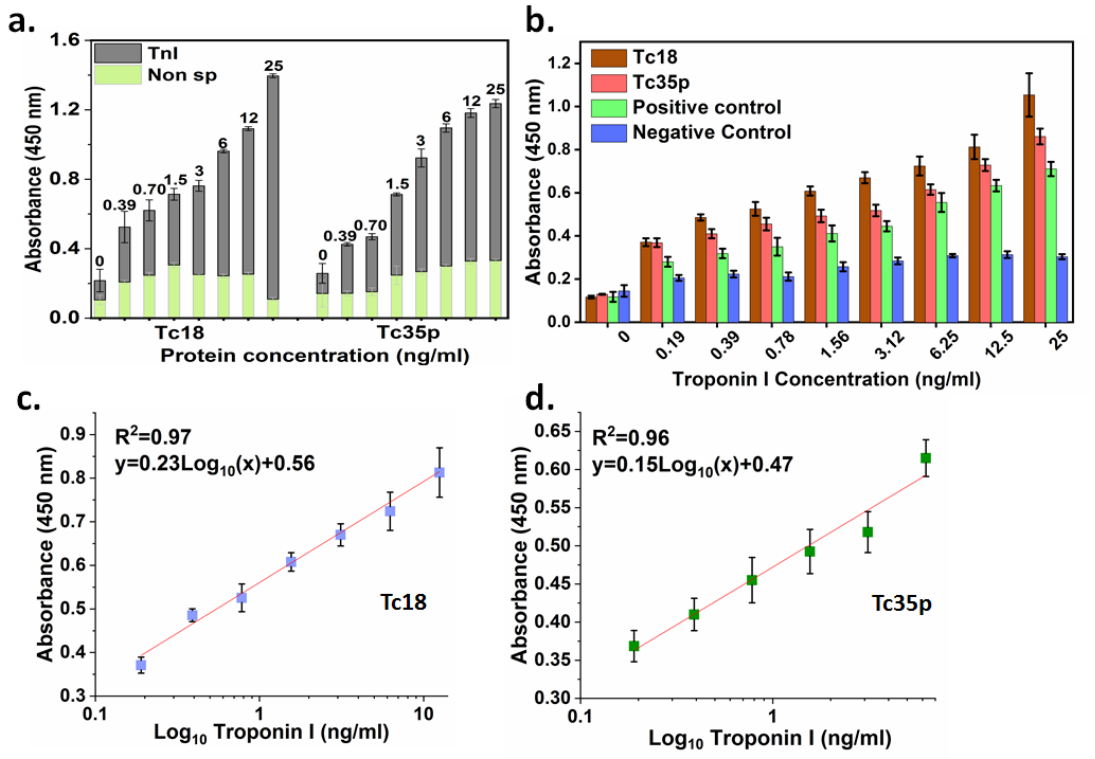

Fig.4.2 Sandwich ELISA of **Tc18 and Tc35p aptamers used as capture probes** (a) Aptamers detecting TnI in experimental buffer (b) Aptamers detecting commercial human heart TnI spiked in serum along with positive control Tro4 aptamer (c) and (d) Calibration curves of both the aptamers Tc18 and Tc35p for serum spiking studies

The performance of aptamers as capture probes was also examined to detect commercial human heart TnI spiked in healthy serum sample. A positive control aptamer (Tro4) selected from literature generated against full length TnI was also investigated along with Tc18 and Tc35p aptamers [117]. As observed in Fig.4.2 (b) both the aptamers could target as low as 0.2 ng/ml of TnI delineating their exceptional target specificity in complex matrix. Both aptamers were observed to perform better than commercial Tro4 aptamer. A calibration curve for each aptamer was plotted to identify TnI concentration in unknown sample in Fig.4.2(c) for Tc18 and (d) for Tc35p.

Simultaneously, potency of aptamers Tc18 and Tc35p was displayed for recognizing TnI as **target bioreceptors**. In reverse configuration, only Tc18 detected TnI, probably due to its flexible hair-pin loop like structure whereas Tc35p did not. It was speculated that long stem-loop straight conformation of Tc35p offered steric hindrance in binding TnI along with PolyAb in sandwich ELISA format. The assay displayed sensitive TnI detection for Tc18 at 0.15 ng/ml avoiding non-specific interactions in Fig.4.3(a). The competence of Tc18 as an effective target bioprobe was also displayed to detect human heart TnI spiked in complex serum medium in Fig.4.3(b). As a result, efficient response of Tc18 aptamer target probe was observed that was plotted as standard curve showing linear fitting for TnI dilutions Fig.4.3(c).

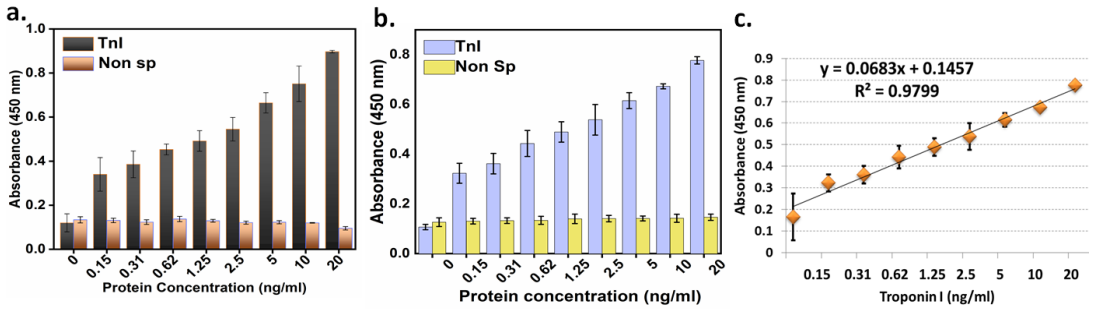

Fig.4.3 Sandwich ELISA of **Tc18 aptamer used as target probe** (a) Tc18 detecting TnI in experimental buffer (b) Tc18 detecting commercial human heart TnI spiked in serum (c) Calibration curve of Tc18 aptamer for serum spiking studies

4.3.2 Aptamer-Peptide match-pair sandwich ELISA

The peptide used here was selected from the literature synthesized by Banta *et al* that has been mentioned in the second chapter. As inferred from the last chapter that aptamer binds at C-terminal region and peptide binds distantly; this unique match-pair of aptamer and peptide was studied for the first time in sandwich based configuration to detect TnI. Peptide-BSA carrier conjugate was captured for detecting TnI along with Tc18 aptamer as target bioprobes. As a result, only Tc18 aptamer exhibited efficient targeting of TnI in combination with peptide owing to its flexible hair-pin loop folding. The match-pair could detect a lowest dilution of 0.4 ng/ml TnI avoiding interference from non-specific proteins further displaying immuno-sandwich detection of TnI in Fig.4.4(a). When the assay was performed with human heart TnI spiked in serum, Tc18 aptamer-peptide match-pair displayed effective competency upto 0.7 ng/ml in Fig.4.4(b). A standard calibration curve with linear fitting was plotted for identifying TnI in unknown sample [Fig.4.4(c)].

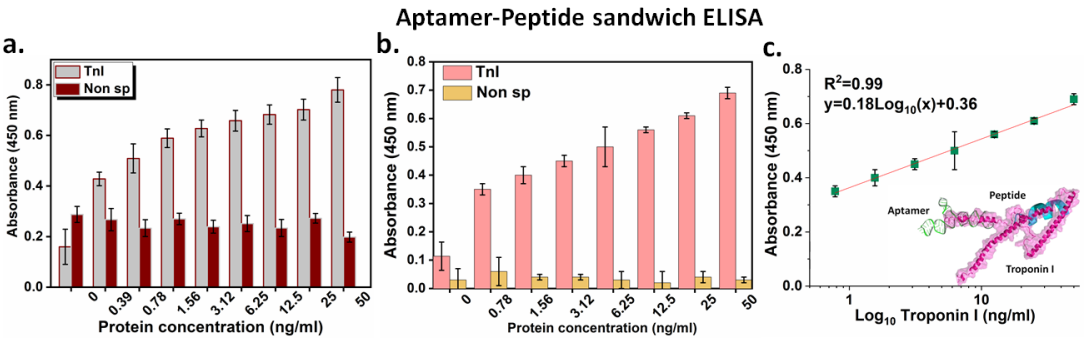

Fig. 4.4 Aptamer-peptide sandwich ELISA (a) TnI detection in experimental buffer (b) Detection of commercial human heart TnI spiked in serum (c) Calibration plot for aptamer-peptide sandwich assay serum spiking studies with schematic showing TnI targeting by match-pair bioreceptors

4.3.3 Aptamer based ELISA verification in clinical samples

After examining the efficacy of aptamers Tc18 and Tc35p to detect natural TnI spiked in serum samples, their competency in clinical samples was validated. A total of 40 AMI positive samples along with 20 negative samples were analyzed for presence of TnI content. Alternate sandwich ELISA for all clinical samples was performed wherein both aptamers were used as capture bioprobes and PolyAb was used for recognition. Tc18 aptamer based clinical sandwich assay displayed three false negative in Fig.4.5(a). Similarly, Tc35p demonstrated only 1 sample to be false negative and 1 out of 20 negative samples displayed false positive absorbance values as shown in scatter plot of Fig.4.5(b).

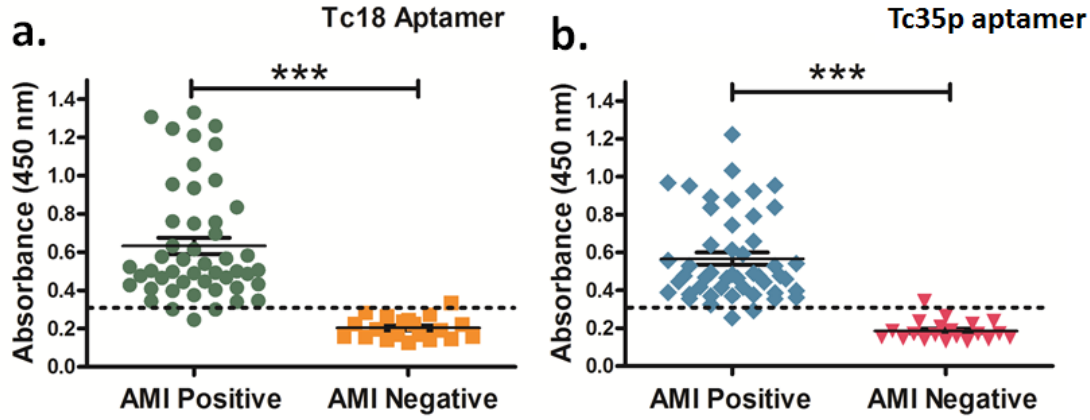

Fig. 4.5 Aptamer based ELISA of clinical samples (a) Sandwich ELISA of Tc18 for detecting TnI in clinical samples (b) Sandwich ELISA of Tc35p detect TnI in clinical samples

The statistical unpaired t-test for both aptamers Tc18 and Tc35p based sandwich ELISA of clinical samples demonstrated two-tailed P-value<0.0001 with positive

predictive value (PPV)=100% and 98% respectively and negative predictive value (NPV)=86.95% and 95% respectively. However, the sensitivity of Tc18 with 93.75% was less than Tc35p with 98% nevertheless, Tc18 was 100% specific than Tc35p with only 95% specificity [Fig. 4.6(a)]. The better binding efficiency of Tc18 can be attributed to previous results of this chapter and studies in chapter 3 where Tc18 has demonstrated more affinity towards target TnI due to its structural folding.

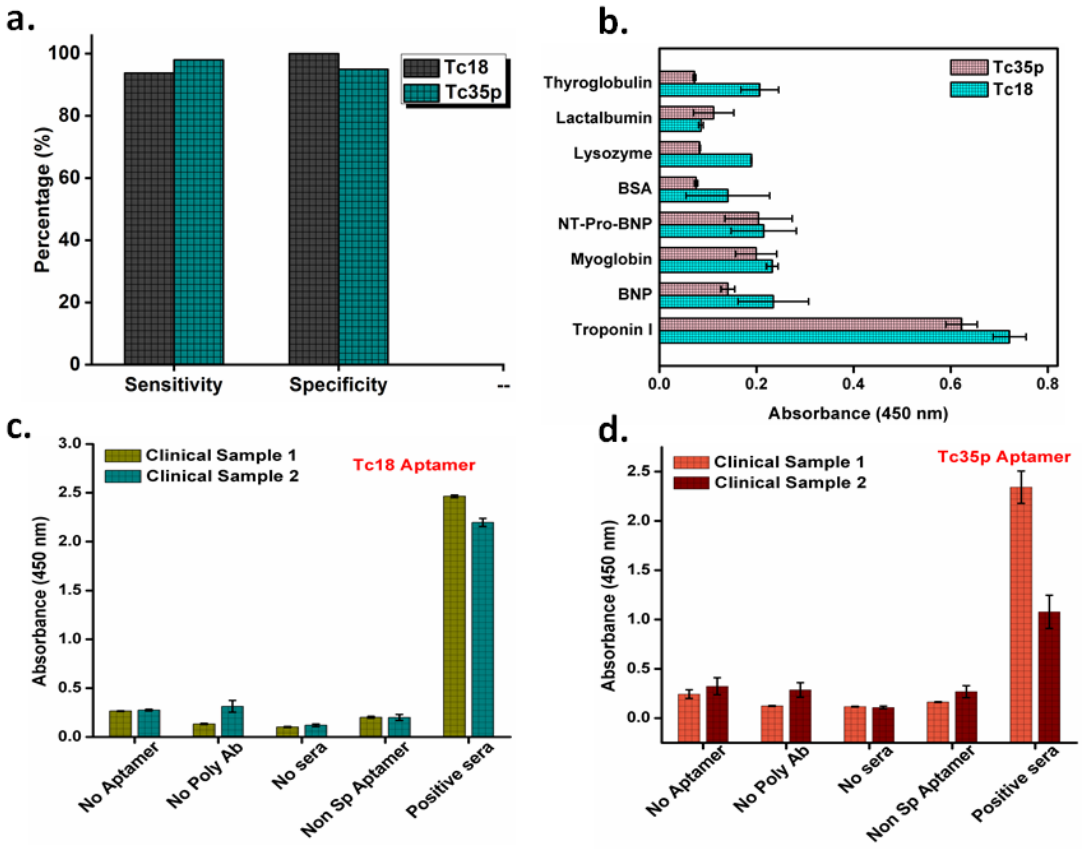

Fig. 4.6 (a) Statistical analysis of both aptamers to detect TnI in AMI clinical samples (b) Sandwich ELISA of aptamers showing specificity studies of non-specific proteins spiked in serum along with TnI containing clinical samples (c) Sandwich ELISA of Tc18 showing control studies by taking two clinical samples (d) Sandwich ELISA of Tc35p showing control studies by taking two clinical samples

Moreover, Tc18 and Tc35p aptamer based sandwich assays were also performed to examine significant interference of other possible abundant biomarker proteins found in sera. Both the aptamers didn't demonstrate any non-specific interactions with other targets spiked in very high dilutions into serum, maintaining their specificity for TnI in Fig.4.6(b). A sandwich ELISA with all possible controls was also performed for both the aptamers alternatively along with two random AMI positive clinical samples.

As observed in Fig.4.6(c) and (d), we can conclude that no interference was restricting categorical recognition of TnI by both the aptamers in clinical samples. Thus we can contemplate that both the aptamers Tc18 and Tc35p are exhibiting efficacious binding in sandwich ELISA platform for target TnI that has been validated in clinical samples as well.

4.3.4 Dot-blot immunoassay: Tc18 aptamer nanobioprobe

Tc18 aptamer gold nanoconjugates based dot-blot assay was adopted to develop a simple diagnostic approach for detecting TnI. By using strong thiol-gold covalent linkage (~ 45 kcal/mol) [157], chemical conjugation of aptamer onto GNPs was achieved as shown in Fig.4.7 [158][144][154]. An optimized 2 µM aptamer assembly was immobilized at pH~ 8 to form stable GNP-A nanoconjugates. GNP-A were stabilized by salt aging phenomenon through stepwise addition of NaCl to promote maximum receptor loading by decreasing the repulsive forces between alike charged DNA moieties [159].

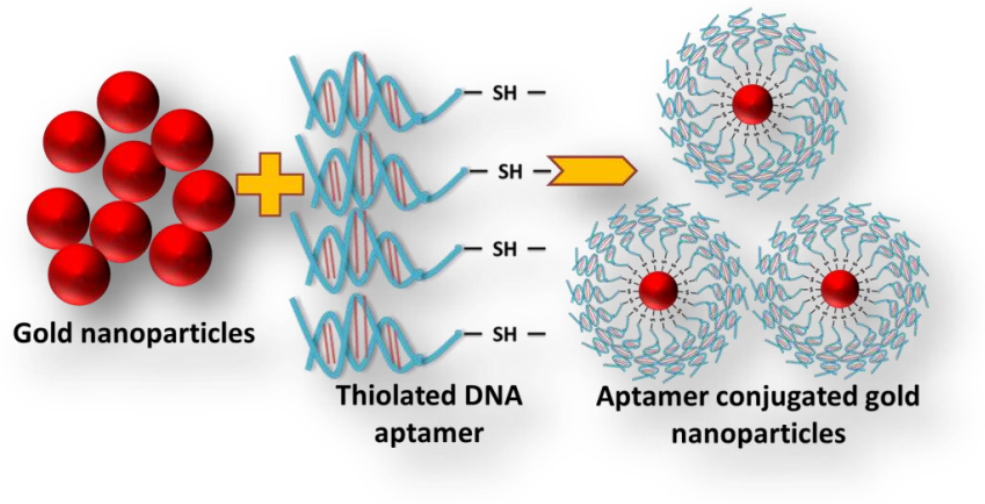

Fig.4.7 Schematic illustration for synthesis of Tc18 GNP-A nanoconjugates

The GNP-A nanobioprobe was characterized for its morphological stability by TEM showing subtle change in shape of spherical GNPs (Fig.4.8a inset) compared to GNP-A in Fig.4.8(a). UV-spectroscopic measurement in Fig.4.8b displayed a red shift of 4 nm post conjugation. Furthermore, an increase of 5 nm in hydrodynamic radii of GNP-A was observed via DLS measurement as shown in Fig. 4.8(c and d).

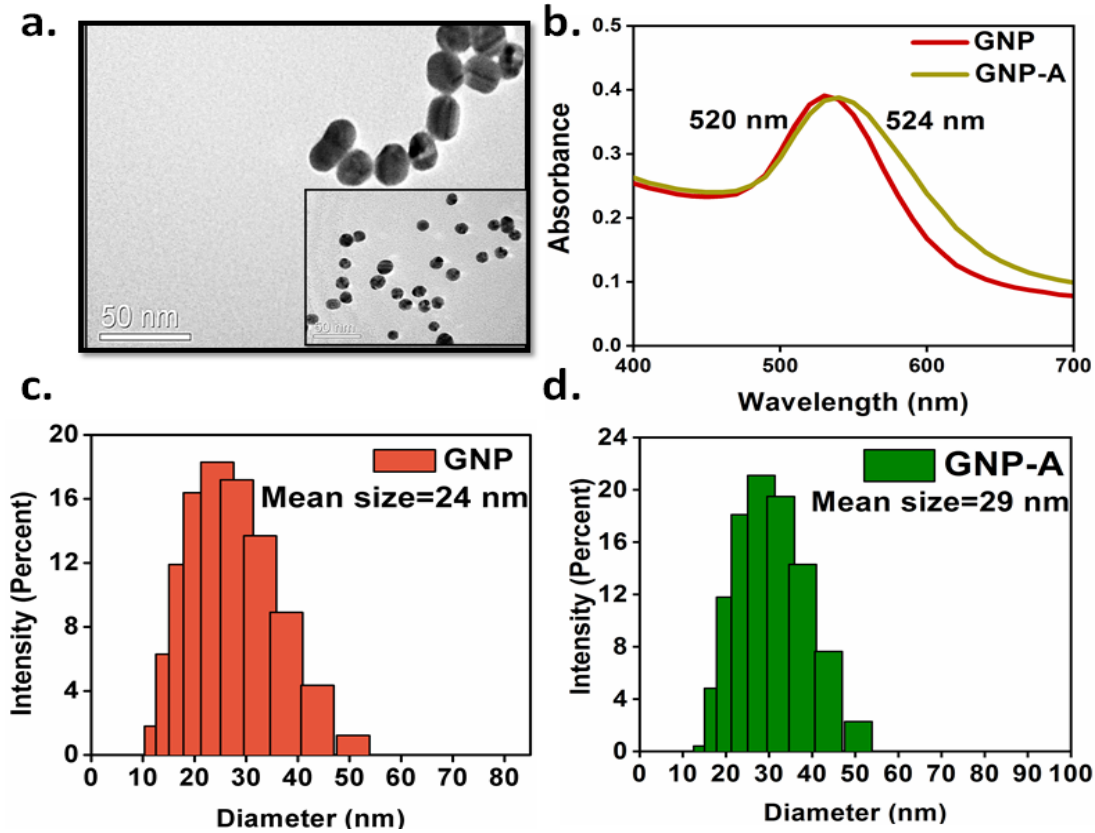

Fig.4.8 Characterization of GNP and GNP-A (a) TEM micrograph of GNP-A with inset showing spherical GNP (b) UV spectrum showing 4 nm peak shift for GNP-A conjugation (c and d) DLS histogram of GNPs and GNP-A

After confirmation of GNP-A bioconjugation, dot-blot assay was performed where silver enhancement solution was used to develop spot intensity by precipitation of metallic silver that enlarges GNP-A bound to TnI [16]. Fig.4.9(a) depicted clear spots that intensified with increasing TnI concentration as compared to no protein control. This visual qualitative analysis was corroborated with quantification of dots using ImageJ analyzer that measured raw integrated density for each spot.

Additionally, dot-blot analysis for analyzing interference of other cardiac biomarkers was investigated which was found to be non-significant as seen from blot visual. This diplays selective specificity of Tc18 aptamer gold conjugate GNP-A for TnI in Fig.4.9(b) and graphical plot of ImageJ. In serum spiking studies, GNP-A could detect spots of commercial TnI explaining binding efficiency of Tc18 for dot-blot assay performed in complex serum matrix. To this context, Fig.4.9(c) diplays visible spots quantified as raw integrated density of eact natural TnI concentration with Fig.4.9(d) depicting a standard plot for spot density conferring to different log values of TnI in ng/ml.

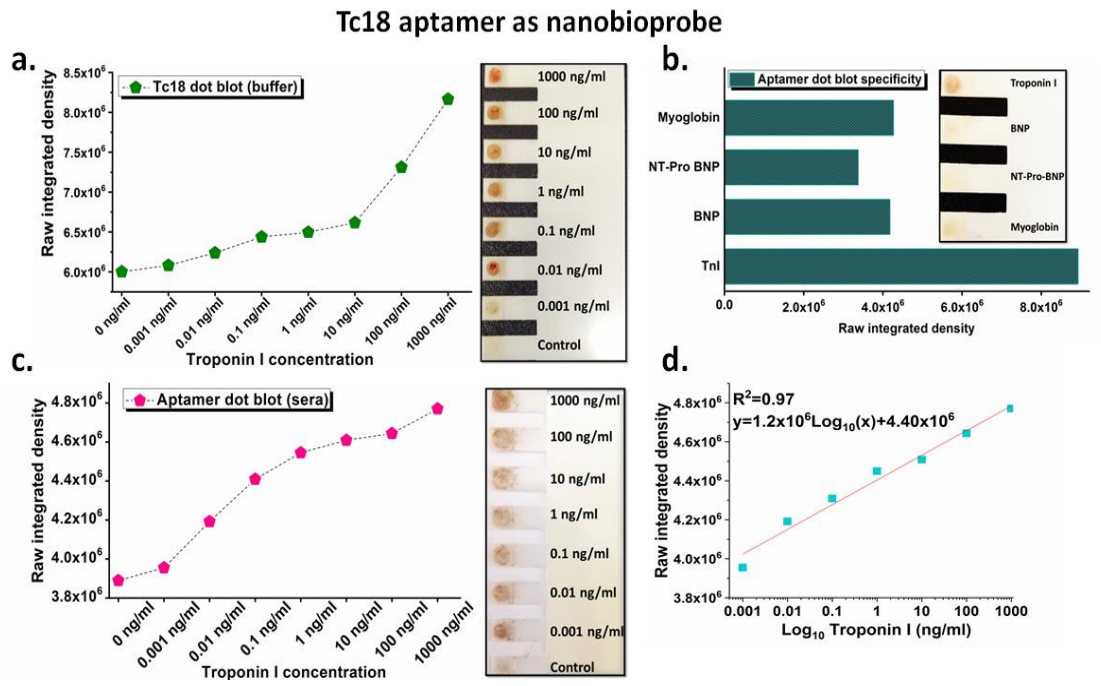

Fig.4.9 TnI detection using GNP-A based dot-blot assay (a) Spot density curve and visual image for TnI dot-blot assay in buffer (b) Specificity analysis of Tc18 based dot-blot assay for TnI detection (c) Spot density curve and visual image for natural TnI dot-blot assay in serum (d) Calibration curve of serum spiking dot-blot for raw integrated densities of TnI dilutions

4.3.5 Aptamer based lateral-flow immunoassay

TnI sandwich ELISA was further reciprocated to lateral-flow immunoassay wherein anti-TnI PolyAb was lined onto NC membrane and Tc18 aptamer as gold nanoconjugates was adsorbed onto conjugate pad. After assembling all the components of LFIA strip, when TnI was added to sample pad in varying dilutions, red color test line was observed upto 0.1 ng/ml. Moreover, aptamer being specific to its target obviated non-specific interactions as seen in Fig.4.10.

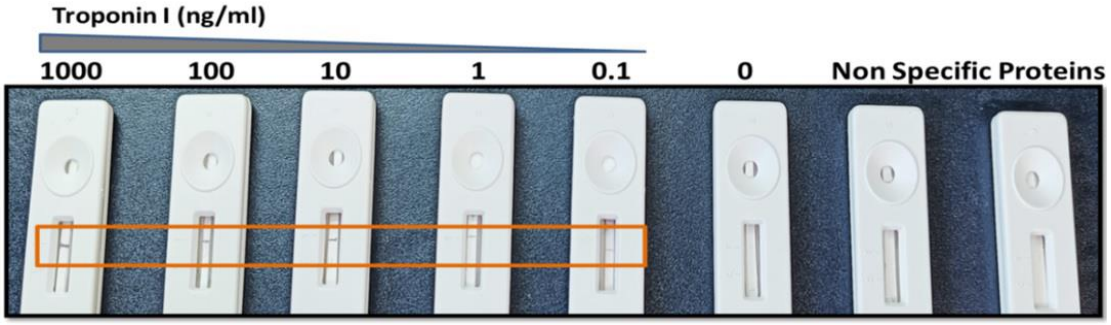

Fig.4.10 Tc18 aptamer based LFIA for rapid detection of TnI

4.4 Conclusion

The major highlight of this chapter is underlined by the affinity of Tc18 and Tc35p towards TnI in designing aptamer based immunodiagnostic assays such as ELISA and dot-blot. Both the aptamers have demonstrated dynamic efficacy towards TnI via binding to its apical C-terminal peptide fragment. Their ability to detect 0.2 ng/ml TnI as capture bioprobes using avidin-biotin interaction is exceptional even in serum spiking studies. This is indicative of their relevance in developing advanced TnI biosensing platforms in spite of strong interference from abundant non-specific components present in serum matrix. Moreover, Tc18 aptamer even recognized TnI as target bioprobe with 0.15 ng/ml dilution, further establishing its applicability as a strong bioreceptor probe to design diagnostic platforms. Therefore, **Tc18 aptamer can be used in the form of capture as well as target bioreceptor** corroborates its applicability towards designing biosensing platforms to detect TnI. Besides, an important assay incorporating **Tc18 aptamer-peptide as a novel match-pair to bind TnI** at distinct sites enabled a cost effective replacement for antibodies for developing TnI detection assays. The match-pair provided 0.4 ng/ml TnI detection that further unfolds their utility in establishing dual-receptor match-pair based biosensing platform discussed in the next chapter.

This chapter also describes the validation studies of sandwich ELISA to investigate the competency of both aptamers to detect TnI in AMI clinical specimens. A small cohort of 40 positive and 20 negative samples was procured from PGIMER for this study. Various hs-TnI assays from Abott, Roche, Siemens, Beckman Coulter, etc. rely upon monoclonal antibodies (Mab) based TnI detection for risk stratification in acute conditions of myocardial infarction [160,161]. They are very costly and inaccessible to patients for which these aptamers can serve as promising bioreceptors in developing stable point-of-care testing assays for AMI diagnosis.

However, dot-blot assay circumvents the disadvantage of lengthy processing hours of ELISA and costs associated with reagents and enzyme. The assay explores **Tc18 aptamer conjugated gold nanoparticles as nanobioprobes** to detect TnI as another cost-effective alternative to antibodies based detection assays. The assay produced visual signal as colored spots upto 0.1 ng/ml TnI achieved by signal enhancement of

GNP-A nanoconjugates. Furthermore, the competency of Tc18 aptamer was investigated in paper based LFIA system wherein 0.1 ng/ml sensitivity was obtained in the form of visible red color test line.

Though, in this chapter the dot-blot assay surpassed ELISA in sensitive detection of TnI as visual signal, nevertheless the assay performing time was still a constrain which was averted by LFIA. LFIA provides qualitative estimation of TnI, therefore a quantitative colloidal assay has been discussed in next chapter. This assay eliminates the utility of antibodies used as bioreceptors introducing a synthetic peptide in combination with TnI. Tc18 gold nanobioprobe along with peptide has been described in the next chapter for naked-eye visible quantitative estimation of TnI.

Chapter 5

Aggregator-free gold nano-sandwich based colorimetric detection of cardiac Troponin I

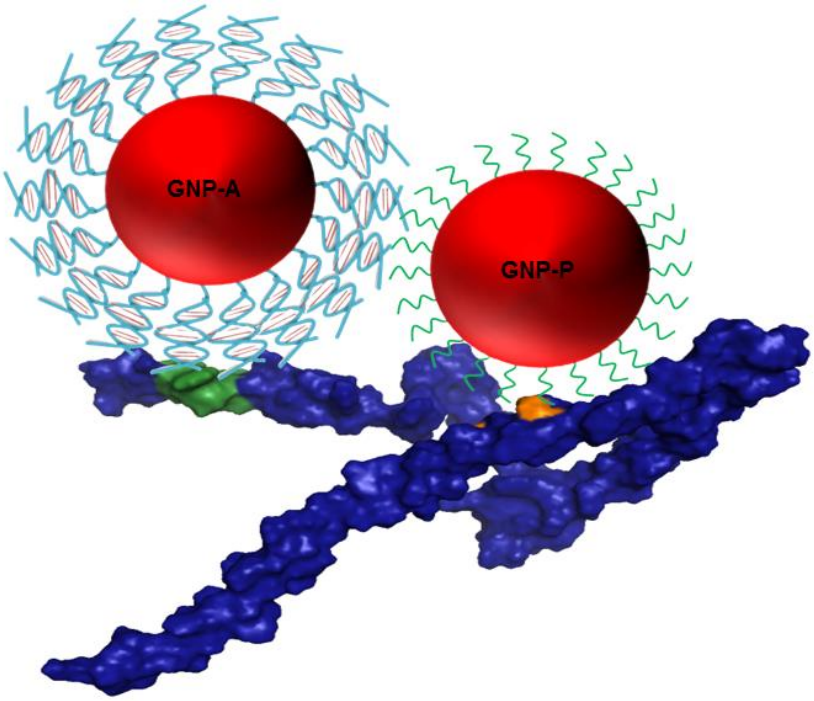

5.1 Overview

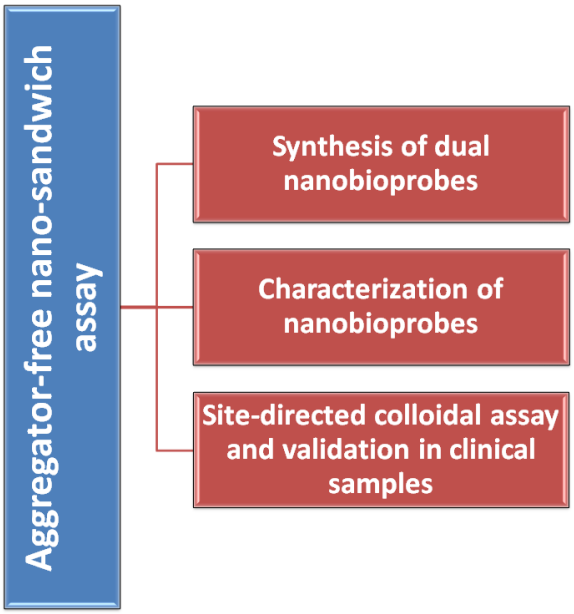

Gold nanoparticles (GNPs) possessing LSPR have turned out to be excellent scaffolds for fabrication of colorimetric biological sensors as point-of-care testing platforms [162,163]. Their exceptional physico-chemical properties such as stability, low toxicity and superficial modifications due to high surface to volume ratio makes it ideal to form nanoconjugates [164,165]. Earlier studies reporting antibody or aptamer GNPs conjugates used an external aggregator such as NaCl/polycationic polymer in colloidal aggregation assays for detection of analyte [166]. Therefore, in marked contrast from the reported studies, the concerned chapter discusses about a simple and cost-effective aggregator-free colorimetric assay that utilizes two site-directed gold nanoconjugates simultaneously for detection of TnI. For the first time, combination of aptamer and peptide functionalized gold nanoconjugates as high affinity nano-bioprobes have been investigated as novel match-pair to detect TnI. Moreover, no external element is required to induce aggregation thereby minimizing the possibility of non-specificity and making it a one-step aggregator-free assay.

5.2 Experimental approaches

5.2.1 Materials and Instrumentation

Trisodium citrate dehydrate, Hydrogen tetrachloroaurate (III) trihydrate, Monobasic dihydrogen phosphate and Dibasic monohydrogen phosphate were obtained from Sigma Aldrich (India). Thiol modified Tc18 aptamer was taken from IDT technologies comprising -SH-$(CH_2)_6$ linker at 5′ end. Peptide containing cysteine

moiety was selected from literature and chemically synthesized following HPLC purification (CFYSHSFHENWPS) [167]. Recombinant cardiac TnI and commercial human heart TnI (Sigma) was taken for experimentation. Blood samples of AMI patients were collected from PGIMER, Chandigarh and commercial ELISA TnI detection kit was procured from *RayBiotech* for validation studies. All the experiments were performed in phosphate buffer (PB) pH 7-8 medium and all solutions were prepared with 18.2 MΩ cm resistivity ultra-pure water of Merck Millipore (milli-Q water). The glasswares were rinsed with aqua regia and retreated with GOPS prior to use.

UV-Visible spectroscopy measurements were taken using BioTek Synergy H1 spectrophotometer (UK). Transmission electron microscopy (TEM) was performed using JEOL 2100 (USA). Gel based characterizations were done with BioRad gel assembly. CD measurements were performed using Jasco J-815 instrument and BLI experiments on ForteBio Octet K2 system (Pall Life sciences, Fremont, CA 94538 USA). DLS (Dynamic Light Scattering) for size and ζ- potential studies for charge analysis were performed using a Zetasizer Nano ZS (Malvern, UK).

5.2.2 Synthesis of gold nanoparticles and development of gold nanoconjugates

Smaller sized and concentrated citrate capped gold particles were synthesized as discussed in last chapter in higher volume. As prepared GNPs concentrated upto an OD of 1 @ 520 nm with 7.00×10^{11} particles per ml were used for preparing aptamer (GNP-A) and peptide (GNP-P) nanoconjugates. Bioconjugation protocols were followed as described in chapter 4 for dot-blot assay. An optimized 2 μM of Tc18 aptamer was reduced with 0.1 M DTT for 30 minutes at 37˚C and added dropwise to 1 ml GNPs under constant rotation. For peptide bioconjugation, an optimized 40 μM of peptide solution along with 0.1 M DTT was added dropwise to GNPs at 4˚C overnight incubation [154]. Both the nanoconjugates were characterized using UV-Visible spectroscopy, DLS/ζ- potential, TEM, gel shift assay, CD and BLI and were stable at 4˚C for long time.

5.2.3 Characterization of nanoconjugates

a. UV-spectroscopy: The prepared GNPs along with both nanoconjugates of GNP-A and GNP-P were subjected to UV-spectroscopic measurement in a wavelength range from 400-700 nm to analyze the red shift for standard gold plasmon peak at 520 nm.

b. Transmission electron microscopy (TEM): Samples of GNP-A and GNP-P with reference bare GNPs were diluted in 10 mM phosphate buffer pH 7.5. Respective drops of samples were placed onto carbon coated TEM grids with negative staining via 2% phosphotungstic acid (PTA) for 30 minutes. The measurements were performed at an accelerating voltage of 120 kV.

c. DLS and Zeta measurements: Size distribution analysis for GNPs and nanoconjugates GNP-A and GNP-P were investigated using DLS by 10 fold diluting the samples making the final volume 1 ml. Alongside charge distribution studies were performed via ζ-potential using Malvern zetasizer.

d. Agarose gel electrophoresis (AGE): The conjugation of nanoconjugates was confirmed by observing their electrophoretic mobility on 0.5% agarose gel under a voltage of 80 volts in 1x TAE buffer for an hour. 30 µl of both nanoconjugates GNP-A and GNP-P were added onto the gel along with bare GNPs.

e. CD spectroscopy and BLI: The conformational isomerization of aptamer and peptide was measured by CD spectroscopy after forming nanoconjugates with GNPs. Far-UV measurements for 2 µM Tc18 aptamer and GNP-A were taken in the range of 190-250 nm λ at a scanning speed of 50 nm/min. Subsequently, near-UV CD measurements for 40 µM peptide along with GNP-P were measured in range of 260-350 nm λ. All dilutions of 200 µl each were made in PB (pH 7.5) to which scans were baseline corrected. Final spectrum depicts average of three accumulations for each measurement.

BLI studies were performed for analyzing binding strength of gold nanoconjugates GNP-A and GNP-P towards TnI target. Briefly, 5 µg/ml 6x His-tagged rTnI was immobilized onto Ni-NTA sensor for 600 seconds. After 60 seconds washing in 10 mM PB (pH 7.5) as baseline, 300 seconds each of association and dissociation steps were performed for GNP-A and GNP-P gold nanoconjugates along with referencing against bare GNPs. The data analysis was performed with *ForteBio* software analysis 9.0.

5.2.4 Conjugation efficiency and flocculation assay

For GNP-A synthesis, 2 µM corresponding to 30 ng/µl DNA in 1 ml GNP solution were used. After centrifugation, the absorption of supernatant was recorded as 11 ng/µl corresponding to 0.7 µM. For GNP-P synthesis, 40 µM peptide in 1 ml GNP

solution was used. Post purification, supernatant was 10 µM indicating 30 µM bound to GNPs. Furthermore, in accordance to a recent study [168], calculations for immobilization of aptamer and peptide onto GNPs were performed as amount of capping that was inferred in terms of efficiency of aptamer/peptide immobilization in a percentile**:**

% Immobilization = (A - B) * 100/A

Where: A = total aptamer/peptide used for conjugation,

B = aptamer/peptide content in supernatant of GNP conjugate.

The stability of GNP-A and GNP-P nano-bioconjugates were investigated by performing a simple flocculation assay using NaCl based aggregation. Briefly, 100 µl of 0.1 M NaCl was added to 20 µl each of GNP-A and GNP-P conjugates making the final volume of reaction mixture to be 150 µl with 10 mM PB (pH 7.5). Bare GNPs were also taken as control and mixture was incubated at room temperature for 5 minutes.

5.2.5 Gold nano-sandwich assay for TnI detection

For performing the colorimetric assay, different concentrations of TnI varying from 0.1 ng/ml to 500 ng/ml were freshly prepared in PB (pH 7.5). 20 µl each of the nanoconjugates- GNP-A and GNP-P were simultaneously added to 60 µl of TnI diluted in 10 mM PB (pH 7.5) making the final reaction volume 100 µl. Afterwards, photographic images were captured and UV -spectrum was recorded in 400-1000 nm λ range. TEM of nanoconjugates was also performed to analyze the aggregation phenomenon. Various other cardiac biomarkers such as BNP, NT-pro BNP, Myoglobin and other proteins BSA and lysozyme were also investigated in higher concentration compared to TnI for analyzing selectivity and specificity of nano-sandwich assay.

5.2.6 Aggregation assay by individual nanoconjugates

Both nanobioprobes-GNP-A and GNP-P were examined for their individual competency to cause aggregation. To this context, an excess amount of individual nanoconjugates were tested to detect sufficiently high concentration of TnI. Experimentally, 40 µl GNP-A and GNP-P were mixed separately with 20 µl of 5

μg/ml TnI making final volume 100 μl with 10 mM PB (pH 7.5) and incubated at room temperature for 5-10 minutes.

5.2.7 Nano-sandwich assay in TnI spiked serum

The nano-sandwich colorimetric assay was performed for targeting TnI in human sera. Various human heart isolated TnI concentrations were spiked in 1:10 μl diluted serum using 10 mM PB (pH 7.5) along with 0.1% Tween 20 and 1% BSA to avoid non-specific interactions. Briefly, 20 μl of each GNP-A and GNP-P nanoconjugates were uniformly blended with TnI spiked sera samples in duplicates followed by UV-spectroscopic measurements. The ratio of the aggregated nanoparticles at λ_{620} to non-aggregated particles at λ_{520} was measured to generate a standard curve of $\lambda_{620}/\lambda_{520}$ plotted against Log_{10} TnI (ng/ml).

5.2.8 Validation in clinical samples

Subsequently, potential of the developed colorimetric TnI nano-sandwich assay was analyzed in clinical samples of AMI patients. A total of twenty blood samples were investigated comprising ten AMI patient's (positive) and ten healthy subject's (negative). In brief, 20 μl of each GNP-A and GNP-P nanoconjugates were simultaneously mixed with 60 μl of undiluted serum of positive and negative clinical samples. The absorbance values were recorded at 520 nm and 620 nm respectively and ratio $\lambda_{620}/\lambda_{520}$ was analyzed for quantification.

To further compare and contemplate the competence of nano-sandwich assay, all the clinical samples were evaluated by standard commercial TnI ELISA kit comprising high affinity anti-TnI Mab. A standard curve was plotted by spiking different TnI dilutions in serum to achieve a linear curve equation where absorbance @ 450 nm was plotted across Log_{10} TnI (ng/ml).

5.3 Results and discussion

The conceptual illustration for aggregator free gold nano-sandwich assay has been explained in Fig.5.1(a). In presence of TnI, receptor conjugated gold nanobioprobes-GNP-A and GNP-P binds TnI at distinct interface inducing greater inter-particle cross-linking. TnI acting as an interconnecting bridge causes both nanoconjugates to come in close proximity in a sandwich-type arrangement inducing aggregation. This

results in changing the color of particles from red to blue. However, in absence of TnI, gold nanoconjugates are separated by each other as a result of inter-particle distance along with steric hindrance and similar charge based repulsion [101]. The realized aggregator-free colorimetric assay is distinguished from conventional salt based aggregation phenomenon of Chad Mirkin's standard gold-nanoparticle agglomeration assay and heterofunctionalized GNPs [169,170].

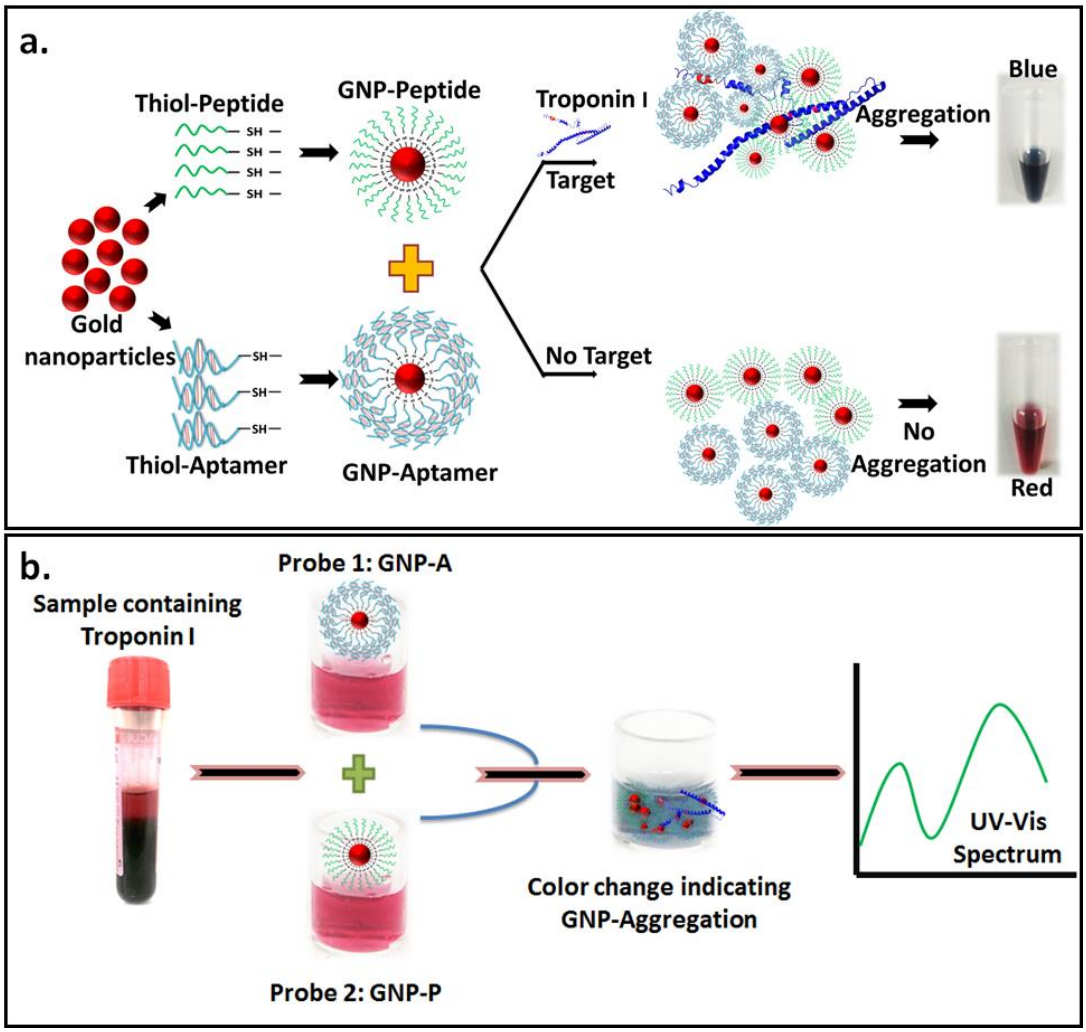

Fig.5.1 (a) Schematic illustration of aggregator-free gold nano-sandwich assay (b) Single step process for aggregator-free assay to detect TnI

The sequential process of colorimetric nano-sandwich assay has been clearly illustrated in Fig.5.1(b) which displays direct addition of sample containing TnI to a mixture of both nanobioprobes. The sandwich pair produces instant transition in color which is further measured by UV-Visible Spectroscopy.

5.3.1 *In silico* characterization of match-pair binding interface

The comprehensive architecture of nano-sandwich aggregation assay is laid on discrete interface of binding for GNP-A and GNP-P to target TnI as described in the last chapter via sandwich ELISA and dot-blot immunoassay. *In silico* docking and binding site prediction of aptamer with TnI has been discussed in chapter 3 that demonstrates Asp190-C43, Trp191-A42 and Trp191-T33 binding residues for TnI-Tc18 interaction. While, Trp10 of peptide was predicted to interact with Glu66 and Lys58 residues of TnI as suggested by literature as well [144]. A schematic representation of aptamer and peptide binding at different sites on TnI has been displayed in Fig.5.2.

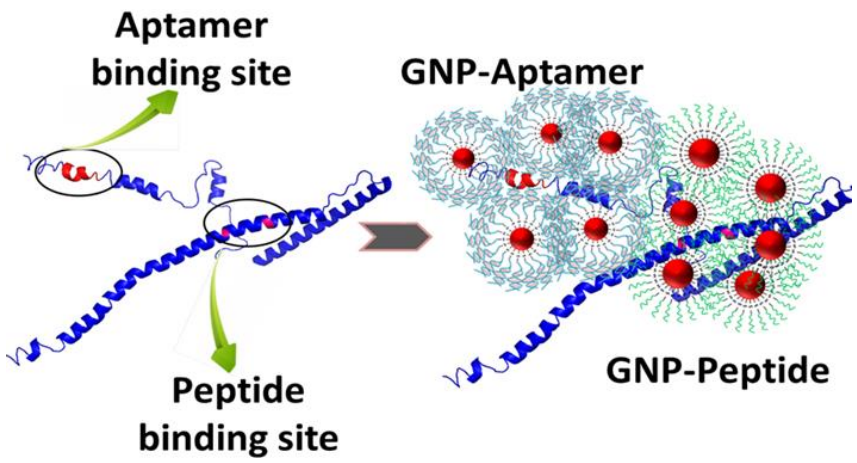

Fig.5.2 Schematic representation depicting biomolecular interaction of nanobioprobes with TnI

5.3.2 Optimization of gold nanobioprobes

An optimized concentration of 2 µM of thiolated aptamer and 40 µM of cysteine peptide were used at pH~ 8 for effective thiol-gold interaction to prepare nanobioprobes with maximum graft density (Fig.5.3). The significant affinity of gold-thiol has been extensively employed to chemically conjugate bioreceptors via strong covalent interactions [155][156][171][144]. The bioconjugation was theoretically calculated in terms of immobilization efficiency that estimated approximately 65% aptamer and 75% peptide immobilization onto GNPs. The biofunctionalized gold nanoconjugates were further stabilized by salt aging that decrease the repulsive forces between alike charged bioreceptors. Stepwise addition of NaCl promotes maximum receptor loading further stabilizing nanoconjugates [159].

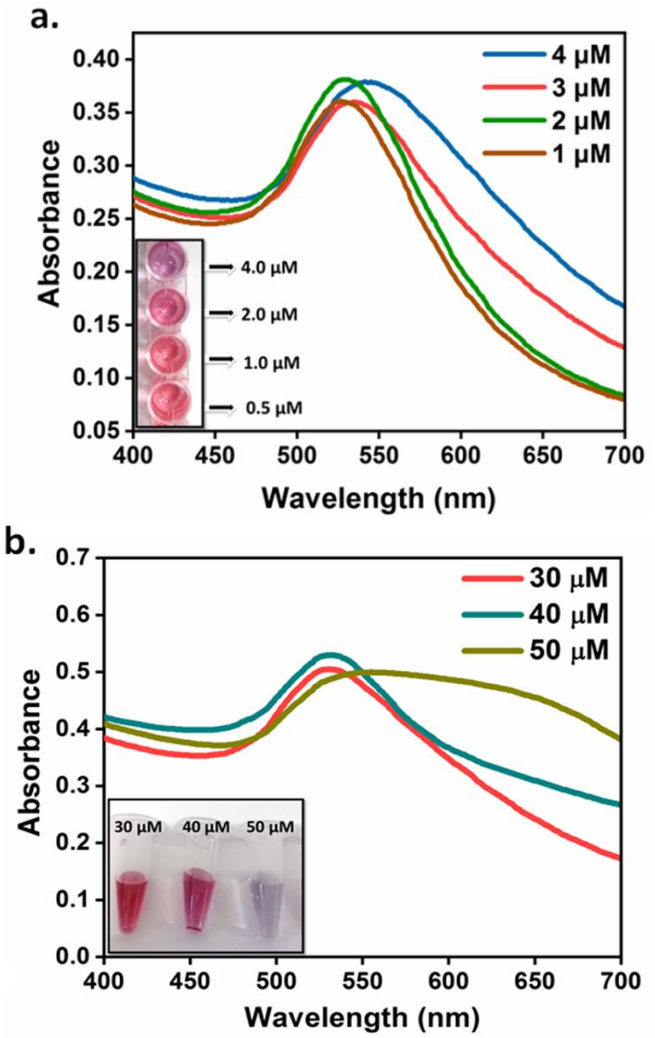

Fig.5.3 Bioconjugation optimization of (a) Aptamer and (b) Peptide onto GNPs

5.3.3 Characterization of gold nanobioprobes

The characteristic absorption peak of uniformly prepared GNPs was obtained at 520 nm as a result of a cherry red colloidal solution. The monodisperse feature was analyzed by TEM micrograph with approximate diameter of 11±5 nm. The confirmation of conjugation for gold-nanoprobes was obtained by a characteristic red shift in surface plasmon peak at 530 nm for GNP-A and 526 nm for GNP-P nanobioprobes in Fig.5.4(a-b). TEM micrographs also depict uniformity in morphology of GNP-A and GNP-P ruling out the formation of large aggregates Fig.5.4(c-d).

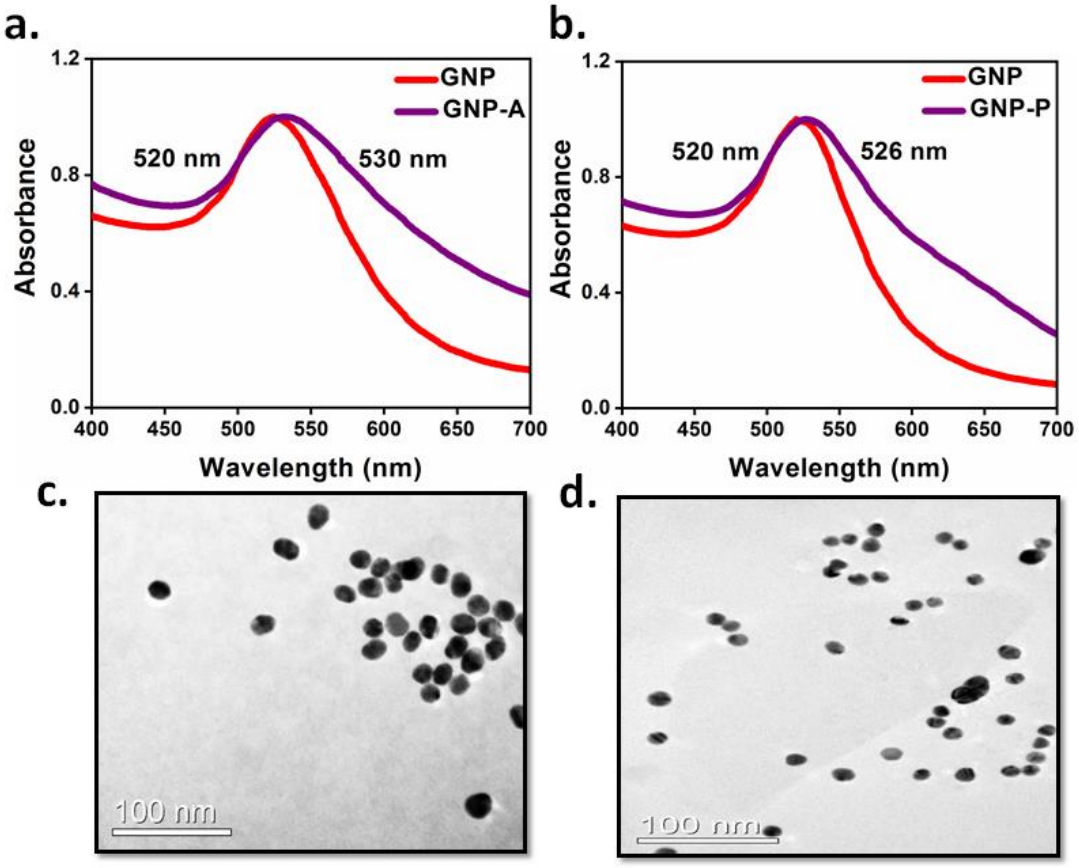

Fig.5.4 Characterization of gold nanobioprobes (a and b) UV-spectra of GNP-A and GNP-P respectively (c and d) TEM micrograph of GNP-A and GNP-P respectively

DLS histogram showed an average diameter of nanobioprobes 29 nm (GNP-A) and 27 nm (GNP-P) as compared to bare GNPs of 24 nm in Fig.5.5(a). An increase in negative charge in Fig.5.5(b) with ζ-potential of -29.5 mV for GNP-A and -26.8 mV for GNP-P. Analogously, agarose gel electrophoresis also corroborated conjugation of nanobioprobes showing restricted mobility as compared to bare GNPs in Fig.5.5(c) [172]. Additionally, the flocculation assessment with 0.1 M NaCl induced disruption in charge based repulsion of GNPs as it turned blue in color. The nanobioprobes GNP-A and GNP-P remained cherry red in color due to conjugation induced stabilization [173]. UV-Visible measurements also displayed a peak shift only in peak of GNPs taken as control with inset corresponding to visual color signal in Fig.5.5(d).

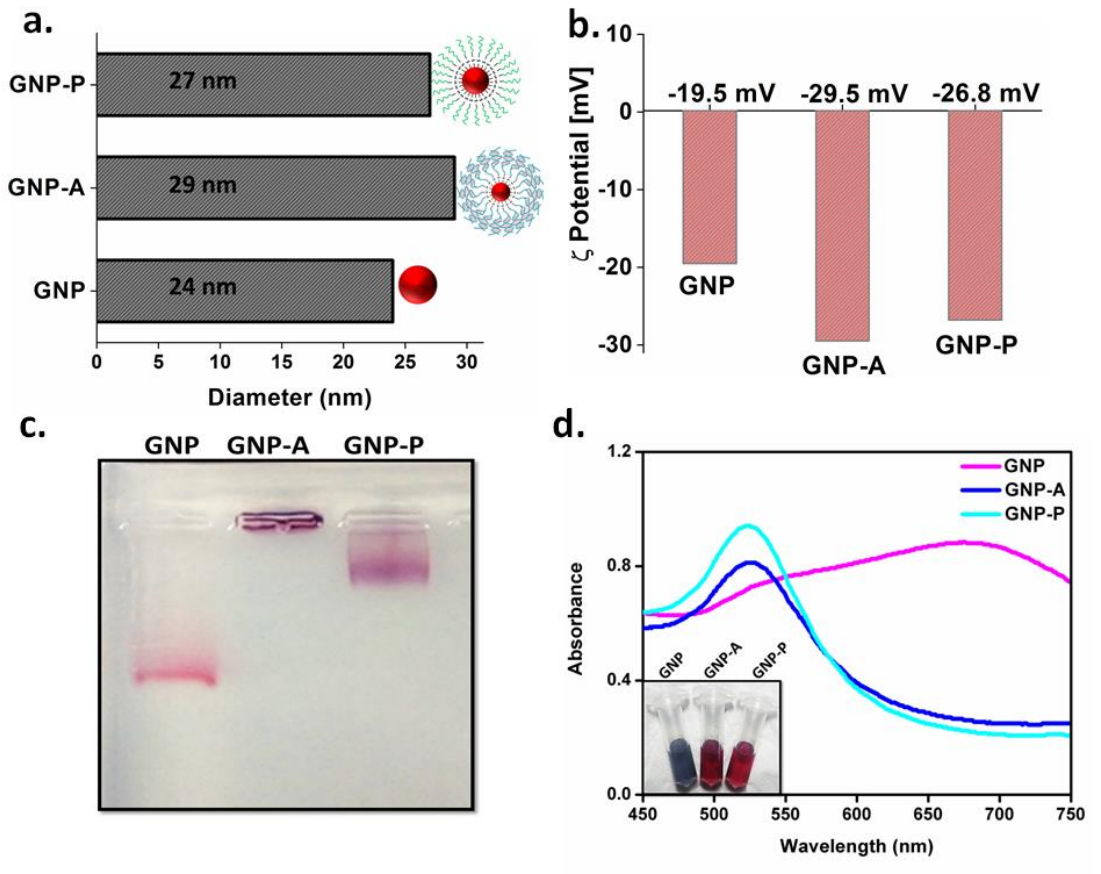

Fig.5.5 Characterization of gold nanoconjugates (a) DLS showing increase in size of nanoconjugates (b) Zeta-potential histogram showing change in charge distribution of nanoconjugates (c) Gel-electrophoresis showing restricted migration of nanoconjugates (d) Flocculation assay for stability of nanoconjugates

CD spectroscopy demonstrates that bare GNPs caused plasmon induced alteration of electromagnetic field inside chiral molecules of aptamer and peptide upon conjugation. The respective change arises from dipolar interactions occurring between aptamer and peptide with GNPs [174]. CD signature of far-UV measurements for aptamer uniformly accords with B-form of DNA showing a negative signal at 240-260 nm and a positive peak signal between 270-290 nm [175]. While dissipation of CD signature for aptamer in GNP-A [Fig.5.6(a)] for both peaks at their respective wavelengths suggested successful conjugation onto GNPs [176]. Correspondingly, near-UV measurement for peptide exhibits a random coil structure with a negative CD signal at 190 nm [177], which gets disrupted after conjugating with GNPs in Fig.5.6(b). In context to this, chiroptical (chiral + optical) properties of nanoconjugates can be explained as non-chiral nanoclusters can modify CD spectra of a chiral molecule after bioconjugation [178].

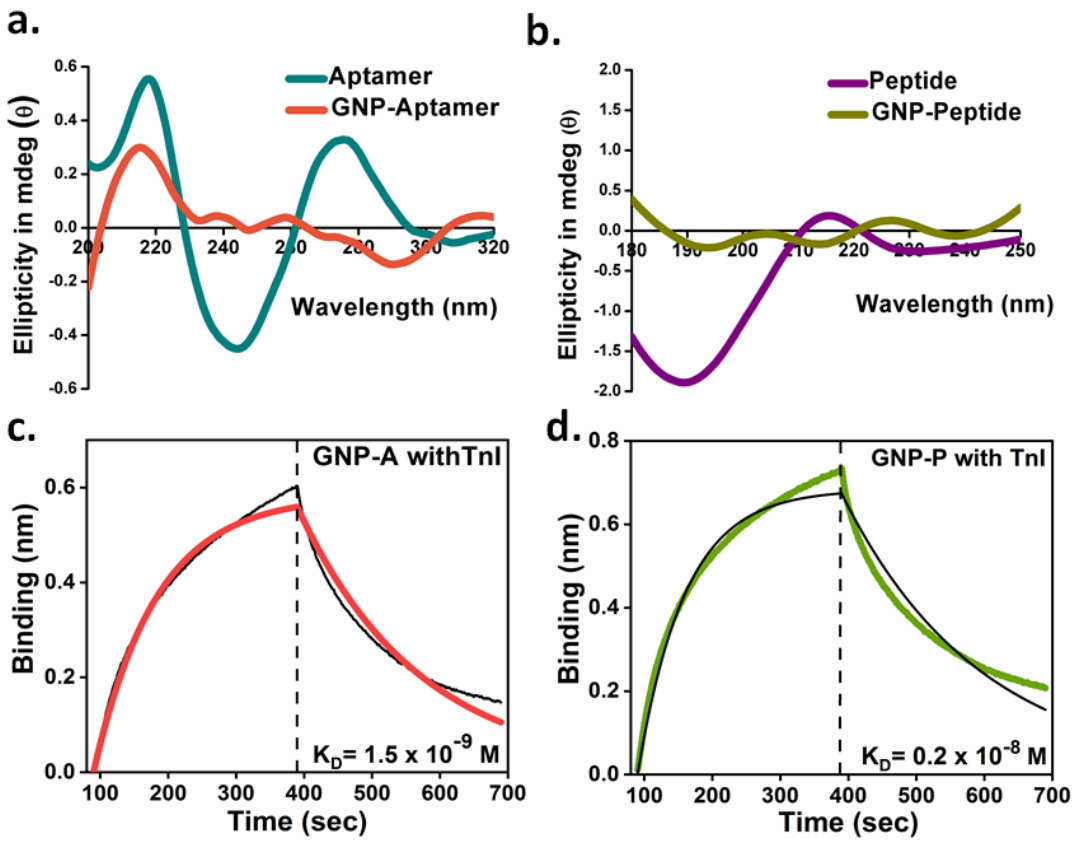

Fig.5.6 (a and b) CD spectroscopy curves showing change in secondary structure of aptamer and peptide after conjugation onto GNPs (c and d) BLI sensogram showing association and dissociation curves for GNP-A and GNP-P interaction with TnI

Furthermore, BLI studies were performed to examine the affinity of nanobioprobes towards target TnI. The binding affinity calculated in terms of K_D (dissociation constant) as a function of association and dissociation for GNP-A was 1.5 x 10^{-9} M with R^2=0.98 and for GNP-P was 0.2 x 10^{-9} M with R^2=0.90 indicating binding affinity of nanoconjugates with TnI [Fig.5.6(c-d)]. The characterization of nanobioprobes by both biochemical techniques suggested their active functionality and binding ability.

5.3.4 Gold nano-sandwich assay

The nanobioprobes GNP-A and GNP-P upon interacting with TnI caused spontaneous aggregator-free agglomeration. The aggregation phenomenon was further profoundly analyzed via TEM depicting monodisperse GNPs corresponding to red color and when aggregated state dominates caused change in color to blue Fig.5.7.

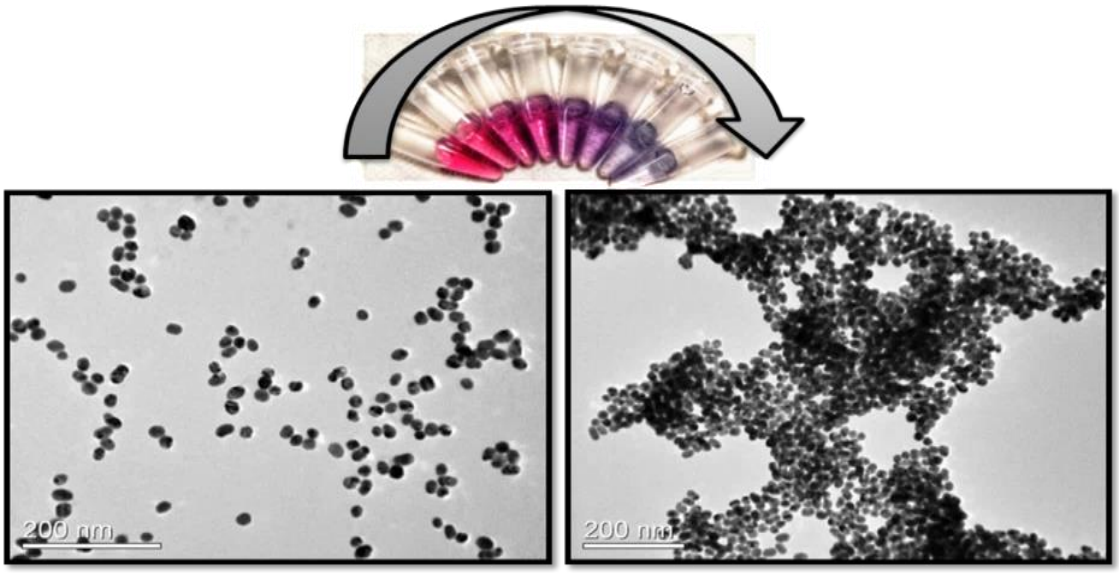

Fig.5.7 TEM image of target induced aggregation with image showing change in color

For nano-sandwich colorimetric assay, GNP-A and GNP-P nanobioprobes were investigated with a series of TnI concentration. The change in color of solution underwent a corresponding visual transition from cherry red to wine red and further purple to blue indicating transition from dispersed to aggregation state of nanoclusters in presence of TnI. With increasing concentration of TnI, the characteristic UV-spectrum of GNPs at 520 nm began to decline and a highly intense band emerged at around 620 nm with concomitant broadening in the peak [Fig.5.8(a)].

5.3.5 TnI serum spiking analysis

An apparent probability of signal loss when applied to real AMI samples due to presence of other non-specific biomolecular moieties in complex serum was analyzed. Therefore, to study the competence of gold nanobioprobes in biological medium, different TnI concentrations were spiked in human serum samples. As a result, an intensive appearance of UV-spectrum peak at 620 nm correlating to spiked TnI in serum was noted [Fig.5.8(b)]. Alongside, visible color change from cherry red to blue was observed which was spectrophotometrically substantiated by recording absorbance ratio A_{620nm}/A_{520nm} to plot a standard calibration curve in Fig.5.8(c).

The limit of detection 0.084 ng/ml was calculated by 3α/slope where α confers to standard deviation of instrument and slope comes from linear calibration plot. Besides the recovery efficiency calculated using straight line equation was in close agreement with spiked TnI concentration implying high practicability of the developed assay (Table 5.1).

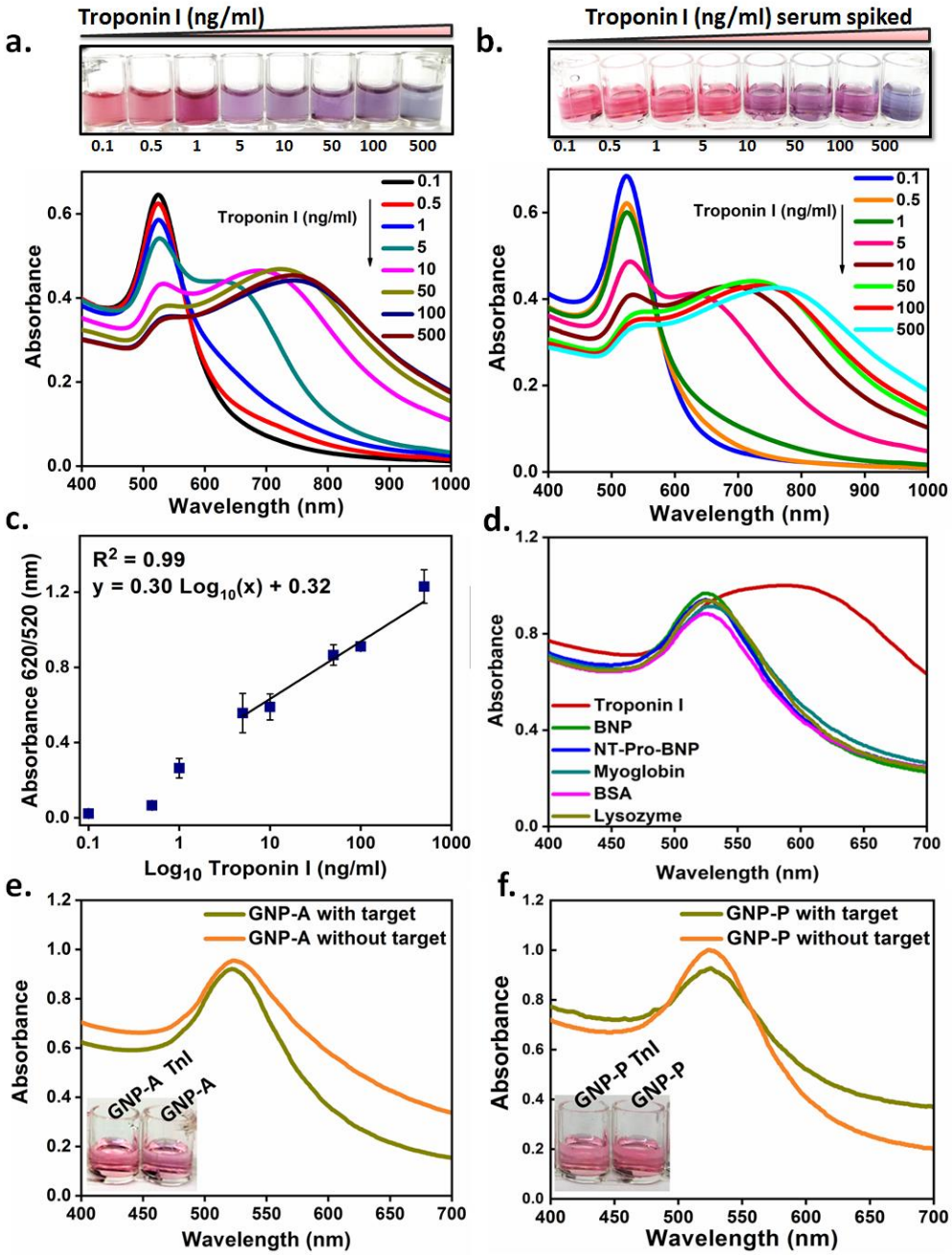

Fig.5.8. (a) Visual signal and UV-spectrum of TnI nano-sandwich assay in buffer (b) Visual signal and UV-spectrum of TnI nano-sandwich assay in TnI spiked serum (c) Calibration curve of nano-sandwich assay for TnI detection in spiked serum (d) UV-spectrum for specificity analysis of nano-sandwich assay for TnI (e) and (f) Nano-sandwich assay by individual GNP-A and GNP-P nanobioprobes respectively with inset visual signal

S.R. No.	Amount added (ng/mL)	Amount found (ng/mL)	Troponin I recovery (%)
1	0.1	0.1	100
2	5	5.7	114
3	100	93.3	93.3

Pearson correlation coefficient (r)=0.99; $p<0.05$

Table 5.1 Percentage recovery table of spiked TnI samples

5.3.6 Interference studies for non-specific targets

The analytical performance of nano-sandwich assay was further examined for investigating nanobioprobes to capture only specific target unhindered by non-specific interactions. The specificity of nanobioprobes was strengthened by an extreme peak shift for TnI as compared to other non-specific targets observed via UV-spectrum in Fig.5.8(d). Alongside UV-absorption maxima at 620 nm for TnI compared to other biomarkers also displayed insignificant interference from other cardiac biomarkers.

5.3.7 Aggregation efficiency of individual nanoconjugates

Independent nanobioprobe assays were performed to speculate whether aggregation is a match pair driven circumstance of aptamer and peptide nanobioprobes or is a result of agglomeration caused by individual nanoconjugates. Fig.5.8(e-f) described a marginal wavelength shift with no significant color change. This corroborated the synergistic effect of both nanobioprobes for development of nano-sandwich colorimetric assay.

5.3.8 Gold nano-sandwich assay verification in clinical samples

Ten positive AMI clinical samples and ten negative sera samples of healthy subjects were taken and analyzed for presence of TnI using nano-sandwich assay. The color change was observed in positive samples after addition of both nanobioprobes which remained stable even after few hours. UV-Visible absorbance at 620 nm of positive samples was noted higher than their values at 520 nm indicating aggregation while an opposite recordings was measured for negative samples. The ratio of varying UV absorbance values for each sample as A_{620nm}/A_{520nm} was calculated for comparative quantitative analysis as shown in Fig.5.9(a).

Furthermore, the comparison and cross-validation of nano-sandwich assay was achieved with commercial TnI ELISA kit. The absorbance values of clinical samples were observed at 450 nm in Fig.5.9(b) and quantitative analysis performed by both the assays demonstrated that nine AMI positive samples displayed a strong association with commercial ELISA. To this context, 100% specificity and 90% sensitivity of nano-sandwich assay was observed estimating 100% positive predicted

value (PPV) and 90.90% negative predicted value (NPV) suggesting that colorimetric assay is less likely to provide any false negative results in Fig.5.9(c). Moreover, Fig.5.10 displays a visual image for c hange in color for all the clinical samples.

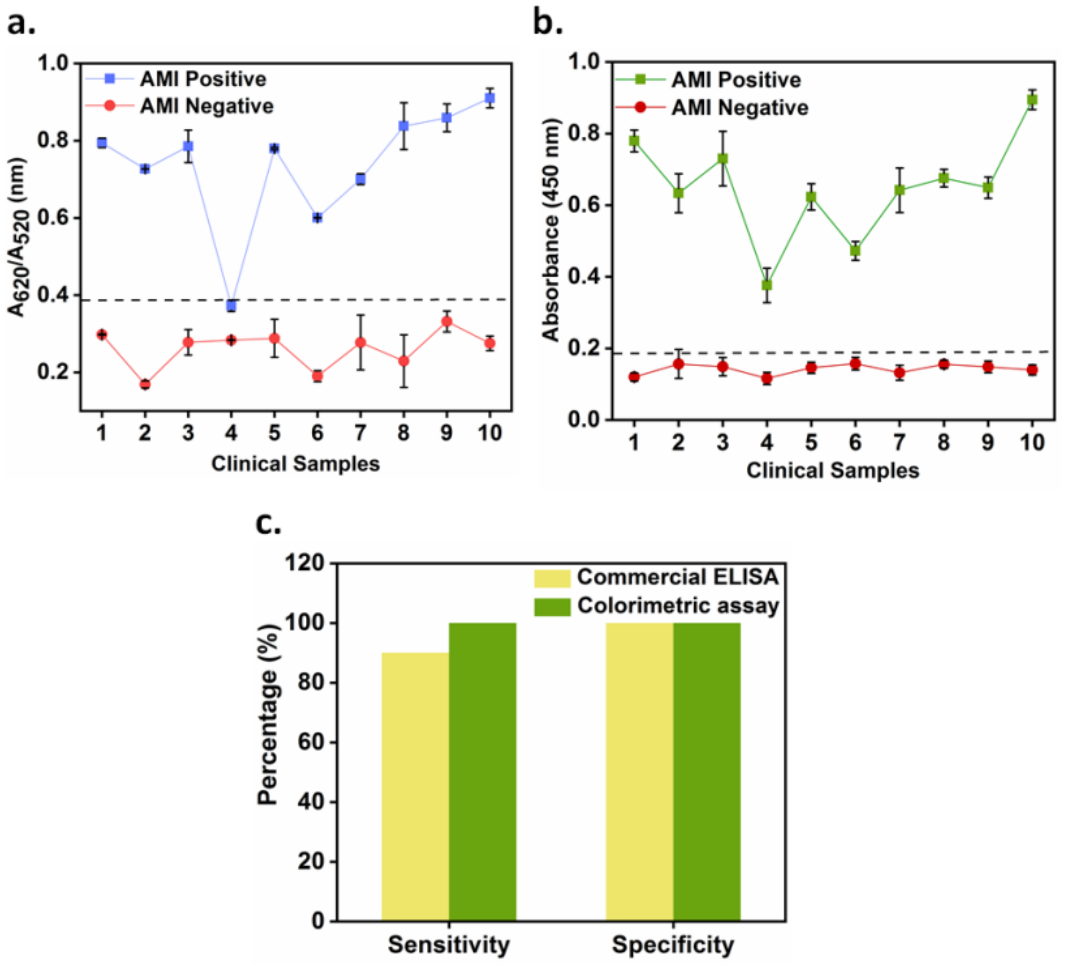

Fig.5.9 Aggregator-free assay for 20 clinical samples (a) Colorimetric assay depicting A_{620}/A_{520} nm ratio (b) Commercial ELISA depicting A_{450} nm (c) Comparative statistical analysis between colorimetric assay and commercial ELISA

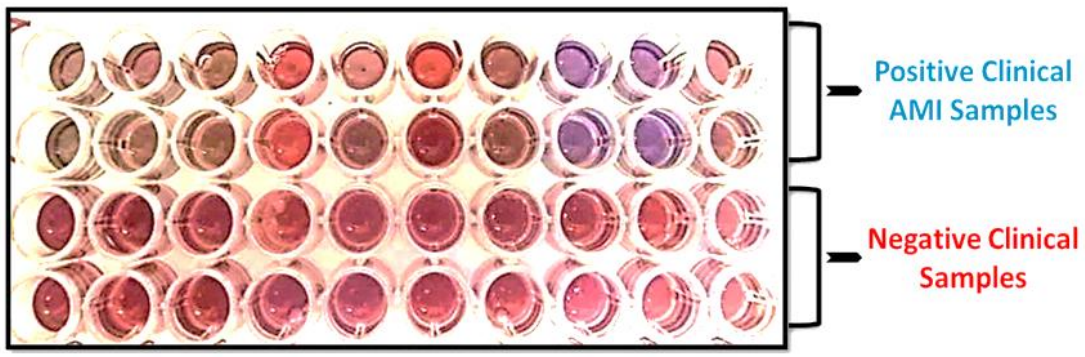

Fig.5.10 Colorimetric visual signal of nano-sandwich assay for clinical samples

5.4 Conclusion

This chapter discusses about **an aggregator-free gold nano-sandwich assay** exhibiting agglomeration of nanobiprobes to detect cardiac TnI. The **distinct molecular binding sites of aptamer and peptide** on TnI were predicted by *in silico* docking described in chapter 2 that enabled the development of this novel match-pair bioreceptors. The match-pair was used for sensitive detection of TnI in sandwich ELISA and dot-blot assay discussed in last chapter which navigated our research towards designing of colorimetric colloidal assay that is rapid and sensitive.

This piece of work comprises **DNA aptamer Tc18 and peptide bioreceptor** moieties bioconjugated onto gold nanoparticles to design **nanobioprobes-GNP-A and GNP-P**. TnI even at a concentration of 0.1 ng/ml behaves as an inter-connecting aggregator to link both the nanobioprobes establishing a site-directed nano-sandwich optical detection system.

As a result, the colorimetric assay develops a reliable and rapid naked-eye detection of TnI that can be easily performed by people not skilled in the art. The performance of proposed optical biosensor has displayed efficient response unhindered by components of compound serum matrix as depicted by UV-spectrum peak shift. The validation of nano-sandwich assay in clinical AMI samples has demonstrated promising comparable output as commercial TnI ELISA technique. Moreover, the specificity of nanobioprobes for TnI along with non-interfered selectivity makes the assay an ideal point-of-care investigation for early diagnosis of AMI. In context to this, direct GNP agglomeration based nanobiosensor without any external aggregator will pave novel pathways in designing sensitive, cost-effective and portable hand-held optical system for cardiac biomedical applications.

The described colorimetric assay based optical biosensor displays an instant response generation concept based on-*all we need is just a drop of serum.* However, TnI detection based on colorimetric and analytical sensitivity is enough for surveillance of AMI, nonetheless, enhanced sensitivity that can fulfill the criteria for hsTnI detection was compromised. Therefore, to fulfill the void of meeting higher sensitivity limits, electrochemical diagnostic platforms were implemented for rapid and early TnI detection discussed in next chapters. Moreover, the ability of Tc18 aptamer to form layers onto the gold surface was explored along with our collaborators at CSIR-CEERI, Pilani.

Chapter 6

Aptamer based electrochemical biosensing for sensitive detection of cardiac Troponin I

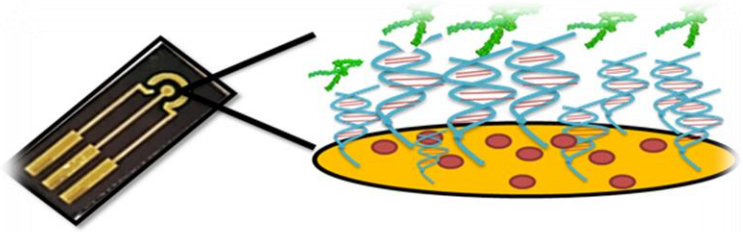

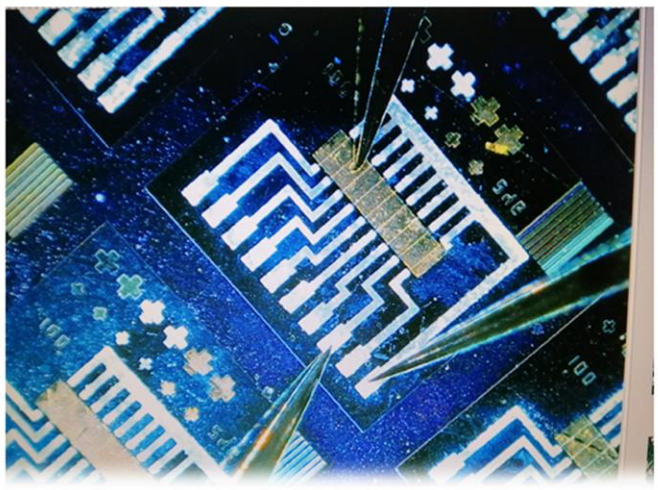

6.1 Overview

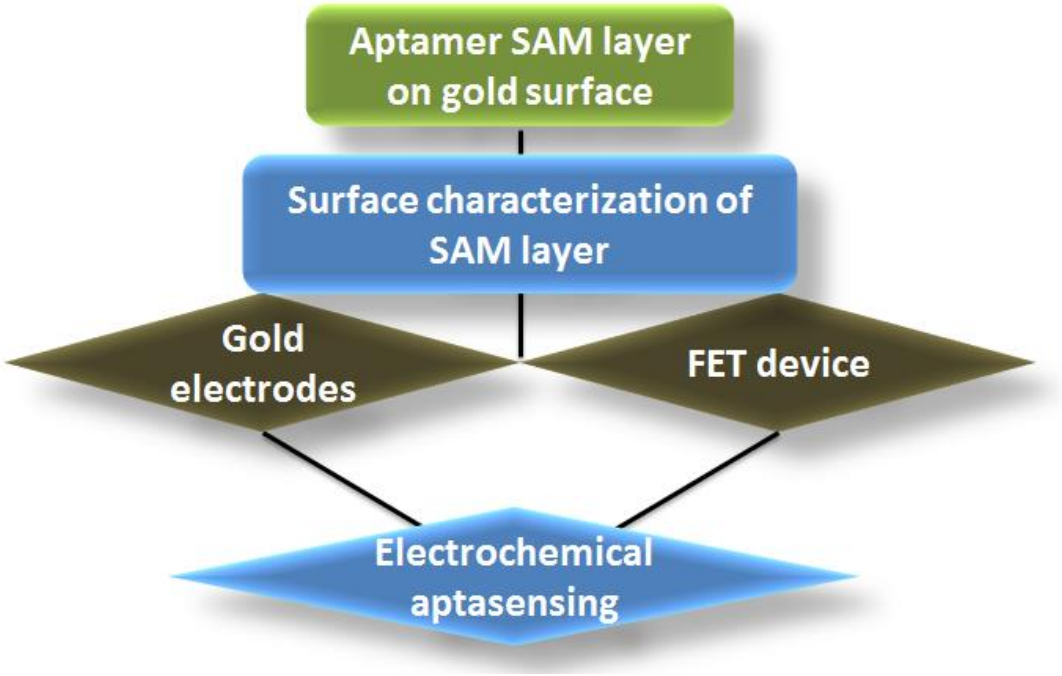

Electrochemical biosensors over the years have gathered attention for the detection of various biomarkers of clinical importance serving as next generation for medical diagnostics due to real-time analysis [179]. Alternatively, electrochemical biosensing via Silicon nanowire field-effect-transistors (Si-NW FETs) that have recently introduced as potential biosensing platforms delivering label-free detection with ultrasensitive, instant and real-time capabilities [120]. In this regard, combining the SPR related properties of gold nanoparticles studied in the last chapter, this chapter unfolds the electrochemical properties of metallic gold coated surface.

For this thiol modified Tc18 aptamer binding to terminal end of TnI was investigated for its property to form SAM (self-assembled monolayer) layer onto the gold surface. The work was performed in collaboration with CSIR-CEERI, Pilani, Rajasthan where they microfabricated gold coated electrodes and Si-NW FETs device with gold coated gate-oxide. A further description of standard microfabrication processes used to design gold coated electrodes and polysilicon FET biosensor is discussed. The use of gold for electrochemical sensing has provided an ideal platform for rapid and early detection of TnI.

6.2 Experimental approaches

6.2.1 Materials and Instrumentation

Device fabrication required acetone (Sigma) and DI water required for cleaning of glass wafer and positive photoresist (S-1818) used for optical photolithography. 6-Mercaptohexanol, KOH, H_2O_2, Trizma base, EDTA, DTT, Tween 20 were procured from Sigma. The electrode reliability and stability studies were performed using 2.5 mM ferricyanide and ferrocyanide solution in 10 mM PBS (pH 7.4). Thiol-modified aptamer Tc18 with a -SH-$(CH_2)_6$ linker at 5′ end. The aqueous solutions were prepared using 18.2 MΩ cm resistivity ultra-pure water of Merck Millipore (milli-Q water). Gold electrodes and device was fabricated at CSIR-CEERI, Pilani.

Electrochemical studies were carried out on EC workstation CHI660D with multiplexer CHI 684-8 at CSIR-IMTECH and an EC workstation Metrohm Autolab; Nova 2.1.4 at CSIR-CEERI. Contact angle measurement (Biolin Scientific), Raman Spectrophotometer, Atomic Force Microscopy were used for gold surface characterization.

6.2.2 Fabrication of gold electrode

The gold electrode/chip was designed at CEERI in L-edit software required for mask fabrication with 1 mm working electrode diameter. Microfabrication technology was used with standard unit processes such as lithography at UV-lamp intensity of 18mWcm^{-2}, deposition, etching, etc. in two-level photolithography (MA6, Suss Microtech, Mask Aligner) steps. The positive photoresist was done at first level to pattern the glass substrate with three-electrode structure. A thin layer of 200 Å titanium (Ti) was deposited by sputtering (TFSP-840, VST Israel) to improvise adhesion of gold followed by 2000 Å gold (Au) sputtering. Thereafter, lift-off process was performed in acetone solution for three-electrode realization. The passivation of patterned structure was done by SiO_2 (0.4 μm) and then Silicon Nitride Si_3N_4 (0.6 μm) via Plasma Enhanced Chemical Vapor Deposition (PECVD, Plasma Lab Oxford) for insulating entire surface of electrode and later second-level lithography was used to open sensing area window and contact pad. Subsequently, CF_4+O_2 gas was used for Reactive Ion Etching (RIE) for etching out layers of passivation from sensing area and contact pads.

6.2.3 Biofunctionalization of aptamer onto gold electrode

All the optimizations regarding biofunctionalization was performed onto gold sputtered glass chips. The Tc18 aptamer was chemically adsorbed onto gold chips by utilizing its 5' -SH-$(CH_2)_6$ linker containing thiolated terminal. Briefly, the gold chips was subjected to extensive cleaning process with piranha solution (KOH: H_2O_2=5:1) wherein 50 mM of KOH solution was used along with 25% H_2O_2 for few minutes and was further rinsed with deionized water followed by 70% ethanol. Approx. 500 nM thiolated Tc18 in TE buffer and was functionalized onto gold surface to develop a homogenous SAM (Self assembled Monolayer) of aptamer at 25˚C or room temperature for 12-16 hours. The gold chips were immersed in aptamer solution and unbound aptamers were washed with TE buffer gently. Afterwards, 2 mM 6-Mercaptohexanol was used to block gold surface for 30 minutes at RT [180]. The characterization for surface functionalization was performed at each step after cleaning, Tc18 aptamer hybridization and blocking by measuring contact angle, AFM, microscopy and Raman spectroscopy. Similarly, gold electrodes were functionalized with Tc18 aptamer.

6.2.4 Electrochemical characterization of gold electrodes

In order to investigate electrochemical sensing efficiency of fabricated gold electrodes, Cyclic Voltammetry (CV) and Impedance Spectroscopy (EIS) was adopted. For studying electrochemical charge transfer properties of gold electrode across a sweeping potential, CV was recorded in range from -0.5 to +0.5 in 6 segments volts at 50 mV/sec scan rate. While EIS scans were measured to examine charge transfer resistance at each successive step of functionalization in a frequency range of 1 Hz to 100 kHz. Both the techniques employed measurements using 2.5 mM $[Fe(CN)_6]^{3-/4-}$ as redox probe.

6.2.5 Aptasensing of Troponin I on gold electrodes

CV and Square Wave Voltammetry (SWV) electrochemical techniques were implemented to detect cardiac TnI onto gold sensor surface. Briefly, varying concentrations from 0.1-1000 pg/ml of TnI was prepared in 10 mM PBS (pH 7.5) and incubated for 30 minutes onto the aptasensor immobilized gold surface. Post incubation, excess of TnI was removed by washing with deionized water and

electrochemical scans were recorded using 2.5 mM redox couple $[Fe(CN)_6]^{-3/-4}$. CV measurements were acquired in a sweeping potential range from -0.5 to +0.5 volts at a scan rate of 50 mV/sec. While SWV scans were acquired in a stepping potential range from -1 to +1 V at 40 mV/sec scan rate.

6.2.6 Polysilicon Field Effect Transistor (FET) device fabrication

After piranha cleaning, thermal oxidation of silicon wafer with p-type, resistivity of 1-10 Ω-cm was done at high temperature of 1050^{o}C for growing 1 μm of SiO_2 to enable electrical isolation. Thereafter, deposition of 0.4 μm of polysilicon by LPCVD was achieved. Then phosphorus diffusion was carried out for 7mins @ 900^{o}C to make polysilicon to be of n-type. Further, i-line lithography was used to pattern the polysilicon to realize wire structures. The etching of polysilicon was done using reactive ion etching in sulfur hexafluoride plasma (SF_6). Gate oxide of approx. ~10 nm was grown on polysilicon wires, following lithography via opening. Then source drain doping (5E15 cm^{-2} @ 40 keV) of wafers was performed in ion implanter. Patterned photoresist was then removed and deposition of metallic gold (Au) was carried out on cleaned wafers further following metal patterning by lithography and wet etching. Thereafter, lift-off process was used to patch gold on gate followed by device passivation using PECVD of Si_3N_4 (0.4 μm) and SiO_2 (0.6 μm). After passivation by silicon nitride and oxide layers, rest of the area leaving only pads and gold gate remained exposed.

6.2.7 Aptamer immobilization onto FET device

The preliminary step for designing a FET based biosensor offering POC applications is to design biofunctionalization methodology involving maximum immobilization of bioreceptor abolishing non-specific interactions [181]. Before biofunctionalization on actual SiFET, separate pieces of glass substrate were taken to optimize the process was optimized coated with 0.2 μm thickness gold. The Tc18 aptamer SAM layer was formed by strong chemisorption of Tc18 aptamer via thiol-gold covalent bond as described in section 6.2.3 and blocked further.

6.2.8 Poly-SiFET based Troponin I aptasensing

After removing blocking solution, TnI was added in varying concentrations from 0.1-1000 ng/ml and the results were recorded. The biofunctionalization optimized

protocol was applied to SiFET and TnI response for various dilutions of was measured. Current-voltage (I-V) measurements were also performed to investigate the device functionalization.

6.3 Results and discussion

Gold electrodes manufactured at CSIR-CEERI under collaborative project were microfabricated to realize electrochemical detection of TnI based on biofunctionalization of Tc18 aptamer as detection probe. The schematic illustration of thiolated aptamer immobilization onto gold electrodes followed by electrochemical aptasensing of TnI is depicted in Fig.6.1.

Alternatively, a highly sensitive and robust SiFET device was developed at CSIR-CEERI for detection of TnI. A thin film of gold layer is integrated with device as gate terminal biofunctionalized with specific TnI binding Tc18 aptamer.

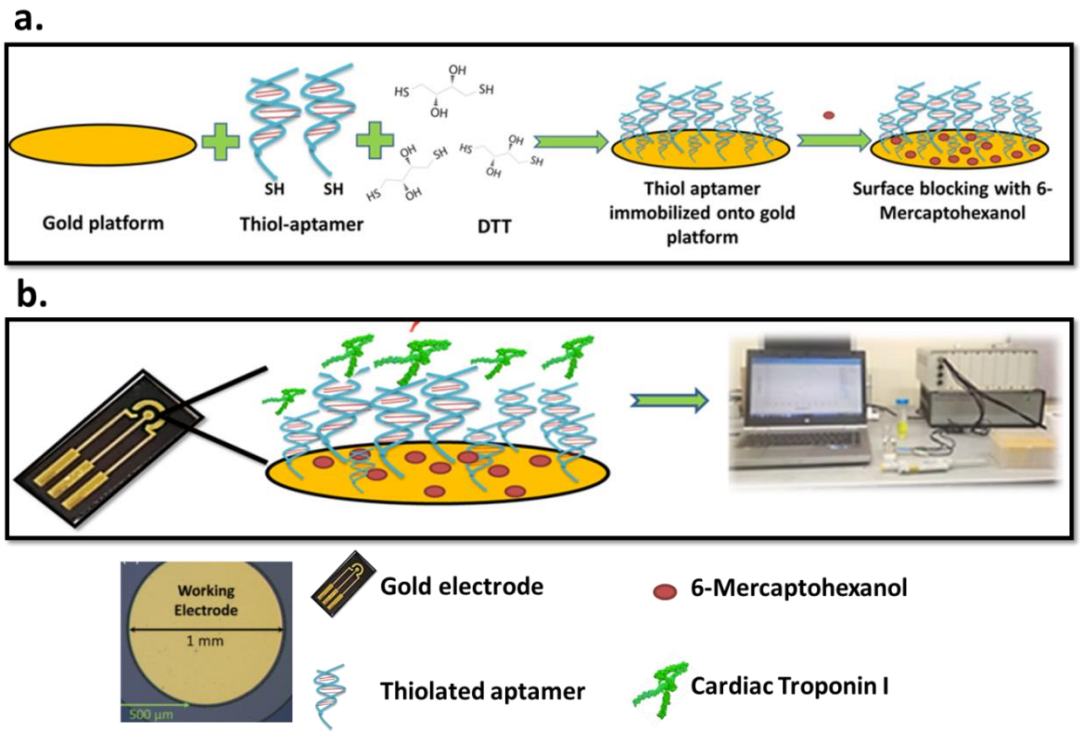

Fig.6.1 Schematic illustration of (a) Biofunctionalization of thiolated Tc18 aptamer onto gold surface (b) Electrochemical aptasensing of TnI onto gold electrode

6.3.1 Characterization of gold surface

Gold surface of electrodes enabled direct covalent biofunctionalization of thiolated aptamer without any elaborated coupling mechanisms. Similarly, gold coated gate

terminal of FET device offered high thermal stability enabling efficient immobilization of aptamer via gold-thiol linkage [154]. The gold chips as a prototype for biofunctionalization was studied using surface characterization techniques of Raman spectroscopy for functional group analysis, AFM for morphological analysis and Contact angle measurements to confirm aptamer SAM layer formation.

Contact angle measurements in Fig. 6.2 displayed the measurement angle for bare gold surface (~83.5^{o}) that decreased in for aptamer SAM (~64.4^{o}) providing increased surface wettability that suggests hydrophilic nature of the aptamer bioprobe. After incubating the chip with TnI (1000 ng/ml), the contact angle measurement declined (~44 ^{o}) further suggesting hydrophilicity of gold surface.

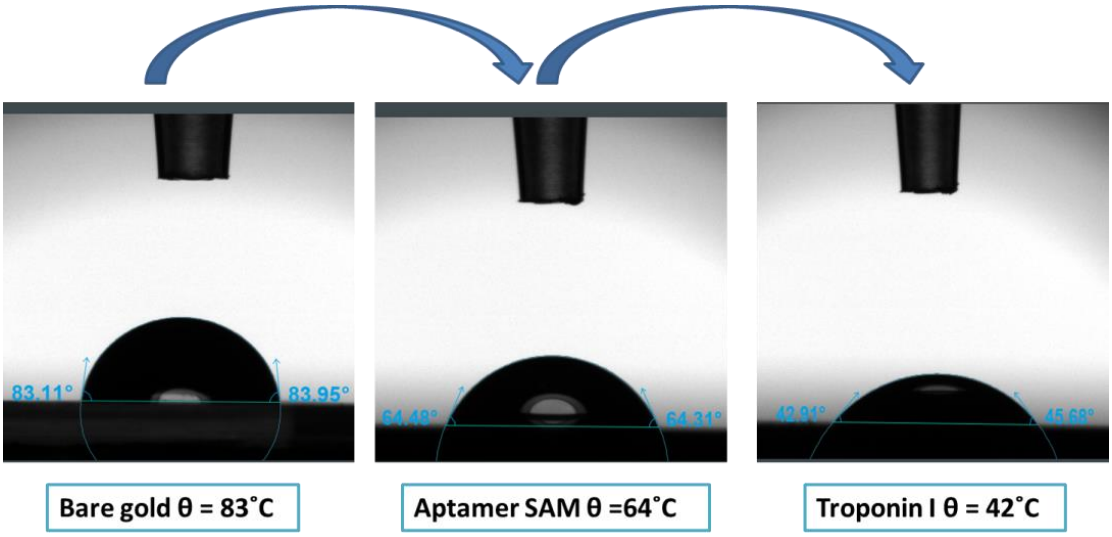

Fig.6.2 Contact-angle measurement for bare gold surface, aptamer SAM layer and TnI

The Raman peaks of at 1551 cm^{-1} corresponded to bare gold whereas an emergence of peaks at 780, 918, 1414, 1553, 2095 and 2480 cm^{-1} displayed aptamer functionalization and target TnI binding to coated aptamer was observed at 1160 cm^{-1} and 1595 cm^{-1} [182,183] (Fig.6.3).

Furthermore, Fig.6.4 shows AFM analysis at different stages of biofunctionalization. Bare gold displayed 5.59 nm peak-to-peak height, 53.07 nm for SAM of aptamer on gold surface and 118.6 nm for TnI sample onto it.

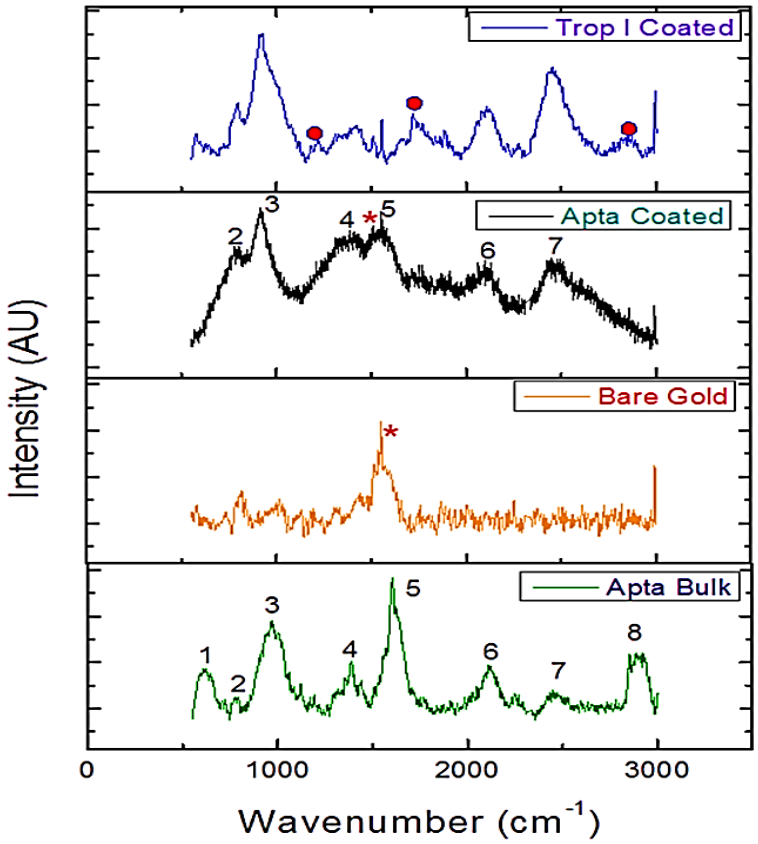

Fig.6.3 Raman spectroscopy scans for surface immobilization of aptamer and TnI onto gold surface

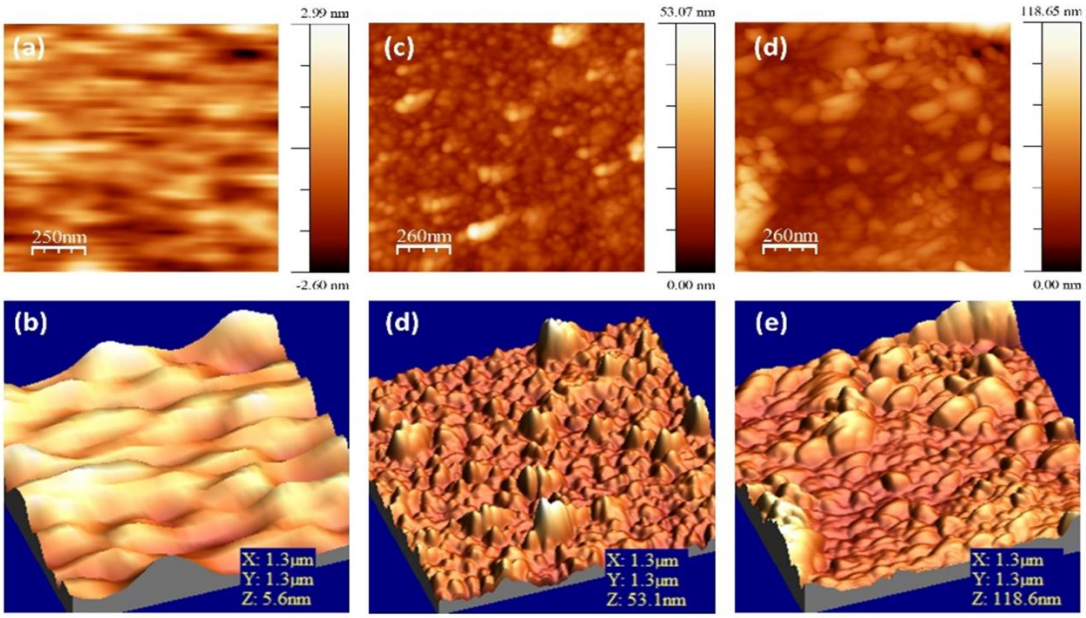

Fig.6.4 AFM analysis of (a and b) Bare gold surface (c and d) Aptamer SAM (e and f) TnI

6.3.2 Electrochemical characterization of gold electrodes

The gold electrode was electrochemically characterized by CV and EIS using 2.5 mM $[Fe(CN)_6]^{3-/4-}$ as redox couple probe. CV spectroscopic analysis in Fig. 6.5(a) exhibited an increase of 1.5 µA current signal when compared to bare gold electrode which further enhanced to 2 µA redox current upon TnI target sensing. Complying with the CV voltammogarm, EIS analysis in Fig.6.5 (b) demonstrated a decrease in electron to charge transfer resistivity upon aptamer SAM formation that further diminished upon TnI sensing. The increase in current can be attributed primarily to the negative phosphate backbone and aromatic ring containing nucleobases that act as nanowire for charge transfer. While, addition of TnI caused ligand induced structural rearrangement of aptamer that generated signal amplification of redox current and decreased charge transfer resistance [184][185].

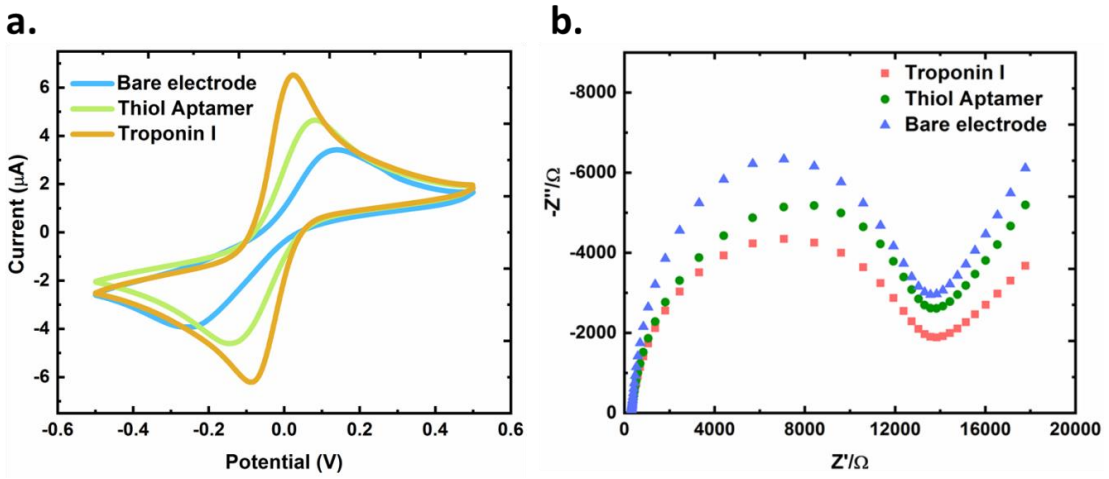

Fig.6.5 Electrochemical characterization for gold electrode fabrication after adding aptamer and TnI via (a) CV spectroscopy voltammogram (b) Impedance spectroscopy Nyquist plot

6.3.3 Aptasensing of Troponin I on gold electrodes

CV and SWV electrochemical techniques were employed for aptasensing TnI with 2.5 mM redox couple $[Fe(CN)6]^{3-/4-}$ solution in 10 mM PBS (pH 7.5). As seen in Fig.6.6 (a), an increase in redox current was noted with increasing TnI dilution. Similarly, Fig.6.6 (b) demonstrated SWV curves conferring to increasing oxidative peak current. The signal amplification was related to unfolding of DNA aptamer upon consecutive binding with TnI which contributed to enhanced electrochemical readout. Moreover, aptamer undergoes conformational isomerization upon TnI interaction which was sensed by redox probe which caused flow of current via negatively charged phosphate backbone [184] [186].

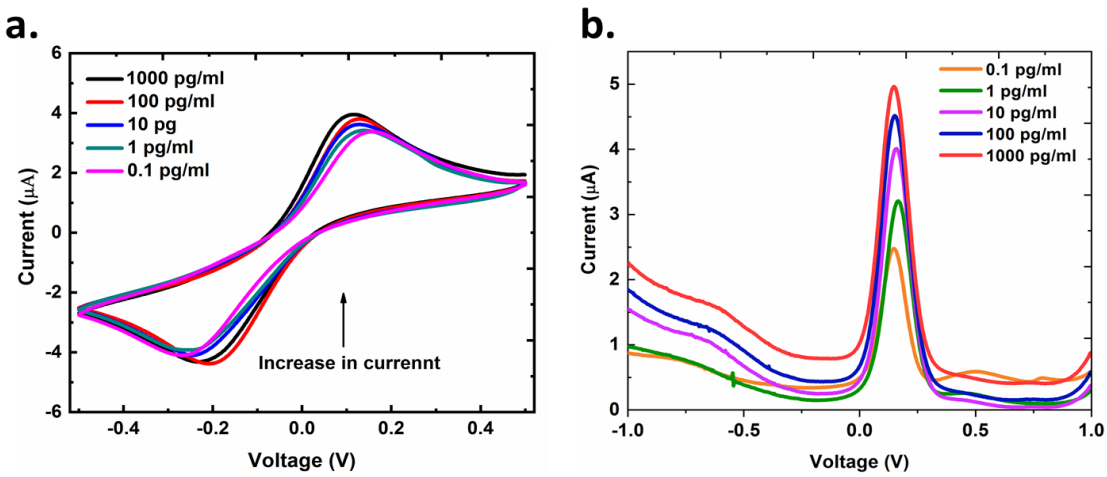

Fig.6.6 Electrochemical aptasensing at different concentrations of TnI (a) CV voltammogram showing increase in redox current (b) SWV curves showing increase in oxidation peak current

6.3.4 Electrical characterization of Polysilicon wire FET

A schematic illustration of SiFET device biofunctionalization of aptamer followed by electrochemical sensing of TnI is represented in Fig.6.7. The standard microfabrication technology was used to fabricate polysilicon FET device and was characterized using Keithley-4200 parameteric analyzer for accessing properties of transistor. Fig.6.8(a) and (b) demonstrates nine patterned polysilicon wires array on silicon wafer and gold coated gate surface fabricated biosensor device.

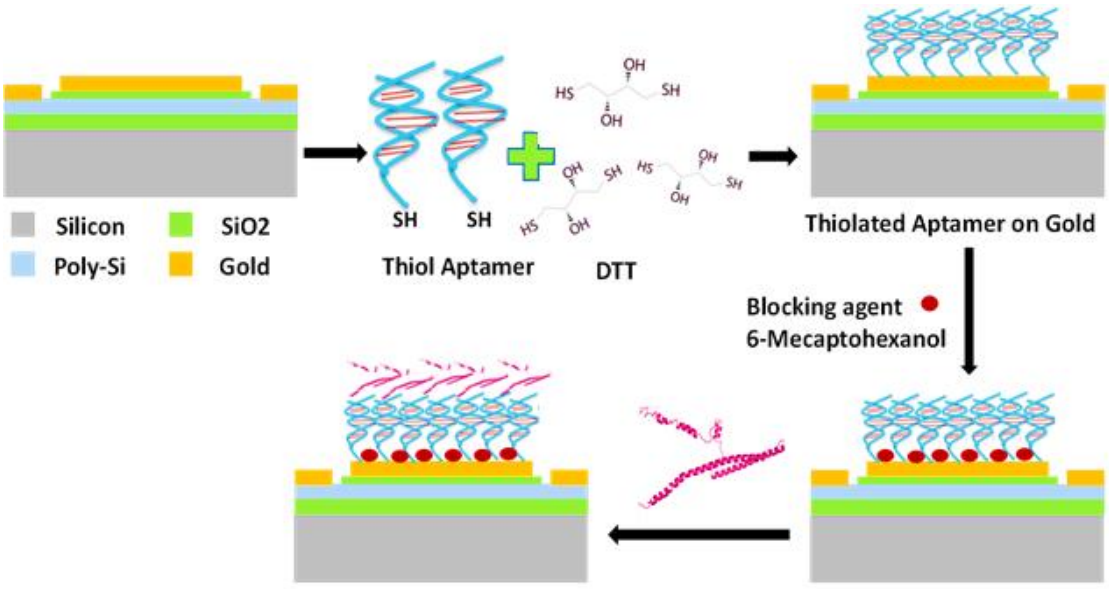

Fig.6.7 Schematic representation of biofunctionalization of aptamers onto gate terminal of FET device

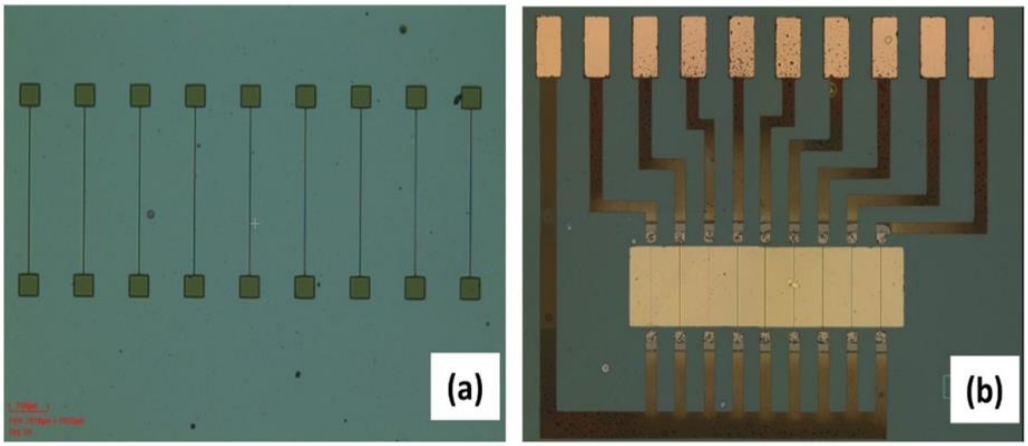

Fig.6.8 Micrographs for (a) Polysilicon wires array patterned on silicon wafer (b) Fabricated biosensor device with gold coating on gate-terminal

The array of 9 wires was characterized by maintaining constant voltage at drain to source (VDS) at 2.5 V and VGS varied in -0.4V to 0.4V range. Fig.6.9(a) represents the I-V characteristics of transistor i.e. different gate voltages (VGS) drain to source current (IDS). Although minute variation was noted for all 9 wires however, linear response with similar slope was displayed for all wires. This showed that fabricated wires were responding similarly irrespective to applied gate voltage of different base current. All the wires was found to be sensitive with ~ 4.9 to 6.4 nA/V as shown in the Figure 6.9(b).

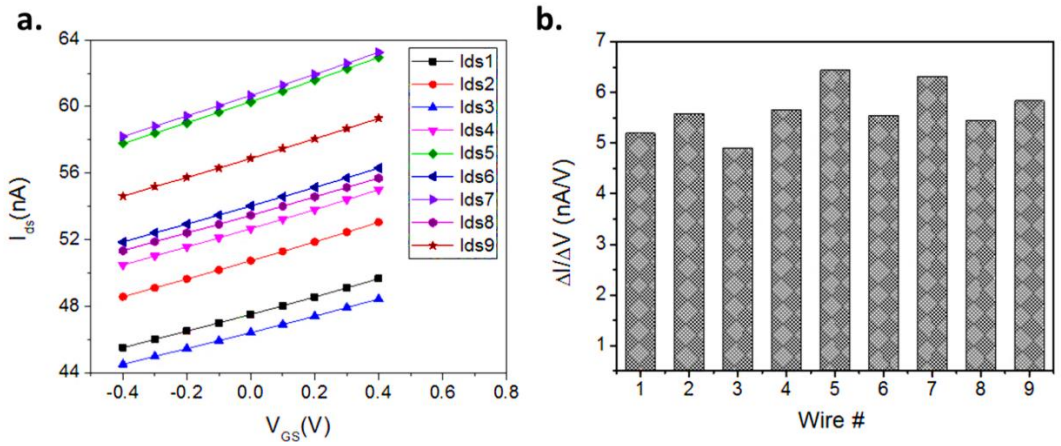

Fig.6.9 FET characteristics of all 9 wires (a) I-V data of various gate voltages at 2.5 V V_{DS} (b) Calculated slope for I-V data of all 9 wires for applied gate voltage

6.3.5 Troponin I detection using FET device

The sensor with aptamer biofunctionalized was characterized by Keithley-4200 parametric analyser. Different dilutions of Trop-I (0.1-1000 ng/ml) were dropcasted

on aptamer conjugated gate of varying sensors (similar electrical characteristics) and IDS was recorded at 2.5 V of VDS. Fig.6.10 demonstrates the electrical response of sensor with significant increase in current corresponding to concentration of TnI. The repeatability studies of sensor functioning for all tested TnI concentrations was also performed with less than 1% deviation.

An equipotential surface was provided by gold patch on gate terminal as it is preferred material for biofunctionalization. Increasing TnI dilutions on gate terminal in turn altered the accumulated charge which resulted in drain-source current modulation. TnI with 9.86 isoelectric point (pI), which means at physiological pH below its pI will develop positive charge on the surface of gate. On the contrary, for an n-type channel, current enhancement was recorded with each escalating TnI concentration. Addition of positively charged TnI in turn caused charge reversal on the gate surface immobilized with negatively charged aptamer, which led to highly stable label-free electronic signal generation [186].

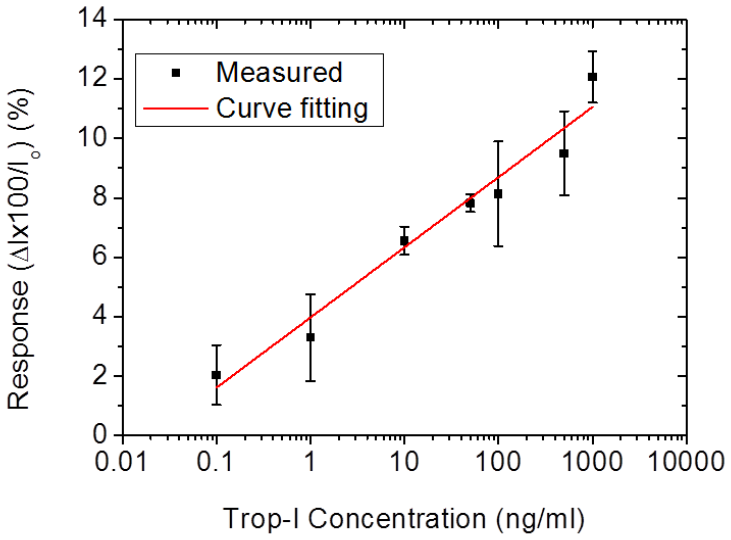

Fig.6.10 FET device response with varying dilutions of TnI detected using Tc18 aptamer

6.4 Conclusion

The current chapter comprises **applicability of metallic gold to fabricate electrochemical sensing devices** with enhanced sensing properties. Gold film coated gate terminal of polysilicon FET device and gold electrodes were synthesized at CSIR-CEERI, Pilani for electrochemical aptasensing of TnI. Due to excellent properties of metallic gold for biofunctionalization, thiol-gold interaction has been

investigated for formation of even aptamer SAM layer. In a way, **Tc18 aptamer was explored to examine its TnI binding ability in an electrochemical biosensing platform.**

The first part of this chapter describes about **gold electrodes** that were tested for their efficacy to be incorporated in TnI electrochemical aptasensing. The glass chips coated with gold film were used for immobilizing Tc18 aptamer and then TnI which was surface characterized by high end techniques such as AFM, contact angle measurement and Raman spectroscopy. CV and EIS techniques were used for testing functionality of gold chips at different steps of functionalization while CV and SWV were applied for aptasensing TnI upto 0.1 pg/ml. As deciphered from CD studies in chapter 3, the conformational isomerization of aptamer upon TnI binding has been transduced for electrochemical aptasensing. To this context, the observed increase in current signal can be attributed to the nanowire behavior of negatively charged DNA aptamer Tc18 that undergoes structural switching upon TnI binding.

On the other hand, a **poly-silicon wire FET** was fabricated and developed on silicon substrate consisting of gold coated gate terminal to functionalize thiolated Tc18 aptamer for detection of TnI. Electrical characteristics favored the fabrication scheme that can be employed for mass production due to low device-to-device variation with efficient repeatability. The current-voltage characterization for device functionality was examined and TnI biomarker concentration as low as 0.1 ng/ml was detected. Polysilicon can suggest applicability of developed FET device as point-of-care AMI diagnostics.

Apart from achieving promising TnI detection upto 0.1 ng/ml with FET device and certainly improved sensitivity of 0.1 pg/ml with gold electrodes, we thought of incorporating advanced nanomaterials for enhancing sensitivity of assay. In this regard, next chapter comprises graphene based nanomaterials for enhancing electrochemical conductivity in context of improvising TnI aptasensing.

Chapter 7

A graphene-gold nanohybrid for electrochemical aptasensing of cardiac Troponin I

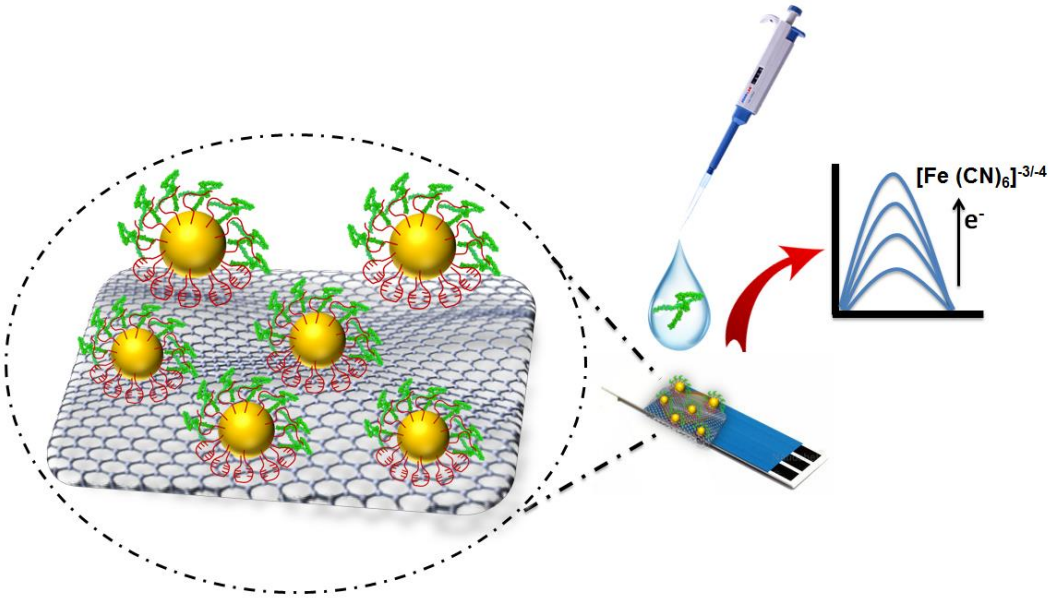

7.1 Overview

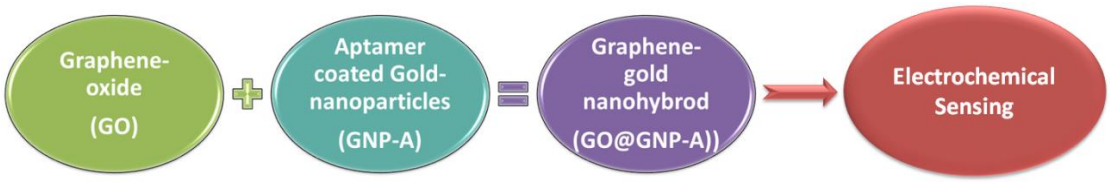

With advancement in the field of nanotechnology, electrochemical signal amplification employing nanomaterials enables fast recognition of target biomarkers using biological receptors [187]. Moreover, diversified applications of nanocomposite hybrids such as graphene-metal nanoparticles have offered synergistic physicochemical properties becoming substrates of interest in electrochemical sensing of biological markers. Among metal nanoclusters, graphene-gold nanocomposite hybrid exhibits remarkable catalytic activity and high stability promoting superior electrolytic current density and stronger raman signals [188].

Hence, after studying the efficient applicability of aptamers associated with metallic gold in the previous chapter to offer rapid electrochemical signal readout, this chapter was focused towards enhancing the sensitivity for TnI detection. To this concern, an advanced nanomaterial graphene-oxide was synthesized and conjugated with aptamer gold nanobioprobes (as synthesized in chapter 4 and 5) developing a nanohybrid based electrochemical sensing platform. Sufficiently high electrochemical signal amplification was achieved that gave us novel insights to conformational changes in the aptamer due to consecutive TnI binding.

7.2 Experimental approaches

7.2.1 Materials and Instrumentation

Sodium citrate tribasic dehydrate, Monobasic dihydrogen phosphate (KH_2PO_4), Dibasic monohydrogen phosphate (K_2HPO_4), Gold (III) chloride ($HAuCl_4$), Potassium permanganate ($KMnO_4$), graphite flakes were obtained from Sigma Aldrich (India). Sulphuric acid (H_2SO_4), Hydrochloric acid (HCl,) Phosphoric acid (H_3PO_4), Ethanol (Analytical grade) were procured from Thermo Scientific. Recombinant cardiac TnI and commercial human heart TnI (Sigma) was taken for experimentation. Blood samples of AMI patients were procured from PGIMER, Chandigarh. Thiol-modified aptamer Tc18 having -SH-$(CH_2)_6$ linker was used. Screen printed electrodes (SPE) Zensor were used for aptasensor fabrication. The aqueous

solutions were prepared using 18.2 MΩ cm resistivity ultra-pure water of Merck Millipore (milli-Q water).

Ultraviolet-Visible (UV-Vis) spectrophotometry was measured using BioTek Synergy H1 spectrophotometer (UK). Fourier Transform Infrared (FTIR) spectrum of Bruker-Vertex 70. Electron microscopy using JEOL 2100 transmission electron microscope (TEM) and Zeiss EVO 40 scanning electron microscope (SEM). For charge distribution analysis, Zetasizer NanoZS (Malvern, UK) was used. Electrophoretic characterizations were done with BioRad gel assembly. Electrochemical studies were carried out on EC workstation CHI660D with multiplexer CHI 684-8 and compact electronic interface: PalmSens using PSTrace software.

7.2.2 Synthesis and characterization of aptamer gold nanoconjugates (GNP-A)

GNPs were synthesized by citrate reduction method as mentioned in chapter 4. The GNP-A nanoconjugates were characterized by the following methods:

a. TEM: Drops of unmodified GNPs and GNP-A were placed onto carbon coated TEM grids. After drying the film, residual solution was discarded and negative staining via 2% phosphotungstic acid (PTA) was done for GNP-A nanoconjugates.

b. UV-Visible spectroscopy: UV-spectrum from 400-700 nm wavelength range was observed for GNPs and GNP-A nanoconjugates.

c. AUC: The samples were prepared by resuspending nanoconjugates in 10 mM PB (pH 7.5) with final OD=2. Bare GNPs taken as control for measurement was recorded in AUC sapphire cell of pathlength 1.2 cm. Continuous distribution AUC measurement was performed at 6000 rpm with An50 Ti Rotor. Real-time absorbance scans were recorded at λ 520 nm and 260 nm corresponding to GNP and DNA aptamer respectively. Data analysis was performed using SEDFIT by selecting continuous distribution c(s) model.

d. Agarose gel electrophoresis: GNPs and GNP-A nanoconjugates were run onto 0.8% agarose gel made in 0.5x Tris Borate EDTA buffer for an hour at 80 volts.

e. Dot Blot immunoassay: The dot blot immunoassay was performed to characterize GNP-A binding with TnI. Briefly, 2 µl of TnI concentrations 1000 ng/ml, 500 ng/ml and 250 ng/ml in diluent 10 mM PB (pH 7.5) along with no

protein control was spotted along with 2 µg/ml of BSA onto comb-shaped nitrocellulose membrane. The protein was incubated for 2 hours at room temperature. After blocking for 30 minutes with 1% BSA solution in phosphate buffer containing 0.1 % Tween 20, the comb was dipped in GNP-A solution at 37˚C for another two hours under constant shaking. Afterwards, comb was washed thrice with block buffer for 30 seconds each to remove unbound GNP-A. Silver enhancement solution was added to develop the spot signal and excess solution was washed away with deionized water.

7.2.3 Synthesis of Graphene Oxide (GO)

Improved Hummer's method was used to synthesize graphene oxide (GO) as reported in literature with slight modifications [189]. Briefly, a mixture of 0.75g graphite flakes and 4.5 g $KMnO_4$ was added to 100 ml volume of 9:1 concentrated H_2SO_4 and H_3PO_4 mixture in a round bottom flask. The mixture was raised to 50°C temperature using an oil bath along with overnight stirring on a magnetic stirrer. Next day, reaction was brought to room temperature in an ice bath and then mixed with 3 ml of 30% H_2O_2 suspended in 100 ml of deionized (DI) water. The aqueous mixture was then centrifuged at 11,000 rpm for 1 hour and supernatant was removed. The remaining pellet was washed multiple times with DI water to remove residual acid until pH of suspension reached 6.0. Then solution was sonicated and centrifuged at 6000 rpm for 1 hour. GO was separated from supernatant and freeze-dried. An amount of 1 mg lyophilized GO was suspended in 1 ml of 10 mM PB (pH 7.5) as 100x stock solution. The prepared GO was characterized using Zeta-sizer for charge analysis, SEM and TEM for morphology studies, UV-spectroscopy and FTIR to study functional groups predominant in GO.

7.2.4 Synthesis and characterization of graphene-gold nanohybrid (GO@GNP-A)

To prepare graphene-gold nanohybrid (GO@GNP-A), 750 µl of GNP-A gold nanoconjugates was mixed with 350 µl GO making final mixture volume to 1 ml containing 35x GO. The mixture was left for overnight binding at 4˚C under constant rotation. Further, the mixture was centrifuged at low speed of 5000 rpm for 1 hour to remove unbound GNP-A. After separating supernatant, soft precipitate was washed thrice with 10 mM PB (pH 7.4) and was resuspended in same buffer. GO@GNP-A

was characterized by SEM, TEM, UV-spectroscopy, FTIR and ζ-potential described as follows:

a. **Electron Microscopy:** SEM and TEM was performed to examine morphology of GO and GO@GNP-A nanohybrid. Briefly, GO and GO@GNP-A nanohybrid suspension was dropcasted onto pre-cut clean silicon wafer and dried for about 30 minutes and then scans for surface morphology of samples were taken using a SEM equipped with thermal field emission emitter. Similarly, TEM images were taken by dropcasting GO and GO@GNP-A onto copper coated grids and kept for drying at room temperature for 20 minutes. The measurements were performed at an accelerating voltage of 120 kV.
b. **UV-Spectroscopy:** The prepared GO, GNP-A nanoconjugates and GO@GNP-A nanohybrid were analyzed for their spectroscopic properties under wavelength range from 200-1000 nm.
c. **FTIR:** FTIR spectrum was measured in of 500-4000 cm^{-1} range. Briefly, GO and nanohybrid GO@GNP-A were lyophilized by freeze-drying followed by mixing with potassium bromide (KBr) powder in ratio 2:98 respectively by vigorous grinding of mixture using mortar and pestle to a fine powder. Due to its transparency in IR, KBr remains inert as window material between 4000–400 cm^{-1}.
d. **Zeta Potential:** Samples of GO, GNP-A nanoconjugates and GO@GNP-A nanohybrid were suspended in 10 mM phosphate buffer (pH 7.5) and diluted 10 folds to measure charge distribution.

7.2.5 Fabrication of GO@GNP-A aptasensor

The aptasensor was fabricated by simply dropcasting the prepared nanohybrid suspension of GO@GNP-A onto screen printed electrode (SPE) consisting 3-mm-diameter carbon-paste working-electrode, carbon/graphite counter electrode and reference-electrode Ag/AgCl. Prior to nanohybrid modification, SPE was subjected to extensive cleaning by uniformly polishing the working area of electrode with 0.3 µm and 0.05 µm sized alumina granules. The electrode was washed with DI water and ultrasonicated for 1 min in absolute ethanol and DI water respectively. Subsequent cleaning sonication was repeated after polishing with 0.05 µm alumina slurry. Afterwards, 50 µl nanohybrid GO@GNP-A was dropcasted onto working area of SPE and dried at 37˚C for 12-16 hours. The fabricated aptasensor was then characterized and assessed for their electrochemical performance using cyclic voltammetry (CV) and

chronoamperometry. CV scan was accumulated at 50 mV s^{-1} scan rate to study charge transfer properties along a potential range of -0.4 to +0.8 V at each successive step contributing to nanohybrid formation. Chronoamperometry was performed at constant 0.25 V potential measuring change in current as a function of time (0-5 s/20 ms scan rate) to study diffusion process on sensing platform.

7.2.6 Biosensing of Troponin I and selectivity of aptasensor

Square Wave Voltammetry (SWV) technique was employed for GO@GNP-A nanohybrid based aptasensing of TnI. Briefly, varying TnI dilutions (0.001-1000 pg/mL) in 1x PB (pH 7.4) was incubated on fabricated aptasensor for 20 min followed by washing unbound protein with DI water. SWV signal was recorded in duplicates using 5 mM redox couple $[Fe(CN)6]^{-3/-4}$ within potential range from -0.5 V to +0.5 V at 40 mV/s scan rate. A standard calibration curve was plotted for logarithmic TnI concentrations (pg/mL) and their corresponding peak current values of SWV scans. Alongside, chronoamperometry was performed for lower concentrations of TnI (0.001-1 pg/mL) to study consistent diffusion process occurring at aptasensor fabricated electrode surface. A fixed voltage of 0.25 V was set to measure electrode decay process for 0-4 s at 20 ms scan rate. Moreover, serum samples in 1:10 µL dilution was used to spike various concentrations of TnI and SWV signal was measured and the peak current values were used to plot a calibration curve with linear fitting as mentioned above.

Additionally, interference of other cardiac biomarkers such as BNP, N-terminal Pro-BNP, Myoglobin and BSA was examined in duplicates at excess concentration than TnI for selectivity of aptasensor. The reproducibility of electrochemical performance for aptasensor was analyzed by recording six SWV scans for TnI 10 pg/ml after every 2 hours interval. Moreover, the efficiency and long-term stability of the fabricated GO@GNP-A nanohybrid aptasensor was observed.

The electrochemical sensor was also examined for generating current signal response by replacing Tc18 aptamer with peptide bioreceptor (discussed in chapter 4 and 5) to detect TnI. The nanoconjugates of cysteine containing peptide functionalized gold particles as GNP-P were synthesized using Au-thiol linkage. Simultaneously, GNP-P was attached with GO to form nanohybrid of GO@GNP-P which was further employed to record SWV scans for varying concentrations of TnI at potential range from -1 to 1 V using redox couple $[Fe(CN)_6]^{-3/-4}$.

7.2.7 Clinical samples evaluation by developed GO@GNP-A aptasensor

Five AMI positive and five AMI negative (healthy individual serum) samples were taken and proficiency of fabricated GO@GNP-A nanohybrid aptasensor was investigated. Briefly, 50 µl of each undiluted serum sample was incubated for 15 minutes onto GO@GNP-A aptasensor and SWV scans were recorded in duplicates in 5 mM redox couple [Fe $(CN)_6$ $]^{-3/-4}$ in similar stepping voltammetric range.

7.3 Results and Discussion

The proposed biosensor consists nanohybrid of GO and GNP biointerfaced with DNA aptamer to design an electrochemical aptasensor for rapid and early detection of TnI. Fig.7.1(a) depicts graphical illustration of GO synthesis using graphite flakes. Further, thiolated Tc18 aptamer was functionalized onto gold particles to form GNP-A nanoconjugates depicted in Fig.7.1(b) [154] [190] [155]. Subsequently, Fig.7.1(c) displays interaction of GNP-A with GO sheets to construct nanohybrid of GO@GNP-A onto which aptasensing of TnI was performed as shown in Fig.7.1(d) [191].

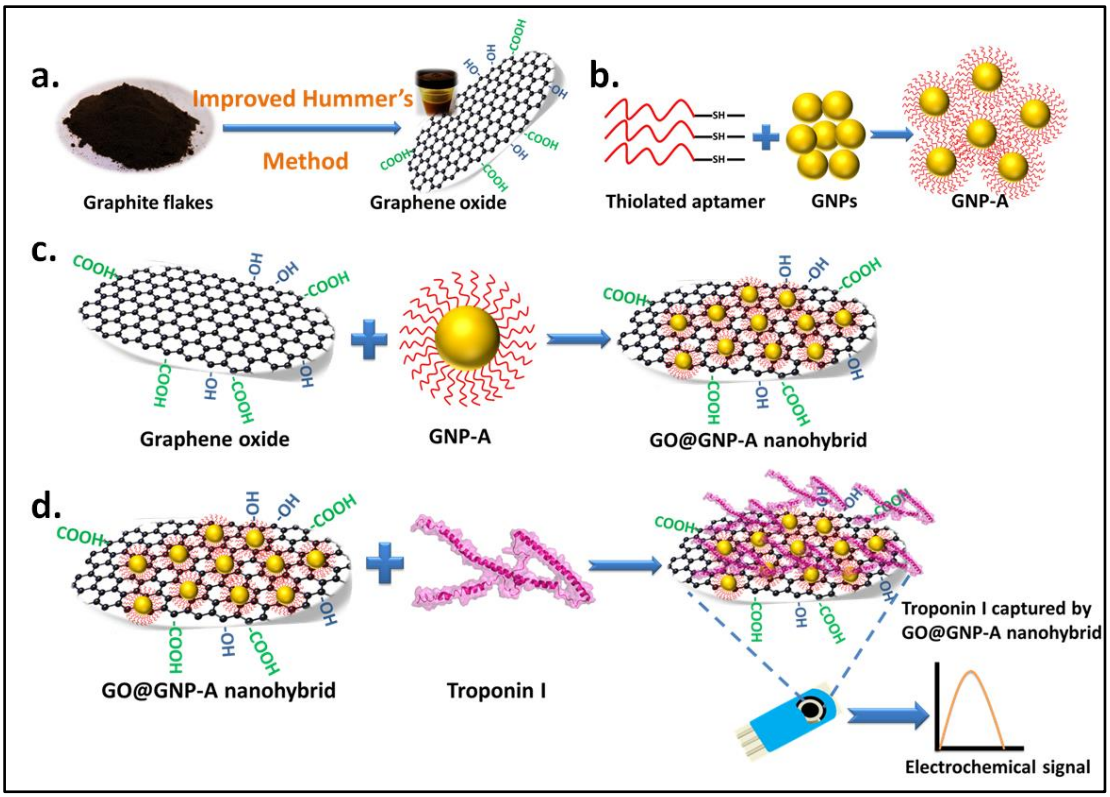

Fig.7.1 Schematic illustration of graphene-gold based electrochemical aptasensing of TnI (a) Synthesis of graphene oxide (GO) using improve hummer's method (b) Synthesis of aptamer conjugated gold nanoparticles (GNP-A) (c) Formation of gold-graphene nanohybrid (GO@GNP-A) (d) Detection of TnI onto GO@GNP-A fabricated screen printed electrode

7.3.1 Characterization of GNP-A nanoconjugates

GNP-A nanoconjugates bearing Tc18 aptamer were studied for their morphological properties by TEM providing 16±3 nm size corresponding to 80% immobilization efficiency as calculated in previous studies [Fig. 7.2(a) and (b)] [192]. Gel electrophoresis in Fig.7.2(c) demonstrates restricted mobility of GNP-A nanoconjugates as compared to unmodified GNPs suggesting the bulkiness of aptamer conjugated nanoclusters.

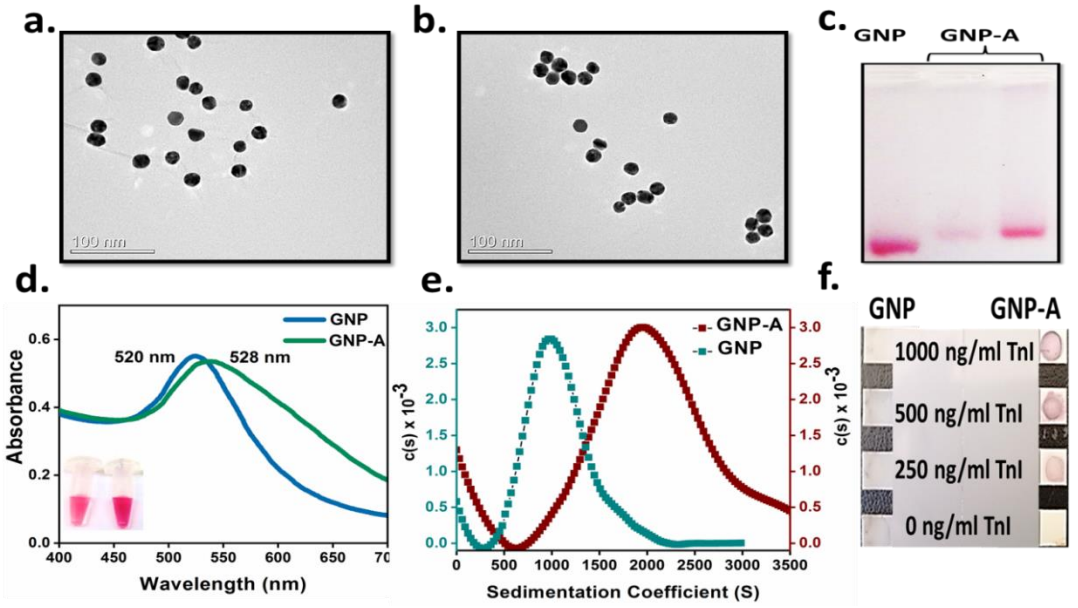

Fig.7.2 Characterization of GNP-A (a and b) TEM micrograph of GNP and GNP-A (c) Agarose gel electrophoresis showing restricted mobility of GNP- A compared to bare GNPs (d) UV-spectra showing 8 nm peak shift in GNP-A (e) SV-AUC of GNP-A showing higher sedimentation coefficient value than GNP (f) Dot-blot showing binding of GNP-A to TnI

UV-spectroscopy also corroborated Tc18 aptamer conjugation onto GNPs with a characteristic red peak shift of 8 nm in plasmon resonance of nanoconjugates from its characteristic gold peak at λ520 nm [Fig.7.2(d)]. Moreover, an increase in sedimentation coefficient (S) via Sedimentation Velocity AUC experiments (SV-AUC) for GNP-A nanoconjugates was observed to be in close agreement with other characterizations in Fig.7.2(e). To this support, a dot-blot immunoassay was performed that substantiated binding ability of GNP-A for TnI as visible dots with reference to bare GNPs in Fig.7.2(f).

7.3.2 Synthesis of GO and nanohybrid GO@GNP-A for TnI aptasensing

Further, for synthesizing nanohybrid, GO was made using Improved Hummer's method which produced hydrophilic oxidized regular-structured carbon material as compared to conventional Hummer's method. This method is useful for large scale production of GO under controlled temperature without generating toxic gases [189][193]. The well-structured morphology of GO enabled efficient attachment of GNP-A nanoconjugates producing gold-graphene nanohybrid. The rationale behind generating GO@GNP-A nanohybrid intrigues high prospects to explore multiple properties of both nanomaterials cooperatively attributing to enhanced conductivity and ease of bio-molecular functionalization [194][195]. As shown in previous studies, covalent interaction of GNP-A with GO instead of electrochemical reduction of gold onto GO sheets eliminates two-step nanohybrid fabrication [196]. Tc18 aptamer and GO utilizes π–π stacking interactions to form GO@GNP-A nanohybrid [197][198]. The nucleoside units of Tc18 aptamer forms strong cooperative π–π stacking with hexagonal rings of GO along with hydrophobic, hydrogen and vander waals bonding [199][200]. The unengaged aptamer moieties functionalized onto GNP interact with TnI transducing biological interaction to enhanced electrochemical response.

7.3.3 Characterization of GO and GO@GNP-A nanohybrid

a. Electron microscopy: The morphological studies of GO and GO@GNP-A nanohybrid was subjected to SEM and TEM analysis. SEM micrograph displayed grooved texture with flexible and large lateral graphene sheets stacked within itself due to π-π linkage in two dimensions in Fig.7.3(a). This in turn promotes greater mechanical tensile strength and minimizes surface energy [201]. While SEM of GO@GNP-A in Fig.7.3(b) reveals evenly decorated GNP-A nanoconjugates on large surface of GO sheets. TEM micrograph in Fig.7.3(c) presents crumbled and layered sheets of GO exhibiting flake-like shape, whereas nanohybrid GO@GNP-A in Fig.7.3(d) displays homologous distribution of GNP-A onto smooth and planar surface of GO sheets. To our assumption, presence of discrete GNP-A on surface of graphene remarkably suppressed the wrinkling of graphene without any clustering. Additionally, synthesis mechanism of nanohybrid by incubation of GNP-A nanoconjugates with GO suspension yielded even settling of GNP-A avoiding their clustering as aggregates.

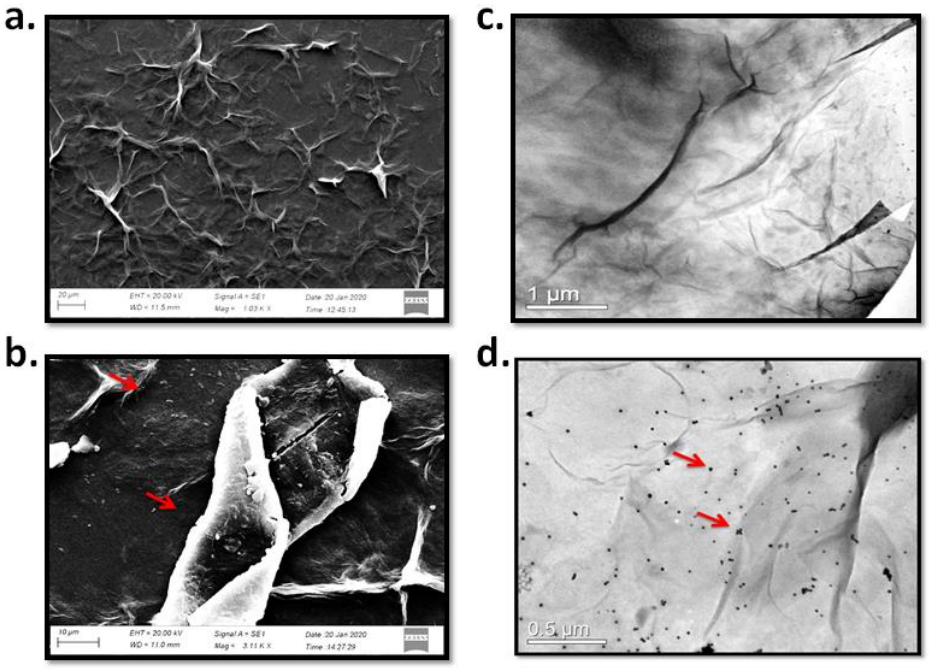

Fig.7.3 Morphological characterization showing (a and b) SEM micrograph of GO and GO@GNP-A (c and d) TEM images of GO and GO@GNP-A nanohybrid

b. UV-Spectroscopy: Furthermore, optical properties were examined via UV-spectroscopy in Fig.7.4(a). Primarily, GO represented a characteristic peak of π- π* transition for aromatic C-C bond and sp2 hybridized C=C bond at 230 nm [202]. GNP-A nanoconjugates demonstrated another peak near 530 nm conferring to red-shift in gold plasmon absorbance (520 nm) which was prominent in nanohybrid GO@GNP-A as well [203]. A peak representing C=C-C=C conjugated double bond of purine and pyrimidine base at 260 nm was observed, clatifying immobilization of GNP-A on GO.

c. FTIR: Moreover, nanohybrid synthesis by attachment of GNP-A onto GO was confirmed using FTIR analysis in Fig.7.4(b) which demonstrates broad band at 3423 cm^{-1} of various -OH stretching in GO along with peak at 1623 cm^{-1} conferring to sp^2 carbon network of C=C stretch. Another band coinciding to C=O stretch confirms presence of carboxylic acid observed at 1400 cm^{-1} and peaks related to stretch -C-O-C- at wavenumber 1056 cm^{-1} suggested presence of alkoxy and epoxy groups on surface of GO [204]. After synthesis of nanohybrid, FTIR spectra exhibited all characteristic peaks corresponding to GO along with some additional peaks at 862 cm^{-1} relating to symmetrical stretching vibrations of deoxyribose-phosphate linkage and strong bending vibrations of phosphate backbone was seen

at wavenumbers 996 cm^{-1} and 1082 cm^{-1}[202]. Additionally, an intense peak relating to presence of nucleoside bases of Adenine/Guanine of DNA aptamer at 1378 cm^{-1} was also observed, confirming successful immobilization of GNP-A onto GO. These additional and flexible variation in IR intensities was corroborated to partial reformation of C=C linkages in GO@GNP-A nanohybrid due to GO reduction during synthesis.

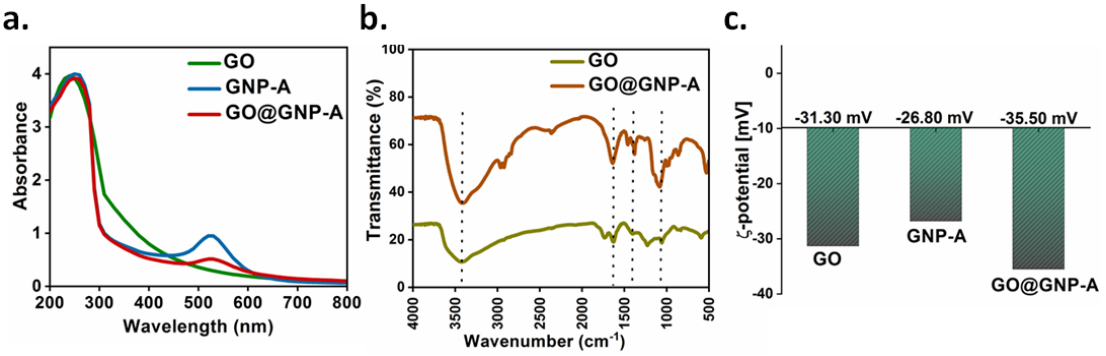

Fig.7.4 Characterization of GO@GNP-A nanohybrid (a) UV-spectra of GO, GNP-A and nanohybrid GO@GNP-A (b) FTIR spectra of GO and its nanohybrid with GNP-A (c) Charge distribution analysis involving synthesis of GO, GNP-A and GO@GNP-A

d. ζ-potential: Charge distribution of synthesized GO sheets and its complementary nanohybrid GO@GNP-A was analyzed by inspecting their ζ-potential. A negative potential of -31.30 mV was observed for GO suspension in 10 mM PB, pH 7.5 due to presence of C=O linkages [199]. While after addition of GNP-A, potential value declined to -26.80 mV and eventually decreased to -35.50 mV for nanohybrid GO@GNP-A in Fig.7.4(c).

7.3.4 Characterization of fabricated GO@GNP-A aptasensor

CV and chronoamperometry techniques were employed to analyze electrochemical performance of fabricated aptasensor assessed at each successive step of nanohybrid synthesis. CV voltammogram obtained at 50 mVs^{-1} scan rate in 5mM $[Fe(CN)_6]^{3-/4-}$ solution displayed an increase in anodic and cathodic peak current at subsequent electrode modification in Fig.7.5(a). GO to GO@GNP synthesis step depicted 10 µA elevation in redox peak current. While, a sharp increase of 35 µA redox current for GO@GNP-A clearly indicated that Tc18 aptamer is responsible for huge signal amplification. This suggested that GO@GNP-A

nanohybrid has better electron transfer capacity due to combined enhanced conductivity and increased surface area contributed by both nanomaterials. Further, when TnI was incubated onto the nanohybrid fabricated aptasensor (GO@GNP-A@TnI), electrochemical current signal escalated by 10 μA redox current. Additionally, chronoamperogram obtained at constant 0.25 V potential to analyze the redox species diffusion process for electrode modification step is shown in Fig.7.5(b). A subsequent increase in current at each successive step of nanohybrid formation was observed under 0-5 s time duration. Simultaneously, a distinctive escalation of amperometric signal from GO@GNP to GO@GNP-A corresponded to Tc18 aptamer.

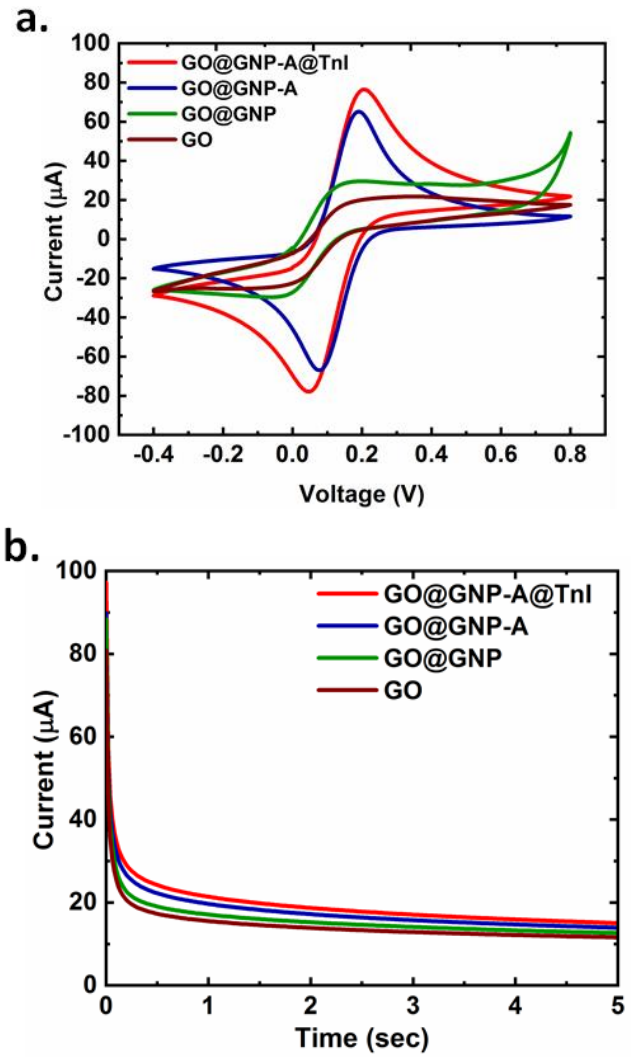

Fig.7.5 Electrochemical characterization of fabricated aptasensor (a) CV voltammogram depicting increasing current with each step of nanomaterial functionalization (b) Chronoamperometry curves showing increasing current with time at constant voltage

7.3.5 Electrochemical aptasensing of TnI

SWV was applied for label-free aptasensing of TnI using 5 mM $[Fe(CN)6]^{3-/4-}$ as redox probe. TnI in experimental buffer from 0.001-1000 pg/mL concentration was captured on GO@GNP-A nanohybrid biointerface. SWV scans depicted linearity in increase of peak current in Fig.7.6(a) upon increasing concentrations of TnI that was substantiated to cooperative electron transfer properties of synthesized nanohybrid [34]. A calibration curve was best fitted with a correlation regression coefficient of R^2=0.98 between logarithmic concentration of TnI and SWV peak current values in Fig.7.6(b). Additionally, chronoamperometry curves in Fig.7.6(c) for lower TnI dilutions also revealed increasing current signal. Further, Fig.7.6(d) displayed SWV curves of serum spiking studies showing increasing current corresponding to TnI dilutions along the calibration curve in Fig.7.6(e) with R^2=0.97. This revealed efficient performance of GO@GNP-A nanohybrid aptasensor in compound serum matrix. Moreover, repeatability studies performed at 0.01 pg/mL TnI revealed similar SWV curves with almost aligning peak currents that suggested reproducibility of electrochemical aptasensing assay in Fig.7.6(f).

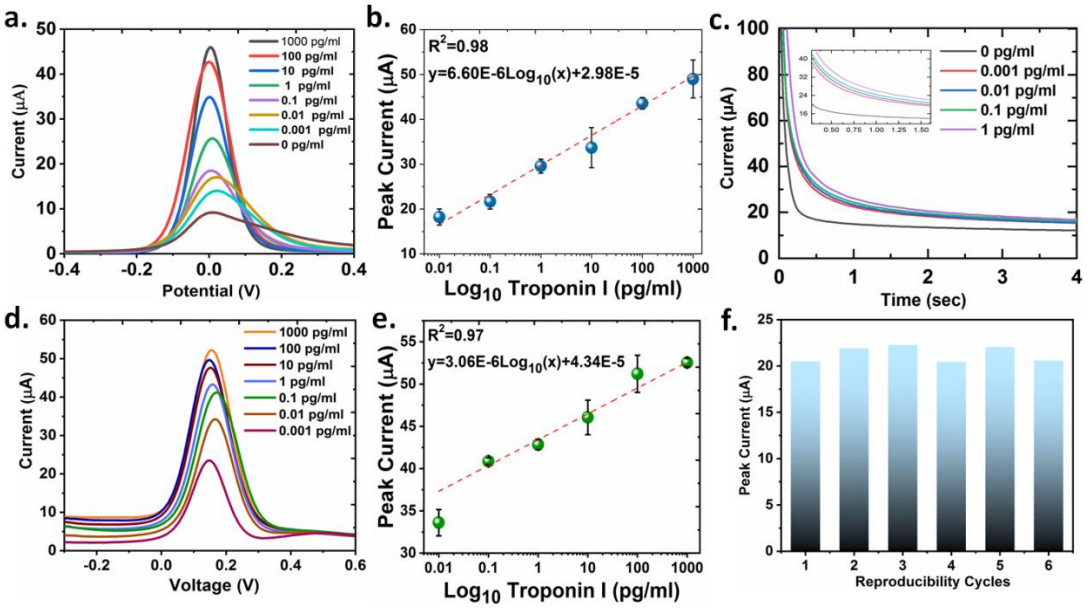

Fig.7.6 Electrochemical aptasensing of TnI (a) SWV curves for TnI sensing in buffer (b) Calibration curve for linear fitting of peak current values for TnI sensing in buffer with R^2=0.98 (c) Chronoamperometry analysis for TnI aptasensing at low concentrations (d) SWV curves of TnI sensing spiked in serum (e) Calibration curve for linear fitting of peak current values for TnI spiked in serum with R^2=0.97 (f) Reproducibility cycles of GO@GNP-A based aptasensing of 10 pg/mL TnI

To further study the effect of any nonspecific moiety which might interfere in specific target detection, the fabricated aptasensor was investigated to analyze other possible biomarkers found in blood circulation. SWV revealed highest peak current signal for TnI as compared to other non-specific targets in Fig.7.7(a) which is more prominently identified by SWV curves in Fig.7.7(b). Consequently, this suggested insignificant hindrance from non-specific targets depicting selectivity of developed aptasensor towards TnI.

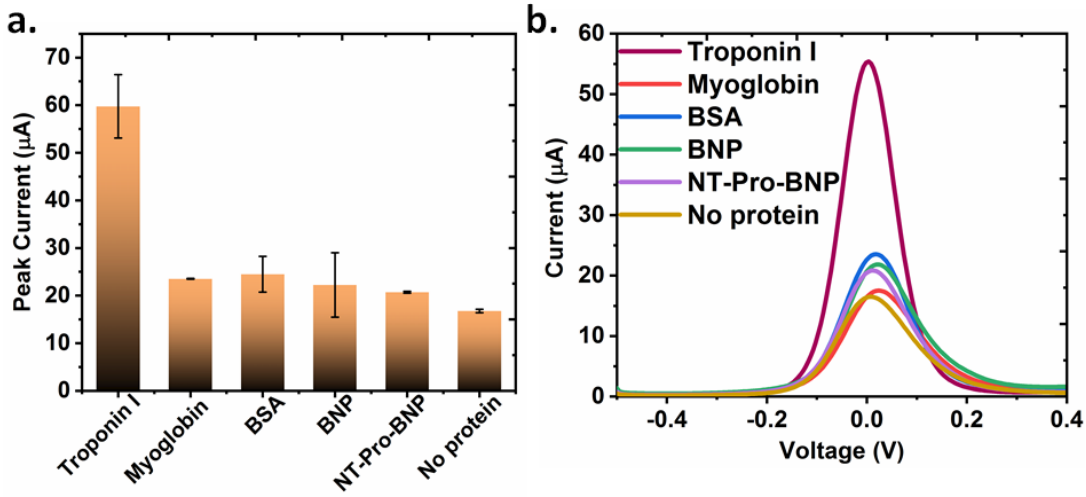

Fig. 7.7 Specificity studies for GO@GNP-A based TnI aptasensing (a) Peak current values of SWV curves of TnI along with non-specific targets (b) SWV curves of TnI compared to non-specific biomarkers

The average recovery of TnI in low concentration standards of 0.1 pg/ml TnI was 115%, 1 pg/ml was 93% and for higher range 100 pg/ml was 112%. This depicts determined consistency with aptasensor detected results eliminating non-specificity due to serum components. A detection limit of 0.001 fg/ml was calculated by 3α/slope where α is standard deviation of blank measurement and slope was obtained from standard plot which is much lower than studies enlisted in literature.

7.3.6 Cause of increase in current signal

The increase in current is associated with conformational isomerization of Tc18 aptamer upon TnI binding which was further sensed by redox probe $[Fe(CN)_6]^{3-/4-}$ resulting in transfer of electrons between the redox couple and SPE [205][206]. Herein, phosphate backbone of DNA aptamer is supposed to act as nanowire for conducting charge transfer which structurally rearranges with each increase in TnI

[207]. Besides, according to a previous study, it can be hypothesized that binding of TnI to aptamer in 10 mM PB, pH 7.5 (pH less than pI of protein) reverses the surface charge that leads to changing from repulsion to attraction of redox probe, thus increasing conductivity [186]. This induced charge reversal at aptamer-GO interface in-turn is sensed by SPE facilitating label-free electrochemical aptasensing of TnI [186,208]. Fig.7.8 clearly explains both the phenomenon inducing increase in current signal.

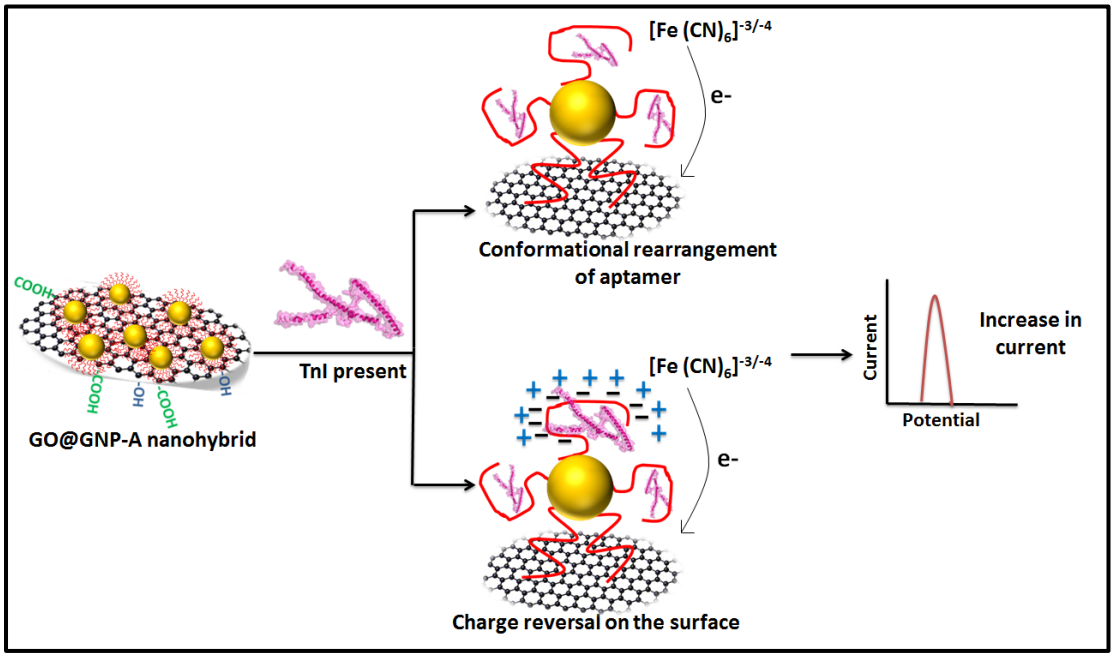

Fig.7.8 Schematic showing TnI aptasensing causing increase in current due to structural-rearrangement of aptamer on GO interface and charge-reversal phenomenon

Alongside, when aptamer was replaced by peptide as biorecognition element to detect TnI, the peptide based GO@GNP-P nanohybrid electrochemical sensing demonstrated decrease in current signal in Fig.7.9(a-c). This observation further emphasized upon aptamer to be resolutely responsible for increasing the electrochemical signal [167].

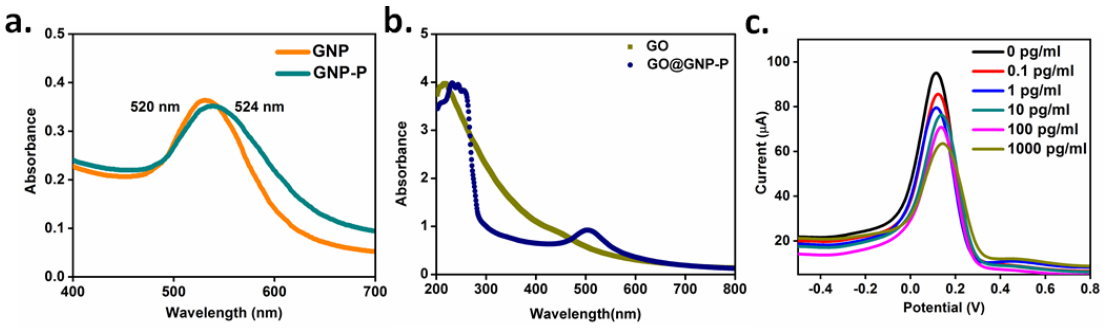

Fig.7.9 Peptide based detection of TnI (a) UV-spectrum of GNP-P nanoconjugate (b) UV-spectrum for GO@GNP-P nanohybrid formation (c) GO@GNP-P based TnI detection SWV curves

7.3.7 GO@GNP-A aptasensing verification in clinical samples

Five blood samples from AMI patients collected from PGIMER, Chandigarh were inspected to validate competency of discussed aptasensor. SWV scans were recorded for each positive and negative sample onto GO@GNP-A fabricated aptasensor revealing differential oxidative peak current values depicted in Fig.7.10(a). A statistical analysis depicted 80% sensitivity and 100% specificity of GO@GNP-A aptasensor correlating to 100% PPV (positive predictive value) and 83.33% NPV (negative predictive value) in Fig.7.10(b).

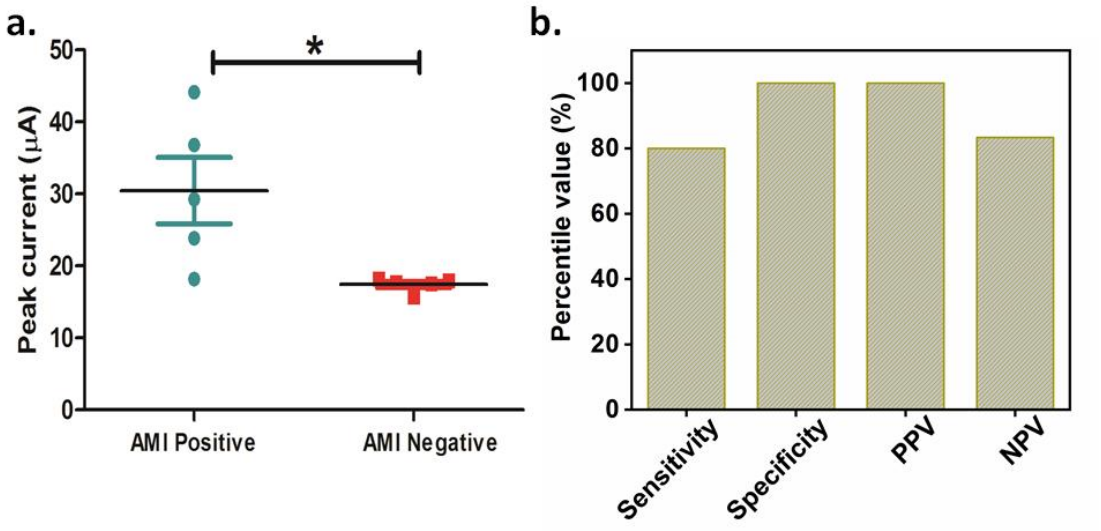

Fig.7.10 GO@GNP-A aptasensing of TnI in clinical samples (a) Peak current values for SWV curves of clinical samples (b) Statistical evaluation of clinical samples assessment via GO@GNP-A aptasensing

7.4 Conclusion

The current chapter encompasses advanced **nanomaterial GO along with Tc18 GNP-A nanoconjugates to form nanohybrid GO@GNP-A**. GO was synthesized by improved hummer's technique and was characterized by SEM and TEM for its morphological properties accompanied by UV-spectroscopy and FTIR for optical properties conferring to presence of functional groups. Moreover, Tc18 aptamer bearing GNP-A nanoconjugates were characterized separately as mentioned in previous chapter 4 and 5 describing dot-blot assay and colorimetric assay respectively.

GO was surface anchored to aptamer nanoconjugates (GNP-A) via π-π interactions between DNA and GO functional groups for specific TnI capturing. The

electrochemical assessment of fabricated aptasensor was achieved by CV and chronoamperometry that displayed step by step increase in current with each nanomaterial being fabricated on SPE as: GO to GO@GNP to GO@GNP-A to GO@GNP-A@TnI. The stable, robust and reproducible output generation for as low as 0.001pg/ml or 1fg/ml TnI targeting was achieved by using SWV technique with ultralow detection limit of 0.001fg/ml. **The obtained consecutive increase in charge transfer current signal can be correlated with CD signatures of TnI induced structural-rearrangement of aptamer** as discussed in chapter 3. **The aptamer consecutively opens/unfolds its secondary structure to bind increasing concentration of TnI. We can speculate that aptamer here acts as a nanowire that has contributed to increasing current signal.** The designed aptasensor is specific abolishing any non-specific binding with other cardiac biomarkers. Its promising performance to detect TnI in AMI clinical samples even avoids interference from components of serum matrix with repeatable reproducibility. In this regard, the proposed GO@GNP-A nanohybrid based label-free electrochemical aptasensing offers dynamic applicability in point-of-care surveillance and regular periodic monitoring of TnI for rapid and early AMI diagnostics in hospitals.

Summary & Future perspectives of the study

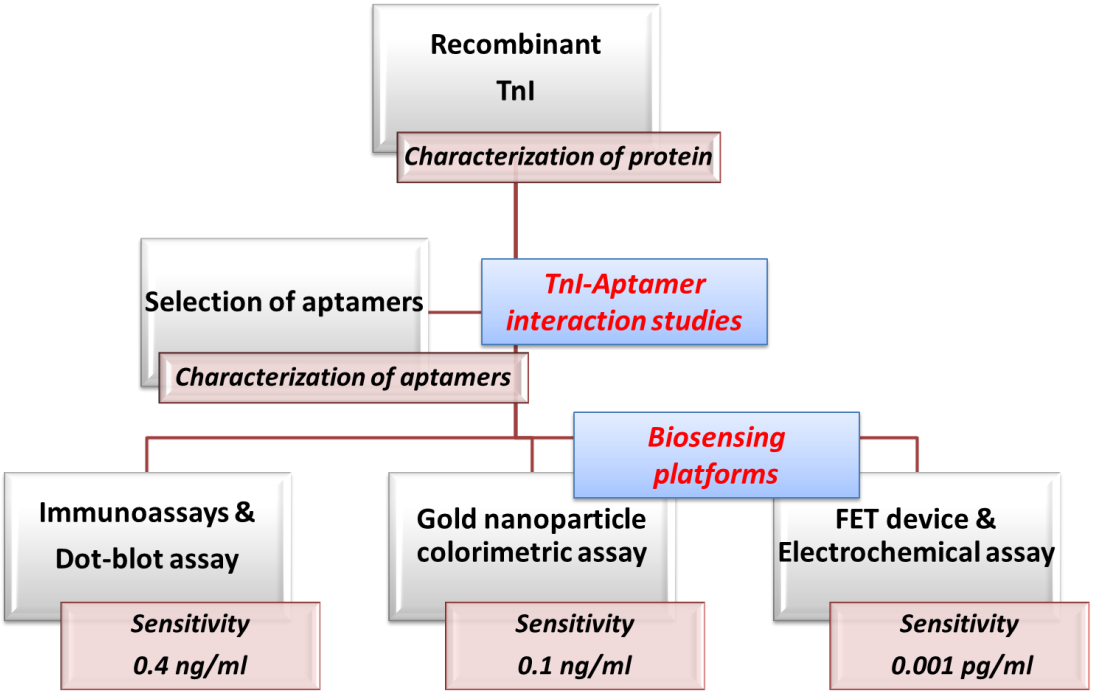
Recombinant
TnI
Characterization of protein
Selection of aptamers
TnI-Aptamer interaction studies
Characterization of aptamers
Biosensing platforms
Immunoassays &
Dot-blot assay
Sensitivity
0.4 ng/ml
Gold nanoparticle colorimetric assay
Sensitivity
0.1 ng/ml
FET device &
Electrochemical assay
Sensitivity
0.001 pg/ml

Summary

The **first chapter** covers the basic literature one should be aware of regarding the cardiovascular diseases and importance of biochemical markers for diagnosing AMI. It also comprises details regarding relevance of TnI as biomarker of choice for cardiac disorders of acute coronary syndrome along with particulars of its mechanism of release and degradation in the bloodstream. Moreover, an elementary introduction to SELEX and aptamer generation have been given with maximum focus drawn on aptamers to be used as potential biorecognition elements compared to conventional antibodies. The current state-of-art comprising antibodies based market for TnI detection consists of Abott iSTAT microfabricated device. It gives quantitative detection of TnI but is extremely costly and is not accessible to common man. Although, various AMI diagnostics strategies are available to detect TnI but the absence of a quantitative test that is rapid and at the same time cost effective is the current need in medical settings. All this literature review was studied to build knowledge on already available techniques for biosensing further bridging the gap to design novel methodologies of TnI detection on a view to improvise available detection limits of rapid, sensitive and early diagnosis.

As the cost associated with natural human heart TnI was extremely high, hence the **second chapter** investigates the heterologous gene expression of human TnI was achieved in *E. coli* bacterial system with several modifications applied to previously described protocols for achieving high protein yield. Recombinant TnI was expressed in soluble fraction and on-column urea refolding protocol was adopted for Ni-NTA based Immobilized Metal Affinity Chromatography (IMAC) purification. A yield of approx. 1-2 mg/ml TnI was obtained that was measured using nanodrop from 500 µl of bacterial culture. Various characterizations were performed based on SDS-PAGE displaying single band near 28 kDa **(Fig. 2.3)** and MALDI-TOF analysis showing 100% intensity peak of 28.5 kDa for its purity **(Fig. 2.4)**. Moreover, secondary structural identification was performed using biophysical technique of CD spectroscopy that deduced α-helix feature of recombinant TnI with a negative peak at 208 nm coinciding with commercial human heart TnI **(Fig.2.5)**. This was further supported with 3-D structure of TnI deduced by I-TASSER tool due to unavailability

of its PDB structure in repository that predicted a filamentous structure containing 4 α-helices **(Fig.2.6)**. Additionally, a biochemical assay of indirect microtiter ELISA with commercial Mab supported binding ability of recombinant TnI which was used for further aptamer binding studies.

Consequently, four aptamers (Tn13.2a, Tn24.1 for N-terminal and Tc18, Tc35p for C-terminal) were selected; two each from both the peripheral peptide targets of TnI **(Fig.2.10)**. It was found via indirect binding ELISA that only C-terminal peptide specific aptamers firmly bind with recombinant TnI protein in **Fig.2.11**, so we propagated our studies with Tc18 and Tc35p. Both the aptamers were monomeric in nature displaying an intense band of Tc18 near 55 bp and an accelerated migration of Tc35p near 50 bp as observed by gel electrophoresis **(Fig.2.12)**. The binding strength of aptamers towards TnI protein was quantified by biophysical biomolecular interaction technique of BLI. The method deduced binding in terms of dissociation constant (K_D) via global fitting of association and dissociation curves as $1.06x10^{-9}$ M for Tc18 and $1.84x10^{-7}$ M for Tc35p **(Fig.2.13)**. Besides, secondary structural folding of both aptamers as determined by CD spectroscopy demonstrated B-form of DNA helix with a negative peak at around 245 nm and a positive peak at around 280 nm relating to poly[d(AT)] configuration **(Fig.2.14)**. Secondary structure analysis was performed with Mfold that revealed Tc18 attaining hairpin loop and Tc35p as an extended stem-loop configuration **(Fig.2.15)**. While tertiary structures of aptamers were predicted using webserver RNA Composer **(Fig.2.16)**.

Although aptamers were shown to bind recombinant TnI nevertheless there were many aspects to acknowledge for gaining profound insights of interaction pattern for aptamers. Hence, in **chapter three,** interaction studies of Tc18 and Tc35p aptamers were performed as a function of varying amount of recombinant TnI. To this context, various biochemical and biophysical experimentations were performed further corroborated with *in silico* docking studies. Preliminary, sandwich ELISA was performed to identify the binding efficacy of both aptamers as match-pair candidates in combination with commercial Mab, which described that Tc18 surpassed Tc35p in detecting 0.1 ng/ml TnI **(Fig.3.2)**. In support to this, binding kinetics using BLI displayed dissociation constant for Tc18 (2×10^{-9}) and Tc35p (3.5×10^{-8}) for varying TnI dilutions **(Fig.3.3)**. Alongside, the conformational transition based CD studies revealed rearrangement of Tc18 and Tc35p secondary structures by interacting with

increasing concentration of TnI envisaging a strong concept of TnI induced structural-switching of aptamers **(Fig.3.5)**. The results from both BLI and CD can be conferred to large hair-pin loop like structure of Tc18 enabling better interaction with TnI as compared to Tc35p. Apart from studying interaction of aptamers with TnI, the property of forming in-solution complex was inspected by non-radioactive electrophoretic mobility shift assay (EMSA)-a DNA-protein interaction technique, size exclusion chromatography (SEC) and analytical ultracentrifugation (AUC). Agarose gel based EMSA displayed decrement in aptamer band intensity with increasing TnI as they get involved in complex formation showing restricted mobility **(Fig.3.8)**. Additionally, velocity experiments of AUC resulted in increased sedimentation coefficients corresponding to settling of Tc18-TnI and Tc35p-TnI complexes due to bulky behavior as compared to individual aptamers taken as controls **(Fig.3.9)**. Moreover, SEC purification also eluted the aptamer-TnI complex prior to elution of TnI taken as control **(Fig.3.10)**. All these results deciphered stable complex formation that can be exploited for targeting ultralow concentration of TnI in compound serum samples and real clinical samples. Consequently, the precise understanding of biomolecular interaction of aptamer-TnI were supported with docking studies performed using HDOCK-a DNA-protein docking tool **(Fig.3.12)**. Subsequently, first highest scoring model out of ten predicted models was analyzed to identify interacting residues via PDBsum-an EMBL-EBI server. Generally, aptamer-target binding can result due to spatial adjustment, electrostatic interactions, hydrogen bonding, van der waals forces, aromatic group interactions, etc. Only hydrogen bonding was prioritized to study the binding partners residues within 4Å distance range using visualization software PyMOL to which Tc18-TnI (C43-Asp190, A42-Trp191, T33-Trp191) **(Fig.3.13)** and Tc35p-TnI (G8-Asp196, C37-P-C38-Leu198, A22-Asn194) **(Fig.3.14)** were predicted.

So far in in chapters 2 and 3, we have achieved the expression and purification of cardiac biomarker TnI and determined its stable interaction with DNA aptamers specific to its terminal peptide fragments by various biochemical and biophysical techniques. Moreover, the binding efficacies of both aptamers towards TnI have also been displayed in complex serum matrix. On the basis of aforementioned accomplishments, we navigated our research towards developing various TnI detection platforms for early diagnosis of AMI.

The **chapter 4** encompasses the preliminary biosensing platform of immunodiagnostic assays as sandwich microtiter ELISA and dip-stick based dot-blot assays for TnI detection. Two configurations of sandwich ELISA were designed with PolyAb as counterpart forming match-pair with aptamer. First version comprised capturing of biotinylated aptamers using avidin-biotin linkage **(Fig.4.2)** and second version comprises of aptamers to be used as target bioreceptors **(Fig.4.3)**. Both the aptamers detected 0.2 ng/ml TnI as capture bioprobes even in spiked serum samples. While only Tc18 aptamer displayed affinity for TnI as target probe with 0.2 ng/ml sensitivity Standard curves were plotted for serum spiking studies to quantitate unknown concentration of TnI. Simultaneously, a peptide was studied from literature to bind TnI as a bioreceptor reported by Banta *et al.* In order to avoid the use of antibodies for developing biosensing platforms, a sandwich microtiter assay employing the novel match-pair of aptamer-peptide was performed that detected 0.4 ng/ml of TnI **(Fig.4.4)**. This unique combination of stable and easily reproducible bioreceptors further suggests its applicability in designing advanced TnI diagnostic platforms.

The target recognizing ability of both the aptamers was validated to detect TnI in clinical samples of AMI patients which were procured from PGIMER, Chandigarh under collaborative project. Tc18 and Tc35p aptamers were immobilized via avidin-biotin linkage as capture bioprobes to perform sandwich ELISA in combination with PolyAb. Both the aptamers detected TnI content in clinical samples with Tc18 aptamer displaying positive predictive value (PPV)=100% and negative predictive value (NPV)=86.95% and Tc35p aptamer depicting PPV=98% and NPV=95% **(Fig.4.5)**. Consequently, complying with the *in vitro* studies of chapter 3, Tc18 due to its structural hair-pin loop folding was found to be more sensitive and specific than Tc35p for detecting TnI in clinical samples. A cohort study for 40 positive and 20 negative samples was performed along with the interference studies from possible biomarker proteins that may be abundant in human sera was examined.

Another aspect of study was to examine the Tc18 aptamer as a nanobioprobe that could provide visible naked-eye detection of TnI. In view of this, dot-blot immunoassays were implemented subsequently expanding binding affinity of Tc18 aptamer for TnI. This reduced the time duration of ELISA making the diagnosis cost-

effective without requiring any labeled enzymes. The signal was further intensified with silver-enhancement solution that enlarges the colloidal gold nanoconjugates by precipitating silver to produce high-contrast visible signals as dots. GNP-A were synthesized by functionalizing an optimized concentration of thiolated Tc18 aptamer onto gold nanoparticles (GNPs) using gold-thiol covalent linkage which was characterized by UV-spectroscopy, electron microscopy, Dynamic Light Scattering (DLS) and gel electrophoresis **(Fig.4.8)**. The assay resulted in appearance of different intensity of spots corresponding to TnI concentration after silver enhancement of GNP-A **(Fig.4.9)**. The dot-blot assay was specific for TnI even spiked in serum upto 1 pg/ml without any interference from other cardiac biomarkers such as Myoglobin, BNP (Brain Natriuretic Peptide) and NT-Pro-BNP (N-terminal Pro-BNP). Image J software was employed for quantification of spots that calculated the individual spot density to plot linear calibration curves.

Moreover, the ability of Tc18 aptamer nanobioprobe to effectively detect TnI in dot-blot suggested its applicability to design a test card assay that would produce results rapidly. To this context, a lateral-flow immunoassay was designed where Tc18 aptamer conjugated GNPs were used as signaling molecule. A red color line was observed when TnI was added to the strips with sensitivity of 0.1 ng/ml **(Fig.4.10)**.

We wanted to design aptamer-aptamer based assays eliminating the utility of antibodies due to their bulky nature and batch-to-batch variation. But the limitation of similar negative charge based repulsion of aptamers did not provide any successful leads. Therefore, as we discussed in chapter 4 about the aptamer-peptide match-pair sandwich ELISA, we reciprocated the respective assay into a colloidal platform. Hence, **chapter 5** proposes a site-directed GNP sandwich aggregation assay enabling rapid naked-eye detection of TnI. The docking analysis in chapter 2 revealed structural binding interface of Tc18 aptamer at C-terminal peptide whereas peptide interacts with a fragment located distantly on TnI. These discrete binding regions for both bioreceptors laid the foundation for developing a nano-sandwich assay that does not require any external agent to cause aggregation **(Fig.5.1)**. The nanoconjugates for both bioreceptors-GNP-A (aptamer conjugated gold nanoparticles) and GNP-P (peptide conjugated gold nanoparticles) were synthesized using gold-thiol linkage by optimizing maximum graft density. Various characterization methods such as UV-

spectroscopy, TEM, DLS, zeta-potential and agarose gel electrophoresis further corroborated the formation of stable nanoconjugates **(Fig.5.4 and 5.5)**. Biophysical analysis via CD spectroscopy and BLI was also performed to study TnI binding of gold nanoconjugates **(Fig.5.6)**. Most importantly, individual GNP-A and GNP-P nanoconjugates did not induce aggregation. This in turn strengthened the foundation of colorimetric nano-sandwich assay involving cooperative effect of GNP-A and GNP-P to varying TnI dilutions from 0.1-500 ng/ml. Both nanobioprobes interact with TnI at distinct regions causing a visible color change from cherry red to wine red and further purple to blue. This naked-eye color change induces a considerable spectral shift corresponding to TnI concentration depicting a decline at λ_{520} of surface plasmon for GNPs with highly intense broadening of peak at λ_{620} **(Fig.5.8)**. The essential feature of the demonstrated colorimetric assay is distinguished from Chad Mirkin's conventional salt based aggregation phenomenon in an aspect of being aggregator-free. The specificity of the aggregation assay was determined towards TnI as examined by incorporating other cardiac biomarkers **(Fig.5.8)**. Furthermore, both gold nanobioprobes detected and induced aggregation in serum spiked with natural TnI causing a visible color change **(Fig.5.8)**. For quantification of aggregation in unknown samples, absorbance ratio of A_{620nm}/A_{520nm} was calculated to plot a standard calibration curve. The practical applicability of colorimetric assay was validated with ten AMI clinical samples along with ten negative samples. The instant visible color change was observed in positive samples as compared to negative samples. Adding more to verify the proposed assay, commercial TnI ELISA kit was incorporated to analyze the same samples. It was observed that results of colloidal assay for nine samples correlated with commercial ELISA. The specificity of nano-sandwich colorimetric assay is 100% as compared to commercial ELISA, whereas the assay was 90% sensitive **(Fig.5.9)**. Therefore, the discussed TnI detection nano-sandwich colorimetric strategy illustrates a rapid and cost-effective GNP nanobiosensor without any involvement of external aggregator.

Subsequently, we were approached by our collaborators at CSIR-CEERI, Pilani, Rajasthan to examine the efficiency of their microfabricated devices by using Tc18 aptamer synthesized by our lab at CSIR-IMTECH. They developed gold electrodes/chips of 1mm working area by using photolithography technique. Moreover, a highly sensitive and robust polysilicon Field Effect Transistor (SiFET)

device integrated with a thin film of gold layer as gate terminal was also developed using standard microfabrication process. The functionality of both devices was characterized by electrochemical aptasensing of TnI through biofunctionalization of Tc18 aptamer as detection probe. Thiol-gold interaction was exploited for formation of self-assembled monolayer (SAM) of Tc18 aptamer onto gold surface with surface characterization performed at each step. Contact angle measurements, Raman spectroscopy and AFM were performed after cleaning, aptamer SAM formation and TnI sensing **(Fig.6.2, 6.3 and 6.4)**. The electrochemical characterization of gold electrode for each step of functionalization was performed via Cyclic Voltammetry (CV) and Electrochemical Impedance Spectroscopy (EIS). Following that, electrochemical aptasensing of varying concentration of TnI from 0.1-1000 pg/ml was performed with Square Wave Voltammetry (SWV) on gold devices **(Fig.6.6)**. An increase in current signal of oxidative peak current in SWV was obtained corresponding to increasing concentration of TnI. On the other hand, a FET device was fabricated and developed on silicon consisting of gate terminal coated with gold **(Fig.6.7)**. The gate terminal was biofunctionalized with thiolated Tc18 and I-V measurements were taken with slope calculated for I-V data of all 9 wires for applied gate voltage **(Fig.6.9)**. For FET device, any change in TnI concentration from 0.1-1000 ng/ml altered the accumulated charge on gate terminal resulting in the drain-source current modulation **(Fig.6.10)**. Consequently, an illustrative work of FET device was achieved measuring ng/ml of TnI due to some technical limitations.

As the last chapter provided some insights regarding electrochemical sensing of TnI, the next purpose was to enhance the sensitivity of the assay. In this regard, another electrochemical aptasensing platform was explored by using advanced nanomaterials for ultra-sensitive detection of TnI. Therefore, **chapter 7** describes a nanohybrid of graphene oxide (GO) and gold nanoparticles (GNP) for exploiting the synergistic physicochemical properties of both nanocomposites **(Fig.7.1)**. Tc18 as GNP-A gold nanoconjugates were synthesized and characterized as mentioned in chapter 4 and 5. On the other hand, GO was synthesized by Improved Hummer's method which is better than conventional methods to generate regular-structured hydrophilic oxidized graphene material in higher amount without generating toxic gas. The GO@GNP-A nanohybrid was made by utilizing π–π stacking interactions of hexagonal rings of GO interacting with nucleoside DNA bases. GO and its corresponding nanohybrid was

examined for morphological properties using electron microscopy (SEM/TEM) **(Fig.7.3)** and optical properties via UV-spectroscopy along with fourier-transform infrared spectroscopy (FTIR) displaying IR peaks corresponding to functional groups of GO and nanohybrid **(Fig.7.4)**. The fabricated nanohybrid aptasensor was dropcasted onto screen printed electrode (SPE) and CV and chronoamperometry techniques were performed for electrochemical characterization. An increased current signals at each step of nanohybrid synthesis from GO to GO@GNP complex followed by GO@GNP-A nanohybrid was observed using redox couple $[Fe(CN)6]^{3-/4-}$ which further increased with GO@GNP-A@TnI **(Fig.7.5)**. After all the optimizations, TnI aptasensing was performed in an ultralow range from 0.001-1000 pg/ml using SWV technique **(Fig.7.6)**. A consecutive increase in the oxidative peak current corresponding to TnI concentration was obtained. This increase in current is corroborated to conformational rearrangement of aptamer upon TnI binding as characterized by CD studies in chapter 3. Adding more to what has been mentioned, it was suggested that phosphate backbone of DNA aptamer acts as a nanowire for causing charge transfer phenomenon corresponding to increasing concentration of TnI. The analytical performance of GO@GNP-A aptasensor was determined in serum spiking studies as well and a calibration curve was plotted. A detection limit of 0.0001 fg/ml was calculated and it was observed that electrochemical performance of nanohybrid aptasensor abolished any background effect from other non-specific cardiac biomarkers **(Fig.7.7)**. The fabricated aptasensor was verified for its efficacy by analyzing AMI clinical samples to detect TnI. Five positive and negative samples were validated by GO@GNP-A based aptasensor to record SWV scans which resulted in increased oxidative peak current values of positive samples as compared to negative samples **(Fig.7.10)**.

As of now, the last four chapters compile the biosensing platforms for sensitive detection of cardiac TnI. We have demonstrated four different TnI detection strategies by overcoming the limitations of our own former methods and enhancing the sensitivity for the latter and advanced platforms. The ability of both the aptamers to recognize TnI from clinical specimens further defines their potency as promising bioreceptor candidates to develop cost-effective, sensitive and portable point-of-care testing hand-held devices detecting TnI in myocardial infarction patients.

Future perspectives of the study

The present investigation can be explored in various aspects to augment the utility of aptamers synthesized in the discussed work for real-time practical biosensing applications. For the first time, this novel technique of generating aptamers against apical peptide fragments of biomarker TnI enables capturing of target from its C-terminal tail even when it gets degraded in bloodstream. This led us to discover other bioreceptor moieties that can bind TnI at other distant region facilitating sensitive detection using match-pair. The recently described combination of aptamer and peptide discussed in present work unfolds novel TnI detection platform, as colorimetric assay mentioned in chapter 5. Hence these target specific aptamers can be utilized as high affinity substitutes of conventional antibodies based immunodiagnostic assays such as ELISA/dot-blots/lateral-flow assay. Moreover, the reproducibility of synthesis process avoiding batch-to batch variation of aptamer generation can provide cost-effective and sensitive alternatives for monoclonal antibodies based current digital cardiac biomarkers detection devices such as Quidel triage or Abott i-STAT. These aptamers can further be integrated to fabricate hand-held optical or electrochemical multimeric devices implementing simultaneous rapid detection of multiple biomarkers. Moreover, applicability of aptamer based rapid TnI lateral-flow test can be a cost-effective self-care approach to avoid delayed diagnosis that sometimes lead to heart attack.

A detailed study regarding the conformational isomerization upon target binding can be further investigated to study the mechanisms involved to acquire deep insights into aptamer-target interaction. Furthermore, the unique property of structural rearrangement can be integrated with other fluorescent probes to develop advanced nano-enabled naked-eye detection platforms. These high affinity DNA binders can be commercialized for their applicability in separating and purifying human heart TnI protein from bulk serum samples. The aptamer based colorimetric platform incorporating nano-sandwich assay can be incorporated as a rapid diagnostic for visible signal readout with only small amount of serum sample. The developed lateral-flow test cards are better prospective as a cost-effective solution and rapid diagnosis of AMI. While, the electrochemical aptasensing platforms can be extended to fabricate a handheld portable device for detecting TnI providing instant digital response as point-of-care devices in hospitals.

Bibliography

Each source that I read,
I would look through the
Bibliography and the footnotes,
And use that as a map for
the next thing I would read…
-Alexander Chee

[1] W. Zhou, K. Li, Y. Wei, P. Hao, M. Chi, Y. Liu, Y. Wu, Ultrasensitive label-free optical microfiber coupler biosensor for detection of cardiac troponin I based on interference turning point effect, Biosens. Bioelectron. 106 (2018) 99–104. doi:10.1016/j.bios.2018.01.061.

[2] Cardiovascular diseases, (n.d.). https://www.who.int/health-topics/cardio vascular-diseases (accessed June 29, 2021).

[3] Cardiovascular diseases (CVDs), (n.d.). https://www.who.int/news-room/fact-sheets/detail/cardiovascular-diseases-(cvds) (accessed June 29, 2021).

[4] J. Rao, P. St, S.S. Quest, P. View, C.D. View, Cardiac bioMarkers : the troponins and CK-MB, (2010). doi:10.4103/1947-489X.210998.

[5] A. Qureshi, Y. Gurbuz, J.H. Niazi, Biosensors for cardiac biomarkers detection: A review, Sensors Actuators, B Chem. 171–172 (2012) 62–76. doi:10.1016/j.snb.2012.05.077.

[6] K. Thygesen et al, Fourth Universal Definition of Myocardial Infarction (2018), Circulation. 138 (2018) e618–e651. doi:10.1161/CIR.0000000000000617.

[7] M.I. Ahmad, Biomarkers in Acute Myocardial Infarction, J. Clin. Exp. Cardiolog. 03 (2012). doi:10.4172/2155-9880.1000222.

[8] P. Garg, P. Morris, A.L. Fazlanie, S. Vijayan, B. Dancso, A.G. Dastidar, S. Plein, C. Mueller, P. Haaf, Cardiac biomarkers of acute coronary syndrome: from history to high-sensitivity cardiac troponin, Intern. Emerg. Med. 12 (2017) 147–155. doi:10.1007/s11739-017-1612-1.

[9] K. Thygesen, J. Mair, H. Katus, M. Plebani, P. Venge, P. Collinson, B. Lindahl, E. Giannitsis, Y. Hasin, M. Galvani, M. Tubaro, J.S. Alpert, L.M. Biasucci, W. Koenig, C. Mueller, K. Huber, C. Hamm, A.S. Jaffe, Recommendations for the use of cardiac troponin measurement in acute cardiac care, (2010) 2197–2206. doi:10.1093/eurheartj/ehq251.

[10] M. Panteghini, F. Pagani, K.T.J. Yeo, F.S. Apple, R.H. Christenson, F. Dati, J. Mair, J. Ravkilde, H.B.W. Alan, Evaluation of Imprecision for Cardiac Troponin Assays at Low-Range Concentrations, Clin. Chem. 50 (2004) 327–332. doi:10.1373/clinchem.2003.026815.

[11] A.J. Saleh Ahammad, Y.H. Choi, K. Koh, J.H. Kim, J.J. Lee, M. Lee, Electrochemical detection of cardiac biomarker troponin I at gold nanoparticle-modified ITO electrode by using open circuit potential, Int. J. Electrochem. Sci. 6 (2011) 1906–1916.

[12] A.H.B. Wu, F.S. Apple, W.B. Gibler, R.L. Jesse, M.M. Warshaw, R. Valdes, National Academy of Clinical Biochemistry Standards of Laboratory Practice : Recommendations for the Use of Cardiac Markers in Coronary Artery Diseases, 1121 (1999) 1104–1121.

[13] M. Shan, M. Li, X. Qiu, H. Qi, Q. Gao, C. Zhang, Sensitive electrogenerated chemiluminescence peptide-based biosensor for the determination of troponin i with gold nanoparticles amplification, Gold Bull. 47 (2014) 57–64. doi:10.1007/s13404-013-0113-x.

[14] X. Han, S. Li, Z. Peng, A.M. Othman, R. Leblanc, Recent Development of Cardiac Troponin i Detection, ACS Sensors. 1 (2016) 106–114. doi:10.1021/acssensors.5b00318.

[15] C. Tuerk, L. Gold, Systematic evolution of ligands by exponential enrichment: RNA ligands to bacteriophage T4 DNA polymerase, Science (80-.). 249 (1990) 505–510. doi:10.1126/science.2200121.

[16] G.S. Dorraj, M.J. Rassaee, A.M. Latifi, B. Pishgoo, M. Tavallaei, Selection of DNA aptamers against Human Cardiac Troponin I for colorimetric sensor based dot blot application, J. Biotechnol. (2015) 1–7. doi:10.1016/j.jbiotec.2015.05.002.

[17] B.T.M. T., N. Mhamadian, M. Ghorbani, F. Khorshidi, F. Akbari, C. Knaup, Original 1111. 0 (2000) 51–60.

[18] D. Liu, X. Lu, Y. Yang, Y. Zhai, J. Zhang, L. Li, A novel fluorescent aptasensor for the highly sensitive and selective detection of cardiac troponin I based on a graphene oxide platform, Anal. Bioanal. Chem. 410 (2018) 4285–4291. doi:10.1007/s00216-018-1076-9.

[19] X. Fu, Y. Wang, Y. Liu, H. Liu, L. Fu, J. Wen, J. Li, P. Wei, L. Chen, A graphene oxide/gold nanoparticle-based amplification method for SERS immunoassay of cardiac troponin I, Analyst. 144 (2019) 1582–1589. doi:10.1039/c8an02022a.

[20] R. Prajesh, V. Goyal, S. Kakkar, J. Sharma, M.A. Alam, R.K. Maurya, V. Bhalla, A. Agarwal, Polysilicon Field Effect Transistor Biosensor for the Detection of Cardiac Troponin-I (cTnI), J. Electrochem. Soc. 168 (2021) 27501. doi:10.1149/1945-7111/abdde6.

[21] P. Gopinathan, A. Sinha, Y. Da Chung, S.C. Shiesh, G. Bin Lee, Optimization of an enzyme linked DNA aptamer assay for cardiac troponin i detection: Synchronous multiple sample analysis on an integrated microfluidic platform, Analyst. 144 (2019) 4943–4951. doi:10.1039/c9an00779b.

[22] G.H. Metrics, Global , regional , and national age-sex-specific mortality for 282 causes of death in 195 countries and territories , 1980 – 2017 : a systematic analysis for the Global Burden of Disease Study 2017, 392 (2018) 1980–2017. doi:10.1016/S0140-6736(18)32203-7.

[23] Global status report on noncommunicable diseases 2010. (Book, 2011) [WorldCat.org], (n.d.). https://www.worldcat.org/title/global-status-report-on-noncommunicable-diseases-2010/oclc/740739598 (accessed June 1, 2021).

[24] J. Stewart, G. Manmathan, P. Wilkinson, Primary prevention of cardiovascular disease: A review of contemporary guidance and literature, JRSM Cardiovasc. Dis. 6 (2017) 204800401668721. doi:10.1177/2048004016687211.

[25] Risk Factors for Heart Disease, (n.d.). https://www.webmd.com/heart-disease/risk-factors-for-heart-disease (accessed June 2, 2021).

[26] S.E. Kjeldsen, Hypertension and cardiovascular risk: General aspects, Pharmacol. Res. 129 (2018) 95–99. doi:10.1016/j.phrs.2017.11.003.

[27] Chart: Top Global Causes of Death, Statista, (n.d.). https://www.statista.com/chart/20522/most-common-causes-of-death-global/ (accessed May 11, 2022).

[28] V. Fuster, Global burden of cardiovascular disease: Time to implement feasible strategies and to monitor results, J. Am. Coll. Cardiol. 64 (2014) 520–522. doi:10.1016/j.jacc.2014.06.1151.

[29] M. Nishiga, D.W. Wang, Y. Han, D.B. Lewis, J.C. Wu, COVID-19 and cardiovascular disease: from basic mechanisms to clinical perspectives, Nat. Rev. Cardiol. 17 (2020) 543–558. doi:10.1038/s41569-020-0413-9.

[30] G.W. Reed, J.E. Rossi, C.P. Cannon, Acute myocardial infarction, (2017). doi:10.1016/S0140-6736(16)30677-8.

[31] X. Han, S. Li, Z. Peng, A.M. Othman, R. Leblanc, Recent Development of Cardiac Troponin I Detection, (2016). doi:10.1021/acssensors.5b00318.

[32] A.M. Infarction, Acute Myocardial Infarction, (2017) 2053–2064. doi:10.1056/ NEJMra1606915.

[33] M.I. Ahmad, Biomarkers in Acute Myocardial Infarction, J. Clin. Exp. Cardiolog. 03 (2012). doi:10.4172/2155-9880.1000222.

[34] F. Combined, Risk factors for coronary heart disease (CHD), (n.d.) 6–7.

[35] A. Malik, A. Malik, R. Khurshid, R. Khurshid, S. Rashid, The Diagnostic Value of Biochemical Cardiac Markers in in Acute Myocardial Infarction Acute Myocardial Infarction Shazia, (2018). doi:10.5772/intechopen.76150.

[36] W.C. Be, HHS Public Access, (2020). doi:10.1055/s-0039-1679104.Cardiac.

[37] B.A. Karmen, F. Wroblewski, J.S. Ladue, amino nitrogen, (1954) 126–133.

[38] P. Garg, P. Morris, A.L. Fazlanie, S. Vijayan, B. Dancso, A.G. Dastidar, S. Plein, C. Mueller, P. Haaf, Cardiac biomarkers of acute coronary syndrome: from history to high-sensitivity cardiac troponin, Intern. Emerg. Med. 12 (2017) 147–155. doi:10.1007/s11739-017-1612-1.

[39] C. I-w, Myoglobin as an Early Indicator of Acute Myocardial Infarction, (1987).

[40] S. Aydin, K. Ugur, S. Aydin, İ. Sahin, M. Yardim, Biomarkers in acute myocardial infarction: Current perspectives, Vasc. Health Risk Manag. 15 (2019) 1–10. doi:10.2147/VHRM.S166157.

[41] C. Biomarkers, I. Ahs, Corporate Medical Policy Cardiac Biomarkers for Myocardial Infarction AHS – G2150, (2022) 1–12.

[42] A New Protein Factor Promoting Aggregation of Tropomyosin, 58 (1965).

[43] B. Cummins, M.L. Auckland, P. Cummins, P.D. Birmingham, the Diagnosis Ic T Ropon of Acute Myocarwl Oassay Infarction in, (1987).

[44] M. Panteghini, F. Pagani, K.J. Yeo, F.S. Apple, R.H. Christenson, F. Dati, J. Mair, J. Ravkilde, Evaluation of Imprecision for Cardiac Troponin Assays at Low-Range Concentrations, 332 (2004) 327–332. doi:10.1373/clinchem.2003.026815.

[45] S. V. Perry, Background to the discovery of troponin and Setsuro Ebashi's contribution to our knowledge of the mechanism of relaxation in striated muscle., Biochem. Biophys. Res. Commun. 369 (2008) 43–48. doi:10.1016/j.bbrc.2007.11.185.

[46] S. Mythili, N. Malathi, Diagnostic markers of acute myocardial infarction (Review), (2015) 743–748. doi:10.3892/br.2015.500.

[47] Elevation of cardiac troponin I indicates more than myocardial ischemia - PubMed, (n.d.). https://pubmed.ncbi.nlm.nih.gov/12858947/ (accessed June 3, 2021).

[48] I.A. Katrukha, Human cardiac troponin complex. structure and functions, Biochem. 78 (2013) 1447–1465. doi:10.1134/S0006297913130063.

[49] Y. Cheng, M. Regnier, Cardiac troponin structure-function and the influence of hypertrophic cardiomyopathy associated mutations on modulation of contractility, Arch. Biochem. Biophys. 601 (2016) 11–21. doi:10.1016/j.abb.2016.02.004.

[50] S.B. Marston, J.W. Walker, Back to the future: New techniques show that forgotten phosphorylation sites are present in contractile proteins of the heart whilst intensively studied sites appear to be absent, J. Muscle Res. Cell Motil. 30 (2009) 93–95. doi:10.1007/s10974-009-9184-y.

[51] H. Nordrhein-westfalen, R. Bochum, L. Heilmeyer, R. Bochum, and Dephosphorylation, 490 (1995) 486–490.

[52] S. Marston, J.E. Zamora, Troponin structure and function: a view of recent progress, J. Muscle Res. Cell Motil. 41 (2020) 71–89. doi:10.1007/s10974-019-09513-1.

[53] S. Takeda, A. Yamashita, K. Maeda, Y. Maéda, Structure of the core domain of human cardiac troponin in the Ca2+-saturated form, Nature. 424 (2003) 35–41. doi:10.1038/nature01780.

[54] R. Zhang, J.J. Zhao, J.D. Potter, Phosphorylation of both serine residues in cardiac troponin I is required to decrease the Ca2+ affinity of cardiac troponin C, J. Biol. Chem. 270 (1995) 30773–30780. doi:10.1074/jbc.270.51.30773.

[55] Recommendations for the Use of Cardiac Markers in Coronary Artery Disease | AACC.org, (n.d.). https://www.aacc.org/science-and-research/practice-guidelines/cardiac-markers (accessed June 3, 2021).

[56] A. Maqsood, K. Kaid, M. Cohen, Clinical Significance Of Borderline Cardiac Troponin (cTnI) Are Referred For Cardiac Catheterization, 4 (2006) 2002–2005.

[57] J. Peela, A. Jarari, A. Hai, A. Rawal, S. Kolla, S. Sreekumar, L. Khurana, N. Sidhanathi, Cardiac biomarkers: The troponins and CK- MB, Ibnosina J. Med. Biomed. Sci. 2 (2010) 190. doi:10.4103/1947-489x.210998.

[58] M.H.M. Hessel, D.E. Atsma, E.J.M. Van Der Valk, W.H. Bax, M.J. Schalij, A. Van Der Laarse, Release of cardiac troponin I from viable cardiomyocytes is mediated by integrin stimulation, Pflugers Arch. Eur. J. Physiol. 455 (2008) 979–986. doi:10.1007/s00424-007-0354-8.

[59] D. Amgalan, R. Pekson, R.N. Kitsis, Troponin Release Following Brief Myocardial Ischemia: Apoptosis Versus Necrosis, JACC Basic to Transl. Sci. 2 (2017) 118–121. doi:10.1016/j.jacbts.2017.03.008.

[60] B.R. Weil, G. Suzuki, R.F. Young, V. Iyer, J.M. Canty, Troponin Release and Reversible Left Ventricular Dysfunction After Transient Pressure Overload, J. Am. Coll. Cardiol. 71 (2018) 2906–2916. doi:10.1016/j.jacc.2018.04.029.

[61] J. Mair, B. Lindahl, O. Hammarsten, C. Müller, E. Giannitsis, K. Huber, M. Möckel, M. Plebani, K. Thygesen, A.S. Jaffe, How is cardiac troponin released from injured myocardium?, Eur. Hear. Journal. Acute Cardiovasc. Care. 7 (2018) 553–560. doi:10.1177/2048872617748553.

[62] A.H.B. Wu, Release of cardiac troponin from healthy and damaged myocardium, Front. Lab. Med. 1 (2017) 144–150. doi:10.1016/j.flm.2017.09.003.

[63] O. Hammarsten, J. Mair, M. Möckel, B. Lindahl, A.S. Jaffe, Possible mechanisms behind cardiac troponin elevations, Biomarkers. 23 (2018) 725–734. doi:10.1080/1354750X.2018.1490969.

[64] A.G. Katrukha, A. V Bereznikova, V.L. Filatov, T. V Esakova, O. V Kolosova, K. Pettersson, T. Lo, T. V Bulargina, I.R. Trifonov, N.A. Gratsiansky, K. Pulkki, N.B. Gusev, Degradation of cardiac troponin I : implication for reliable immunodetection, 2440 (1998) 2433–2440.

[65] R. Labugger, L. Organ, C. Collier, D. Atar, J.E. Van Eyk, Clinical Investigation and Reports Extensive Troponin I and T Modification Detected in Serum From Patients With Acute Myocardial Infarction, (2000).

[66] J. Mair, What is new on cardiac troponin degradation ?, (2017) 3–5. doi:10.21037/jlpm.2017.07.06.

[67] B. Regan, R.O. Kennedy, D. Collins, Point-of-Care Compatibility of Ultra-Sensitive Detection Techniques for the Cardiac Biomarker Troponin I — Challenges and Potential Value, (2018) 1–32. doi:10.3390/bios8040114.

[68] S. Upasham, A. Tanak, S. Prasad, Cardiac troponin biosensors: where are we now?, Adv. Heal. Care Technol. Volume 4 (2018) 1–13. doi:10.2147/ahct.s138543.

[69] M.C. Kontos, J.S. Turlington, High-Sensitivity Troponins in Cardiovascular Disease, (2020).

[70] A.H.B. Wu, A.S. Jaffe, S. Francisco, The clinical need for high-sensitivity cardiac troponin assays for acute coronary syndromes and the role for serial testing, (2008). doi:10.1016/j.ahj.2007.10.016.

[71] C.S. Kosack, A.L. Page, P.R. Klatser, A guide to aid the selection of diagnostic tests, Bull. World Health Organ. 95 (2017) 639–645. doi:10.2471/BLT.16.187468.

[72] S. Carrara, K. Adamson, H. Ma, R.O. Kennedy, L. De Cola, R.J. Forster, U. De Strasbourg, Cardiac Troponin I: Ultrasensitive Detection Using Faradaic Electrochemical Impedance, (2018). doi:10.1021/acsomega.8b01758.

[73] F. Microspheres, Y. Cai, Rapid and Sensitive Detection of Cardiac Troponin I for Point-of-Care Tests Based on Red, (2018). doi:10.3390/molecules23051102.

[74] X. Fu, Y. Wang, Y. Liu, H. Liu, L. Fu, J. Wen, cardiac troponin I †, (2019) 1582–1589. doi:10.1039/c8an02022a.

[75] K.R. Kim, H.J. Chun, Y.D. Han, K.W. Lee, D.K. Hong, K.N. Lee, H.C. Yoon, A Time-resolved fluorescence immunosensing platform for highly sensitive detection of cardiac troponin i ajou university , suwon , South Korea and Korea Electronics Technology Institute , Seongnam , South Korea Synthesis and Bioconjugation of LESNPs Const, (2017) 1640–1643.

[76] A. Buhot, devices to emerging technologies, (2020).

[77] T. Lee, J.H. Ahn, J. Choi, Y. Lee, J.M. Kim, C. Park, H. Jang, T.H. Kim, M.H. Lee, Development of the troponin detection system based on the nanostructure, Micromachines. 10 (2019). doi:10.3390/mi10030203.

[78] H. Yoo, H. Jo, S.S. Oh, Detection and beyond: challenges and advances in aptamer-based biosensors, Mater. Adv. 1 (2020) 2663–2687. doi:10.1039/d0ma00639d.

[79] J. Hidding, A therapeutic battle: Antibodies vs. Aptamers, Nanosci. Master Progr. (2017) 1–20. https://www.rug.nl/research/zernike/education/topmasternanoscience/programme-documents/ns190-papers/ns_190_hidding-atherapeuticbattleantibodiesvs.aptamers.pdf.

[80] P.K. Kulabhusan, B. Hussain, Current Perspectives on Aptamers as Diagnostic Tools and Therapeutic Agents, (2020).

[81] A. Biosensing, N.I. Khan, E. Song, Lab-on-a-Chip Systems for, (2020).

[82] M. Bauer, M. Strom, D.S. Hammond, S. Shigdar, Anything you can do, i can do better: Can aptamers replace antibodies in clinical diagnostic applications?, Molecules. 24 (2019) 1–13. doi:10.3390/molecules24234377.

[83] S.Y. Toh, M. Citartan, S.C.B. Gopinath, T.H. Tang, Aptamers as a replacement for antibodies in enzyme-linked immunosorbent assay, Biosens. Bioelectron. 64 (2015) 392–403. doi:10.1016/j.bios.2014.09.026.

[84] S. Ni, Z. Zhuo, Y. Pan, Y. Yu, F. Li, J. Liu, L. Wang, X. Wu, D. Li, Y. Wan, L. Zhang, Z. Yang, B.T. Zhang, A. Lu, G. Zhang, Recent Progress in Aptamer Discoveries and Modifications for Therapeutic Applications, ACS Appl. Mater. Interfaces. 13 (2021) 9500–9519. doi:10.1021/acsami.0c05750.

[85] A.D. Ellington, J.W. Szostak, In vitro selection of RNA molecules that bind specific ligands, Nature. 346 (1990) 818–822. doi:10.1038/346818a0.

[86] Z. Wang, W. Xu, L. Liu, T.F. Zhu, A synthetic molecular system capable of mirror-image genetic replication and transcription, Nat. Chem. 8 (2016) 698–704. doi:10.1038/nchem.2517.

[87] SOMAmer® reagents focus on single proteins in living cells - SomaLogic, (n.d.). https://somalogic.com/news_press_releases/somamer-reagents-focus-on-single-proteins-in-living-cells/ (accessed June 7, 2021).

[88] M. Berezovski, M. Musheev, A. Drabovich, S.N. Krylov, Non-SELEX selection of aptamers, J. Am. Chem. Soc. 128 (2006) 1410–1411. doi:10.1021/ja056943j.

[89] K. Han, Z. Liang, N. Zhou, Design strategies for aptamer-based biosensors, Sensors. 10 (2010) 4541–4557. doi:10.3390/s100504541.

[90] A.K. Deisingh, Aptamer-based biosensors: Biomedical applications, Handb. Exp. Pharmacol. 173 (2006) 341–357. doi:10.1007/3-540-27262-3_17.

[91] Immunoassay - an overview | ScienceDirect Topics, (n.d.). https://www.sciencedirect.com/topics/neuroscience/immunoassay (accessed June 8, 2021).

[92] Traber & Atkinson, NIH Public Access, Bone. 23 (2007) 1–7. doi:10.1021/ac8009559.Effect.

[93] C. Zhu, J. Liu, Y. Ling, H. Yang, Z. Liu, R. Zheng, L. Qin, Z. Hu, Correction to Evaluation of the clinical value of ELISA based on MPT64 antibody aptamer for serological diagnosis of pulmonary tuberculosis [BMC Infect Dis, 12, (2012) 96], BMC Infect. Dis. 13 (2013) 1. doi:10.1186/1471-2334-13-410.

[94] K. Kitamura, M. Biyani, M. Futakami, S. Ueno-Tsuji, M. Suzuki, Peptide Aptamer-Based ELISA-Like System for Detection of Cathepsin E in Tissues and Plasma, J. Mol. Biomark. Diagn. 02 (2011) 2–5. doi:10.4172/2155-9929.1000104.

[95] Dot Blot - an overview | ScienceDirect Topics, (n.d.). https://www.sciencedirect.com/topics/biochemistry-genetics-and-molecular-biology/dot-blot (accessed June 8, 2021).

[96] M. Citartan, Aptamers as the powerhouse of dot blot assays, Talanta. 232 (2021) 122436. doi:10.1016/j.talanta.2021.122436.

[97] Y. Liu, D. Zhang, E.C. Alocilja, S. Chakrabartty, Biomolecules detection using a silver-enhanced gold nanoparticle-based biochip, Nanoscale Res. Lett. 5 (2010) 533–538. doi:10.1007/s11671-010-9542-0.

[98] Y. Wang, D. Li, W. Ren, Z. Liu, S. Dong, E. Wang, Ultrasensitive colorimetric detection of protein by aptamer-Au nanoparticles conjugates based on a dot-blot assay, Chem. Commun. (2008) 2520–2522. doi:10.1039/b801055b.

[99] C. Wang, D. Liu, Z. Wang, Gold nanoparticle based dot-blot immunoassay for sensitively detecting Alzheimer's disease related β-amyloid peptide, Chem. Commun. 48 (2012) 8392–8394. doi:10.1039/c2cc33568a.

[100] M. Pal, R. Khan, Biosensor platforms for detection of cardiovascular disease risk biomarkers, Elsevier Ltd., 2019. doi:10.1016/B978-0-08-102555-0.00012-1.

[101] C.C. Chang, C.P. Chen, T.H. Wu, C.H. Yang, C.W. Lin, C.Y. Chen, Gold nanoparticle-based colorimetric strategies for chemical and biological sensing applications, Nanomaterials. 9 (2019) 1–24. doi:10.3390/nano9060861.

[102] R. Article, N. Xu, S. Jin, L. Wang, O. Access, Metal nanoparticles-based nanoplatforms for colorimetric sensing : A review, (2021) 1–11.

[103] F. Zhang, J. Liu, Label-Free Colorimetric Biosensors Based on Aptamers and Gold Nanoparticles : A Critical Review, (2021) 30–43.

[104] J.P. Park, D.M. Cropek, S. Banta, High affinity peptides for the recognition of the heart disease biomarker troponin I identified using phage display, Biotechnol. Bioeng. 105 (2010) 678–686. doi:10.1002/bit.22597.

[105] W. Wang, W.Y. Wu, X. Zhong, W. Wang, Q. Miao, J.J. Zhu, Aptamer-based PDMS-gold nanoparticle composite as a platform for visual detection of biomolecules with silver enhancement, Biosens. Bioelectron. 26 (2011) 3110–3114. doi:10.1016/j.bios.2010.10.034.

[106] L. Sciences, www.els-journal.com Page 1 Engineering in Life Sciences, (2014) 1–32. doi:10.1002/elsc.201500188.This.

[107] V. Raj, S. Alex, Non-enzymatic colorimetric sensor for cardiac Troponin I (cTnI) based on self-assembly of gold nanorods on heparin, Gold Bull. 54 (2021) 1–7. doi:10.1007/s13404-020-00287-w.

[108] B. Mondal, S. Ramlal, P.S. Lavu, N. Bhavanashri, J. Kingston, Highly sensitive colorimetric biosensor for staphylococcal enterotoxin B by a label-free aptamer and gold nanoparticles, Front. Microbiol. 9 (2018) 1–8. doi:10.3389/fmicb.2018.00179.

[109] S.A. Kitte, F.A. Bushira, T.R. Soreta, An impedimetric aptamer-based sensor for sensitive and selective determination of cardiac troponin I, J. Iran. Chem. Soc. 2021 192. 19 (2021) 505–511. doi:10.1007/S13738-021-02324-7.

[110] H. Jo, H. Gu, W. Jeon, H. Youn, J. Her, S.K. Kim, J. Lee, J.H. Shin, C. Ban, Electrochemical Aptasensor of Cardiac Troponin i for the Early Diagnosis of Acute Myocardial Infarction, Anal. Chem. 87 (2015) 9869–9875. doi:10.1021/acs.anal chem.5b02312.

[111] A. Idili, J. Gerson, C. Parolo, T. Kippin, K.W. Plaxco, An electrochemical aptamer-based sensor for the rapid and convenient measurement of l-tryptophan, Anal. Bioanal. Chem. 411 (2019) 4629–4635. doi:10.1007/s00216-019-01645-0.

[112] T. Lee, J. Ahn, J. Choi, Y. Lee, J. Kim, C. Park, H. Jang, T. Kim, M. Lee, Development of the Troponin Detection System Based on the Nanostructure, (n.d.). doi:10.3390/mi10030203.

[113] A. Villalonga, I. Estabiel, A.M. Pérez-Calabuig, B. Mayol, C. Parrado, R. Villalonga, Amperometric aptasensor with sandwich-type architecture for troponin I based on carboxyethylsilanetriol-modified graphene oxide coated electrodes, Biosens. Bioelectron. 183 (2021) 113203. doi:10.1016/j.bios.2021.113203.

[114] M. Saremi, A. Amini, H. Heydari, An aptasensor for troponin I based on the aggregation-induced electrochemiluminescence of nanoparticles prepared from a cyclometallated iridium(III) complex and poly(4-vinylpyridine-co-styrene) deposited on nitrogen-doped graphene, Microchim. Acta. 186 (2019) 0–10. doi:10.1007/s00604-019-3352-6.

[115] G. Liu, M. Qi, Y. Zhang, C. Cao, E.M. Goldys, AC SC, Anal. Chim. Acta. (2016). doi:10.1016/j.aca.2015.12.023.

[116] J. Lei, J. Kim, D.H. Kim, Y. Hoon, W. Kim, Author ' s Accepted Manuscript, (2018). doi:10.1016/j.bios.2018.11.012.

[117] H. Jo, H. Gu, W. Jeon, H. Youn, J. Her, S. Kim, J. Lee, J.H. Shin, C. Ban, Electrochemical Aptasensor of Cardiac Troponin I for the Early Diagnosis of Acute Myocardial Infarction, (2015). doi:10.1021/acs.analchem.5b02312.

[118] X. Qiao, K. Li, J. Xu, N. Cheng, Q. Sheng, W. Cao, T. Yue, Biosensors and Bioelectronics Novel electrochemical sensing platform for ultrasensitive detection of cardiac troponin I based on aptamer-MoS 2 nanoconjugates, Biosens. Bioelectron. 113 (2018) 142–147. doi:10.1016/j.bios.2018.05.003.

[119] C.A. Vu, W.Y. Chen, Field-effect transistor biosensors for biomedical applications: Recent advances and future prospects, Sensors (Switzerland). 19 (2019). doi:10.3390/s19194214.

[120] K. Kim, C. Park, D. Kwon, D. Kim, M. Meyyappan, S. Jeon, J.S. Lee, Silicon nanowire biosensors for detection of cardiac troponin I (cTnI) with high sensitivity, Biosens. Bioelectron. 77 (2016) 695–701. doi:10.1016/j.bios.2015.10.008.

[121] P. Cummins, S.V. Perry, Troponin I from human skeletal and cardiac muscles, Biochem. J. 171 (1978) 251–259. doi:10.1042/bj1710251.

[122] S.M. Selimoglu, M. Kasap, G. Akpinar, A. Karadenizli, Overcoming difficulties on synthesis of cardiac troponin-I, Prep. Biochem. Biotechnol. 47 (2017) 94–99. doi:10.1080/10826068.2016.1172894.

[123] K. Lohmann, B. Westerdorf, R. Maytum, M.A. Geeves, K. Jaquet, Overexpression of human cardiac troponin in escherichia coli: Its purification and characterization, Protein Expr. Purif. 21 (2001) 49–59. doi:10.1006/prep.2000.1328.

[124] W. Zhou, P.J. Huang, J. Liu, Critical review, (2014) 2627–2640. doi:10.1039/c4an00132j.

[125] A. Yamashita, K. Maeda, Y. Mae, Structure of the core domain of human cardiac troponin in the, 424 (2003) 35–41.

[126] J. Liu, M. Li, Z. Zeng, K. Song, P. Xu, J. Zhang, Selection of aptamers against cardiac troponin i by SELEX, ITME 2011 - Proc. 2011 IEEE Int. Symp. IT Med. Educ. 1 (2011) 536–539. doi:10.1109/ITiME.2011.6130894.

[127] L. Tian, R. Wang, Hwilv, 1 (2014).

[128] D.N.A. Aptamer, S. Binding, W)", 1 (2012).

[129] Z.J. Tolnai, J. András, Z. Szeitner, K. Percze, L.F. Simon, R.E. Gyurcsányi, T. Mészáros, Spiegelmer-based sandwich assay for cardiac troponin i detection, Int. J. Mol. Sci. 21 (2020) 1–11. doi:10.3390/ijms21144963.

[130] M. Zuker, Mfold web server for nucleic acid folding and hybridization prediction, (2014). doi:10.1093/nar/gkg595.

[131] M. Biesiada, K. Pachulska-wieczorek, R.W. Adamiak, K.J. Purzycka, RNAComposer and RNA 3D structure prediction for nanotechnology, (2016). doi:10.1016/j.ymeth.2016.03.010.

[132] M. Vorlickova, I. Kejnovska, Circular Dichroism Spectroscopy of DNA : From Duplexes to Quadruplexes Review Article Circular Dichroism Spectroscopy of DNA : From Duplexes to, (2012). doi:10.1002/chir.22064.

[133] D. Renc, M. Vorlı, Circular dichroism and conformational polymorphism of DNA, 37 (2009) 1713–1725. doi:10.1093/nar/gkp026.

[134] A.C. Grodzki, E. Berenstein, Antibody purification: ammonium sulfate fractionation or gel filtration., Methods Mol. Biol. 588 (2010) 15–26. doi:10.1007/978-1-59745-324-0_3.

[135] S. Hober, K. Nord, M. Linhult, Protein A chromatography for antibody purification, J. Chromatogr. B Anal. Technol. Biomed. Life Sci. 848 (2007) 40–47. doi:10.1016/j.jchromb.2006.09.030.

[136] A. Lamiable, P. Th, J. Rey, M. Vavrusa, P. Derreumaux, P. Tuff, PEP-FOLD3 : faster denovo structure prediction for linear peptides in solution and in complex, 44 (2016) 449–454. doi:10.1093/nar/gkw329.

[137] J.P. Elskens, J.M. Elskens, A. Madder, Chemical Modification of Aptamers for Increased Binding A ffi nity in Diagnostic Applications : Current Status and Future Prospects, (2020).

[138] K.A.Y. Ohlendieck, S.E. Harding, Centrifugation and Ultracentrifugation, (n.d.) 424–453.

[139] J.L. Cole, J.W. Lary, T. Moody, T.M. Laue, NIH Public Access, (2009). doi:10.1016/S0091-679X(07)84006-4.Analytical.

[140] J.A. Ream, L.K. Lewis, K.A. Lewis, Rapid agarose gel electrophoretic mobility shift assay for quantitating protein: RNA interactions, Anal. Biochem. 511 (2016) 36–41. doi:10.1016/j.ab.2016.07.027.

[141] M. Seo, L. Lei, M. Egli, Label-Free Electrophoretic Mobility Shift Assay (EMSA) for Measuring Dissociation Constants of Protein-RNA Complexes, Curr. Protoc. Nucleic Acid Chem. 76 (2019) 1–12. doi:10.1002/cpnc.70.

[142] P. Schuck, Size-Distribution Analysis of Macromolecules by Sedimentation Velocity Ultracentrifugation and Lamm Equation Modeling, Biophys. J. 78 (2000) 1606–1619. doi:10.1016/S0006-3495(00)76713-0.

[143] A.T. Brunger, J.A. Wells, Warren L. DeLano 21 June 1972-3 November 2009., Nat. Struct. Mol. Biol. 16 (2009) 1202–1203. doi:10.1038/nsmb1209-1202.

[144] S. Tadepalli, Z. Kuang, Q. Jiang, K.K. Liu, M.A. Fisher, J.J. Morrissey, E.D. Kharasch, J.M. Slocik, R.R. Naik, S. Singamaneni, Peptide Functionalized Gold Nanorods for the Sensitive Detection of a Cardiac Biomarker Using Plasmonic Paper Devices, Sci. Rep. 5 (2015) 1–11. doi:10.1038/srep16206.

[145] I.A. Darwish, Immunoassay Methods and their Applications in Pharmaceutical Analysis : Basic Methodology and Recent Advances, (n.d.) 217–235.

[146] M. Bauer, M. Strom, D.S. Hammond, Anything You Can Do , I Can Do Better : Can Aptamers Replace Antibodies in Clinical Diagnostic Applications ?, (2019) 1–13.

[147] J. Kang, G. Yeom, S. Ha, M. Kim, Development of a DNA aptamer selection method based on the heterogeneous sandwich form and its application in a colorimetric assay, (2019) 6883–6889. doi:10.1039/c8nj06458j.

[148] F. Torrini, P. Palladino, A. Brittoli, V. Baldoneschi, M. Minunni, S. Scarano, Characterization of troponin T binding aptamers for an innovative enzyme-linked oligonucleotide assay (ELONA), (2019).

[149] L. Kaiser, J. Weisser, M. Kohl, H. Deigner, Small molecule detection with aptamer based lateral flow assays : Applying aptamer-C-reactive protein cross-recognition for ampicillin detection, Sci. Rep. (2018) 6–15. doi:10.1038/s41598-018-23963-6.

[150] C. Wang, Z. Wang, ChemComm Gold nanoparticle based dot-blot immunoassay for sensitively detecting Alzheimer ' s disease related b -amyloid peptide w, (2012) 8392–8394. doi:10.1039/c2cc33568a.

[151] © 1973 Nature Publishing Group, (1973).

[152] Gold Colloid, (n.d.). https://www.bbisolutions.com/en/reagents/gold-colloid (accessed June 28, 2021).

[153] I. Extraction, Reduction Protocol for Thiol-Modified Oligonucleotides, 1 (2014) 2–3.

[154] Y. Xue, X. Li, H. Li, W. Zhang, the efficient strength control, (2014). doi:10.1038/ncomms5348.

[155] Y. Xie, Y. Huang, D. Tang, H. Cui, L. Yang, H. Cao, W. Yun, Sensitive colorimetric detection for lysozyme based on the capture of a fixed thiol-aptamer on gold nanoparticles, New J. Chem. 43 (2019) 4531–4538. doi:10.1039/c9nj00016j.

[156] N.S. Lopa, M.M. Rahman, F. Ahmed, T. Ryu, S.C. Sutradhar, J. Lei, J. Kim, D.H. Kim, Y.H. Lee, W. Kim, Simple, low-cost, sensitive and label-free aptasensor for the detection of cardiac troponin I based on a gold nanoparticles modified titanium foil, Biosens. Bioelectron. 126 (2019) 381–388. doi:10.1016/j.bios.2018.11.012.

[157] N.G. Bastús, E. Sánchez-Tilló, S. Pujals, C. Farrera, C. López, E. Giralt, A. Celada, J. Lloberas, V. Puntes, Homogeneous conjugation of peptides onto gold nanoparticles enhances macrophage response, ACS Nano. 3 (2009) 1335–1344. doi:10.1021/ nn8008273.

[158] W. Zhao, W. Chiuman, J.C.F. Lam, S.A. McManus, W. Chen, Y. Cui, R. Pelton, M.A. Brook, Y. Li, DNA aptamer folding on gold nanoparticles: From colloid chemistry to biosensors, J. Am. Chem. Soc. 130 (2008) 3610–3618. doi:10.1021/ja710241b.

[159] Me232290, Title of the 232290th document, 78 (2008) 8313–8318. doi:10.1021/ac0613582.Maximizing.

[160] A.S.V. Shah, A. Anand, Y. Sandoval, K.K. Lee, S.W. Smith, P.D. Adamson, A.R. Chapman, T. Langdon, D. Sandeman, A. Vaswani, F.E. Strachan, A. Ferry, A.G. Stirzaker, A. Reid, A.J. Gray, P.O. Collinson, D.A. McAllister, F.S. Apple, D.E. Newby, N.L. Mills, High-sensitivity cardiac troponin i at presentation in patients with suspected acute coronary syndrome: A cohort study, Lancet. 386 (2015) 2481–2488. doi:10.1016/S0140-6736(15)00391-8.

[161] M.W. Sherwood, L. Kristin Newby, High-sensitivity troponin assays: evidence, indications, and reasonable use., J. Am. Heart Assoc. 3 (2014) 1–10. doi:10.1161/JAHA.113.000403.

[162] K. Saha, S.S. Agasti, C. Kim, X. Li, V.M. Rotello, Gold nanoparticles in chemical and biological sensing, Chem. Rev. 112 (2012) 2739–2779. doi:10.1021/cr2001178.

[163] C.S. Tsai, T. Bin Yu, C.T. Chen, Gold nanoparticle-based competitive colorimetric assay for detection of protein-protein interactions, Chem. Commun. (2005) 4273–4275. doi:10.1039/b507237a.

[164] S.O. Pereira, A. Barros-Timmons, T. Trindade, Biofunctionalisation of colloidal gold nanoparticles via polyelectrolytes assemblies, Colloid Polym. Sci. 292 (2014) 33–50. doi:10.1007/s00396-013-3037-3.

[165] W. Zhou, X. Gao, D. Liu, X. Chen, Gold Nanoparticles for in Vitro Diagnostics, Chem. Rev. 115 (2015) 10575–10636. doi:10.1021/acs.chemrev.5b00100.

[166] D.H. Choi, S.K. Lee, Y.K. Oh, B.W. Bae, S.D. Lee, S. Kim, Y.B. Shin, M.G. Kim, A dual gold nanoparticle conjugate-based lateral flow assay (LFA) method for the analysis of troponin I, Biosens. Bioelectron. 25 (2010) 1999–2002. doi:10.1016/j.bios.2010.01.019.

[167] J.P. Park, D.M. Cropek, S. Banta, High affinity peptides for the recognition of the heart disease biomarker troponin I identified using phage display, Biotechnol. Bioeng. 105 (2010) 678–686. doi:10.1002/bit.22597.

[168] P. Singh, S. Kakkar, Bharti, R. Kumar, V. Bhalla, Rapid and sensitive colorimetric detection of pathogens based on silver-urease interactions, Chem. Commun. 55 (2019) 4765–4768. doi:10.1039/C9CC00225A.

[169] D.A. Giljohann, D.S. Seferos, W.L. Daniel, M.D. Massich, P.C. Patel, C.A. Mirkin, Gold Nanoparticles for Biology and Medicine Angewandte, (2010) 3280–3294. doi:10.1002/anie.200904359.

[170] P.C. Patel, D.A. Giljohann, D.S. Seferos, C.A. Mirkin, Peptide antisense nanoparticles, (2014). doi:10.1073/pnas.0801609105.

[171] X. Liu, Y. Wang, P. Chen, A. McCadden, A. Palaniappan, J. Zhang, B. Liedberg, Peptide Functionalized Gold Nanoparticles with Optimized Particle Size and Concentration for Colorimetric Assay Development: Detection of Cardiac Troponin i, ACS Sensors. 1 (2016) 1416–1422. doi:10.1021/acssensors.6b00493.

[172] K. Kim, C. Park, D. Kwon, D. Kim, M. Meyyappan, S. Jeon, J. Lee, Biosensors and Bioelectronics Silicon nanowire biosensors for detection of cardiac troponin I (cTnI) with high sensitivity, 77 (2016) 695–701. doi:10.1016/j.bios.2015.10.008.

[173] E.M. Nelson, L.J. Rothberg, Kinetics and mechanism of single-stranded DNA adsorption onto citrate-stabilized gold nanoparticles in colloidal solution, Langmuir. 27 (2011) 1770–1777. doi:10.1021/la102613f.

[174] J.M. Slocik, A.O. Govorov, R.R. Naik, Plasmonic circular dichroism of peptide-functionalized gold nanoparticles, Nano Lett. 11 (2011) 701–705. doi:10.1021/nl1038242.

[175] J. Kypr, I. Kejnovská, D. Renčiuk, M. Vorlíčková, Circular dichroism and conformational polymorphism of DNA, Nucleic Acids Res. 37 (2009) 1713–1725. doi:10.1093/nar/gkp026.

[176] H. Kurt, M. Yüce, B. Hussain, H. Budak, Dual-excitation upconverting nanoparticle and quantum dot aptasensor for multiplexed food pathogen detection, Biosens. Bioelectron. 81 (2016) 280–286. doi:10.1016/j.bios.2016.03.005.

[177] N.J. Greenfield, Using circular dichroism spectra to estimate protein secondary structure, Nat. Protoc. 1 (2007) 2876–2890. doi:10.1038/nprot.2006.202.

[178] A.O. Govorov, Z. Fan, P. Hernandez, J.M. Slocik, R.R. Naik, Theory of circular dichroism of nanomaterials comprising chiral molecules and nanocrystals: Plasmon enhancement, dipole interactions, and dielectric effects, Nano Lett. 10 (2010) 1374–1382. doi:10.1021/nl100010v.

[179] G. Maduraiveeran, Bionanomaterial-based electrochemical biosensing platforms for biomedical applications, Anal. Methods. 12 (2020) 1688–1701. doi:10.1039/d0ay00171f.

[180] S. Mehennaoui, S. Poorah, G.C. Jimenez, M. Siaj, Selection of high affinity aptamer-ligand for dexamethasone and its electrochemical biosensor, (2019) 1–9. doi:10.1038/s41598-019-42671-3.

[181] X. Zhang, V.K. Yadavalli, Biosensors and Bioelectronics Surface immobilization of DNA aptamers for biosensing and protein interaction analysis, Biosens. Bioelectron. 26 (2011) 3142–3147. doi:10.1016/j.bios.2010.12.012.

[182] L.D. Tuyen, A.C. Liu, C. Huang, P. Tsai, J.H. Lin, C. Wu, L. Chau, T.S. Yang, L.Q. Minh, H. Kan, C.C. Hsu, Doubly resonant surface-enhanced Raman scattering on gold nanorod decorated inverse opal photonic crystals, 20 (2012) 29266–29275.

[183] S. Moghaddamjoo, A.P. Tashakor, S.T. Fard, Y.T. A, E. Kwok, Y.A. Li, N. Tavassoli, Characterization of Cardiac Troponin I Raman Signature in Bovine Serum Albumin and Human Blood Serum for the Potential Diagnosis of Myocardial Natural Products Chemistry & Research Characterization of Cardiac Troponin I Raman Signature in Bovine Serum Alb, (2016) 1–6. doi:10.4172/2329-6836.1000200.

[184] H. Yoo, H. Jo, S.S. Oh, Materials Advances in aptamer-based biosensors, Mater. Adv. 1 (2020) 2663–2687. doi:10.1039/D0MA00639D.

[185] M. Jarczewska, Ł. G, Analytical Methods potential tools for clinical diagnostics, (2016) 3861–3877. doi:10.1039/C6AY00499G.

[186] M.C. Rodriguez, A. Kawde, J. Wang, Aptamer biosensor for label-free impedance spectroscopy detection of proteins based on recognition-induced switching of the surface charge {, (2005) 4267–4269. doi:10.1039/b506571b.

[187] Q. Sheng, X. Qiao, M. Zhou, J. Zheng, Recent progress in electrochemical sensing of cardiac troponin by using nanomaterial-induced signal amplification, (2017) 1573–1585. doi:10.1007/s00604-017-2219-y.

[188] I. Khalil, N.M. Julkapli, W.A. Yehye, W.J. Basirun, S.K. Bhargava, Graphene–Gold Nanoparticles Hybrid—Synthesis, Functionalization, and Application in a Electrochemical and Surface-Enhanced Raman Scattering Biosensor, n.d. doi:10.3390/ma9060406.

[189] D.C. Marcano, D. V Kosynkin, J.M. Berlin, A. Sinitskii, Z. Sun, A. Slesarev, L.B. Alemany, W. Lu, J.M. Tour, Improved Synthesis of Graphene Oxide, 4 (n.d.).

[190] X. Zhang, V.K. Yadavalli, Surface immobilization of DNA aptamers for biosensing and protein interaction analysis, Biosens. Bioelectron. 26 (2011) 3142–3147. doi:10.1016/j.bios.2010.12.012.

[191] L. Yang, Y. Tseng, G. Suo, L. Chen, J. Yu, W. Chiu, C. Huang, C. Lin, Photothermal Therapeutic Response of Cancer Cells to Aptamer − Gold Nanoparticle-Hybridized Graphene Oxide under NIR Illumination, (2015). doi:10.1021/am508117e.

[192] S. Vijayender, As featured in : ChemComm, (2019). doi:10.1039/c9cc00225a.

[193] H. Yu, B. Zhang, C. Bulin, R. Li, R. Xing, High-efficient Synthesis of Graphene Oxide Based on Improved Hummers Method, Sci. Rep. 6 (2016) 1–7. doi:10.1038/srep36143.

[194] G. Liu, M. Qi, Y. Zhang, C. Cao, E.M. Goldys, Nanocomposites of gold nanoparticles and graphene oxide towards an stable label-free electrochemical immunosensor for detection of cardiac marker troponin-I, Anal. Chim. Acta. 909 (2016) 1–8. doi:10.1016/j.aca.2015.12.023.

[195] F. Chekin, A. Vasilescu, R. Jijie, S.K. Singh, S. Kurungot, M. Iancu, G. Badea, R. Boukherroub, S. Szunerits, Sensitive electrochemical detection of cardiac troponin I in serum and saliva by nitrogen-doped porous reduced graphene oxide electrode, Sensors Actuators, B Chem. 262 (2018) 180–187. doi:10.1016/j.snb.2018.01.215.

[196] F. Jia, N. Duan, S. Wu, X. Ma, Y. Xia, Z. Wang, X. Wei, Impedimetric aptasensor for Staphylococcus aureus based on nanocomposite prepared from reduced graphene oxide and gold nanoparticles, Microchim. Acta. 181 (2014) 967–974. doi:10.1007/s00604-014-1195-8.

[197] L. Tang, Y. Wang, Y. Liu, J. Li, DNA-directed self-assembly of graphene oxide with applications to ultrasensitive oligonucleotide assay, ACS Nano. 5 (2011) 3817–3822. doi:10.1021/nn200147n.

[198] P.J.J. Huang, J. Liu, DNA-length-dependent fluorescence signaling on graphene oxide surface, Small. 8 (2012) 977–983. doi:10.1002/smll.201102156.

[199] Y.H. So, H.T. Chang, W.J. Chiu, C.C. Huang, Graphene oxide modified with aptamer-conjugated gold nanoparticles and heparin: A potent targeted anticoagulant, Biomater. Sci. 2 (2014) 1332–1337. doi:10.1039/c4bm00156g.

[200] C. Soc, Y. Wang, Chem Soc Rev, (2015) 6954–6980. doi:10.1039/c4cs00519h.

[201] S. Li, G. Zhao, R. Zhang, A sensitive and selective nitrite sensor based on a glassy carbon electrode modified with gold nanoparticles and sulfonated graphene, (2013) 821–827. doi:10.1007/s00604-013-0999-2.

[202] N. Deng, B. Jiang, Y. Chen, Z. Liang, L. Zhang, Y. Liang, K. Yang, Y. Zhang, Aptamer-conjugated gold functionalized graphene oxide nanocomposites for human - thrombin specific recognition ଌ, J. Chromatogr. A. 1427 (2016) 16–21. doi:10.1016/j.chroma.2015.12.018.

[203] H. Bhardwaj, M.K. Pandey, G. Sumana, Electrochemical Aflatoxin B1 immunosensor based on the use of graphene quantum dots and gold nanoparticles, (2019) 1–12.

[204] S. Verma, A. Singh, A. Shukla, J. Kaswan, K. Arora, J. Ramirez-vick, P. Singh, S.P. Singh, Anti-IL8 / AuNPs-rGO / ITO as an Immunosensing Platform for Noninvasive Electrochemical Detection of Oral Cancer, (2017). doi:10.1021/acsami.7b06839.

[205] E. Farjami, R. Campos, J.S. Nielsen, K. V Gothelf, J. Kjems, E.E. Ferapontova, RNA Aptamer-Based Electrochemical Biosensor for Selective and Label-Free Analysis of Dopamine, (2013).

[206] E.E. Ferapontova, E.M. Olsen, K. V Gothelf, An RNA Aptamer-Based Electrochemical Biosensor for Detection of Theophylline in Serum, (2008) 4256–4258. doi:10.1021/ja711326b.

[207] J. Song, L. Xu, R. Xing, Q. Li, C. Zhou, D. Liu, H. Song, Synthesis of Au / Graphene Oxide Composites for Selective and Sensitive Electrochemical Detection of Ascorbic, (2014) 1–7. doi:10.1038/srep07515.

[208] A. Radi, C.K.O. Sullivan, Aptamer conformational switch as sensitive electrochemical biosensor for potassium ion recognition {, (2006) 3432–3434. doi:10.1039/b606804a.

Buffers and Stocks

IPTG Stock solution	
1 M IPTG Stock solution	2.38g IPTG and DI water.

Kanamycin stock solution	
Kanamycin stock solution	0.5g Kanamycin monosulfate and DI water.

Protein purification buffers	
Binding buffer (200ml)	20 mM Tris pH-8, 500 mM NaCl, 0.5 mM β-mercaptoethanol, 3% glycerol,0.01% Tween 20 , 8M urea and 5 mM Imidazole.
Wash buffer I (200ml)	20 mM Tris pH-8, 500 mM NaCl, 0.5 mM β-mercaptoethanol, 3% glycerol,0.01% Tween 20 , 6 M urea and 15 mM Imidazole.
Wash buffer II (200ml)	20 mM Tris pH-8, 500 mM NaCl, 0.5 mM β-mercaptoethanol, 3% glycerol, 0.01% Tween 20 , 4 M urea and 15 mM Imidazole.
Wash buffer III (200ml)	20 mM Tris pH-8, 500 mM NaCl, 0.5 mM β-mercaptoethanol, 3% glycerol, 0.01% Tween 20 , 2 M urea and 15 mM Imidazole.
Wash buffer IV (200ml)	20 mM Tris pH-8, 500 mM NaCl, 0.5 mM β-mercaptoethanol, 3% glycerol, 0.01% Tween 20 and 15 mM Imidazole.
Elution buffer (200ml)	20 mM Tris pH-8, 500 mM NaCl, 0.5 mM β-mercaptoethanol, 3% glycerol, 0.01% Tween 20 and 300 mM Imidazole.
Dialysis buffer I (1000ml)	20 mM Tris pH-8, 500 mM NaCl, 0.5 mM β-mercaptoethanol, 3% glycerol and 0.01% Tween 20.
Dialysis buffer II (1000ml)	20 mM Tris pH-8, 300 mM NaCl, 0.5 mM β-mercaptoethanol, 3% glycerol and 0.01% Tween 20.

SDS-PAGE buffer

30% acrylamide-bisacrylamide solution (100ml)	29.2g Acrylamide, 0.8g Bisacrylamide.
Tris-HCl, pH 6.8, 0.5M (100ml)	6.06g Tris base, pH adjusted to 6.8 with 2N HCl.
Tris-HCl, pH 8.8, 1.5M (100ml)	18.18g of Tris base, pH adjusted to 8.8 with 2N HCl.
Gel running buffer (10X)	30.0g of Tris base, 144.0g of glycine and 10.0g of SDS in 1000ml of water.
SDS gel loading buffer (2X)	100mM Tris/HCl (pH 6.8), 4% (w/v) SDS, 0.2% (w/v) Bromophenol blue, 20% (v/v) glycerol, 200mM DTT or β-mercaptoethanol
Staining solution (Coomassie brilliant blue staining) (100ml)	10ml Orthophosphoric acid, 10 g w/v ammonium sulphate, 0.12 g w/v CBB G250, 20ml methanol and 70 ml water.
Destaining solution (1000ml)	HPLC grade water, 50% (v/v) methanol and 10% (v/v) acetic acid.

Agarose gel electrophoresis

Tris Borate EDTA (TBE) (10X) 1 Litre	Tris 108g, Boric acid 55g, 0.5M EDTA 40ml (pH-8).
TAE buffer (50X)	50mM EDTA disodium salt, 2M Tris and 1M Glacial acetic acid.

Phosphate buffer saline (PBS) pH-7.4

Phosphate Buffer Saline (PBS) pH-7.4 1 Liter	1.37 M NaCl, 27 mM KCl, 100 mM Na_2HPO_4, and 18 mM KH_2PO_4.

Phosphate buffer pH-7.4

Phosphate buffer (0.1M) pH-7.4 1 Liter	Sodium dihydrogen phosphate (NaH_2PO_4) 2.7g and Disodium hydrogen phosphate (Na_2HPO_4)10.9g.

Western Blot buffer	
Transfer buffer	25mM Tris, 192 mM Glycine, 20% methanol.
Block buffer	5% skim milk in 1x PBS pH-7.4
Wash buffer	1x PBST (0.1% Tween 20)

EMSA buffer	
EMSA binding buffer	50 mM Tris pH 8, 50 mM NaCl, 200 mM KCl, 5 mM MgCl2, 5 mM EDTA, 5 mM DTT, 5% glycerol, 0.25 mg/ml BSA.

ELISA coating buffer	
Sodium carbonate/bicarbonate buffer (0.1M) pH-9.6, 1 Litre	Sodium carbonate (Na_2CO_3) 3.03g and Sodium bicarbonate ($NaHCO_3$) 6g.

TE buffer	
Tris EDTA buffer	40 mM Tris HCl pH 8, 0.02% Tween 20 and 10 mM EDTA and 50 mM DTT

List of Patents…

- **A pH based colorimetric bioassay method for bacterial detection in water by naked.**

  Inventors: Vijayender Bhalla, Pargat Singh, ***Saloni kakkar***, Bharti, Virendra Nishad.

  Application No. 201811035461; 20/09/2018. Published patent; 14/08/2020.

- **DNA aptamers directed against cardiac biomarker peptides.**

  Inventors: Vijayender Bhalla, Virendra Nishad, ***Saloni kakkar***, Bharti.

  Application No. 202111043591; 24/09/2021. Completely filed.

List of publications…

- **Rapid and sensitive colorimetric detection of pathogens based on silver–urease interactions.**

  Pargat Singh*, ***Saloni Kakkar**,*** Bharti, Rajesh Kumar and Vijayender Bhalla (2019); Chemical Communications (The Royal Society of Chemistry), 55: 4765-4768. (* Equal First author)

  doi: 10.1039/c9cc00225a.

- **Polysilicon Field Effect Transistor Biosensor for the Detection of Cardiac Troponin-I (cTnI).**

  Rahul Prajesh, Vinay Goyal, ***Saloni Kakkar***, Jyayasi Sharma, M. A. Alam, Ranjan Kumar Maurya, Vijayender Bhalla, Ajay Agarwal (2021) Journal of The Electrochemical Society 168-027501.

  doi:10.1149/1945-7111/abdde6

- **Site-directed dual bioprobes inducing single-step nano-sandwich assay for detection of cardiac Troponin I.**

  Saloni Kakkar, Sakshi Chauhan, Rajni Bala, Bharti, Virendra Kumar, Manojkumar Rohit, Vijayender Bhalla. (Under review)

- **Conformational switching of aptamer biointerfacing graphene-gold nanohybrid for ultrasensitive label-free sensing of cardiac Troponin I.**

  Saloni Kakkar, Sakshi Chauhan, M. A. Alam, Bharti, Manojkumar Rohit, Vijayender Bhalla.

  (Under review)

Journal featured cover page…

- **Rapid and sensitive colorimetric detection of pathogens based on silver–urease interactions.**

  Pargat Singh*, ***Saloni Kakkar**,*** Bharti, Rajesh Kumara and Vijayender Bhalla (2019); Chemical Communications, (The Royal Society of Chemistry), 55: 4765-4768. (* Equal First author)

  doi: 10.1039/c9cc00225a.

Research news highlight…

- **Low-cost, portable kit to detect pathogens in drinking water.**

  Nature India; doi:10.1038/nindia.2019.76 Published online 12 June 2019

  https://www.natureasia.com/en/nindia/article/10.1038/nindia.2019.76

सी. एस. आई. आर. - सूक्ष्मजीव प्रौद्योगिकी संस्थान

विज्ञान एवं प्रौद्योगिकी मंत्रालय, भारत सरकार

CSIR- INSTITUTE OF MICROBIAL TECHNOLOGY

Ministry of Science and Technology, Govt. of India

सेक्टर - 39 ए, चण्डीगढ़/ Sector – 39A, Chandigarh-160036

प्रमाण-पत्र/ Certificate

Best PhD Research Presentation Award- 2021

सुश्री सलोनी कक्कड़ को पीएचडी कार्यक्रम के दौरान उत्कृष्ट शोध कार्य के लिए वर्ष 2021 के सर्वश्रेष्ठ पीएचडी अनुसंधान प्रस्तुति पुरस्कार से सम्मानित किया जाता है/ *Ms. Saloni Kakkar* has been awarded the Best PhD Research Presentation Award for the year 2021 for her outstanding research work while undergoing the PhD Programme.

दिनांक/Dated: 24.01.2022

निदेशक/Director

Journal of The Electrochemical Society, 2021 **168** 027501
1945-7111/2021/168(2)/027501/7/$40.00 © 2021 The Electrochemical Society ("ECS"). Published on behalf of ECS by IOP Publishing Limited

Polysilicon Field Effect Transistor Biosensor for the Detection of Cardiac Troponin-I (cTnI)

Rahul Prajesh,[1,2,z] Vinay Goyal,[1,2] Saloni Kakkar,[3] Jyayasi Sharma,[1,4] M. A. Alam,[1] Ranjan Kumar Maurya,[1,2] Vijayender Bhalla,[3] and Ajay Agarwal[1,2]

[1]*CSIR-Central Electronics Engineering Research Institute, Pilani-333031 (Rajasthan), India*
[2]*Academy of Scientific and Innovative Research (AcSIR), Ghaziabad-201002 (U.P.), India*
[3]*CSIR-Institute of Microbial Technology, Chandigarh-160036, India*
[4]*University of Rajasthan, Jaipur, 302004, India*

A highly sensitive and robust polysilicon Field Effect transistor (SiFET) has been developed for the detection of an gold standard biomarker of myocardial infarction (AMI) Cardiac Troponin I (cTnI). This paper reports a polysilicon FET device integrated with a thin film of gold layer as a gate terminal which is biofunctionalized with specific cTnI binding single stranded DNA receptor aptamer to detect cTnI. The reported SiFET is fabricated using standard microfabrication unit processes. The detailed characterization of reported device is performed and thoroughly discussed at different stages of device development. The assessment of bio-interface is also studied using various surface characterization techniques such as Raman spectroscopy, Atomic force microscopy (AFM) and Contact angle measurements. The experimental results showed the significant response for cTnI concentration as low as 0.1 ng ml^{-1} for label free detection.
 [DOI: 10.1149/1945-7111/abdde6]

Manuscript submitted January 7, 2021; revised manuscript received January 18, 2021. Published February 1, 2021.

Silicon nanowire field-effect-transistors (Si-NW FETs) have recently emerged as potential diagnostic platforms due to its ultrasensitive, instant, real-time and label-free detection capabilities. FET biosensor works similar to a conventional field effect transistor with a precise difference as it has receptors as gate and channel is replaced by Silicon/poly silicon wires which makes it more sensitive to the detection of biomarkers and simplifies the binding of biological analytes.[1–4] Point-of-care testing devices (POCT)[5,6] have emerged variedly in the field of biology nowadays. This is because these are cost-effective, easy to operate and convenient as compared to the conventional laboratory tests.[7,8]

Generally, a biosensor is a point-of-care device which senses the target analyte on its surface with limited amount of biological sample (Blood/Urine/Saliva etc.) expressing high accuracy of signal output (cTnI) present in it. cTnI is an explicit biomarker of Acute Myocardial Infarction (AMI).[9–12] In biological terms, levels of cTnI in blood express the condition of heart being damaged.[13] cTnI comes in blood from cardiac muscles, as cardiac muscles shrink or block due to some factors, leading to AMI or heart attack.[14] As a consequence, the criticality lies in early and accurate diagnosis of AMI which is indicated by the elevated levels of gold standard biomarker cTnI. The high specificity and sensitivity of cTnI demarcates it as a preferred indicator of monitoring heart condition.[15] The advancement in development of biosensing platforms to detect cTnI have been exhibited by many conventional methodologies such as enzyme-linked immunosorbent assay (ELISA),[16] radioimmunoassay,[17] fluorescent based detection,[18] surface plasmon resonance (SPR) based sensors[19] and colorimetric sensors.[20] Nevertheless, rapid detection along with point of care management of cardiac patients suffers prolonged diagnosis producing non-specific output. To this context, FET based detection platforms offer real time administration of patient's health by measuring accurate levels of cTnI via specific DNA aptamer-based probe hence providing a label-free aptasensor based biosensor. FET based biosensor can be fabricated by using Top-down or bottom-up approach.[21–25] Top-down approach is mostly preferred because this is industry friendly enabling mass production. Conventional FET suffers from some measurement drawbacks and limitations. They generally have gate current leakage, low subthreshold voltage and high detection time. To overcome all these issues Si-FET is fabricated with top-down approach with a gold coated gate.[26–28] The presence of a gold layer on the gate minimizes the leakage of gate current diminishing the detection time. In this work, standard microfabrication processes are used to fabricate the poly silicon FET biosensor. Fabricated device is characterized using I–V measurements, functionalized surface is characterized by Raman spectroscopy, atomic force microscopy (AFM) and bio sensing. The ease of operation principle of SiFET sensor with simplified integration with transducer extends low device-to-device variations providing a promising platform for early and rapid detection of cTnI as compared to previously reported electrochemical sensing strategies.

[z]E-mail: rahul@ceeri.res.in

Experimental

Chemicals and reagents.—Standard semiconductor grade chemicals namely, acetone, isopropyl alcohol (IPA), H_2SO_4 and H_2O_2 *(purchased from Merck)* are used for cleaning of silicon wafer. The DNA aptamer binding to cTnI was chemically synthesized by SELEX (Systematic evolution of ligands by exponential enrichment) method and purified by column method[29] at CSIR-IMTECH, Chandigarh, India. Thiol modified aptamer was procured from IDT technologies with a $–SH–(CH_2)_6$ linker at 5′ end. The aptamer is a 55-nucleotide DNA sequence generated against a specific peptide region of Troponin I.

Device fabrication.—The Si-FET device was fabricated using standard microfabrication technology. The detailed fabrication steps are elaborated in Fig. 1. Briefly, after cleaning (Piranha), silicon wafer (p-type, resistivity 1–10 Ω-cm) was thermally oxidized (at 1050 °C) to grow 1 μm of SiO_2 for electrical isolation. Thereafter, 0.4 μm of polysilicon was deposited by low pressure chemical vapor deposition (LPCVD). Then diffusion of phosphorus (7 min @ 900 °C) was carried out for making the poly silicon to be n-type. Further, the polysilicon was patterned using i-line (365 nm) lithography to realise wire structures. Polysilicon wass etched using reactive ion etching (RIE) using SF_6 and O_2 gases. Gate oxide (~10 nm by dry thermal oxidation @950 °C for 8 min) wass then grown on the polysilicon wires, followed by lithography of via opening. Wafers were thereafter taken to ion implanter for source drain doping (5E15 cm^{-2} @ 40 keV). Patterned photoresist was removed and metal (Au or Al) deposition on the cleaned wafers was carried out, followed by metal patterning using lithography and wet etching. Further, gold patch on gate was patterned by lift-off process followed by passivation of the device by plasma enhanced chemical vapor deposition (PECVD) of Si_3N_4 (0.4 μm) and SiO_2 (0.6 μm). After passivation, only the pads and gold gate remain exposed and rest of the area got passivated by silicon nitride and oxide layers. Figure 2 shows the optical images of polysilicon array patterned on silicon wafer.

ChemComm

COMMUNICATION

View Article Online
View Journal | View Issue

Cite this: *Chem. Commun.*, 2019, **55**, 4765

Received 9th January 2019,
Accepted 8th March 2019

DOI: 10.1039/c9cc00225a

rsc.li/chemcomm

Rapid and sensitive colorimetric detection of pathogens based on silver–urease interactions†

Pargat Singh,‡[ab] Saloni Kakkar,‡[b] Bharti,[b] Rajesh Kumar[a] and Vijayender Bhalla *[b]

Herein, we demonstrate a facile and economic approach for colorimetric detection of microbial pathogens in drinking water, employing silver–urease interactions. In the presence of harmful pathogens, receptor coated silver nanoparticles (AgNPs) preferentially bind to the bacterial surface and urease catalytically elevates the pH of the solution, which is sensed by a pH responsive chromogenic dye. The assay demarcates bacterial contamination levels up to 10^2 cells mL^{-1} in a field-friendly method.

Bacterial contamination in drinking water poses a serious threat to public health and safety.[1] Monitoring of drinking water for microbial contamination is a major step in the prevention of various infectious diseases.[2] An array of techniques has been reported for detection of bacterial contamination to date, with many being restricted to laboratory settings only. Traditional methods of culturing and immunological assays are accurate and reliable but their utility is constrained by time and the requirement of trained manpower.[3] Modern molecular diagnostics such as polymerase chain reaction and loop mediated amplification remain unavailable, impractical and too expensive for poor economies.[4] Besides, the breakthrough of diagnostics introduced for areas with confined resources still comes at a considerable expense.[5] Therefore, a cost-effective and portable assay platform for detection of pathogenic microorganisms will not only conserve precious human lives, but also avert the unnecessary cost associated with medical treatments.

Recent advances in colorimetric detection strategies have already secured an edge in the commercial arena of diagnostics.[6] pH monitoring based on visual signal readout *via* dyes such as litmus, phenol red, bromothymol blue, and phenolphthalein is one of the most simple, cost effective and routinely used methods.[7]

Urease is a highly efficient metalloenzyme which increases the pH of the solution by hydrolyzing urea to ammonia and carbon dioxide.[8,9] Over the past few years, efforts have been made to utilize the catalytic activity of urease for detecting bacterial contamination. For instance, Li and co-workers have reported a strategy by engineering RNA cleaving DNA aptazyme and urease using magnetic beads for detection of *Escherichia coli*.[7] However, the system is quite complex as it is difficult to engineer and conjugate functional nucleic acids. Recently, Lin and his group demonstrated a combinatorial approach of urease catalysis and immunomagnetic separation for pH based detection of *Listeria monocytogenes*.[10] The methodology suffers various drawbacks like tedious bioconjugation steps and use of multiple receptor biomolecules, which eventually increases the cost of the assay. In this perspective, a robust and cost effective pH-based colorimetric sensing framework that can exploit the catalytic activity of urease for a bacterial detection event is highly desirable.

AgNPs with their diversified applications are paving new avenues in biomedical research.[11–14] Yen *et al.* demonstrated a study of multicolor silver nanoparticle based lateral flow assays for simultaneous detection of yellow fever, dengue and ebola virus.[15] The significance of AgNPs as a SERS probe for detection of bacteria in water has been reported by Haibo and co-workers.[16] Their work along with various other studies signifies the strong relevance of AgNPs for sensitive detection of bioanalytes. Silver has long been well-acknowledged to inhibit urease activity by blocking its active site through sulfhydryl linkages.[17,18] With advances in nanotechnology many groups have explored this inhibition phenomenon in nanostructured silver also.[19,20]

Herein, we report a distinct approach for bacterial sensing by employing molecular recognition of AgNPs and catalytic activity of urease to detect bacterial contamination in drinking water. In the presence of bacterial contamination, receptor coated AgNPs adhere to the bacterial cell membrane rendering urease active in solution. Upon addition of urea and phenol

[a] *UIET-Panjab University, Sector 25, Chandigarh, India*
[b] *CSIR-Institute of Microbial Technology, Sector 39A, Chandigarh, India. E-mail: vkbhalla@imtech.res.in*

† Electronic supplementary information (ESI) available: Experimental procedures, synthesis of silver nanoparticles, real sample testing and other characterization methods. See DOI: 10.1039/c9cc00225a

‡ Both of these authors contributed equally.

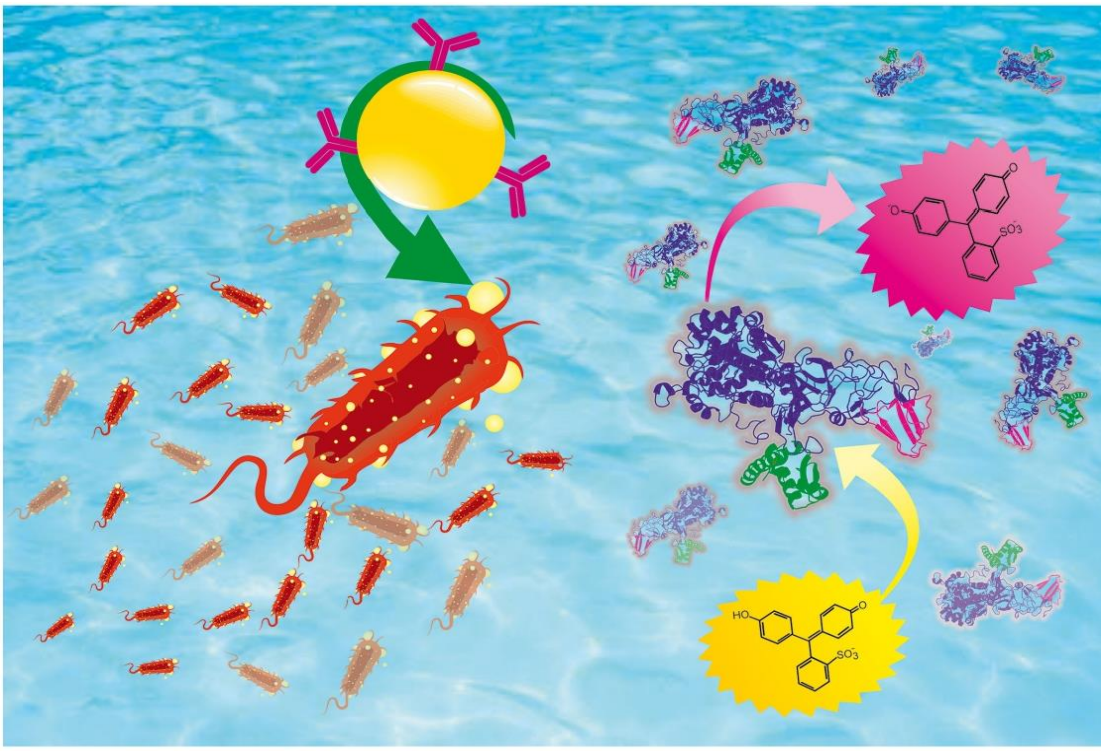

Showcasing research from Dr Vijayender Bhalla's laboratory, CSIR – Institute of Microbial Technology, Chandigarh, India.

Rapid and sensitive colorimetric detection of pathogens based on silver–urease interactions

A pH based sensing strategy for onsite pathogen detection using a receptor coated silver nanoparticle–urease pair is reported. The device detects bacterial contamination as low as 10 cells mL^{-1} and can be used for both broad range and specific bacterium detection.

As featured in:

See Vijayender Bhalla *et al.*, *Chem. Commun.*, 2019, **55**, 4765.

ROYAL SOCIETY OF CHEMISTRY | Celebrating IYPT 2019

rsc.li/chemcomm

Registered charity number: 2078

Office of the Controller General of Patents, Designs & Trade Marks
Department of Industrial Policy & Promotion,
Ministry of Commerce & Industry,
Government of India

सत्यमेव जयते

INTELLECTUAL PROPERTY INDIA
PATENTS | DESIGNS | TRADE MARKS
GEOGRAPHICAL INDICATIONS

1. IN201811035461 - A PH BASED COLORIMETRIC BIOASSAY METHOD FOR BACTERIAL DETECTION IN WATER BY NAKED EYE

National Biblio. Data | Description | Claims | Documents

PermaLink | Machine translation ▼

Office
India

Application Number
201811035461

Application Date
20.09.2018

Publication Number
201811035461

Publication Date
14.08.2020

Publication Kind
A

IPC
C12Q 1/00

Applicants
COUNCIL OF SCIENTIFIC AND INDUSTRIAL RESEARCH

Inventors
BHALLA, VIJAYENDER
SINGH, PARGAT
KAKKAR, SALONI
BHARTI
NISHAD, VIRENDRA

Title
[EN] A PH BASED COLORIMETRIC BIOASSAY METHOD FOR BACTERIAL DETECTION IN WATER BY NAKED EYE

Abstract
[EN]
The current invention describes a portable and facile platform for detection of bacterial contamination in drinking water. The invention provides an absolutely novel methodology that associates bacterial detection technique to a pH change event and produces a colorimetric readout that can be visualized by naked eyes. The novelty of the disclosed study lies in the urease-silver interaction based bacteria detection. The recognition elements used in the study are Ag+ itself or the polycationic coating of the nanoparticle or the specific receptor layer on the nanoparticle. The assay is based on the inhibition of the urease enzyme by silver nanoparticles/ silver ions in the absence of bacteria that inactivates the enzymatic response. Whereas, in case of a small concentration of any bacterial contamination, the silver nanoparticles/ ions attaches to the bacterial cell membrane rendering enzyme functional. This can be seen by a chromogenic pH responsive dye that produces colorimetric transition on addition of substrate urea. The technique is extremely sensitive to a least number of bacterial count.